Innate Immune Surveillance in Coronavirus Disease-2019 (COVID-19)

A thesis submitted in fulfilment of the requirement for the
Degree of Doctor of Philosophy

By Nazar Beirag
February 2024

Division of Biosciences
College of Health, Medicine, and Life Sciences
Brunel University London

Declaration

I declare that the research presented in this thesis is my work, except where others specified and have not been submitted for any other degree.

Nazar Beirag

ACKNOWLEDGEMENTS

With great pleasure and profound gratitude, I extend my heartfelt thanks to my supervisor, Dr Uday Kishore, for his continuous support during my PhD and related research. Also, I would like to thank Dr Anthony Tsolaki for talking over the supervision and my second supervisor, Dr Evgeny Makarov.

Every result described in this thesis was accomplished with the help of our collaborators in providing kindly research reagents; Dr Robert B. Sim, MRC Immunochemistry Unit, Department of Biochemistry, University of Oxford for providing the primary antibodies (anti-human SP-D, anti-human C1q, anti-human C4BP, anti-human properdin, and anti-human factor H). Dr Nigel Temperton, Viral Pseudotype Unit, Medway School of Pharmacy, University of Kent and Greenwich, Kent, for supplying SARS-CoV-2 spike lentiviral pseudoparticles. Dr Mohamed H. Shamji, Immunomodulation and Tolerance Group, Department of Allergy and Clinical Immunology, National Heart and Lung Institute, Imperial College London, London, for providing SARS-CoV-2 S protein. Dr Chandan Kumar and Dr Susan Idicula, Biomedical Informatics Centre, National Institute for Research in Reproductive and Child Health, ICMR, Mumbai, Maharashtra, India for In-silico Docking Analysis. Dr Robert B. SIM, MRC Immunochemistry Unit, Department of Biochemistry, University of Oxford, and Dr Anna Blom, Lund University, Malmo, Sweden provided C4BP.

I would also like to thank my PhD progression panel, Dr Annabelle Lewis, Dr Su-Ling Li, and Dr Sabrina Tosi. Their participation and valuable insights during the PhD review meetings greatly supported my research journey. Furthermore, I express my deepest gratitude to the PGR office and the laboratory staff at the Department of Biosciences at Brunel University London for their assistance throughout my project.

Finally, I want to acknowledge my colleagues and friends, Dr Praveen Mathews and Dr Valarmathy Murugaiah, for validating my experiments, supporting me during challenging times, and engaging in stimulating discussions.

List Of Symbols and Abbreviations

ARDS	–	Acute Respiratory Distress Syndrome
A549	–	Adenocarcinoma Human Alveolar Basal Epithelial Cells
BALF	–	Bronchoalveolar Lavage Fluid
ACE2	–	Angiotensin-converting enzyme 2 receptor
C1q	–	Complement component 1q
C4BP	–	C4b Binding Protein
CRD	–	Carbohydrate Recognition Domain
CBC	–	Carbonate/Bicarbonate
CD	–	Cluster of Differentiation
CCP	–	Complement Control Protein
CNBR	–	Cyanogen Bromide
CTL	–	Cytotoxic T Lymphocytes
℃	–	Degree Celsius
DC	–	Dendritic Cells
DEAE	–	Diethyl Aminoethyl
DMSO	–	Dimethyl Sulfoxide
DMEM	–	Dulbecco's Modified Eagle Medium
E protein	–	SARS-CoV-2 Envelope Protein
ELISA	–	Enzyme-Linked Immunoassay
EDTA	–	Ethylenediamine Tetra-Acetic Acid
FH	–	Factor H
FBS	–	Fetal Bovine Serum
Fabs	–	Fragment-Antigen Binding Region
Gh	–	Globular Head
GP	–	Glycoprotein
HA	–	Hemagglutinin
HRP	–	Horseradish Peroxidase

HEK	–	Human Embryonic Kidney
HIV	–	Human Immunodeficiency Virus
HTLV	–	Human T Lymphotropic Virus
ISGs	–	IFN-Stimulated Genes
Ig	–	Immunoglobulin
IAV	–	Influenza A Virus
IFN	–	Interferon
IRF	–	Interferon Regulatory Factor
Il	–	Interleukin
IPTG	–	Isopropyl B-D-1-Thiogalactopyranoside
kDa	–	Kilo Daltons
LB	–	Luria-Bertani
M protein	–	SARS-CoV-2 Membrane Protein
MHC	–	Major Histocompatibility Complex
MBL	–	Mannose-Binding Lectin
mRNA	–	Messenger Ribonucleic Acid
MW	–	Molecular Weight
N protein	–	SARS-CoV-2 nucleoprotein
NK	–	Natural Killer
CAPS	–	N-Cyclohexyl-3-Aminopropanesulfonic Acid
fMLP	–	N-Formylmethionine-Leucyl-Phenylalanine
NF-κB	–	Nuclear Factor Kappa-Light-Chain-Enhancer of Activated B Cells
PAMPs	–	Pathogen-Associated Molecular Patterns
PRRs	–	Pattern Recognition Receptors
PS	–	Penicillin-Streptomycin
PBS	–	Phosphate-Buffered Saline
PAGE	–	Polyacrylamide Gel Electrophoresis
PVDF	–	Polyvinylidene Difluoride

RANTES	–	Regulated Upon Activation, Normal T Cell Expressed and Presumably Secreted
rfhSP-D	–	A recombinant fragment of human SP-D
RNA	–	Ribonucleic Acid
RT	–	Room Temperature (~20℃)
S protein	–	SARS-CoV-2 envelope protein
SARS-CoV-2	–	Severe Acute Respiratory Syndrome Coronavirus 2
SDS	–	Sodium Dodecyl Sulfate
SD	–	Standard Deviation
SEM	–	Standard Error of The Mean
SP-A	–	Surfactant Protein A
SP-D	–	Surfactant Protein D
TSR	–	Thrombospondin Type 1 Repeats
TLR	–	Toll-Like Receptors
TNF	–	Tumor Necrosis Factor
WHO	–	World Health Organization
TMB	–	3,3’,5,5’-Tetramethylbenzidine

Table of Contents

1. Introduction 27

1.1 COVID-19 Pandemic 28

1.2 The origin and evolution of SARS-CoV-2 29

1.3 Structure and genomic of SARS-CoV-2 29

1.4 The life cycle of SARS-CoV-2 31

1.4.1 Priming viral S protein, binding, and entry into the target host cell: 31

1.4.2 Replication, assembly, and release: 32

1.5 Major cellular receptor recognition by SARS-CoV-2 34

1.5.1 ACE2 34

1.5.2 TMPRSS2 & TMPRSS4 and Furin 35

1.5.3 DC-SIGN/L-SIGN 35

1.6 Pathogenesis of COVID-19 36

1.7 Immune Response to SARS-CoV-2 37

1.8 Innate immune response to SARS-CoV-2 37

1.8.2 Adaptive immune response in SARS-CoV2 infection 55

1.9 Main aims of this study 56

2 Introduction ..... **Error! Bookmark not defined.**

2.1 Native Complement Protein Purification from Human Plasma 58

2.1.1 Purification of native human C1q 58

2.1.2 Purification of Factor H 58

2.1.3 Purification of native human C4BP 59

2.1.4 Purification of properdin 59

2.2 Expression of recombinant proteins 59

2.2.1 Expression of rfhSP-D, DC-SIGN, ghA, ghB, ghC modules of human C1q, and properdin-TSR4+5 59
2.2.2 Endotoxin Removal of DC-SIGN, rfhSP-D, ghA, ghB, ghC modules of human C1q and MBP, and properdin-TSR4+5 and Limulus Amoebocyte Lysate Assay 63
2.3 Sodium Dodecyl Sulphate-Polyacrylamide Gel Electrophoresis (SDS-PAGE) 63
2.3.1 SDS PAGE preparation 63
2.3.2 Sample Preparation and Electrophoresis 64
2.3.3 Staining of SDS-PAGE gel 64
2.4 Western Blotting 64
2.5 Direct-Binding ELISA 65
2.6 Cell Culture 67
2.7 Viral cell entry assay 67
2.7.1 Preparation of SARS-CoV-2 Spike Protein Pseudotyped lentiviral particles 67
2.7.2 Treatment of SARS-CoV-2 Pseudotyped lentiviral particles 67
2.7.3 Luciferase reporter assay 68
2.7.4 NF-κB activity assay 68
2.8 Cell binding assay 69
2.9 Fluorescence microscopy 69
2.10 Modulation of SARS-CoV-2 Pseudoparticle-Induced Infection by C1q, C4BP, FH, FP or TSR4+5 70
2.10.1 SARS-CoV-2 S protein treatment 70
2.10.2 SARS-CoV-2 alphaviral pseudoparticles treatment 70
2.10.3 Quantitative Real-time (qRT) Polymerase Chain Reaction (PCR) analysis 70
2.11 *In-silico* Docking Analysis 73
2.11.1 rfhSP-D interaction with Spike and DC-SIGN 73
2.11.2 FP interaction with Spike and ACE2 73

2.12 Statistical analysis 74

3 Interaction between rfhSP-D and SARS-CoV-2 virus in DC-SIGN expressing cells 75

3.1 Abstract 76

3.2 Background ..... **Error! Bookmark not defined.**

3.3 Results 79

3.3.1 Both DC-SIGN and rfhSP-D bind to SARS-CoV 2 spike protein. 79

3.3.2 rfhSP-D treatment enhances DC-SIGN mediated binding and uptake of SARS-CoV-2 pseudotyped viral particles 80

3.3.3 rfhSP-D modulates pro-inflammatory cytokines and chemokines response in SARS-CoV-2 spike protein-challenged DC-HEK cells 83

3.3.4 Modulation of immune response in SARS-CoV-2 spike protein-challenged DC-THP-1 cells by rfhSP-D 85

3.3.5 SP-D interacts with RBD, and DC-SIGN interacts with NTD of the SARS-CoV-2 spike protein 87

3.3.6 SP-D stabilises DC-SIGN and SARS-CoV-2 spike protein interaction 89

3.4 Discussion 91

4 Complement Activation-Independent Attenuation of SARS-CoV-2 Infection by C1q and C4b-Binding Protein 96

4.1 Abstract 97

4.2 Introduction 98

4.3 Results 100

4.3.1 Human C1q and C4BP interact with SARS-CoV-2 Spike and RBD Proteins 100

4.3.2 Human C1q, Recombinant Globular Head Modules, and C4BP Inhibit SARS-CoV-2 Pseudoparticle Transduction 102

4.3.3 Human C1q, Recombinant Globular Head Modules, and C4BP Inhibit SARS-CoV-2 Pseudoparticle Binding to ACE2- and TMPRSS2-Expressing A549 Cells 104

4.3.4 C1q and C4BP Attenuate Inflammatory Response in SARS-CoV-2 Pseudoparticles Challenged A549-hACE2+TMPRSS2 Cells 106
4.4 Discussion 111
5 Human complement Properdin and Factor H differentially modulate SARS-CoV-2 Infection 116
5.1 Abstract 117
5.2 Introduction 118
5.3 Results 120
5.3.1 SARS-CoV-2 Spike and RBD Proteins interact with FH and FP 120
5.3.2 FH restricted SARS-CoV-2 Pseudoparticle transduction, while FP and TSR4+5 promoted 122
5.3.3 SARS-CoV-2 Pseudoparticle binding to the target cells was inhibited by FH and enhanced by FP and TSR4+5 123
5.3.4 SARS-CoV-2 infection-associated inflammation can be attenuated by FH but promoted by FP 126
5.3.5 FP interacts with spike and ACE2 in a tripartite complex 132
5.4 Discussion 135
6 Conclusion 140
7 References 144
8 Appendix 163

List of Figures

Figure 1.1: Genomic and molecular characteristics of the SARS CoV-2 virus. A. The genome of SAR-CoV-2 is a large, positive-sense, single-stranded RNA consisting of 29,903 nucleotides. It is non-segmented and contains two open-reading frames (ORFs), ORF1a and ORF1b, which encode non-structural proteins (nsps). The structural proteins, including the viral spike protein (S), envelope protein (E), membrane protein (M), and nucleocapsid protein (N), are encoded by subgenomic RNA (sgRNA). The genome also encodes several putative accessory proteins (3a, 6, 7a, 7b, 8, and 10). The leader 3' sequence (L) is at the beginning, with a 5' untranslated region (UTR). B. The structure of the SARS-CoV-2 virion reveals an enveloped virus with major surface antigens, such as hemagglutinin-esterase (HE) and the spike (S) protein trimer. The genomic RNA is packaged inside the nucleocapsid (N), surrounded by the envelope. The protein structure of the spike (S) protein monomer exhibits key molecular domains involved in the pathogenesis of the virus. C. The primary cellular host receptor and co-receptor for SAR-CoV-2 are angiotensin-converting enzyme 2 (ACE2) and transmembrane serine protease 2 (TMPRSS2), respectively. The attachment and entry of SAR-CoV-2 into host cells require priming by TMPRSS2, which cleaves the S protein into S1 and S2 portions. This cleavage facilitates the targeting and binding of the S1 portion to the ACE2 receptor. D. Following ACE2 receptor binding, the virion is internalised into the host cell through receptor-mediated endocytosis, enabling viral entry and infection (Figure 1.1 was taken from (10)). 31

Figure 1.2: SARS CoV-2 Life cycle. (1a) SARS-CoV-2 utilises the ACE2 receptor on the cell surface to bind and initiate infection. The S1 subunit of the spike protein facilitates this binding. Once bound, the S2 subunit promotes fusion between the viral and cellular membranes through the formation of a six-helix bundle (6-HB) fusion core comprising heptad repeats 1 (HR1) and heptad repeats 2 (HR2). That brings the viral and cellular membranes into proximity for fusion and subsequent infection. (1b) In cells lacking TMPRSS2, cathepsin B/L may facilitate endosomal entry of the virus. (After fusion, the virus releases its positive-sense single-stranded RNA (ssRNA), which spans approximately 30 kilobases (kb), into the host cytoplasm. (4a) Using the host ribosomal machinery, the 5' end of the ssRNA is translated into a viral polyprotein. (4b) This polyprotein is then auto-proteolytically cleaved by virus-encoded proteinases, forming 16 non-structural proteins that assemble into the replicase-transcriptase complex. This complex includes essential enzymes like the viral RNA-dependent RNA

polymerase and endo- and exonucleases involved in nucleic acid metabolism. (5a) Simultaneously, the 3' end of the viral genome expresses 13 open-reading frames (ORFs) that encode the four major structural proteins: Spike (S), Envelope (E), Membrane (M), and Nucleocapsid (N). These structural proteins are also synthesised using the host ribosomal machinery. (5b) Concomitantly, the ssRNA undergoes replication with viral RNA-dependent RNA polymerase assistance. The S, E, and M viral structural proteins are inserted into the endoplasmic reticulum (ER). (7a) They move to the ER-Golgi intermediate compartment through the secretory pathway. (7b) The viral RNA, encapsulated by the N protein, buds into membranes of the ER-Golgi intermediate compartment. Finally, the N protein encapsulates viral RNA, and the S, E, and M structural proteins assemble to form mature virions. After assembly, the virions are transported in vesicles to the cell surface, fusing with the plasma membrane for exocytosis and releasing many virions (**Figure 1.2** was taken from (10). 34

Figure 1.3: Various soluble and membrane-bound pattern-recognition receptors (PRRs**).** The term "extracellular pattern-recognition receptors" (PRRs) refers to soluble lectins, which include lung surfactants and mannose-binding lectins, ficolins, and pentraxins (such as C-reactive proteins and serum amyloid-P). Extracellular C-type lectin PRRs include dendritic cell-specific intercellular adhesion molecule 3-grabbing non-integrin (DC-SIGN), dectin 1, and the mannose receptor on macrophages. Scavenger receptors, complement receptors, and natural killer (NK) cell receptors are other extracellular receptors. Nuclear factor-κB (NF-κB) is the mechanism by which leucine-rich repeat-rich extracellular Toll-like receptors and intracellular nucleotide-binding oligomerization domain (NOD) receptors activate immune genes. Membrane-associated and soluble lectins mediate interactions with pathogens that result in immunological recognition, attachment, opsonization, host invasion, and immune response. CARD: Caspase recruitment domain, CRP: C-reactive protein, ITAM: Immunoreceptor tyrosine-based activation motif, ITIM: Immunoreceptor tyrosine-based inhibition motif, KIR2DL3: Killer cell immunoglobulin-like receptor 2DL3, LBP: Lipopolysaccharide-binding protein, MBL: Mannan-binding lectin, NBS: Nucleotide-binding site, NKGA: Natural killer glycoprotein C-type lectin receptor, NITR: Novel immune-type receptor, SAP: Serum amyloid protein, TICAM1: TIR domain-containing adapter molecule 1, TIRAP: Toll/interleukin-1 receptor domain-containing adapter protein. (**Figure 1.3** was taken from (31)). 39

Figure 1.4: Illustrates the structure of human Surfactant Protein D (SP-D). The monomeric form of SP-D consists of distinct regions, including a cysteine-rich N-terminal region

responsible for forming disulfide bonds for oligomers, a collagen region containing repeated Gly-X-Y triplets, an α-helical coiled-coil neck region, and a C-type lectin domain known as the carbohydrate recognition domain (CRD). Human SP-D comprises three identical polypeptide chains, each weighing 43 kDa, which form a trimer subunit of 130 kDa. Four trimer subunits further assemble to create a tetrameric structure of SP-D, weighing 520 kDa. The CRDs of SP-D are responsible for binding to various ligands. At the same time, the collagen region plays a role in recruiting immune cells to facilitate the clearance of pathogens, allergens, and apoptotic/necrotic cells (**Figure 1.4** adapted from (38))..... 40

Figure 1.5: Three pathways of the Complement system. The classical pathway of complement activation occurs when the C1 complex binds to immune complexes, forming the C4bC2b enzyme complex (C3 convertase). It can also be initiated by the binding of C1 to apoptotic cells. The lectin pathway is activated by binding mannose-binding lectin (MBL) or MBL-associated serine proteases (MASPs) to mannose groups on bacterial cell surfaces, generating C3 convertase. The alternative pathway is activated by hydrolysed C3 and factor B, forming C3 convertase. All three pathways converge at the C3 convertase stage. C3 convertase generates the C5 convertase enzyme, including the membrane attack complex (MAC). Various factors, including CR1, DAF, C4BP, and MCP, can inhibit the activity of C3 and C5 convertases. Proteins like CD59, clusterin, and vitronectin can block the assembly of the MAC complex. Complement activation leads to bacterial lysis through the MAC complex, recruitment of immune cells, platelet activation, and activation of endothelial and epithelial cells. Furthermore, complement proteins opsonise pathogens, enhancing their phagocytosis. (Figure 1.5 adapted from (57))..... 44

Figure 1.6: Structural Organization of C1q Molecule**.** The C1q molecule (460 kDa) comprises 18 polypeptide chains (6A, 6B, and 6C). (a) Each A, B, and C chain has a short N-terminal region with a half-cystine residue involved in forming interchain disulfide bonds. That is followed by a collagen region (CLR) consisting of approximately 81 residues and a C-terminal globular region (gC1q domain) comprising about 135 residues. (b) The interchain disulfide bonding results in the formation of 6A-B dimer subunits and 3C-C dimer subunits. The A and B chains of an A-B subunit and one of the C chains from a C-C subunit form a structural unit (ABC-CBA) held together by both covalent and non-covalent bonds. (c) Three of these structural units associate through non-covalent solid bonds in the central portion, resembling a fibril-like structure, to form the hexameric C1q molecule with a tulip-like shape, like mannose-binding

protein, surfactant protein A, and ficolins. (d) The crystal structure of the gC1q domain of human C1q (Protein Data Bank code 1PK6) reveals a compact, spherical, heterotrimeric assembly with a diameter of approximately 50 Å. Non-polar interactions primarily hold it together and exhibit non-crystallographic pseudo-threefold symmetry. (e) The three gC1q modules show different electrostatic surface potentials, partly explaining the modularity in ligand recognition (Figure 1.6 adapted from (61))..... 46

Figure 1.7: Schematic Structure of C4BP. C4BP comprises seven identical a-subunits, each containing a binding site for C4b. Each a-chain consists of eight complement control protein modules, SCR modules, along with a C-terminal linking domain. The b-chain, which includes the protein S binding site, comprises three SCR modules and a linking domain (Figure 1.7 adapted from (64)). 47

Figure 1.8: The Schematic Structure of Factor H. Factor H comprises 20 short consensus repeat (SCR) domains. The molecule has two central functional regions at the N- and C-termini. SCRs 1-4 mediate the complement regulatory activities of factor H (Figure 1.8 adapted from (67)). 48

Figure 1.9: Schematic Structure of Properdin**.** The structure of properdin consists of seven thrombospondin repeat (TSR) domains labelled TSR0-6. Under normal physiological conditions, properdin monomers assemble into cyclic dimers, trimers, and tetramers, with a ratio of approximately 1:2:1. Molecular modelling suggests that the vertices of properdin oligomers are formed by a combination of four domains derived from two different monomers, arranged in a head-to-tail organisation. While the organisation of domains at the vertices is still not fully understood, theoretical models propose that the TSR0-1 domains from one monomer are involved in vertex formation along with TSR5-6 domains from the other monomer (Figure 1.9 adapted from (70)). 50

Figure 3.1: ELISA shows SARS-CoV-2 S protein binds DC-SIGN(A) and rfhSP-D (B), where rfhSP-D increases S protein and DC-SIGN binding (C). SARS-CoV-2 Spike protein (2 µg /well) was incubated with microtiter wells coated with DC-SIGN or rfhSP-D proteins at varying doses (2, 1, 0.5, or 0 µg/ well). The binding of DC-SIGN and rfhSP-D to Spike protein was shown to be dose-dependent. A competitive ELISA (C) was performed to investigate the impact of rfhSP-D on DC-SIGN and Spike protein interaction. The addition of rfhSP-D enhanced the binding of Spike protein to DC-SIGN. The increased detectable amount of Spike protein with increasing concentrations of rfhSP-D suggests the presence of distinct binding sites for Spike protein on

both C-type lectins. MBP was used as a negative control. The data were expressed as the mean of triplicates ± SD. Statistical significance was determined using the unpaired t-test (compared mean of rfhSP-D or DC-SIGN binding with S-protein to MBP) (**p < 0.01, and ***p < 0.001) (n = 3). 80

Figure 3.2: SARS-CoV-2 Spike Pseudotypes bind to DC-SIGN expressing using fluorescence microscopy. DC-HEK cells were incubated with SARS-CoV-2 Spike Pseudotypes at 37°C for 30 minutes. After incubation, the cells were fixed using 4% paraformaldehyde, washed, and blocked with 5% FCS. The cells were probed with rabbit anti-SARS-CoV-2 Spike antibody and mouse anti-DC-SIGN antibody to detect Spike-Pseudotypes and DC-SIGN expression in the cells. Alexa Fluor 647 conjugated goat anti-mouse antibody (Abcam) and Alexa Fluor 488 conjugated goat anti-rabbit antibody (Abcam) were used to detect the primary antibodies. The nucleus was stained using Hoechst dye (Invitrogen, Life Technologies). 81

Figure 3.3: rfhSP-D promotes the binding of SARS-CoV-2 Spike pseudotypes in DC-HEK (A) and DC-THP-1 cells (B). rfhSP-D enhances the interaction between SARS-CoV-2 Spike Pseudotypes and DC-SIGN expressing cells. DC-HEK cells (Panel A) and DC-THP-1 cells (Panel B) were treated with rfhSP-D and SARS-CoV-2 Spike Pseudotypes. The binding of cells to the pseudotypes was assessed using fluorescent probes, Alexa Fluor 488 (FTIC) and Alexa Fluor 647 (APC), and the fluorescence intensity was measured using a GloMax 96 Microplate Luminometer (Promega). Increased fluorescence intensity was observed in DC-HEK and DC-THP-1 cells treated with 20 µg/ml of rfhSP-D compared to cells challenged with Spike pseudotypes alone. The experiments were conducted in triplicates, and the error bars represent ± SEM. Statistical significance was calculated using an unpaired t-test (compared mean of treated to untreated cells) (***p < 0.001) (n = 3). The x-axis represents the treatment conditions (0 for untreated and 20 for treated samples). 82

Figure 3.4: rfhSP-D enhances the transduction of SARS-CoV-2 Spike pseudotypes in DC-HEK (A) and DC-THP-1 cells (B). Purified Spike pseudotypes were used to transduce DC-HEK cells (Panel A) and DC-THP-1 cells (Panel B), and the luciferase reporter activity was measured. Significantly higher levels of luciferase reporter activity were observed in DC-HEK and DC-THP-1 cells treated with 20 µg/ml of rfhSP-D compared to cells challenged with Spike pseudotypes alone. The experiments were conducted in triplicates, and the error bars represent ± SEM. Statistical significance was calculated using an unpaired t-test(compared mean of treated to untreated cells) (***p < 0.001) (n = 3). 83

Figure 3.5: rfhSP-D reduces the expression of pro-inflammatory cytokines and chemokines in DC-HEK cells. DC-HEK cells were challenged with SARS-CoV-2 Spike protein incubated with 20 μg/ml of rfhSP-D. After 6 hours, the cells were harvested for analysis of cytokine expression. RNA was purified and converted into cDNA, and the gene expression levels of NF-κB (Panel A), IFN-α (Panel B), TNF-α (Panel C), and RANTES (Panel D) were assessed using RT-qPCR. The expression levels were normalised to the endogenous control 18S rRNA, and the relative expression (RQ) was calculated using cells challenged with Spike protein without rfhSP-D as the calibrator. The assays were performed in triplicates, and the error bars represent ± SEM. Statistical significance was determined using the two-way ANOVA test (***p < 0.0001) (n = 3). 84

Figure 3.6: rfhSP-D modulates the immune response in DC-THP-1 cells. DC-THP-1 cells were challenged with SARS-CoV-2 Spike protein incubated with 20 μg/ml of rfhSP-D. The cells were harvested at 6 hours, 12 hours, 24 hours, and 48 hours to analyse the expression of cytokines and MHC class II. RNA was purified from the lysed cells and converted into cDNA. The expression levels of NF-κB (Panel A), TNF-α (Panel B), IL-1β (Panel C), IL-6 (Panel D), IL-8 (Panel E), and MHC class II (Panel F) were measured using RT-qPCR, and the data were normalised against the expression of 18S rRNA as a control. The experiments were conducted in triplicates, and the error bars represent ± SEM. The relative expression (RQ) was calculated using cells challenged with Spike protein without rfhSP-D as the calibrator. The RQ value was calculated using the formula RQ = 2−ΔΔCt. Statistical significance was determined using the two-way ANOVA test (***p < 0.0001, and ns = no significance) (n = 3). 86

Figure 3.7: DC-SIGN interacts with both SP-D and SARS-CoV-2 Spike. The docked poses of complex A (A) and complex B (B) were selected for docking and molecular dynamics (MD) simulations, respectively. The spike protein interacts with DC-SIGN (CRD) in complex B through the N-terminal domain (NTD, shown in orange). 88

Figure 3.8: DC-SIGN, SP-D and SARS-CoV-2 spike interaction. A tripartite complex of SP-D, DC-SIGN, and SARS-CoV-2 Spike was formed, and the docked poses of the tripartite complexes were selected for analysis using molecular dynamics (MD) simulations. In complex C1, DC-SIGN (CRD) interacts with the N-terminal domain (NTD) of Spike (A). In complex C2, DC-SIGN (CRD) interacts with the NTD of Spike, while SP-D interacts with the receptor binding domain (RBD) of Spike (B). 88

Figure 3.9: SP-D stabilises SARS-CoV-2 Spike interaction with DC-SIGN. SP-D plays a stabilising role in the interaction between SARS-CoV-2 Spike and DC-SIGN. Comparative analysis of MD simulations was conducted for complexes B, C1, and C2, considering (A) root mean square deviation (RMSD) and (B) potential energy (PE). The RMSD and PE profiles of complexes C1 and C2 were lower than those of complex B, indicating greater tripartite complex C1 and C2 stability. 89

Figure 3.10: SP-D stabilises the interaction between SARS-CoV-2 Spike and DC-SIGN. Comparative analysis of MD simulations was performed for complexes B, C1, and C2, considering the average distance (A–C) and H-bonds (D–F) between DC-SIGN and Spike. In contrast to complex B, the intermolecular distance between DC-SIGN and Spike remained relatively constant throughout the simulation period in tripartite complexes C1 and C2. Additionally, the number of intermolecular H-bonds between DC-SIGN and Spike was higher in complexes C1 and C2 compared to complex B. These findings suggest that SP-D stabilises Spike and DC-SIGN (CRD) interaction. 90

Figure 4.1: ELISA shows that the SARS-CoV-2 S protein binds C1q (A, B) and C4BP (C, D). SARS-CoV-2 virus exhibits direct interactions with both C1q and C4BP proteins. To investigate this interaction, a 96-well plate was coated with varying concentrations of immobilised C1q (1, 0.5, 0.125, and 0 µg per well) (A, C) or constant concentrations of viral proteins (spike or RBD 1 µg per well) (B, D) using a carbonate–bicarbonate (CBC) buffer at pH 9.6, and then incubated at 4 °C overnight. Subsequently, a constant concentration of viral proteins (1 µg per well) (A) or decreasing amounts of C1q/C4BP (1, 0.5, 0.125, and 0 1 µg per well) (B) was added to the corresponding wells and incubated at 37 °C for 2 hours. After the incubation, the wells were washed, and primary antibodies (rabbit anti-SARS-CoV-2 spike or rabbit anti-human C1q/C4BP) were added (1:5000 dilution, 100 µL/well). MBP was used as a negative control. The data were expressed as the mean of triplicates ± SD. Statistical significance was determined using the two-way ANOVA (* $p < 0.05$, ** $p < 0.01$, and *** $p < 0.001$) (n = 3). 101

Figure 4.2: C1q (A) and C4BP (B) inhibit the transduction of SARS-CoV-2 Spike pseudotypes in A549-hACE2+TMPRSS2 cells**.** C1q (A) and C4BP (B) were found to inhibit the entry of SARS-CoV-2 pseudoparticles into A549-hACE2+TMPRSS2 cells. To assess the impact of complement protein treatment on the ability of lentiviral pseudoparticles to enter the cells, luciferase reporter activity was measured in A549-hACE2+TMPRSS2 cells transduced with either treated

or untreated SARS-CoV-2 lentiviral pseudoparticles that were pre-treated with C1q or C4BP (20µg/ml). Background values were subtracted from all data points, and the obtained data were normalised with 0% luciferase activity representing the mean relative luminescence units recorded from the control sample (A549-hACE2+TMPRSS2 cells + SARS-CoV-2 lentiviral pseudoparticles). The pseudoparticles pre-treated with C1q and C4BP demonstrated a substantial reduction in viral transduction. The data are presented as the normalised mean of three independent experiments, each carried out in triplicates, with the error bars representing the standard error of the mean (SEM). Statistical significance was determined using the two-way ANOVA test (*** $p < 0.001$) (n = 3)..... 103

Figure 4.3: C1q globular head modules inhibit the transduction of SARS-CoV-2 Spike pseudotypes in A549-hACE2+TMPRSS2 cells. Recombinant ghA, ghB, and ghC modules of human C1q were found to inhibit SARS-CoV-2 pseudoparticle entry into A549-hACE2+TMPRSS2 cells. To assess the interference of these recombinant C1q modules with pseudoparticle entry, SARS-CoV-2 pseudoparticles were pre-treated with ghA (A), ghB (B), or ghC (C) at a concentration of 20µg/ml. Luciferase reporter activity was measured in A549-hACE2+TMPRSS2 cells transduced with pseudoparticles pre-treated with ghA, ghB, or ghC. The background was subtracted from all data points. The obtained data were normalised, with 0% luciferase activity defined as the mean of the relative luminescence units recorded from the control sample (A549-hACE2+TMPRSS2 cells + MBP + SARS-CoV-2 pseudoparticles). The results are presented as the normalised mean of three independent experiments conducted in triplicates, with error bars expressed as ± SEM. Statistical significance was determined using the two-way ANOVA test (*** $p < 0.001$) (n = 3)..... 104

Figure 4.4: C1q (A) and C4BP (B) reduce the binding of SARS-CoV-2 Spike pseudotypes in A549-hACE2+TMPRSS2 cells. The binding of C1q (A) or C4BP (B) treated SARS-CoV-2 pseudoparticles to A549-hACE2+TMPRSS2 cells was examined. SARS-CoV-2 lentiviral pseudoparticles were used to transduce A549-hACE2+TMPRSS2 cells pre-incubated with C1q or C4BP (20µg/ml). After washing and fixation with 1% v/v paraformaldehyde for 1 minute, the wells were probed with rabbit anti-SARS-CoV-2 spike (1:200) polyclonal antibodies. The obtained data were normalised with 0% fluorescence representing the mean of the relative fluorescence units recorded from the control sample (A549-hACE2+TMPRSS2 cells + SARS-CoV-2 lentiviral pseudoparticles). Three independent experiments were conducted in triplicates, and the error

bars are presented as ± SEM. Statistical significance was determined using the two-way ANOVA test (*** p < 0.001) (n = 3)..... 105
Figure 4.5: C1q globular head modules block the binding of SARS-CoV-2 Spike pseudotypes in A549-hACE2+TMPRSS2 cells. The ability of recombinant ghA (A), ghB (B), or ghC (C) to interfere with the binding of SARS-CoV-2 lentiviral pseudoparticles to A549-hACE2+TMPRSS2 cells was investigated. A549-hACE2+TMPRSS2 cells were transduced with SARS-CoV-2 pseudoparticles following pre-incubation with or without ghA, ghB, or ghC at a 20μg/ml concentration. After removing unbound protein and viral particles, the wells were fixed with 1% v/v paraformaldehyde for 1 min and probed with rabbit anti-SARS-CoV-2 spike (1:200) polyclonal antibodies. The obtained data were normalised, with 0% fluorescence as the mean of the relative fluorescence units recorded from the control sample (cells + MBP + pseudoparticles). Three independent experiments were carried out in triplicates, and error bars represent ± SEM. Statistical significance was determined using the two-way ANOVA test (*** p < 0.001) (n = 3). 106
Figure 4.6: C1q and C4BP inhibit NF-κB. C1q and C4BP exhibit inhibitory effects on NF-κB activation in A549-hACE2-TMPRSS2 cells challenged with SARS-CoV-2 spike protein. A549-hACE2+TMPRSS2 cells were transfected with pNF-κB-LUC and subsequently exposed to SARS-CoV-2 spike protein (500ng/mL) that was pre-treated with C1q (A) or C4BP (B) at a concentration of 20 μg/mL. After 24 hours of incubation, luciferase reporter activity was measured. The background was subtracted from all data points, and the obtained data were normalised, with 0% luciferase activity defined as the mean of the relative luminescence units recorded from the control sample (A549-hACE2+TMPRSS2 cells + SARS-CoV-2 spike protein). The data are presented as the normalised mean of three independent experiments carried out in triplicates ± SEM. Statistical significance was determined using the two-way ANOVA test (*** p < 0.001) (n = 3). 108
Figure 4.7: C1q reduces the expression of proinflammatory cytokines and chemokines in A549-hACE2+TMPRSS2 cells. C1q reduces the inflammatory response in A549-hACE2+TMPRSS2 cells challenged with SARS-CoV-2 alphaviral pseudoparticles. The pseudoparticles were pre-incubated with a 20μg/ml of C1q before being used to challenge the cells. At 6 hours and 12 hours post-challenge, the cells were harvested to measure the mRNA levels of proinflammatory cytokines and chemokines. The cells were lysed, and purified RNA was converted into cDNA. RT-qPCR was then used to measure the mRNA levels of NF-κB

(A), IL-6 (B), IFN-α (C), IL-1β (D), TNF-α (E), RANTES (F), and IL-8 (G). The data were normalised against 18S rRNA expression as a control, and the relative expression (RQ) was calculated using A549-hACE2+TMPRSS2 cells challenged with SARS-CoV-2 alphaviral pseudoparticles alone as the calibrator. The RQ value was determined using the RQ = $2^{\wedge(-\Delta\Delta Ct)}$. The experiments were carried out in triplicates, and error bars represent ± SEM. Statistical significance was determined using the two-way ANOVA test (* $p < 0.05$, *** $p < 0.001$, ns $p > 0.05$) (n = 3).109

Figure 4.8: C4BP attenuate the expression of proinflammatory cytokines and chemokines in A549-hACE2+TMPRSS2 cells. C4BP attenuates the inflammatory response in A549-hACE2+TMPRSS2 cells challenged with SARS-CoV-2 alphaviral pseudoparticles. The gene expression profile of cytokines and chemokines in these cells was examined after being challenged with SARS-CoV-2 alphaviral pseudoparticles pre-treated with and without C4BP 20µg/mlL). The expression levels of NF-κB (A), IL-6 (B), IFN-α (C), IL-1β (D), TNF-α (E), RANTES (F), and IL-8 (G) were measured using RT-qPCR at 6 hours and 12 hours post-challenge. A549-hACE2+TMPRSS2 cells challenged with SARS-CoV-2 alphaviral pseudoparticles alone were used as a calibrator to calculate the relative quantitation (RQ), which was determined using the formula RQ = 2^(-ΔΔCt). The experiments were conducted in triplicates, and error bars represent ± SEM. Additionally, 18S rRNA was used as an endogenous control. Statistical significance was established using the two-way ANOVA test (** $p < 0.01$, *** $p < 0.001$, ns $p > 0.05$) (n = 3). 110

Figure 5.1: SARS-CoV-2 Spike protein directly interacts with FH and FP via its RBD**.** In a dose-dependent manner, FH was found to bind both SARS-CoV-2 Spike and RBD proteins. Decreasing concentrations of FH or FP (1, 0.5, 1.25, and 0 µg/well) were immobilised on a 96-well plate using Carbonate-Bicarbonate (CBC) buffer, pH 9.6, and left overnight at 4°C. After washing off the excess CBC buffer with PBS, a constant concentration of viral proteins (1 µg/well) was added to the corresponding wells and incubated at 37°C for 2 hours. Unbound proteins were then washed off, and the wells were probed with corresponding primary antibodies (1:5000; 100 µl/well), namely rabbit anti-SARS-CoV-2 Spike or rabbit anti-human FH or FP polyclonal antibodies. MBP was used as a negative control. The data were expressed as the mean of triplicates ± SD. Statistical significance was determined using the two-way ANOVA (* $p < 0.05$, ** $p < 0.01$, and *** $p < 0.001$) (n = 3). 121

Figure 5.2: Modulation of SARS-CoV-2 pseudotype viral entry in A549-hACE2+TMPRSS2 cells by FH, FP or TSR4+5 treatment. FH, FP, or TSR4+5 at a concentration of 20µg/ml were utilised

to pre-treat SARS-CoV-2 lentiviral pseudoparticles in three separate experiments (A), (B), and (C), respectively. The objective was to assess if the treatment influenced the virus's ability to enter the cells. Both treated and untreated lentiviral pseudoparticles were then transduced into A549-hACE2+TMPRSS2 cells, and luciferase reporter activity was examined to measure viral transduction. The background signal was subtracted from all data points, and the obtained data were normalised using the mean of the relative luminescence units recorded from the control sample (Cells + lentiviral pseudoparticles), defined as 0% luciferase activity. The results were presented as the normalised mean of three independent experiments conducted in triplicates, with error bars expressing ±SEM. Significance was determined using the two-way ANOVA test (***p < 0.001) (n= 3)..... 123

Figure 5.3: Modulation of SARS-CoV-2 pseudoparticle binding to A549-hACE2+TMPRSS2 cells by FH, FP or TSR4+5**.** Cell binding assay demonstrated distinct effects of FH, FP, and TSR4+5 on SARS-CoV-2 binding to cell-surface receptors, as illustrated in Figures (A), (B), and (C), respectively. For this assay, A549-hACE2+TMPRSS2 cells at a concentration of 2×10^4 cells/ml were exposed to SARS-CoV-2 lentiviral pseudoparticles that were pre-incubated with or without FH, FP, or TSR4+5 at a concentration of 20 µg/ml. The cells and viral particles were incubated at 37°C for 2 h. Following the incubation, unbound protein and viral particles were removed, and the wells were fixed using 1% v/v paraformaldehyde for 1 minute. Subsequently, the wells were probed with a polyclonal rabbit anti-SARS-CoV-2 spike antibody at a dilution of 1:200. The obtained data were normalised using 0% fluorescence as the mean of the relative fluorescence units recorded from the control sample (Cells + lentiviral pseudoparticles). The experiments were independently conducted three times in triplicates, and the error bars are expressed as ± SEM. Significance was determined using the two-way ANOVA test (***p < 0.001) (n = 3)..... 124

Figure 5.4: Reversal of FP mediated-SARS-CoV-2 viral entry in and binding to A549-hACE2+TMPRSS2 cells by anti-FP antibody. Lentiviral pseudoparticles, treated with FP (with or without anti-FP antibodies) or untreated, were added to A549-hACE2+TMPRSS2 cells, and luciferase reporter activity or cell binding was evaluated. All data points had the background subtracted. The data were normalised, with 0% luciferase activity defined as the mean of the relative luminescence units recorded from the control sample (Cells + lentiviral pseudoparticles). The data are presented as the normalised mean of three independent experiments performed in triplicates ±SEM. The significance of FP-treated cells (with and

without anti-FP antibodies) compared to the control (cells+ viral pseudoparticles) was determined using the two-way ANOVA test (***p < 0.001). Additionally, the significance of FP-treated cells (with anti-FP antibodies) to cells treated only with FP (cells+ viral pseudoparticles + FP) was also determined (p < 0.001) (n = 3). 125

Figure 5.5: FP increases while FH reduces NF-κB activation in SARS-CoV-2-Spike protein-challenged A549-hACE2-TMPRSS2 cells. SARS-CoV-2 Spike protein pre-treatment with FP (Panel A) or FH (Panel B) led to significant alterations in NF-κB activation. To investigate the immunological impact of FP and FH on NF-κB activation, A549-hACE2+TMPRSS2 cells were transfected with pNF-κB-LUC and then exposed to SARS-CoV-2 Spike protein (500 ng/ml) following pre-treatment with FP or FH (20 µg/ml). After 24 h of incubation, luciferase reporter activity was examined, and the background was subtracted from all data points. The obtained data were normalised, with 0% luciferase activity defined as the mean of the relative luminescence units recorded from the control sample (A549-hACE2+TMPRSS2 cells + SARS-CoV-2 Spike protein). The results are the normalised mean of three independent experiments conducted in triplicates ± SEM. Statistical significance was determined using the two-way ANOVA test (***p < 0.001) (n = 3)..... 128

Figure 5.6: SARS-CoV-2 FH attenuates associated inflammation in A549-hACE2+TMPRSS2 cells. A549-hACE2+TMPRSS2 cells were challenged with SARS-CoV-2 alphaviral pseudoparticles, with and without pre-treatment of FH (20 µg/ml). The mRNA levels of various cytokines and chemokines, including NF-κB (Panel A), IL-6 (Panel B), IFN-α (Panel C), IL-1β (Panel D), TNF-α (Panel E), RANTES (Panel F), and IL-8 (Panel G), were assessed using RT-qPCR. Each target gene's relative expression (RQ) was calculated using untreated cells (A549-hACE2+TMPRSS2 cells + SARS-CoV-2 alphaviral pseudoparticles) as the calibrator. The RQ value was determined using $RQ = 2^{-\Delta\Delta Ct}$. The experiments were performed in triplicates, and the error bars represent ± SEM (n = 3). Statistical significance was assessed using the two-way ANOVA test (****p < 0.0001, and ns= no significance). 129

Figure 5.7: FP promotes SARS-CoV-2-associated inflammation in A549-hACE2+TMPRSS2 cells**.** FP (20 µg/ml). pre-treated SARS-CoV-2 alphaviral pseudoparticles were assessed on the proinflammatory response in A549-hACE2+TMPRSS2 cells at 6h and 12h post-infection. We measured the mRNA expression levels of targeted cytokines and chemokines, including NF-κB (Panel A), IL-6 (Panel B), IFN-α (Panel C), IL-1β (Panel D), TNF-α, RANTES (Panel F), and IL-8 (Panel G), using RT-qPCR. We used 18S rRNA expression as an endogenous control to ensure

accurate normalisation. The relative expression (RQ) was calculated by comparing the data with untreated cells (A549-hACE2+TMPRSS2 cells + SARS-CoV-2 alphaviral pseudoparticles) as the calibrator, and the RQ value was determined using RQ = $2^{-\Delta\Delta Ct}$. All assays were performed in triplicates, and the error bars represent ± SEM. Statistical significance was assessed using the two-way ANOVA test (*p < 0.05, ****p < 0.0001, and ns= no significance) (n = 3)..... 130

Figure 5.8: SARS-CoV-2 infection of A549-hACE2+TMPRSS2 cells induced a greater proinflammatory response in the presence of TSR4+5. In A549-hACE2+TMPRSS2 cells challenged with SARS-CoV-2 alphaviral pseudoparticles pre-treated with TSR4+5 (20 µg/ml) or MBP (20 µg/ml). proinflammatory responses were observed at 6 h and 12 h post-infection. The levels of gene expression for cytokines and chemokines were measured using qRT-PCR, specifically for NF-kB (A), IL-6 (B), IFN-α (C), IL-1β (D), TNF-α (E), RANTES (F), and IL-8 (G). The data were normalised against 18S rRNA expression as a control. Experiments were conducted in triplicates, and error bars represent ±SEM. The relative expression (RQ) was calculated using A549-hACE2+TMPRSS2 cells exposed to SARS-CoV-2 alphaviral pseudoparticles without TSR4+5 as the calibrator. RQ = $2^{-\Delta\Delta Ct}$ was used to calculate the RQ value. The significance of the results was determined using the two-way ANOVA test (*p < 0.05, ****p < 0.0001, and ns= no significance) (n = 3). 131

Figure 5.9: Cartoon representation of FP interaction with spike and ACE2. (A) Interaction of FP with spike RBD and NTD through TSR4 and TSR5 domains. (B) & (C) A tripartite complex representation of FP, spike and ACE2. 133

Figure 5.10: Immune modulator function of FP and FH in SARS-CoV-2 Infection Independent of Complement Activation. The SARS-CoV-2 virus enters host cells by binding to the ACE2 receptor via its spike protein. Upon fusion with the cell membrane, viral RNA is released into the host cytoplasm, initiating viral replication, protein synthesis, and subsequent release of new virions into the extracellular environment, contributing to the spread of SARS-CoV-2 infection. This study investigated the effects of FP and FH separately to understand their roles in SARS-CoV-2 infection without activating the complement cascade. FP enhanced the binding affinity between the SARS-CoV-2 spike protein and ACE2, increasing viral entry into host cells and subsequent infection. This higher viral load triggered the upregulation of proinflammatory cytokines, contributing to the inflammatory response. On the other hand, FH was observed to reduce the binding and entry of SARS-CoV-2 into host cells. Consequently, the decreased viral entry mediated by FH reduced the production of proinflammatory cytokines, potentially

mitigating the immune response. These findings provide valuable insights into FH's immunomodulatory role and FP's immunopathological role in COVID-19. Furthermore, they offer important clues regarding the potential association between elevated levels of properdin and insufficient levels of FH, as observed in severe COVID-19 patients. 134

List of Tables

Table 2.1: Volumes of Resolving and Stacking Components for 12% SDS-PAGE Gel 64

Table 2.2: Target genes, forward primers, and reverse primers used for qPCR analysis 72

Papers Published

1. Beirag N, Varghese PM, Neto MM, Al Aiyan A, Khan HA, Qablan M, et al. Complement Activation-Independent Attenuation of SARS-CoV-2 Infection by C1q and C4b-Binding Protein. Viruses. 2023;15(6):1269. **(IF 4.7; 2023)**

2. Beirag N, Kumar C, Madan T, Shamji MH, Bulla R, Mitchell D, et al. Human surfactant protein D facilitates SARS-CoV-2 pseudotype binding and entry in DC-SIGN expressing cells and downregulates spike protein-induced inflammation. Frontiers in immunology. 2022; 13:960733. **(IF 7.3; 2022)**

3. Hsieh M-H, Beirag N, Murugaiah V, Chou Y-C, Kuo W-S, Kao H-F, et al. Human surfactant protein D binds spike protein and acts as an entry inhibitor of SARS-CoV-2 pseudotyped viral particles. Frontiers in Immunology. 2021; 12:641360. **(IF 7.3; 2021)**

4. Varghese PM, Mukherjee S, Al-Mohanna FA, Saleh SM, Almajhdi FN, Beirag N, et al. Human properdin released by infiltrating neutrophils can modulate Influenza A virus infection. Frontiers in Immunology. 2021; 12:747654. **(IF 7.3; 2021)**

5. Varghese PM, Murugaiah V, Beirag N, Temperton N, Khan HA, Alrokayan SH, et al. C4b binding protein acts as an innate immune effector against influenza a virus. Frontiers in Immunology. 2021; 11:585361. **(IF 7.3; 2021)**

6. Murugaiah V, Varghese PM, Beirag N, DeCordova S, Sim RB, Kishore U. Complement proteins as soluble pattern recognition receptors for pathogenic viruses. Viruses. 2021;13(5):824. **(IF 4.7; 2021)**

7. Singh I, Beirag N, Kishore U, Shamji MH. Surfactant Protein D: A Therapeutic Target for Allergic Airway Diseases. The Collectin Protein Family and Its Multiple Biological Activities. 2021:135-45

In progress

1. Beirag N, Varghese PM, Kumar C, Idicula-Thomas S, Mayora Neto M, Khan HA, et al. Human complement Factor H and Properdin act as soluble pattern recognition receptors and differentially modulate SARS-CoV-2 Infection. bioRxiv. 2023:2023.07. 07.548083.

Abstract

Severe SARS-CoV-2 infection is characterised by an unbalanced immune response, excessive inflammation, and respiratory distress syndrome, often leading to multiorgan failure and death. This study examines the roles number of innate immune membrane-bound and soluble proteins in SARS-CoV-2 infection, including lung surfactant protein D (SP-D), dendritic cell-specific intercellular adhesion molecule-3 grabbing non-integrin (DC-SIGN), complement component 1 q (C1q), C4b-binding protein (C4BP), factor H (FH), and properdin (Factor P/FP). We hypothesised that SP-D, C1q, C4BP, FH, and FP can play protective roles in the immune surveillance against SARS-CoV-2 infection, where hyperinflammation contributes to the disease severity. SP-D and DC-SIGN are C-type lectin receptors involved in pathogen recognition. SP-D clears pulmonary pathogens, while DC-SIGN involves plays role in many viral infections. Both interact with SARS-CoV-2. The study investigates the possible role of recombinant fragment human SP-D (rfhSP-D) in the interaction between DS-SIGN and SARS-CoV-2. We found that rfhSP-D binds to the SARS-CoV-2 Spike protein, enhancing viral binding and uptake in DC-SIGN -expressing cells. Additionally, rfhSP-D reduces pro-inflammatory cytokines in macrophage-like cells. The roles of C1q and C4BP in SARS-CoV-2 infection were also explored. Both proteins directly bind to the SARS-CoV-2 Spike protein, reducing viral attachment and entry into A549 cells expressing human ACE2 and TMPRSS2. Treatment with C1q and C4BP led to the downregulation of pro-inflammatory cytokines, suggesting their potential in mitigating the inflammatory response. Furthermore, the study assessed the impact of FH and FP on SARS-CoV-2 infection. FH inhibited viral binding and cell entry, attenuating the infection-associated inflammatory response. Conversely, FP promoted viral cell entry, binding, and immune response, potentially influencing infection severity. In conclusion, the study highlights the intricate interplay of innate immune proteins in SARS-CoV-2 infection. The findings suggest differential modulatory effects of rfhSP-D, C1q, C4BP, FH, and FP in SARS-CoV-2 infections and offer promising therapeutic interventions targeting these factors. Further *in vivo* research is required to understand the underlying mechanisms and explore their potential clinical applications.

Keywords: SARS-CoV-2, C-type Lectin, Complement System, Soluble PRRs, Innate Immunity, Virus-Host pathogenesis.

Chapter 1

Introduction

The COVID-19 pandemic, caused by severe acute respiratory syndrome corona virus 2 (SARS-CoV-2), posed unprecedented global health challenges (1). Healthcare professionals worldwide have grappled with understanding the transmission dynamics of SARS-CoV-2, its immunopathogenesis, and the urgent need for effective therapeutic interventions. A critical aspect in determining the disease severity and clinical outcomes of COVID-19 patients is the interplay between SARS-CoV-2 and the host's immune responses (1). In-depth knowledge of the pathology of SARS-CoV-2 and the innate humoral and cellular immune responses mounted by the host can provide valuable insights into the disease mechanisms and guide the development of novel preventive and therapeutic strategies (2). Therefore, comprehensive research on the functions of host immune responses to SARS-CoV-2 is essential for enhancing our understanding of the disease and improving patient outcomes.

1.1 COVID-19 Pandemic

The COVID-19 pandemic has profoundly impacted the world, making it one of human history's largest and most significant pandemics (2). This unprecedented crisis originated in Wuhan, China, in December 2019 and was caused by the severe acute respiratory syndrome coronavirus 2 (SARS-CoV-2). The global mortality rate from COVID-19 has surpassed 20 million, highlighting the seriousness of the disease (3). Patients infected with SARS-CoV-2 experience a range of respiratory symptoms, including fever, fatigue, dry cough, and sore throat. In severe cases, acute respiratory distress syndrome (ARDS) may occur in Certain populations, such as older individuals (2). Also, those with comorbidities like obesity, diabetes, and cardiovascular disease are at a higher risk of infection and developing severe symptoms (2). Pregnant women and immune-compromised individuals face an increased likelihood of experiencing severe disease due to physiological changes in immunity and potential complications (2).

While pandemics like COVID-19 are not entirely new phenomena, as we have witnessed outbreaks of other coronaviruses in the twenty-first century, including the Severe Acute Respiratory Syndrome Coronavirus (SARS-CoV) in 2002 and the Middle East Respiratory Syndrome Coronavirus (MERS-CoV) in 2012, these previous coronavirus outbreaks resulted in widespread severe respiratory infectious diseases, causing thousands of deaths and numerous complications even after recovery (4). However, SARS-CoV-2 has a significantly higher transmission rate than its predecessors (4). The emergence of COVID-19 in late 2019 is the latest example of an unexpected, novel, and devastating pandemic disease (4). This

experience has ushered us into a new era of pandemics, requiring in-depth investigations into the multifaceted and complex causes behind this dangerous situation (4).

1.2 The origin and evolution of SARS-CoV-2

Bioinformatic analyses have revealed that SARS-CoV-2 exhibits typical characteristics of the coronavirus family and is classified within the beta-coronavirus 2B lineage (2). During the early stages of the pneumonia outbreak in Wuhan, the complete genome sequences of SARS-CoV-2 were obtained from infected patients (2). These genome sequences share 79.5% sequence identity with SARS-CoV, indicating that SARS-CoV-2 is distinct from its predecessor (2). It is recognised as a novel beta-coronavirus capable of infecting humans (2).

To gain further insights, scientists conducted a comprehensive alignment of the full-length genome sequence of SARS-CoV-2 with other available beta-coronavirus genomes (5). The results revealed the closest genetic relationship between SARS-CoV-2 and a bat SARS-like coronavirus strain called BatCov RaTG13, sharing a high sequence identity of 96% (5). That finding suggests that SARS-CoV-2 may have originated from bats, with the possibility of natural evolution from the bat coronavirus RaTG13 (5). That provides compelling evidence supporting the bat origin hypothesis for SARS-CoV-2, highlighting the close genetic relatedness between SARS-CoV-2 and bat coronaviruses (5). The identification of RaTG13 as the closest known relative emphasises the importance of studying bat coronaviruses to understand the origins and evolution of SARS-CoV-2 (5).

1.3 Structure and genomic of SARS-CoV-2

Enveloped coronaviruses (CoVs) are a diverse group of positive-sense RNA viruses (6). Those are found in various animal species (6). These viruses possess a genome size of approximately 30 kilobases and display pleomorphic forms ranging in diameter from 40 nm to 200 nm (6). They are classified into four major categories (α, β, γ, and δ) based on their genomic structure, with α and β CoVs primarily infecting mammals. SARS-CoV, MERS-CoV , and SARS-CoV-2 belong to the β coronaviruses (6). Genomic analyses suggest that SARS-CoV-2 may have evolved from a bat-originated strain (6). Coronaviruses that infect birds and mammals, including humans, can cause severe infections and even mortality. These viruses possess four structural proteins: E (envelope), M (membrane), N (nucleocapsid), and S (spike) glycoprotein (Figure 1.1) (6).

The spike protein, located on the outer surface of the virion, serves as a recognition factor by binding to membrane receptors on host cells, facilitating fusion with the cellular membrane (7). To understand the invasion of SARS-CoV-2, researchers have modelled and validated the spike protein using available structures from the Protein Data Bank (7). Molecular docking studies have been conducted to investigate its affinity for different receptors and understand its binding to the host cell membrane (7). The trimeric spike protein is a class I transmembrane glycoprotein responsible for viral entry (7). It mediates receptor recognition, cell attachment, and fusion during viral infection (7). Upon interaction with the host cell, extensive structural rearrangement of the spike protein occurs, enabling fusion with the host cell membrane (8). The spike protein is heavily glycosylated to evade the host immune system during entry (8). It consists of two subunits, S1 and S2 (8). The S1 subunit, comprising the N-terminal domain (NTD) and the receptor-binding domain (RBD), is involved in interacting with external proteins (8). The RBD and the host cell receptor ACE2 interaction is crucial for viral entry (8). The S2 subunit in the central region of the spike protein contributes to virus-cell membrane fusion (8).

The N protein of SARS-CoV-2 binds to and packages the viral RNA genome into a ribonucleoprotein complex (RNP) (6). The modular structure and dynamic nature of the nucleocapsid protein contribute to efficient transcription and replication of the viral genome (9). The M and E proteins also play significant roles in SARS-CoV-2 infection (9). The M protein, with its transmembrane structural domains and conserved structural domain, stabilises the nucleocapsid protein during virion assembly (9). Despite its small size, E protein contributes to budding, assembly, and envelope formation (9). These proteins and other viral components work in a coordinated manner, turning SARS-CoV-2 into a complex and sophisticated infectious agent (9).

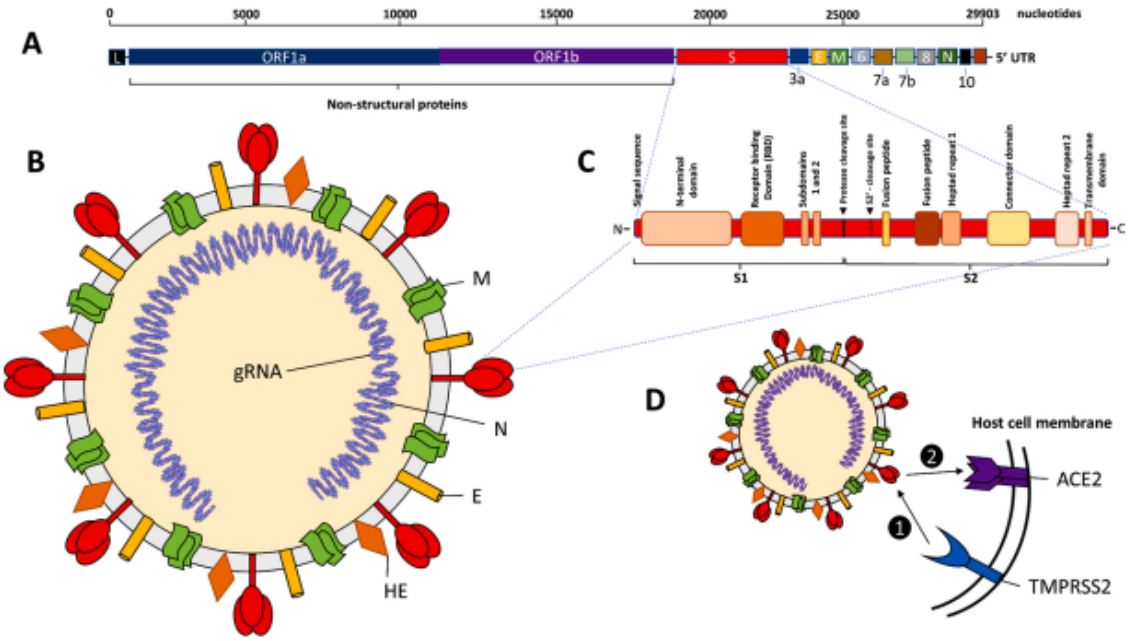

Figure 1.1: *Genomic and molecular characteristics of the SARS CoV-2 virus. A. The genome of SAR-CoV-2 is a large, positive-sense, single-stranded RNA consisting of 29,903 nucleotides. It is non-segmented and contains two open-reading frames (ORFs), ORF1a and ORF1b, which encode non-structural proteins (nsps). The structural proteins, including the viral spike protein (S), envelope protein (E), membrane protein (M), and nucleocapsid protein (N), are encoded by subgenomic RNA (sgRNA). The genome also encodes several putative accessory proteins (3a, 6, 7a, 7b, 8, and 10). The leader 3' sequence (L) is at the beginning, with a 5' untranslated region (UTR). B. The structure of the SARS-CoV-2 virion reveals an enveloped virus with major surface antigens, such as hemagglutinin-esterase (HE) and the spike (S) protein trimer. The genomic RNA is packaged inside the nucleocapsid (N), surrounded by the envelope. The protein structure of the spike (S) protein monomer exhibits key molecular domains involved in the pathogenesis of the virus. C. The primary cellular host receptor and co-receptor for SAR-CoV-2 are angiotensin-converting enzyme 2 (ACE2) and transmembrane serine protease 2 (TMPRSS2), respectively. The attachment and entry of SAR-CoV-2 into host cells require priming by TMPRSS2, which cleaves the S protein into S1 and S2 portions. This cleavage facilitates the targeting and binding of the S1 portion to the ACE2 receptor. D. Following ACE2 receptor binding, the virion is internalised into the host cell through receptor-mediated endocytosis, enabling viral entry and infection (Figure 1.1 was taken from (10)).*

1.4 The life cycle of SARS-CoV-2

1.4.1 Priming viral S protein, binding, and entry into the target host cell:

Understanding the life cycle of SARS-CoV-2 is still evolving (11). The viral ligand-host cell receptor binding and viral entry of SARS-CoV-2 follows a series of steps, although the exact sequence of events is not yet fully elucidated (Figure 1.2) (11). The N-terminal S1 portion of the viral S protein is crucial in targeting the host-cell receptor ACE2. Receptor binding is facilitated by the C-terminal RBD domain on the S1 portion (10). After receptor binding, the S2 portion of the S protein facilitates fusion between the viral and host cell membranes. The S2 portion comprises fusion peptides and heptad repeats (HRs), essential for steering and fusing the virus with the cell membrane (10). The fusion peptides play a crucial role in

attaching to and disrupting the host cell membrane, while the HRs form a trimeric coiled structure that brings the viral envelope and host cell membrane together for fusion. The priming cleavage of the S protein is thought to occur in two steps involving host proteases (11). TMPRSS2, a protease highly expressed in the respiratory tract, plays a significant role in priming the S protein and facilitating viral entry. Other proteases, such as cathepsin B/L, TMPRSS11a, and human airway trypsin-like protease (HAT), may also be involved (11). The S protein of SARS-CoV-2 contains an activation cleavage site located at the S2' position, near the S1-S2 border, which is critical for final priming (11). The exact order of events in S protein priming, the insertion of fusion peptides, and the assembly of HR regions for viral-host cell membrane fusion are still not fully understood (11).

1.4.2 Replication, assembly, and release:

Once the SARS-CoV-2 genome is released into the host cell's cytoplasm, the viral replicase is translated from the genomic RNA (gRNA) (10). The resulting polypeptide is processed and cleaved by viral proteases, leading to the formation of the replicase-transcriptase complex (RTC) within double-membrane vesicles (DMV) (10). This complex is crucial for RNA synthesis, transcription, and replication of the subgenomic RNAs (sgRNAs) (10). The sgRNAs are positive-sense RNA molecules that serve as mRNA for synthesising structural and accessory genes located downstream of the replicase polypeptides (10). The sgRNAs share common leader sequences with the full-length SARS-CoV-2 genome, enabling the creation of nested RNAs, a characteristic of Nidovirales viruses (11). The gRNAs and sgRNAs are synthesised through negative-sense intermediates, with the sgRNAs being present in smaller quantities than the positive-sense RNA species (11). The structural and accessory proteins of SARS-CoV-2, such as HE, 3a/b protein, and 4a/b protein, are translated from the sgRNAs (11). Coronaviruses can utilise homologous and non-homologous recombination to generate genetic diversity, facilitated by the RNA-dependent RNA polymerase, to assemble the viral genome efficiently and contribute to viral evolution (11). After replication and sgRNA synthesis, the S, E, and M genes are translated into viral structural proteins and transported to the endoplasmic reticulum (ER) (11). These proteins are processed through the secretory pathway and transported to the ER-Golgi intermediate compartment, where the full-length viral genomes are packaged with the nucleocapsid N protein. The N protein, along with the assistance of nsp3 protein, binds to the RNA genome and facilitates its packaging into the virion (10). The

M protein, with its transmembrane domains, plays a crucial role in viral assembly, including membrane curvature and nucleocapsid binding (10). The E protein is involved in shaping the viral membrane envelope and inhibiting M protein aggregation (10). Finally, mature virions are transported in vesicles and released from the infected cell via exocytosis (10).

These descriptions outline the current understanding of the SARS-CoV-2 life cycle; however, it is essential to note that research in this area is ongoing, and new insights may emerge as further studies are conducted.

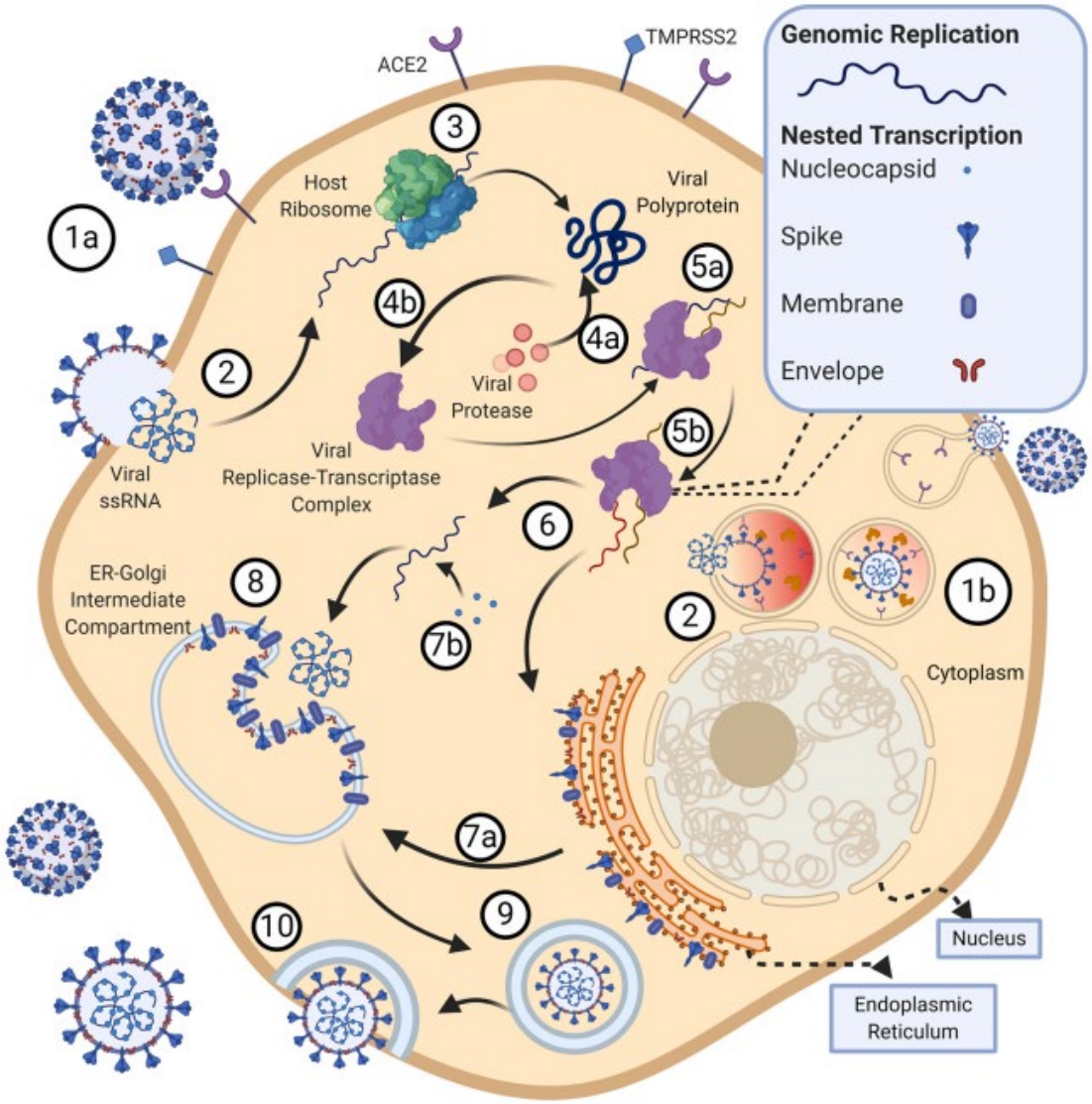

Figure 1.2: *SARS CoV-2 Life cycle. (1a) SARS-CoV-2 utilises the ACE2 receptor on the cell surface to bind and initiate infection. The* S1 subunit of the spike protein facilitates this binding. Once bound, the S2 subunit promotes fusion between the viral and cellular membranes through the formation of a six-helix bundle (6-HB) fusion core comprising heptad repeats 1 (HR1) and heptad repeats 2 (HR2). That brings the viral and cellular membranes into proximity for fusion and subsequent infection. (1b) In cells lacking TMPRSS2, cathepsin B/L may facilitate endosomal entry of the virus. (After fusion, the virus releases its positive-sense single-stranded RNA (ssRNA), which spans approximately 30 kilobases (kb), into the host cytoplasm. (4a) Using the host ribosomal machinery, the 5' end of the ssRNA is translated into a viral polyprotein. (4b) This polyprotein is then auto-proteolytically cleaved by virus-encoded proteinases, forming 16 non-structural proteins that assemble into the replicase-transcriptase complex. This complex includes essential enzymes like the viral RNA-dependent RNA polymerase and endo- and exonucleases involved in nucleic acid metabolism. (5a) Simultaneously, the 3' end of the viral genome expresses 13 open-reading frames (ORFs) that encode the four major structural proteins: Spike (S), Envelope (E), Membrane (M), and Nucleocapsid (N). These structural proteins are also synthesised using the host ribosomal machinery. (5b) Concomitantly, the ssRNA undergoes replication with viral RNA-dependent RNA polymerase assistance. The S, E, and M viral structural proteins are inserted into the endoplasmic reticulum (ER). (7a) They move to the ER-Golgi intermediate compartment through the secretory pathway. (7b) The viral RNA, encapsulated by the N protein, buds into membranes of the ER-Golgi intermediate compartment. Finally, the N protein encapsulates viral RNA, and the S, E, and M structural proteins assemble to form mature virions. After assembly, the virions are transported in vesicles to the cell surface, fusing with the plasma membrane for exocytosis and releasing many virions (***Figure 1.2*** was taken from (10).

1.5 Major cellular receptor recognition by SARS-CoV-2

The SARS-CoV-2 virus adopts some key molecules on host cells, such as receptors or proteases, to establish its infection mainly in the respiratory mucosa in humans (12). That includes (i) ACE2, (ii) TMPRSS2 and Furin, and (iii) DC-SIGN (12-14).

1.5.1 ACE2

In the early stages of SARS-CoV-2 infection, the virus attaches to nasal cavity epithelial cells and rapidly replicates upon inhalation. Angiotensin-converting enzyme 2 (ACE2) has been identified as a primary receptor for SARS-CoV-2 and SARS-CoV (15). The binding between the spike protein of the virus and ACE2 enables the virus to penetrate host cells (12-14). ACE2 receptors are expressed in various organs, including the lungs, brain, heart, intestines, kidneys, and testicles, making them potential targets for SARS-CoV-2 (12-14). Dysregulation of homeostasis in multiple organs, particularly the respiratory, cardiac, renal, and circulatory systems, contributes to the severity and fatality of COVID-19 (12-14). Studies have shown that SARS-CoV-2 has a higher affinity for ACE2 binding than SARS-CoV, which enhances its ability to invade host cells (12-14). Animal models have indicated that SARS-CoV can enter the brain through the olfactory bulb, resulting in rapid spread and neuronal infection (12-14, 16). Dysfunction or death of infected neurons, especially those in the cardiorespiratory centres of the medulla, may contribute to fatality (12-14, 16). Using angiotensin receptor blockers, a

class of antihypertensive drugs, increases ACE2 expression, which may have adverse effects in the context of SARS-CoV-2 infection (12-14, 16).

1.5.2 TMPRSS2 & TMPRSS4 and Furin

TMPRSS2 and TMPRSS4 are cell surface proteases involved in activating the spike protein of SARS-CoV-2, enhancing viral infection (12-14, 16). TMPRSS4 is highly expressed in brain regions associated with the sense of smell and taste (12-14, 16). ACE2 and TMPRSS2 are abundantly expressed in respiratory epithelium and enterocytes of the lower gastrointestinal tract, where they may play a role in viral infection. Furin, a protease enzyme, activates spike proteins in various viruses, including SARS-CoV-2 (12-14, 16). Furin cleavage of the spike protein promotes structural rearrangement and enhances receptor binding affinity. Protein-protein docking studies have shown a strong interaction between furin and the spike protein of SARS-CoV-2, suggesting that the protease may play a role in viral maturation and infection efficiency (12-14, 16). The widespread distribution of furin in various organs increases the likelihood of SARS-CoV-2 infection in multiple organs (12-14, 16). Cleavage of the spike protein by cathepsins B and L can activate SARS-CoV spikes, leading to increased fusion efficiency and binding affinity to the ACE2 receptor (12-14, 16).

1.5.3 DC-SIGN/L-SIGN

Dendritic cell-specific intracellular adhesion molecules (ICAM)-3 grabbing non-integrin (DC-SIGN, CD209) and liver/lymph node-specific ICAM-3 grabbing non-integrin (L-SIGN, DC209L) are members of the C-type lectin superfamily and play a role in viral pathogenesis (17-19). L-SIGN is highly expressed in human type II alveolar cells and the endothelial cells of the lung, liver, and lymph nodes (19, 20). On the other hand, DC-SIGN is primarily found in dendritic cells and tissue-resident macrophages, including alveolar macrophages, dermal macrophages, and peripheral blood mononuclear cells (17, 19). Despite their different expression profiles, CD209L (L-SIGN) and CD209 (DC-SIGN) share a significant amino acid sequence homology of 79.5% (18-20). The distinguishing feature of L-SIGN and DC-SIGN lies in their C-type lectin domain (CRD), which is responsible for recognising glycans in a calcium-dependent manner (18-20). The CRD contains a conserved EPN motif (Glu-Pro-Asn), recognising mannose, fucose, or galactose-containing structures (18-20). Although the CRD of L-SIGN and DC-SIGN share homology, they exhibit differential recognition of oligosaccharide structures (18-20). L-SIGN prefers high mannose oligosaccharides and does not bind well to complex glycans, especially

those with antennary fucose epitopes like LewisX (LeX) (18-20). DC-SIGN binds to fucose and LeX (18-20). Recent studies have demonstrated that RBD of the SARS-CoV-2 spike protein can bind to both DC-SIGN and L-SIGN, facilitating viral entry into the host cells (14, 21). The interaction between SARS-CoV-2 and DC-SIGN may play a role in the pathogenesis of the virus (14, 21).

1.6 Pathogenesis of COVID-19

Coronaviruses encompass a group of viruses that can cause disease in humans and animals (22). While some coronaviruses only lead to mild respiratory symptoms, there are three notable coronaviruses, including SARS-CoV, MERS-CoV, and SARS-CoV-2, that can infect the lower respiratory tract and cause severe pneumonia, which can be fatal (22).

SARS-CoV-2, like other respiratory coronaviruses, primarily spreads through respiratory droplets (22, 23). After infection, the median incubation period is around 5.1 days before symptoms appear, with most symptomatic patients developing symptoms within 11.5 days (22, 23). Common symptoms include fever, dry cough, and, less frequently, difficulty breathing, muscle or joint pain, headache, dizziness, diarrhoea, nausea, and haemoptysis (22, 23). The viral load of SARS-CoV-2 reaches its peak within 5-6 days of symptom onset, which is earlier than the related SARS-CoV (22, 23).

The pathophysiology of SARS-CoV-2 infection mainly resembles aggressive inflammatory responses contributing to airway damage. Disease severity is determined by both the viral infection and the host immune response (22, 24). Like SARS-CoV and MERS-CoV, the severity of COVID-19 tends to increase with age (22, 24). Severe COVID-19 cases often progress to acute respiratory distress syndrome (ARDS), characterised by breathing difficulties and low blood oxygen levels (22, 24). That can lead to secondary bacterial and fungal infections (22, 24). Respiratory failure resulting from ARDS is the leading cause of mortality in 70% of fatal COVID-19 cases(24). Additionally, an excessive release of cytokines in response to viral and secondary infections can trigger a cytokine storm and sepsis, accounting for 28% of fatal COVID-19 cases (22, 24). Uncontrolled inflammation can cause multi-organ damage, particularly affecting the cardiac, hepatic, and renal systems. In SARS-CoV infections, patients with renal failure often succumb to the disease (22, 24). Overall, the pathophysiology of SARS-CoV-2 infection, including the progression to severe disease and potential organ failure, shares

similarities with SARS-CoV and MERS-CoV infections (22, 24). Understanding these mechanisms is crucial for developing effective treatments and interventions(22, 24).

1.7 Immune Response to SARS-CoV-2

Upon encountering the novel pathogen SARS-CoV-2, humans can develop an effective adaptive immune response to neutralise the virus's antigens (25). This response typically takes about 2-3 weeks to develop fully(25). However, in the early stages of infection, in most cases, the control of the infection is likely mediated by the innate immune response (25). Unlike the adaptive immune response, which relies on recognising specific antigens by antibodies and T cells, the innate immune response is activated rapidly (25). It does not require prior exposure to the pathogen (25).

Severe forms of COVID-19 may arise from the failure of innate response mechanisms (26). When this response is dysregulated or amplified, it can potentially become pathogenic to the host (26). That is especially relevant in individuals with underlying comorbidities, as their immune systems may already be compromised (26). The complex interplay between the virus, the immune response, and comorbidities contribute to the severity and clinical outcomes of the disease (26). It is important to note that our understanding of the immune response to SARS-CoV-2 and the pathogenesis of COVID-19 is still evolving (25). Ongoing research is essential to gain further insights into the immune response dynamics and to inform strategies for preventing and treating severe COVID-19 cases (25).

1.8 Innate immune response to SARS-CoV-2

The innate immune system is the initial barrier against pathogens, including viruses (27). It detects viral presence through pattern recognition receptors, which recognise specific patterns associated with viral components (27). Upon recognition, the innate immune system triggers a series of responses involving cellular and inflammatory elements to eliminate the virus from the body. These responses work together to promote viral clearance and prevent infection (27).

1.8.1.1 Innate immune PRRs recognising SARS-CoV-2

Immediate cellular responses to pathogen invasion are crucial for maintaining cell homeostasis and survival in all living organisms (28). These responses are triggered by pattern

recognition receptors (PRRs), which are germline-encoded cellular receptors that recognise specific patterns of non-self and danger molecules known as pathogen-associated molecular patterns (PAMPs) and danger-associated molecular patterns (DAMPs) (Figure 1.3) (28). In mammals, activating PRRs by PAMPs or DAMPs leads to the initiation of innate immune responses and the production of interferons (IFNs) and proinflammatory cytokines (28). Over the past few decades, several PRRs have been discovered, including Toll-like receptors (TLRs), nucleotide-binding oligomerisation domain (NOD)-like receptors (NLRs), C-type lectin receptors (CLRs), AIM2-like receptors (ALRs), cyclic GMP-AMP synthase (cGAS), and retinoic acid-inducible gene I (RIG-I) (28).

TLRs and RLRs are the major receptors responsible for sensing RNA virus infections and triggering antiviral IFN programs (29). TLRs, first identified in Drosophila as antifungal genes, play a fundamental role in innate immune sensing in mammals (29). Multiple TLRs have been discovered in humans (TLR1-TLR10) and mice (TLR1-TLR9 and TLR11-TLR13), each recognising common or distinct PAMPs derived from microbial components (29). TLR3, TLR7, and TLR8 recognise RNA viruses that enter through endocytosis by sensing single- or double-stranded RNA in endosomal compartments (29). In contrast, RLRs are cytoplasmic viral sensors that detect intracellular non-self RNAs with distinct patterns of secondary structures or biochemical modifications. RLRs, including RIG-I, MDA5, and LGP2, possess RNA helicase domains and can recognise non-self RNAs through different mechanisms (29). Activation of RLRs and TLRs initiates immediate antiviral defense programs (29). TLRs recruit adapter proteins, such as MyD88 and TRIF, to initiate downstream signal cascades (29). At the same time, RLRs undergo conformational changes mediated by ATPase/helicase activity and liberate CARDs to bind to the signalling adapter molecule MAVS (29).

The downstream signalling pathways coordinated by MyD88, TRIF, MAVS, and ubiquitin ligases lead to activating antiviral kinases and transcription factors, such as IRF3, IRF7, and NF-κB (30). This activation produces type I IFNs and proinflammatory cytokines, which play crucial roles in the host's antiviral IFN programs (30).

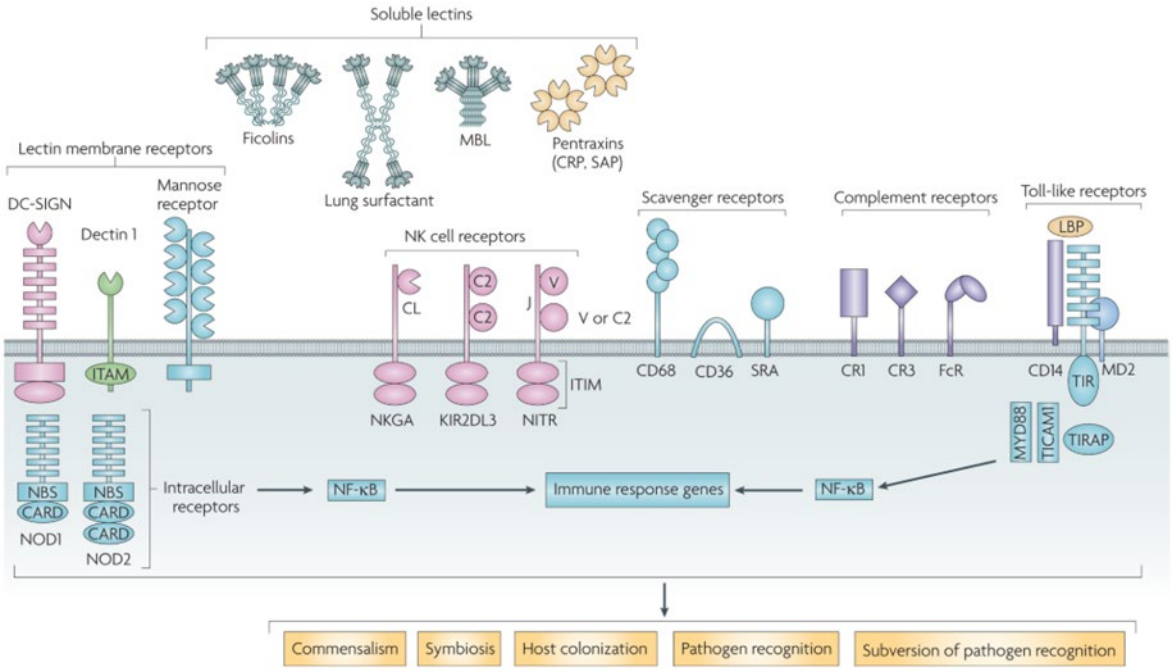

Figure 1.3: *Various soluble and membrane-bound pattern-recognition receptors (PRRs**).** The term "extracellular pattern-recognition receptors" (PRRs) refers to soluble lectins, which include lung surfactants and mannose-binding lectins, ficolins, and pentraxins (such as C-reactive proteins and serum amyloid-P). Extracellular C-type lectin PRRs include dendritic cell-specific intercellular adhesion molecule 3-grabbing non-integrin (DC-SIGN), dectin 1, and the mannose receptor on macrophages. Scavenger receptors, complement receptors, and natural killer (NK) cell receptors are other extracellular receptors. Nuclear factor-κB (NF-κB) is the mechanism by which leucine-rich repeat-rich extracellular Toll-like receptors and intracellular nucleotide-binding oligomerization domain (NOD) receptors activate immune genes. Membrane-associated and soluble lectins mediate interactions with pathogens that result in immunological recognition, attachment, opsonization, host invasion, and immune response. CARD: Caspase recruitment domain, CRP: C-reactive protein, ITAM: Immunoreceptor tyrosine-based activation motif, ITIM: Immunoreceptor tyrosine-based inhibition motif, KIR2DL3: Killer cell immunoglobulin-like receptor 2DL3, LBP: Lipopolysaccharide-binding protein, MBL: Mannan-binding lectin, NBS: Nucleotide-binding site, NKGA: Natural killer glycoprotein C-type lectin receptor, NITR: Novel immune-type receptor, SAP: Serum amyloid protein, TICAM1: TIR domain-containing adapter molecule 1, TIRAP: Toll/interleukin-1 receptor domain-containing adapter protein. (**Figure 1.3** was taken from (31)).*

1.8.1.2 Collectins as soluble PRRs in SARS-CoV-2 infection

Collectins are type of lectins that recognise pathogen glycan which are considered as key soluble pattern-recognition receptors (PRRs) of the innate immune response (32). Collectins such as SP-A, SP-D, and MBL can recognise and bind to various viruses to enhance viral neutralisation and phagocytosis (32, 33). SP-D has been shown to bind to SARS-CoV-2 and inhibits viral cell entry (34). It has been suggested that MBL has an immune function as soluble PRRs against SARS-CoV-2 (35).

1.8.1.2.1 Human Surfactant Protein D

Human surfactant protein-D (SP-D) plays a critical role in innate immunity, protecting against viral infections (33, 34). It acts as a potent opsonin, facilitating the clearance of viruses,

bacteria, and fungi through various mechanisms such as aggregation, enhanced phagocytosis, production of superoxide radicals, and macrophage activation (33, 34). The carbohydrate recognition domain (CRD) of SP-D binds to carbohydrates on the surface of pathogens (36). In contrast, the collagen region binds to its putative receptor, including the calreticulin/CD91 complex, on macrophages and other phagocytic cells, initiating effector functions (36).

SP-D is a hydrophilic protein with a single polypeptide chain (43 kDa) (37). It comprises a cysteine-containing N-terminal region, a collagen sequence region with repeated Gly-X-Y triplets, an α-helical coiled-coil neck region, and a C-type lectin domain or CRD (Figure 1.4) (37). SP-D can form an oligomer of 130 kDa, and four homotrimeric subunits linked through their N-terminal regions form a tetrameric structure of 520 kDa (37). SP-D is secreted by type II pneumocytes and Clara cells in the lungs (37). However, recent studies have reported its presence in extrapulmonary tissues such as the trachea, brain, testis, heart, prostate, kidneys, and pancreas (37).

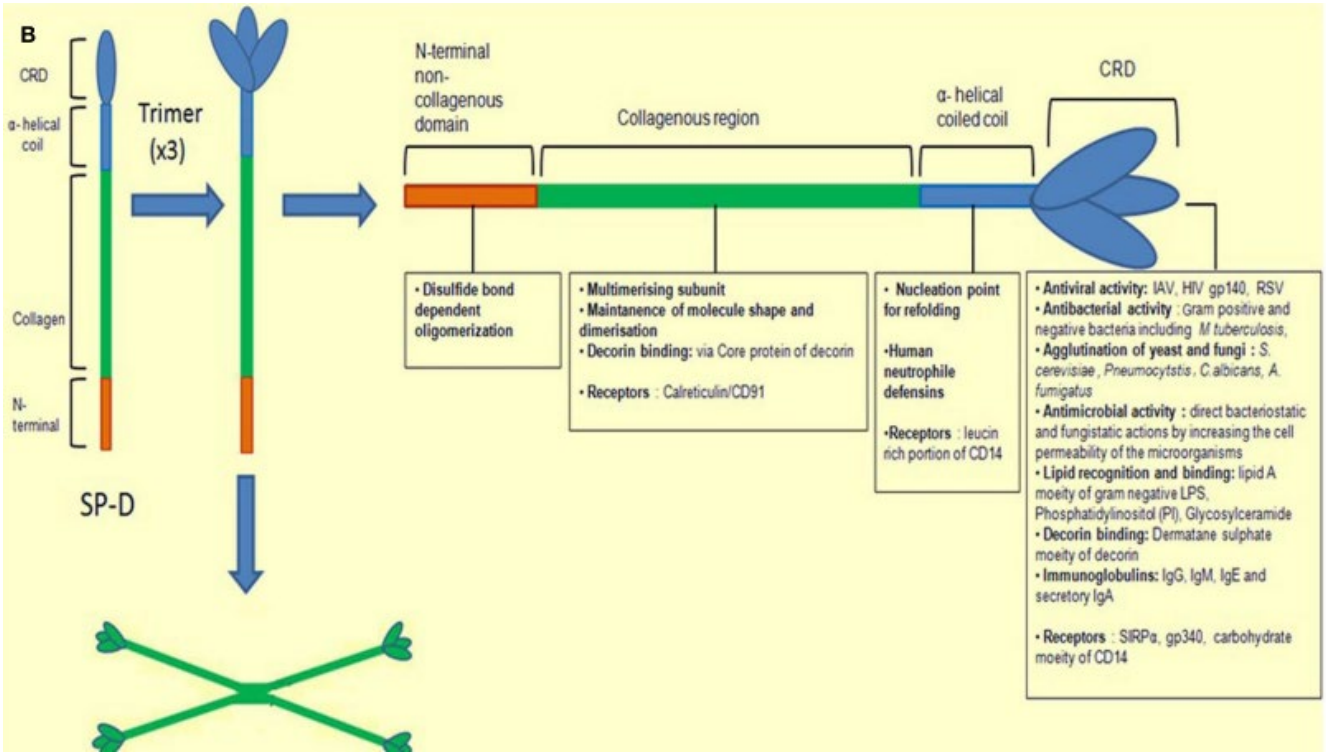

Figure 1.4: *Illustrates the structure of human Surfactant Protein D (SP-D). The monomeric form of SP-D consists of distinct regions, including a cysteine-rich N-terminal region responsible for forming disulfide bonds for oligomers, a collagen region containing repeated Gly-X-Y triplets, an α-helical coiled-coil neck region, and a C-type lectin domain known as the carbohydrate recognition domain (CRD). Human SP-D comprises three identical polypeptide chains, each weighing 43 kDa, which form a trimer subunit of 130 kDa. Four trimer subunits further assemble to create a tetrameric structure of SP-D, weighing 520 kDa. The CRDs of SP-D are responsible for binding to various ligands. At the same time, the collagen region*

*plays a role in recruiting immune cells to facilitate the clearance of pathogens, allergens, and apoptotic/necrotic cells (**Figure 1.4** adapted from (38)).*

1.8.1.2.2 Immune Surveillance of SP-D in viral infections

The interaction between SP-D and various viruses has been extensively studied, revealing its role in viral neutralisation and phagocytosis (39). For instance, SP-D has been found to bind to gp120, inhibiting the infectivity and replication of HIV-1 in a calcium-dependent manner (39). Moreover, a recombinant fragment of human SP-D (rfhSP-D), consisting of a homotrimeric which includes three neck and CRD regions, has demonstrated the ability to bind to gp120, effectively inhibiting HIV-1 infection in different cell types such as U937 monocytic cells, Jurkat T cells, and PBMCs (40). Additionally, rfhSP-D has been shown to suppress the cytokine storm triggered by HIV-1 (40).

Another significant finding is the direct interaction between DC-SIGN and rfhSP-D, which modulates the transfer of HIV-1 to CD4+ T cells *in vitro* (41). Furthermore, rfhSP-D has been observed to prevent and restrict the transfer of HIV-1 across the vaginal epithelial barrier by modulating the gene expression signature of the vaginal epithelium (41). That occurred through the downregulation of genes related to cellular tight junctions and cytoskeleton stability (41).

In the context of severe acute respiratory syndrome (SARS), increased levels of serum SP-D have been detected in patients infected with SARS-CoV (42, 43). SP-D recognises the spike glycoprotein of the SARS-CoV and inhibits viral infection in human bronchial epithelial cells (16HBE) (42, 43). Similarly, SP-D has been found to bind to the glycoprotein of bovine strains of non-enveloped rotavirus and neutralise their infectivity (44). However, it should be noted that the binding of human and porcine SP-D to the glycoprotein of the Ebola virus can enhance viral infection and dissemination (45).

Moreover, SP-D has been shown to bind to the A27 protein of the vaccinia virus, and mice lacking the SP-D gene have exhibited an increased mortality rate when challenged with the vaccinia virus (46). Additionally, rfhSP-D has demonstrated dose-dependent binding to the S1 and RBD of SARS-CoV-2 spike protein, inhibiting their interaction with cells overexpressing ACE2 (34).

In the case of the Influenza A Virus (IAV), SP-D binding to the virus has been extensively studied using SP-D-deficient mice (47). The antiviral effects of SP-D on IAV seem to depend on the viral

subtypes and the glycosylation levels of the virulence factors, such as the hemagglutinin (HA) and neuraminidase (NA) glycoproteins (47). SP-D treatment in a murine model of IAV infection has been shown to enhance lung viral clearance. SP-D neutralises IAV and inhibits the release of viral particles from infected host cells by binding to mannose residues on HA or NA (33, 48). It also inhibits the hemagglutination activity of IAV, leading to viral particle aggregation (33, 48). The anti-IAV activity of SP-D is suggested to occur through its CRD region binding to the carbohydrate pattern (mannosylated, N-linked) on HA and NA (33, 49). Furthermore, SP-D limits the enzymatic activity of HA and NA, thereby neutralising the infectivity of the pH1N1 IAV subtype in human A549 airway epithelial cells (33, 50). However, it has been reported that SP-D can enhance infection in some pandemic pH1N1 strains, which correlates with differences in N-glycosylation in the globular head region of HA (33, 50). Notably, porcine SP-D exhibits potent inhibition of seasonal IAV subtypes and several pandemics and avian strains of IAV (33, 48).

1.8.1.3 The complement system in SARS-CoV-2

The complement system plays a vital role in the innate immune response to viruses, but it can also lead to proinflammatory reactions (51). Mannose-binding lectin (MBL), a member of pattern recognition receptors (PRRs) in innate immunity, recognises mannose residues on viral surfaces (51). This recognition activates the complement system, promoting inflammation and enhancing phagocytosis (51). Studies have shown that MBL can bind to SARS-CoV, leading to C4 deposition on the virus and reducing its infectivity in animal models (51). The presence of mannose-rich glycans on the S1 region of SARS-CoV-2 has raised the possibility that glycan recognition and binding to MBL may inhibit the interaction between S1 and ACE (51).

On the other hand, dysregulation of complement system activation can contribute to severe disease in COVID-19 (52). The complement system has been implicated in the endothelitis and thrombosis observed in COVID-19 (52). Complement activation by coronaviruses was initially observed in mice infected with SARS-CoV (53). Complement activation product depletion was seen in infected mice's lungs as early as one day after infection (53). Mice deficient in C3 complement protein expression showed improved clinical outcomes following SARS-CoV infection, with milder inflammatory responses and reduced levels of inflammatory cytokines and chemokines compared to control mice (53). Similar immunopathogenic complement activation was observed in mice infected with MERS-CoV, and blocking C5a receptor activation

ameliorated clinical disease (53). Evidence of complement activation, including the deposition of complement components and anaphylatoxins, has also been found in COVID-19 patients, particularly those with respiratory failure (52). The involvement of the three complement system pathways has been demonstrated to exacerbate COVID-19 diseases (53). The anaphylatoxins C3a and C5a, produced during complement activation, activate neutrophils and other immune cells, further amplifying the complement cascade (52, 53). In addition, the complement system may also activate coagulation and prothrombotic pathways of SARS-CoV-2 infection through the contact system, contributing to arterial and venous thrombosis and coagulopathy observed in severe cases (53, 54).

1.8.1.3.1 Complement system

The complement system is a vital part of the innate immune system, comprising over 40 plasma proteins that serve various functions: host immunity, microbial defense, clearance of apoptotic cells, regulation of coagulation, and other immunological processes necessary for maintaining homeostasis (55). Activation of the complement system can occur through three pathways, including the classical, lectin, and alternative pathways, depending on the specific triggers (Figure 1.5) (55).

In the classical pathway, the binding of C1q to infectious agents or immune complexes. Activated C1r then cleaves and activates C1s. The latter cleaves C4 and C2, resulting in the generation of the C3 convertase (C4bC2b) (56). Then, The C3 convertase cleaves C3 into C3b and C3a. C3b attaches to the target surface and joins the C3 convertase, forming the C5 convertase (C4bC2bC3b) (56). Cleavage of C5 by the C5 convertase results in the formation of C5a and C5b, which involve the assembly the membrane attack complex (MAC), resulted in cell lysis (56). The lectin pathway is activated when mannose-binding lectin (MBL) recognises and binds to specific carbohydrate patterns on pathogens (56). MBL forms a complex with MBL-associated serine proteases 1(MASP-2), and 2 (MASP-2), which cleaves C4 and C2, generating the C3 convertase C4bC2b, similar to the classical pathway (56). The alternative pathway is initiated by spontaneous hydrolysis of the internal thioester bond of C3, leading to C3 (H_2O) (55). That allows Factor B to bind and be cleaved by Factor D, producing Ba and Bb and generating the alternative pathway C3 convertase (C3 (H_2O)Bb) (55). C3 convertase cleaves C3 into C3b and C3a. C3b can attach to complement-activating surfaces and continue the cascade by binding to Factor B, forming C3 convertase (C3bBb) (55). This amplification

loop is initiated as the C3 convertase cleaves more C3, generating additional C3b to create a new C3 convertase and C5 convertase (55). These pathways induce the activation of complement system, which plays a critical role in immune defense and the maintenance of homeostasis (56).

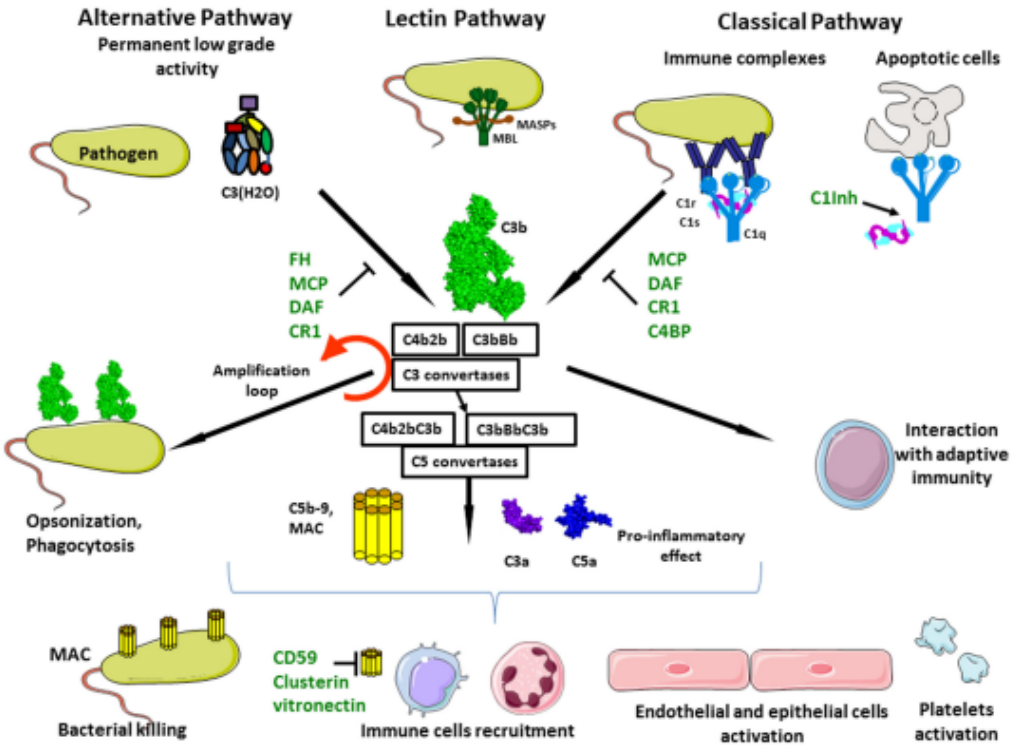

Figure 1.5: *Three pathways of the Complement system. The classical pathway of complement activation occurs when the C1 complex binds to immune complexes, forming the C4bC2b enzyme complex (C3 convertase). It can also be initiated by the binding of C1 to apoptotic cells. The lectin pathway is activated by binding mannose-binding lectin (MBL) or MBL-associated serine proteases (MASPs) to mannose groups on bacterial cell surfaces, generating C3 convertase. The alternative pathway is activated by hydrolysed C3 and factor B, forming C3 convertase. All three pathways converge at the C3 convertase stage. C3 convertase generates the C5 convertase enzyme, including the membrane attack complex (MAC). Various factors, including CR1, DAF, C4BP, and MCP, can inhibit the activity of C3 and C5 convertases. Proteins like CD59, clusterin, and vitronectin can block the assembly of the MAC complex. Complement activation leads to bacterial lysis through the MAC complex, recruitment of immune cells, platelet activation, and activation of endothelial and epithelial cells. Furthermore, complement proteins opsonise pathogens, enhancing their phagocytosis. (Figure 1.5 adapted from (57))*

1.8.1.3.2 Major regulatory complement proteins

1.8.1.3.2.1 The complement component 1q (C1q)

C1q is an integral component of the innate immune system, playing a vital role in the recognition and activation of the classical pathway of complement (58). It serves as the initial

subcomponent of the C1 complex and is responsible for identifying immune complexes containing IgG or IgM antibodies (58). Beyond its role in complement activation, C1q is involved in diverse homeostatic processes, including the clearance of immune complexes, pathogens, necrotic cells, and apoptotic cells (58).

The production of C1q is not limited to Kupffer cells in the liver; it is also synthesised by macrophages, immature dendritic cells (DCs), and adherent monocytes (58). In humans, C1q is a large molecule with a molecular weight of 460 kDa (59). It consists of 18 polypeptide chains, divided into three types: 6A, 6B, and 6C. Each chain, A, B, and C, encompasses a short N-terminal region (3-9 residues), followed by a collagen-like sequence of approximately 81 residues (Figure 1.6) (60). The C-terminal region of each chain forms a globular domain (gC1q) consisting of about 135 residues (60).

The A and B chains are linked by inter-chain disulfide bridges, forming dimer subunits of 6A-B, while the C chains form dimer subunits of 3C-C (59). The triple helical collagen regions from one A-B subunit and one C-C subunit combine to create a structural unit known as ABC-CBA, stabilised by both covalent and non-covalent bonds (59). These three subunits assemble to form the complete C1q protein, held together by non-covalent solid interactions (59).

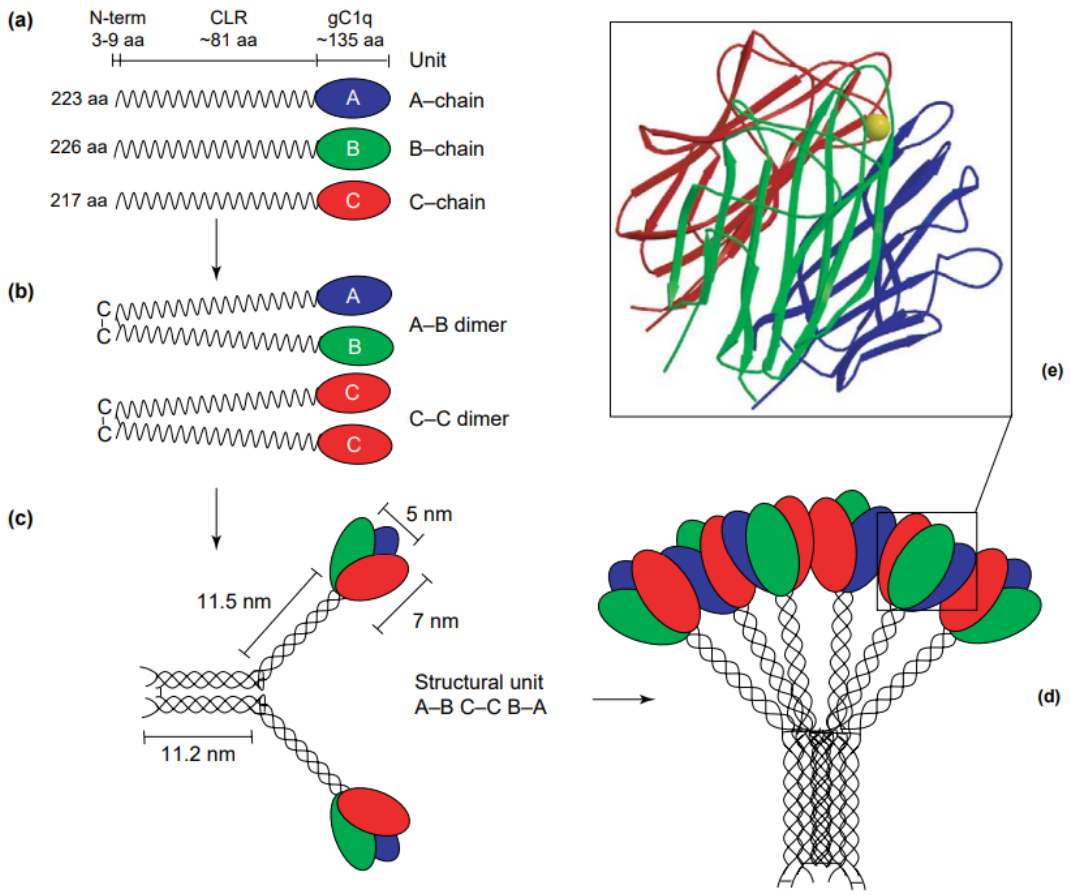

Figure 1.6: *Structural Organization of C1q Molecule. The C1q molecule (460 kDa) comprises 18 polypeptide chains (6A, 6B, and 6C). (a) Each A, B, and C chain has a short N-terminal region with a half-cystine residue involved in forming interchain disulfide bonds. That is followed by a collagen region (CLR) consisting of approximately 81 residues and a C-terminal globular region (gC1q domain) comprising about 135 residues. (b) The interchain disulfide bonding results in the formation of 6A-B dimer subunits and 3C-C dimer subunits. The A and B chains of an A-B subunit and one of the C chains from a C-C subunit form a structural unit (ABC-CBA) held together by both covalent and non-covalent bonds. (c) Three of these structural units associate through non-covalent solid bonds in the central portion, resembling a fibril-like structure, to form the hexameric C1q molecule with a tulip-like shape, like mannose-binding protein, surfactant protein A, and ficolins. (d) The crystal structure of the gC1q domain of human C1q (Protein Data Bank code 1PK6) reveals a compact, spherical, heterotrimeric assembly with a diameter of approximately 50 Å. Non-polar interactions primarily hold it together and exhibit non-crystallographic pseudo-threefold symmetry. (e) The three gC1q modules show different electrostatic surface potentials, partly explaining the modularity in ligand recognition (Figure 1.6 adapted from (61)).*

1.8.1.3.2.2 C4b-binding protein (C4BP)

C4BP is a large plasma glycoprotein with a molecular weight of 570 kDa that plays a crucial role in down-regulating the classical and lectin complement pathways (62, 63). It is present in the human plasma at an estimated concentration of 200 mg/L (62, 63). It comprises seven identical α-chains and one unique β-chain (Figure 1.7). Each α-chain contains eight complement control protein (CCP) domains comprising approximately 60 amino acids (62, 63). The β-chain, on the other hand, shall consist of three CCP domains and is connected to the α-chains through disulfide bridges in a central core structure (62, 63). The main functions of

C4BP include accelerating the decay of the C3 convertase (C4bC2a) by serving as a cofactor for the cleavage of C4b by factor I (62, 63). When recruited to a surface, C4BP inhibits complement activation of the classical pathway and prevents opsonisation and subsequent lysis (62, 63). That regulatory activity protects host cells from excessive complement-mediated damage (62, 63). However, it is worth noting that this regulatory function is not limited to host cells and can also occur on pathogens, exerting an inhibitory effect on their complement activation (62, 63).

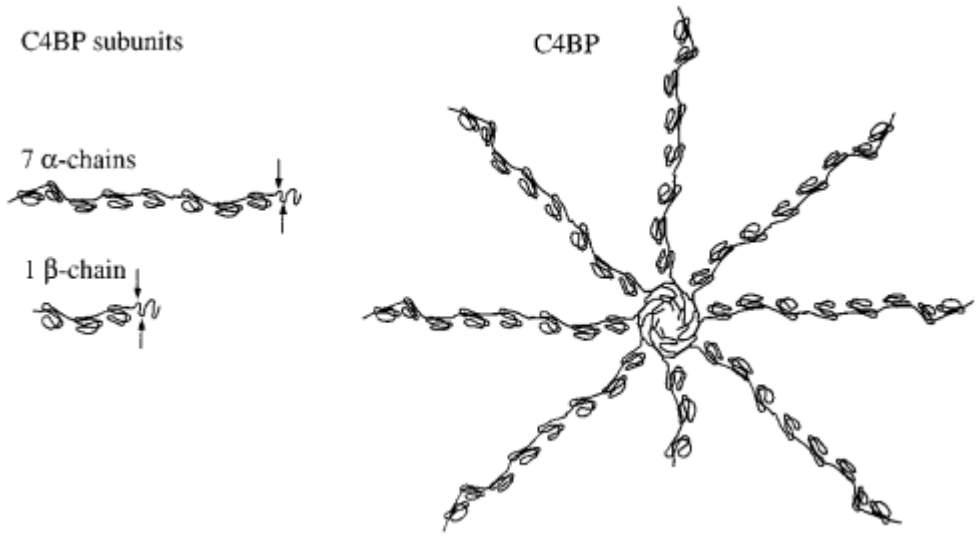

Figure 1.7: *Schematic Structure of C4BP. C4BP comprises seven identical a-subunits, each containing a binding site for C4b. Each a-chain consists of eight complement control protein modules, SCR modules, along with a C-terminal linking domain. The b-chain, which includes the protein S binding site, comprises three SCR modules and a linking domain (Figure 1.7 adapted from (64)).*

1.8.1.3.2.3 Factor H (FH)

The factor H gene (CFH) is situated in the regulators of complement activation (RCA) gene cluster on human chromosome 1 (65). It encodes two main protein products: the 150-kDa factor H protein and a smaller 43-kDa factor H-like molecule known as FHL-1 (66, 67). Additionally, several factor H-related (FHR) molecules share homology with factor H and FHL-1, although they are not transcribed from the factor H gene (65). These molecules possess a common structural motif called the complement control protein (CCP) unit or short consensus repeat (SCR), which comprises approximately 60 amino acids with short spacers between the domains (66, 67). Factor H consists of 20 homologous CCP domains, giving it a flexible

appearance resembling "beads on a string" that can fold back on itself (Figure 1.8) (66, 67). The conformation of factor H can be influenced by the ionic strength and pH of its local microenvironment.

Functional analysis has revealed that the N-terminal four CCP domains of factor H contain a C3b-binding site with decay-accelerating and cofactor activities (66, 67). Additional binding sites for C3b have been identified within CCPs 7-15 and CCPs 19-20. The CCP 19-20 site interacts with C3b, iC3b, and C3d (66, 67). Factor H also possesses multiple binding sites for heparin and other polyanions in CCP 7, CCP 20, and the CCP 9-15 regions (66, 67). The C-terminal site has been shown to bind sialic acids. These binding sites for C3b and polyanions in CCP 19-20 are crucial for factor H's interactions with host surfaces, enabling the regulation of complement activation (66, 67). Recombinant forms of the C-terminal CCPs (rH19-20) can compete with full-length factor H for binding to C3b and host polyanions, increasing complement activation on host surfaces (55). The ability of factor H to distinguish between host and foreign cells is primarily attributed to the two C-terminal domains (55).

Studies utilising deletion mutants and transgenic mice have demonstrated the significance of the C-terminal domains of factor H in recognising host cells and protecting against complement attack (55). These findings suggest that the two C-terminal domains are vital in factor H's ability to recognise and discriminate, particularly in its interactions with host cells (55).

Figure 1.8: *The Schematic Structure of Factor H. Factor H comprises 20 short consensus repeat (SCR) domains. The molecule has two central functional regions at the N- and C-termini. SCRs 1-4 mediate the complement regulatory activities of factor H (Figure 1.8 adapted from (67)).*

1.8.1.3.2.4 Properdin (FP)

Properdin is a protein composed of six complete thrombospondin type 1 repeat (TSR) domains, labelled TSR 1-6, and a truncated N-terminal TSR domain called TSR 0 (Figure 1.9) (68). Properdin has a molecular weight of 53 kDa; each monomer is approximately 26 nm long

and 2.5 nm in diameter, consisting of 442 amino acid residues (69). Properdin monomers undergo glycosylation at an N-glycosylation site in TSR-6 and C-mannosylation at 14 specific tryptophan residues (69). In addition to binding to C3b, C3bB, and C3bBb, properdin interacts with sulfatides and various polyanionic structures (69).

Under normal physiological conditions, properdin forms oligomers consisting of dimers (P2), trimers (P3), and tetramers (P4) in a defined ratio of 26:54:20 (P2:P3:P4) (70). Oligomerisation occurs through head-to-tail associations of the monomers (69, 70). Deletion mutants that lack specific TSR domains have provided insights into the functional properties of individual domains (70, 71). Domains 4, 5, and 6 are essential for properdin's ability to lyse rabbit erythrocytes, as their deletion impairs binding to C3b and sulfatides (70, 71). Deletion of domain three does not affect binding to C3b, sulfatides, or oligomer formation (70, 71). Removal of domains 4 and 5 prevents the formation of trimers and tetramers while allowing dimerisation (70, 71). Complete inhibition of oligomerisation occurs when TSR 6 is deleted (70, 71).

Research indicates that multiple TSR domains work together to mediate properdin oligomerisation and function, with domains 5 and 6 playing crucial roles (69, 71). Antibodies targeting human TSR5-6 and mouse TSR5-6 effectively inhibit properdin function *in vitro* and in vivo, respectively (70). Point mutations, such as Y387D in TSR6, disrupt properdin's binding to C3b and its alternative pathway regulation (70). Mutations in TSR1 (R73W) and TSR5 (Q316R) are associated with type II properdin deficiency, characterised by low levels of circulating properdin and defects in oligomerisation (70). Structural studies propose models for properdin oligomerisation, highlighting the involvement of TSRs 0-1 and 5-6 in forming contacts at the vertices of oligomers (70). The composition of domains at the vertices may vary, and the structural models support the roles of TSR5-6 in properdin function and the impact of the Y387D mutation on C3b binding (70).

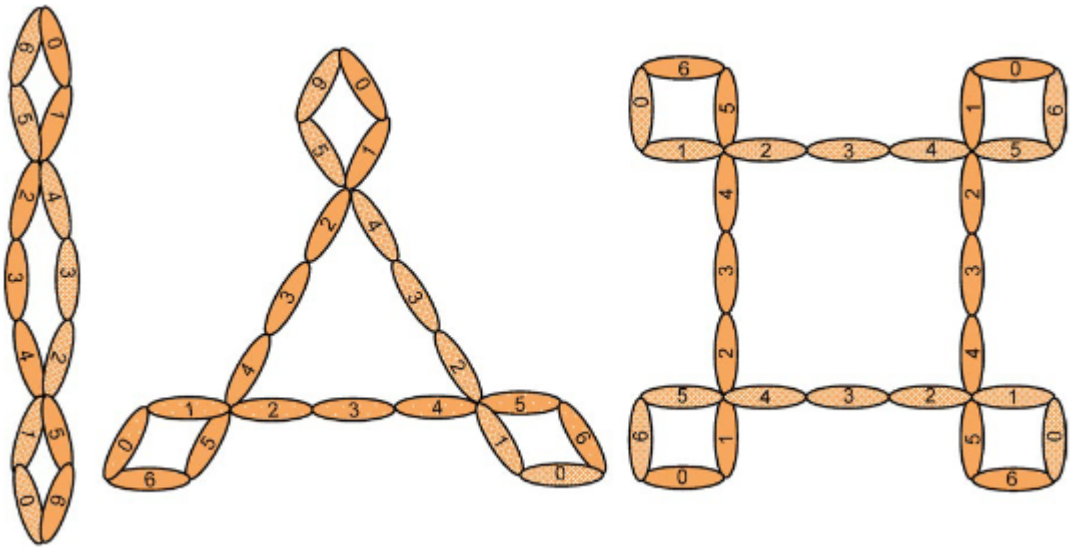

Figure 1.9: *Schematic Structure of Properdin*. *The structure of properdin consists of seven thrombospondin repeat (TSR) domains labelled TSR0-6. Under normal physiological conditions, properdin monomers assemble into cyclic dimers, trimers, and tetramers, with a ratio of approximately 1:2:1. Molecular modelling suggests that the vertices of properdin oligomers are formed by a combination of four domains derived from two different monomers, arranged in a head-to-tail organisation. While the organisation of domains at the vertices is still not fully understood, theoretical models propose that the TSR0-1 domains from one monomer are involved in vertex formation along with TSR5-6 domains from the other monomer (Figure 1.9 adapted from (70)).*

1.8.1.4 Key Cellular innate immune responses in SARS-CoV-2

Various clinical studies have highlighted primary innate immune cells involved in SARS-CoV-2 infection and their role in inflammation, including monocytes, macrophages, DCs, NK, and neutrophils (72, 73).

1.8.1.4.1 Monocytes and Macrophages

Myeloid cells play a significant role in the pathophysiology of coronavirus infections, both as targets of the virus and as producers of proinflammatory cytokines (73). In the case of SARS-CoV-2, macrophage activation syndrome characterised by hyperactivated macrophages has been associated with acute respiratory distress syndrome (ARDS) (73). This hyperactivation is attributed to the activation of alveolar, splenic, and renal macrophages by SARS-CoV-2 through the ACE2 receptor, resulting in increased secretion of proinflammatory cytokines like IL-6, TNF-α and IL-10, even in the absence of active virus replication (73).

In COVID-19 patients, postmortem tissue analysis has revealed the presence of proinflammatory macrophages in various locations (74). SARS-CoV-2 can infect ACE2-expressing resident CD169+ macrophages in secondary lymph nodes, leading to IL-6 production (74). In the peripheral blood, COVID-19 patients have shown a specific subset of

monocytes and macrophages that exhibit mixed M1/M2 polarisation with elevated expression of CD80, CD206, and high secretion of IL-6, IL-10, and TNF-α compared to healthy individuals (74). The abundance of different monocyte subsets varies according to the severity of COVID-19, with an increase in inflammatory monocytes in severe cases (74). Interestingly, critical COVID-19 patients exhibit decreased expression of HLA-DR on CD16+ monocytes, suggesting impaired antigen presentation capability (74). Some reports have also identified monocytes from SARS-CoV-2-infected individuals with high expression of the immune suppressor marker PD-L1 and low expression of the maturation marker CD80, indicating dysfunctional immune responses (74).

In severe cases of COVID-19, bronchoalveolar lavage fluid (BALF) analysis has shown an increased proportion of monocytes, macrophages, and neutrophils expressing specific markers and immunoregulatory genes (75, 76). Severe cases exhibit a predominance of M1-like macrophages producing highly inflammatory chemokines, while mild cases display a gene signature associated with alternative M2-like macrophages with reparative and profibrotic functions (75, 76). Single-cell analysis of BALFs from severe and mild COVID-19 patients has provided insights into cytokine and chemokine production by monocyte-macrophages (75, 76). In severe cases, monocyte-macrophages secrete many cytokines and chemokines but display limited secretion of interferons (75, 76). Additionally, anti-inflammatory molecules are elevated, while IL-18 levels are reduced in severe cases compared to mild cases (75, 76). Monocyte-macrophages from severe cases also produce chemokines that recruit more monocytes and neutrophils, contributing to excessive proinflammatory cytokine production in the infected lungs (75, 76).

1.8.1.4.2 Dendritic Cells

Dendritic cells (DCs) are essential antigen-presenting cells that activate innate and adaptive immune responses (77). In the lung, three subpopulations of DCs are present: CD141+ cDC1, responsible for Th1 response activation; CD1c+ cDC2, involved in regulation and pro-inflammatory chemokine production; and CD123high pDC, the leading producer of antiviral cytokine type I interferon (IFN) (77, 78). In severe and critical COVID-19 patients, pDCs are reduced in bronchoalveolar lavage fluid (BALF) and blood samples compared to moderate infection or healthy controls (77, 78). Furthermore, the functionality of pDCs in terms of IFN-α production is impaired in COVID-19 patients (77, 78). Studies have shown that pDCs can

undergo phenotypical diversification in response to viral infection, giving rise to three effector subpopulations: P1-pDCs specialised for type I IFN production, P2-pDCs exhibiting both innate and adaptive functions, and P3-pDCs with adaptive functions (78, 79). Differences in pDC phenotype have been observed between asymptomatic and hospitalised COVID-19 patients (78, 79). Asymptomatic patients mainly express PD-L1, while severe patients are predominantly represented by the PD-L1+CD80+ phenotype, indicating strong activation for type I IFN production during asymptomatic infection (78, 79).

In vitro studies have demonstrated that SARS-CoV-2 can activate isolated pDCs, leading to their diversification into different subpopulations and the release of high levels of type I and type III IFNs (77, 79). However, these pDCs do not produce proinflammatory cytokines like TNF-α and IL-6 (77, 79). In addition to pDC alterations, severe COVID-19 patients also exhibit a decrease in the frequency of peripheral myeloid DCs (mDCs) (78, 79). The pDC ratio is significantly higher in severe patients compared to other subtypes, suggesting its potential as a biomarker for severe COVID-19 (78, 79). Furthermore, the expression of costimulatory and maturation markers CD86 and CD80 is significantly lower in COVID-19 patients, while the suppressive molecule PD-L1 is enhanced (78, 79). A recent study has shown that DC-SIGN, expressed large on DCs, binds SARS-CoV-2 and mediates viral entry (80).

1.8.1.4.3 Natural Killer Cells

NK cells control viral infections by recognising and killing virus-infected cells (81). They have both cytotoxic activity and immunomodulatory functions to limit host damage and disease progression (81). Human NK cells can be divided into two subsets: CD56brightCD16- NK cells, specialised in cytokine production, and CD56dimCD16+ NK cells, which display potent cytolytic activity (81). The expression of killer-immunoglobulin-like receptors (KIRs) and CD16 is essential for NK cytotoxic functions (81).

In patients infected with SARS-CoV and SARS-CoV-2, there is a significant reduction in the percentage of CD56dimCD16+KIR+ NK cells in whole blood samples (81, 82). That suggests impaired maturation or increased recruitment of NK cells from circulation into infected tissues (81, 82). Moreover, SARS-CoV-2 infection influences NK-mediated cytotoxic activity by upregulating the inhibitory receptor NKG2A (81, 82). Infected patients show increased expression of NKG2A and decreased expression of activation markers CD107a, IFN-γ, IL-2, and TNF-α in NK cells (81, 82). The expression of inhibitory receptors lymphocyte activating-3 and

Tim-3 is also increased, further contributing to the functional impairment of NK cells (81, 82). However, these alterations in NK cell number and NKG2A expression can be restored in convalescent patients (81, 82).

Severe SARS-CoV-2-infected individuals exhibit reduced peripheral NK cell counts and impaired cytotoxic activity compared to mild cases (83, 84). That correlates with increased levels of IL-6, suggesting that the functional impairment of NK cells leads to enhanced activation of innate immune cells and excessive proinflammatory cytokine production (83, 84). The phenotype of NK cells at the early stage of SARS-CoV-2 infection reflects their exhaustion and correlates with disease progression (83, 84). In the alveolar compartment, NK cells in the bronchoalveolar lavage fluid (BALF) of COVID-19 patients are still under investigation, with conflicting results (83, 84). Some studies have shown a significant reduction in resting NK cells in BALF (83, 84). In contrast, others have observed higher percentages of NK cells in severe cases than in moderate infection or healthy donors (83, 84). These discrepancies may be due to differences in sample collection timing or disease severity, necessitating further analysis (83, 84).

1.8.1.4.4 Neutrophils

Neutrophils play a critical role in the immune response against SARS-CoV-2, but their dysregulation can contribute to severe COVID-19 pathology (85). In severe cases, blood samples show a high neutrophil-to-lymphocyte ratio (NLR), indicating inflammation and infection (85). Deceased patients have increased neutrophil counts and decreased lymphocyte numbers compared to survivors (85). Neutrophils in COVID-19 patients exhibit impaired antigen presentation capacity due to reduced HLA-DR expression and increased PD-L1 surface expression (85). They also drive hyperinflammation through enhanced cytokine production and degranulation (85).

The sharp local inflammatory response observed in COVID-19 patients is mediated by chemokines, such as CXCL1, CXCL2, CXCL8, CXCL10, CCL2, and CCL7, which recruit neutrophils to the site of infection (86). Bronchoalveolar lavage fluid (BALF) samples from severe COVID-19 cases show an enrichment of neutrophils, while mild cases exhibit a neutrophil subpopulation with an interferon-stimulated gene (ISG) signature (86). Neutrophils can contribute to COVID-19 pathology by forming neutrophil extracellular traps (NETs) composed of DNA fibres, histones, and microbicidal proteins (86). Excessive NET formation can lead to

inflammation and thrombosis, causing organ damage (86). COVID-19 patients have elevated levels of NET-associated markers, indicating dysregulated NET formation (86).

Experiments demonstrate that COVID-19 patient sera induce NET release from neutrophils of healthy individuals, supporting the pathological role of NETs in severe COVID-19 (86-88). Neutrophils share similarities with polymorphonuclear myeloid-derived suppressor cells (PMN-MDSCs), which have immunosuppressive functions (86-88). In COVID-19 patients requiring intensive care, there is a significant expansion of PMN-MDSCs, suggesting their association with disease severity and serving as a potential biomarker (86-88).

1.8.1.5 Cytokine production in SARS-CoV2 infection

A rapid and coordinated immune response is crucial for combating viral infections, which involves the secretion of various cytokines as a defense mechanism (89). However, reports have indicated dysregulated cytokine production in individuals affected by SARS-CoV or MERS-CoV involving innate and adaptive immune cells (89). In SARS cases, infected hematopoietic cells, monocyte-macrophages, and other immune cells exhibit enhanced secretion of pro-inflammatory cytokines such as TNF-α, IL-6, IL-1β, IL-8, CCL5 and IFN-α/-γ, along with reduced anti-inflammatory cytokines (90-92). Similarly, MERS-CoV infection leads to delayed but increased production of IFN-α and pro-inflammatory cytokines including IL-6, IL-8, and IL-1β. Elevated cytokine levels have been associated with Multi-Organ Dysfunctional Syndrome (MODS) and ARDS due to the accumulation of immune cells in the lungs, causing alveolar damage and oedema (90-92).

In COVID-19 patients, cytokines and chemokines are increased, which attract immune cells to the lungs, resulting in ARDS, particularly in critically ill individuals (90-92). The signature cytokines observed in severe COVID-19 patients are consistent with those seen in SARS and MERS, including elevated expression of IL-6, TNF-α, macrophage inflammatory protein 1-α (MIP-1α), MCP3, GM-CSF, IL-2, and IP-10 (90-92). Elevated chemokines such as IP-10, CCL2/MCP1, CXCL1, and CXCL5 have also been detected in SARS-CoV-2 infection (90-92). In children, increased levels of inflammatory markers such as IL-6, IL-1, C-reactive protein, and procalcitonin have been observed in serum (90-92). Therapeutic approaches to control excessive cytokine production include neutralising antibodies or small molecule drugs that can interrupt the signalling cascade responsible for cytokine production (90-92).

1.8.2 Adaptive immune response in SARS-CoV2 infection

The adaptive immune system plays a critical role in clearing SARS-CoV-2 by utilising cytotoxic T-cells to eliminate infected cells and B-cells to produce neutralising antibodies against virus-specific antigens (93). COVID-19 is characterised by lymphopenia and a reduction in CD4+ T-cells, CD8+ T-cells, and B-cells (94-96). The underlying mechanisms contributing to lymphopenia in COVID-19 involve an abnormal innate immune response with low levels of IFN-I, which is necessary for viral antigen presentation and subsequent induction of adaptive immunity (94-96).

Several factors may contribute to COVID-19-associated lymphopenia, including direct infection of T-cells by SARS-CoV-2, cytokine-induced apoptosis and pyroptosis of lymphocytes, MAS-related haemophagocytosis, sequestration of lymphocytes in the lungs or other organs, reduced bone marrow haematopoiesis, and virus-induced tissue damage to lymphatic organs (94-96). The presence of SARS-CoV-2 in the spleen and lymph nodes, along with pathological alterations such as splenic white pulp atrophy and disruption of lymph node structure, suggests that direct cytotoxicity of SARS-CoV-2 in lymphatic organs may impair the adaptive immune response in COVID-19 (94-96). The absence of germinal centre formation in the spleen and lymph nodes could explain suboptimal humoral immunity, potentially leading to the possibility of re-infection in specific individuals (94-96). However, most individuals with mild-to-moderate COVID-19 experience a robust adaptive immune response characterised by T-cells targeting antigens derived from the S-protein and nucleoprotein/membrane protein, as well as the production of neutralising antibodies against S-protein-derived antigens (94, 95). This immune response persists for months after the primary infection. Coordinated SARS-CoV-2-specific adaptive immune responses are associated with milder disease and are crucial for effectively controlling viral infection (94, 95).

1.9 Main aims of this study

Considering the direct interactions observed between various viruses and innate immune molecules, including SP-D, C1q, C4BP, FH, and FP, the present project aimed to investigate the effects of these innate immune molecules on SARS-CoV-2 infection. The following aims have been outlined:

1. To assess the possible modulating role of rfhSP-D in the interaction between DC-SGN and SARS-CoV-2.
2. To evaluate the regulatory capacity of human C1q, specifically its globular domain, in modulating SARS-CoV-2 infection and associated inflammatory responses.
3. To examine the impact of FP on the modulation of SARS-CoV-2 infection.
4. To investigate the innate immune effector function of C4BP in the context of SARS-CoV-2 infection.
5. To study the complement-independent modulation of SARS-CoV-2 infection by factor H.

By addressing these aims, this project aims to enhance our understanding of the interplay between innate immune molecules and SARS-CoV-2, providing valuable insights into potential therapeutic approaches and immune modulation strategies against COVID-19.

Chapter 2

Methods and Materials

2.1 Native Complement Protein Purification from Human Plasma

2.1.1 Purification of native human C1q

C1q was purified as previously described (97). The lipid from 100 ml of freshly thawed, non-sterile mixed pool human plasma (TCS Biosciences) was isolated by subjecting the plasma to centrifugated at 5000× g for 10 min, and then it was filtered through a Whatman filter paper (GE Healthcare, Hatfield, UK). The lipid -depleted plasma was incubated with IgG-Sepharose (GE Healthcare, Hatfield, UK) for 2 h at room temperature (RT). Beads were loaded into an affinity chromatography column and washed with 3x column volumes of C1q wash buffer (10 mM HEPES) to remove unbound proteins. The bound C1q was eluted using two column volumes of C1q of C1q elution buffer (100 mM CAPS, 1 M NaCl, and 0.5 mM EDTA at pH 11). The flow-through was collected and dialysed against a 0.1 M HEPES buffer at pH 7.5. The protein concentration of the dialysed samples was quantified using the BSA kit (Thermo Fisher, UK). The total yield found to be 3 mg/ml C1q in 100 ml of human plasma. The purified sample was then subjected to SDS-PAGE and western blotting to confirm the identity of the isolated protein as C1q (Appendix 1 F&E).

2.1.2 Purification of Factor H

Human FH was isolated according to the previously reported method (98). 50 mL of non-sterile mixed-pool human plasma (obtained from TCS Biosciences) adjusted to 5mM EDTA, pH 8, then dialysed against buffer I (25 mM Tris-HCL, 140 mM NaCl, and 0.5 mM EDTA at pH 7.5) while being stirred continuously for an entire night at 4°C. The dialysed sample was incubated in an affinity column comprising a monoclonal antibody against human FH (MRCOX23; MRC Immunochemistry Unit, University of Oxford) coupled to CNBr-activated Sepharose (GE Healthcare, UK) after it had been rinsed with five-bed volumes of buffer I and distilled water. The elution buffer contains 3 M magnesium chloride (Merck), 25 mM Tris pH 8.0, 140 mM NaCl, and 0.5 mM EDTA, which was used to elute FH. Using 1 M Tris pH 7.5, the obtained fractions (1 ml each) of the eluted FH fractions were neutralized. The fractions were then dialysed for a whole night against 10 mM potassium phosphate for 4 h. Using a BSA kit (Thermo Fisher, UK), the protein concentration of the protein sample was measured. The total yield found to be 1.5 mg/ml factor H in 50 ml of human plasma. Western blotting and SDS-PAGE were used to verify that the isolated protein was FH (Appendix 1 L&K).

2.1.3 Purification of native human C4BP

Dr Robert B. SIFH ((MRC Immunochemistry Unit, Department of Biochemistry, University of Oxford, and Dr Anna Blom, Lund University, Malmo, Sweden, kindly provided C4BP. It was purified from human plasma as described in (99). The provided samples were subjected to confirming identity using SDS-PAGE and western blotting (Appendix 1 H&G).

2.1.4 Purification of properdin

The purification of FH is done according to the previous protocol (100). 100 ml of plasma was adjusted to final concentration of 5 ml of EDTA at a pH of 8. Contaminants were removed by filtering the plasma using Whatman filter paper after being centrifuged for 10 minutes at 5000 x g. Three-bed volumes of HEPES buffer (10 mM HEPES, 140 mM NaCl, 0.5 mM EDTA, pH 7.4) were used to wash an IgG-Sepharose column. To deplete C1q, the plasma was passed through an IgG-Sepharose column. Depleted C1q samples were passed through the anti-properdin column and rinsed with three-bed volumes of HEPES buffer. The bound properdin was eluted using 3M MgCl2. To get rid of any small minor impurities, they were removed by dialysing the eluted samples against HEPES buffer and stirred overnight at 4°C, followed by passing through an ion exchange column (HiTrap Q FF-Sepharose, GE Healthcare, UK). The total yield found to be 1.2 mg/ml properdin in 100 ml of human plasma. The western blotting and SDS-PAGE analysis were used to confirm the protein identity (Appendix 1 N&M).

2.2 Expression of recombinant proteins

2.2.1 Expression of rfhSP-D, DC-SIGN, ghA, ghB, ghC modules of human C1q, and properdin-TSR4+5

2.2.1.1 Competent Cells

10 ml of Luria Broth (LB) medium (Fisher BioReagents) was inoculated with one colony of E. Coli BL21 (λDE3) pLysS (Invitrogen, UK) and incubated overnight at 37°C on a shaker. The following day, 10 ml of fresh LB media were added to 500 µl of the overnight culture. The bacteria culture growth reached 0.3–0.4 at OD600. Followed by centrifugation at 2000 x g for 5 min. The cells pellet was resuspended in 1 ml of 0.1 M CaCl2. The cell suspension was mixed with a final volume of 12.5 ml of CaCl2 and left on ice for 1 h. Following incubation, the cells

underwent another 5-minute, 2000-x-g centrifugation, and the supernatant was disposed of. The cell pellet was again suspended in 2ml of 0.1 M CaCl2 for transformation.

2.2.1.2 Transformation of cells

1 µg of expression constructs for the properdin-TSR4+5, C1q – globular heads (ghA, ghB, and ghC), DC-SIGN and rfhSP-D were mixed with 100 µl of competent cells (101-104), respectively. For 1h, the mixture was incubated on ice. The bacterial cells were exposed to a 90-second heat shock at 42°C and immediately incubated on ice for 5 min. After adding 800 µl of LB medium to the transformed cells, they were incubated in a shaker for 45 min at 37°C. The cells were spread out on an LB agar plate with 100 µg/ml of ampicillin and kept in an incubator overnight at 37°C.

2.2.1.3 Pilot-Scale Expression

Single bacteria colony was added to 4 sets, each containing 1 ml of LB medium supplemented with 100 µg/ml ampicillin. The cultures were then incubated overnight at 37°C in a shaking incubator. The next day, 500 µl of the primary culture was added to 10 ml of LB medium containing the antibiotics mentioned above, and it was shaken at 37°C for the OD600 to reach 0.6 to 0.8. Followed this, a colony was induced with 0.4 mM Isopropyl β-D-1-thiogalactopyranoside (IPTG) (Sigma Aldrich, UK), and a one ml un-induced sample was obtained as a control. Induced and uninduced cultures were incubated on a shaker for 3 hours at 37°C. After incubation, 1ml samples from both the induced and uninduced cultures were centrifuged for 10 min at 13,800 × g. Then, the cell pellets were combined with 100 µl of 2x treatment buffer, which included 10% glycerol, 2% SDS, 0.1% bromophenol blue, 50% mM Tris pH 6.8, and 2% β-mercaptoethanol. The mixture was then heated for 10 min at 100°C. The expression in the samples have been analysed by loading 20 µl of each sample into a 12% SDS-PAGE gel.

2.2.1.4 Large-Scale Expression

A successful protein expression colony from the pilot scale expression was added into 25 ml of LB medium supplemented with 100 µg/ml ampicillin and incubated overnight at 37°C on a shaker. The next day, 12.5 ml was added to 500 ml of LB medium containing 100 µg/ml ampicillin and incubated at 37°C until the OD600 of 0.6 was reached. Then, 0.4 mM IPTG (isopropyl β-D-1-thiogalactopyranoside) (Sigma Aldrich, UK) was added to the 500 ml sample and incubated for 3 h at 37°C (1 ml un-induced sample was used as a control). After

incubation, the induced and uninduced cultures were centrifuged for 15 min at 12,000 × g. The cell pellet was stored at -20 °C for subsequent purification processes.

2.2.1.5 Purification of rfhSP-D

rfhSP-D was produced and purified as previously described (101). To put it briefly, plasmid pUK-D1, which comprises cDNA sequences for the α-helical neck and CRD region of recombinant fragment human SP-D, was transformed into the Escherichia coli BL21 (λDE3) pLysS bacterial strain (Invitrogen). 500 ml of LB medium supplemented with 100 µg/ml ampicillin and 34 µg/ml chloramphenicol (Sigma-Aldrich) was inoculated with a primary inoculum of 25 ml bacterial culture, and the mixture was grown until an OD600 was 0.6. For 3 h, the bacterial cells were induced with 0.5 mM IPTG (Sigma-Aldrich). The bacteria culture was centrifuged at 13,800 × g for 10 min at 4°C. The lysis solution (50 mM Tris–HCl pH 7.5, 200 mM NaCl, 5 mM EDTA pH 8, 0.1% v/v Triton X–100, 0.1 mM phenyl-methyl-sulfonyl fluoride, 50 µg/ml lysozyme) was added to the IPTG-induced bacterial cell pellet. Then, sonication was performed (five cycles of 30 seconds each). After that, the sonicated mixture was centrifuged for 15 min at 12,000 x g. A refolding buffer (8 M urea, 50 mM Tris–HCl pH 7.5, 100 mM NaCl, and 10 mM 2-mercaptoethanol (BME)) was used to denature and renature the resultant inclusion bodies of rfhSP-D. Then, the dialysate was passed via a 5-ml maltose–agarose affinity column (Sigma–Aldrich). Bound protein was eluted using 10 mM EDTA buffer containing 50 mM Tris–HCl pH 7.5 and 100 mM NaCl (elusion buffer). The protein was verified by western blotting and SDS-PAGE analysis Appendices 1 B&A). The total yield was 3 mg.

2.2.1.6 Purification of soluble DC-SIGN

The production and purification of DC-SIGN were done following the previous protocol (102). BL21 (λDE3) were made to express a tetrameric version of DC-SIGN after being transformed with a pT5T construct. The bacteria were cultured in 500 ml LB medium containing 100 µg/mL ampicillin until the OD600 reached 0.7 at 37°C. 0.4 IPTG was added to the bacteria culture to induce DC-SIGN expression, and it was incubated for 3 h at 37°C. For 15 min, the bacteria culture was centrifuged at 4,500 × g at 4°C. The cell pellet was then treated with 22ml of lysis buffer contains22 mL of lysis buffer containing 100 mM Tris, pH 7.5, 0.5 M NaCl, lysozyme (50 µg/mL), 2.5 mM EDTA, pH 8.0, and 0.5 mM phenylmethylsulfonyl fluoride (PMSF), and left to stir for 1 h at 4°C. Next, the bacteria cells were sonicated (10 cycles of 30 s each, with intervals of 2 min). The sonicated suspension was spun at 10,000 g for 15 min at 4°C. Next,

the inclusion bodies were dissolved in 20 mL of 6 M urea, 10 mM Tris–HCl, pH 7.0, and 0.01% BME. The mixture was centrifuged at 13,000 ×g for 30 min at 4°C, the supernatant was stirred and dropped-wise diluted 5x with loading buffer that contains 25 mM Tris–HCl pH 7.8, 1 mM NaCl, and 2.5 mM CaCl2. Followed by dialysed it against 2 L of loading buffer, changes every 3 h. After a 15 min centrifugation at 12,000 ×g at 4°C, the supernatant was passed through a 5 mL mannan-agarose column (Sigma) previously pre-equilibrated with loading buffer. Then, the protein was eluted using elution buffer containing 2.5 mM EDTA, 1 mM NaCl, 25 mM, and Tris–HCl pH 7.8. The total yield was 1.5 mg. The protein was verified using western blotting and SDS-PAGE analysis Appendix 1 P&O).

2.2.1.7 Purification of ghA, ghB, and ghC- the modules of human C1q

ghA, ghB, and ghC chains fused to maltose-binding protein (MBP0) were produced and purified following the previously described (103). A 500 mL LB medium supplemented with 100 µg/mL ampicillin was inoculated with 12.5 mL of E. Coli BL21 primary culture expressing the proteins. Next, the bacteria culture was incubated on a shaker at 37 °C for 3 h until the OD600 reached 0.6. Then, the culture was induced for protein expression using 0.4 mM IPTG and incubated for 3 h at 37 °C. The culture was then centrifuged at 13,800× g for 10 min at 4°C. The cells pellet was lysed in 25 ml of lysis buffer (20 mM Tris-HCl, pH 8.0, 0.5 M NaCl, 1 mM EGTA, pH 7.5, 1 mM EDTA, pH 7.5, 5% v/v glycerol, 0.2% v/v Tween 20, 0.1 mM PMSF, and 50 µg/mL lysozyme) for 30 min at 4°C. The lysate was sonicated for 12 cycles at 60 Hz for 30 seconds with an interval of 2 min. The sonicated lysate was centrifuged for 30 min at 4 °C at 15,000× g. 125 mL of buffer I (20 mM Tris-HCl, pH 8.0, 100 mM NaCl, 1 mM EDTA, pH 7.5, 0.2% v/v Tween 20, and 5% v/v glycerol) was added to the supernatant. The diluted supernatant was passed through a 5 mL amylose resin column (New England Biolabs). 150 mL of buffer I and 250 mL of buffer II (buffer I without Tween 20) were used to wash the column. 100 mL of buffer II containing 100 mM maltose was used to elute the fusion protein. The proteins were verified by western blotting and SDS-PAGE analysis (Appendices 1 J&I). The total yield found to be 2 mg of each globular fused chain.

2.2.1.8 Expression and purification of properdin-TSR4+5

The production and purification of TSR4+5 fused with MBP are done following the previous protocol(100). A 500 mL LB medium supplemented with 100 µg/mL ampicillin was inoculated with a 12.5 mL E. Coli BL21 primary culture containing the protein. The culture was incubated

for 3 h at 37°C until the OD600 reached 0.6. The bacterial culture was centrifuged at 13,800 x g for 10 min 25 mL of lysis buffer (20 mM Tris-HCl (pH 8.0), 0.5 M NaCl, 1 mM EGTA (pH 7.5), 1 mM EDTA (pH 7.5), 5% v/v glycerol, 0.2% v/v Tween 20, 0.1 mM PMSF, and 50 µg/mL lysozyme) was added to the cells pellet. The lysate was sonicated for 12 cycles at 60 Hz for 30 seconds with an interval of 2 min. The sonicated lysate was centrifuged for 30 min at 4 °C at 15,000× g. The lysate was then suspended with 125 mL of buffer I (20 mM Tris-HCl, pH 8.0, 100 mM NaCl, 1 mM EDTA, pH 7.5, 0.2% v/v Tween 20, and 5% v/v glycerol). The diluted supernatant was loaded onto a 5 mL amylose resin column (New England Biolabs). Next, 150 mL of buffer I and 250 mL of buffer II (buffer I without Tween 20) were used to wash the column. 100 mL of buffer II containing 100 mM maltose was used to elute the fusion protein. The total yield was 2 mg. The protein was verified using western blotting and SDS-PAGE analysis (Appendix 1 D&C).

2.2.2 Endotoxin Removal of DC-SIGN, rfhSP-D, ghA, ghB, ghC modules of human C1q and MBP, and properdin-TSR4+5 and Limulus Amoebocyte Lysate Assay

For the removal of endotoxin contamination of the eluted recombinant proteins, including DC-SIGN, rfhSP-D, C1q globular head ghA, ghB, ghC, and properdin-TSR4+5, a PierceTM High-Capacity Endotoxin Removal Resin (ThermoScientificTM) was utilised. The endotoxin removal resin (10 ml volume column) was washed with 50 ml of sterile H2O and then with 50 ml of 1% sodium deoxycholate (Sigma-Aldrich) more than once. The column was loaded with the pure recombinant DC-SIGN, rfhSP-D, C1q globular head ghA, ghB, ghC, and properdin-TSR4+5. Then, the protein concentration was measured using a Nanodrop spectrophotometer. The endotoxin levels in the purified recombinant protein samples were less than 0.5 pg/µg, measured using the QCL-1000 Limulus amoebocyte lysate technology (Lonza).

2.3 Sodium Dodecyl Sulphate-Polyacrylamide Gel Electrophoresis (SDS-PAGE)

2.3.1 SDS PAGE preparation

The sodium dodecyl sulfate-polyacrylamide gel electrophoresis (SDS-PAGE) separated proteins according to their charge-to-mass ratio. Making the resolving 12% gel (10 ml) and stacking gel (5 ml gel) requires mixing the reagents below in the provided Table 2.1.

Table 2.1: Volumes of Resolving and Stacking Components for 12% SDS-PAGE Gel

Resolving gel (12%)		Stacking Gel (5%)	
Reagents	Volume (mL)	Reagents	Volume (mL)
Distilled water	3.3	dist	3.4
30% Bis-Acrylamide mix	4.0	30% Bis-Acrylamide mix	0.83
1.5M Tris-HCl, pH8.8	2.5	1.0M Tris-HCl, pH6.8	0.63
10% SDS	0.1	10% SDS	0.05
10% Ammonium Persulfate	0.1	10% Ammonium Persulfate)	0.05
Tetramethylethylenediamine	0.015	Tetramethylethylenediamine	0.015

2.3.2 Sample Preparation and Electrophoresis

Treatment buffer (50 mM Tris pH 6.8, 2% β-mercaptoethanol, 2% SDS, 0.1% bromophenol blue, and 10% glycerol) was applied to protein samples that were going to be separated. The samples underwent a 10-min heat treatment at 100°C. The ready-made samples were then put into the SDS-PAGE gel wells with a 10–250 kDa pre-stained protein ladder (Thermo Fisher Scientific). The electrophoresis gel was put together. The samples were separated by running them at 90V in 1× running buffer (0.1% SDS, 192 mM glycine, and 25 mM Tris). The separation process for the protein was run for 120 min. The separated proteins are subjected to western blot analysis.

2.3.3 Staining of SDS-PAGE gel

A staining solution [0.1% Coomassie blue (Fisher Scientific), 10% acetic acid (Fisher Scientific), 40% methanol (Fisher Scientific), and 50% H2O] was used to stain the gels for 2 h. Next, the stained gel is subjected to a destaining solution (10% acetic acid, 40% methanol, and 50% H2O), making the gel's protein bands visible.

2.4 Western Blotting

Western Blotting technique was employed to analyse immunoreactivity and verify the identity of the purified proteins. First, the proteins were separated through SDS-PAGE and then electrophoretically transferred onto an activated PVDF membrane (Millipore). This transfer process was conducted in 1× transfer buffer containing 25mM Tris–HCl pH 7.5,

190mM glycine, and 20% v/v methanol, with an applied current of 320mA for 2 h. Following the transfer, the PVDF membrane was subjected to a blocking step at 4℃ for 2 h, using a solution of 1× PBS containing 5% v/v skimmed milk powder. This blocking process aimed to prevent the nonspecific binding of antibodies. Subsequently, the membrane was washed three times with PBS, each wash lasting 5 min, to remove any residual unbound substances and achieve optimal conditions for subsequent antibody probing.

The membrane was incubated with specific primary antibodies targeting the respective proteins for protein detection and confirmation. The primary antibodies used were polyclonal rabbit anti-human SP-D, rabbit anti-human C1q, rabbit anti-human C4BP, rabbit anti-human properdin polyclonal antibodies, or monoclonal mouse anti-human factor H (MRCOX23), all produced in the MRC immunochemistry unit, Oxford. All primary antibodies were diluted at 1:1000 and applied to the membrane for 1 h at room temperature (RT). The membrane was washed three times with PBST Buffer (PBS + 0.05% Tween 20) for 10 min per wash to remove any unbound primary antibodies. Following the washes, the membrane was probed with either goat anti-mouse IgG-Horseradish peroxidase (HRP)-conjugate or goat anti-rabbit IgG HRP-conjugate, diluted at 1:1000, and incubated at RT for 1h.

Subsequently, the membrane was rewashed with PBST to eliminate excess secondary antibodies. A SIGMAFAST™ 3,3’-Diaminobenzidine (DAB) substrate kit (MERCK) was employed to visualise the proteins on the membrane, and the membrane was developed according to the kit's instructions. That allowed for the visualisation of the proteins of interest.

2.5 Direct-Binding ELISA

In the first set of experiments, polystyrene microtiter plates (PMP) were coated overnight at 4°C with decreasing concentrations (2, 1, 0.5, or 0 µg per 100 µl/well) of recombinant DC-SIGN or rfhSP-D using carbonate/bicarbonate (CBC) buffer, pH 9.6. After washing the wells thrice with PBST Buffer, they were blocked with 2% w/v BSA in PBS for 2 h at 37°C. Following three additional washes with PBST, a constant recombinant SARS-CoV-2 spike protein (RP-87680, Invitrogen, Waltham, MA, USA) (2 µg per 100 µl/well) was added to the wells and incubated for 2 h at 37°C. Subsequently, the wells were washed with PBST to remove unbound protein.

Microtiter wells were coated overnight at 4°C with DC-SIGN protein (2 µg; 100 µl/well) for the competitive ELISA and then blocked. Fixed concentrations of SARS-CoV-2 Spike protein (2 µg;

100 µl/well) and decreasing concentrations (4.0, 2.0, 1.0, 0.5, 0 µg; 100 µl/well) of rfhSP-D in calcium buffer were added to the wells as competing proteins. The plate was incubated at 37°C for 1.5 h, followed by an additional 1.5 h at 4°C. Then, the wells were washed with PBST.

In another set of experiments, PMP were coated with various concentrations of C1q , C4BP, FH or FP (1, 0.5, 0.125, and 0 µg/well) using CBC buffer, pH 9.6, overnight at 4°C. Negative control wells were coated with BSA (1 µg; 100 µl/well). After three washes with PBST buffer, the wells were blocked with 2% w/v BSA in PBS for 2 h at 37°C, followed by three washes with PBST to remove excess BSA. A constant dose of recombinant SARS-CoV-2 S protein (1 µg; 100 µl/well) or recombinant SARS-CoV-2 RBD protein (40592-V08H, SinoBiological, Beijing, China) (1 µg; 100 µl/well) was added to the respective wells coated with C1q, C4BP, FH or FP. In parallel experiments, fixed concentrations of C1q, C4BP, FH or FP (1, 0.5, 1.25, and 0 µg/well) were added to immobilised SARS-CoV-2 S (1 µg; 100 µl/well) or RBD (1 µg; 100 µl/well) coated wells. The wells were then washed with PBST. The binding of viral proteins to immobilised C1q, C4BP, FH or FP, were detected using polyclonal rabbit anti SARS-CoV-2 spike.

The binding of the immobilised virus to the proteins was detected using specific primary antibodies, including rabbit anti-human C1q, rabbit anti-human C4BP, rabbit anti-human properdin polyclonal antibodies, or monoclonal mouse anti-human factor H (MRCOX23) produced in the MRC immunochemistry unit, Oxford. Primary antibodies were diluted at a ratio of 1:5000 and incubated for 1 h at 37 °C. The wells were washed three times with PBST to remove any unbound antibodies.

Appropriate secondary antibodies, such as goat anti-mouse IgG-Horseradish peroxidase (HRP)-conjugate or goat anti-rabbit IgG HRP-conjugate, were used for secondary detection. The secondary antibodies were used at a dilution of 1:5000 and incubated for 1 h at 37°C to tag the primary antibodies. Binding was detected using the 3,3’,5,5’-Tetramethylbenzidine (TMB) substrate set following the manufacturer's instructions, and the reaction was stopped with 1M sulphuric acid. The absorbance was measured at 450 nm using an iMark™ microplate absorbance reader.

2.6 Cell Culture

HEK 293T and A549 cells, both epithelial cell lines, were cultured in growth media comprising Dulbecco's Modified Eagle's Medium (DMEM) with Glutamax (Gibco), supplemented with 10% v/v foetal bovine serum (FBS), 100 U/mL penicillin (Gibco), and 100 µg/mL streptomycin (Gibco). The cells were maintained at 37°C with 5% v/v CO_2 until they reached 70% confluency. In the case of HEK 293T cells, transient transfection was performed using a plasmid encoding human DC-SIGN (HG10200-UT; Sino Biological) and Promega FuGENE™ HD Transfection Reagent (Fisher Scientific). After transfection, the cells were washed and cultured in hygromycin to select HEK-293T cells expressing DC-SIGN (DC HEK) (Thermo Fisher Scientific). Similarly, THP-1 cells were cultured in growth media and stimulated with PMA (10 ng/mL) combined with IL-4 (1000 units/mL) for 72 h to induce the expression of DC-SIGN surface molecules (105).

As for A549, lung epithelial cells were incubated at 37°C with 5% v/v CO_2 until they reached 70% confluency. Transient co-transfection was carried out by introducing a plasmid expressing human ACE2 (pCDNA3.1+-ACE2) and another plasmid encoding TMPRSS2 (pCAGGS-TMPRSS2) into the cells using Promega FuGENETM HD Transfection Reagent. The following day, the transfected cells were cultured with hygromycin and puromycin (Thermo Fisher Scientific, Waltham, MA, USA) to select A549 cells co-expressing human ACE2 and TMPRSS2, referred to as A549-hACE2+TMPRSS2 cells. Evaluation of hACE2 and TMPRSS2 expression was performed through western blotting, employing anti-hACE2 (Sino Biological Inc., Beijing, China, Cat: 80031-RP01) and anti-human TMPRSS2 (Sino Biological Inc., Cat: 204314-T08) antibodies, respectively (Appendices 4 A&B).

2.7 Viral cell entry assay

2.7.1 Preparation of SARS-CoV-2 Spike Protein Pseudotyped lentiviral particles

Pseudotyped lentiviral particles were provided by Dr Nigel Temperton, Viral Pseudotype Unit, Medway School of Pharmacy, University of Kent and Greenwich, Kent, which were generated following established protocols (106).

2.7.2 Treatment of SARS-CoV-2 Pseudotyped lentiviral particles

A luciferase reporter-based cell entry assay was conducted using SARS-CoV-2 lentiviral pseudotyped particles. The latter were pre-incubated with 20 µg/mL of rfhSP-D, C1q, C4BP,

FH, FP, TRS4+5, or ghs modules (ghA, ghB, or ghC) for a duration of 2 h at RT to investigate the effect of these proteins on cell entry. After the pre-incubation, the mixture was used to challenge THP-1 or A549-hACE2 + TMPRSS2 cells. The combination of SARS-CoV-2 lentiviral pseudoparticles and HTP-1 or A549-hACE2 + TMPRSS2 cells served as the untreated control cells for rfhSP-D, C1q, C4BP, FH or FP. Additionally, SARS-CoV-2 lentiviral pseudoparticles + MBP + A549-hACE2 + TMPRSS2 cells were considered the untreated control cells for the ghs modules or TSR4+5.

2.7.3 Luciferase reporter assay

The potential impact of rfhSP-D, C1q, C4BP, FH, FP, TSR+5 or ghs (A, B, and C) on SARS-CoV-2 pseudotype particle cell entry was assessed using a luciferase reporter assay. THP-1 or A549-hACE2 + TMPRSS2 cells were seeded at a density of 20,000 cells per well in a 96-well plate and incubated overnight in complete growth media at 37 °C.

The cells were then challenged with SARS-CoV-2 lentiviral pseudoparticles that had been pretreated with 20 µg/mL of rfhSP-D, C1q, C4BP, FH, FP, TSR+5 or ghs (A, B, and C). That was carried out in incomplete growth medium - DMEM with Glutamax (Gibco), supplemented with 100 U/mL penicillin (Gibco) and 100 µg/mL streptomycin (Gibco). The cells were incubated at 37 °C for 24 hours. Followed by 2x washing steps with PBS, a fresh complete growth medium (incomplete growth medium + 10% v/v FBS) was added. The cells were then incubated for an additional 48 h at 37 °C. The ONE-GloTM Luciferase Assay System (Promega) was used to quantify luciferase activity as a measure of cell entry. The luciferase activity was measured using the Clariostar Plus Microplate Reader (BMG Labtech, Cary, NC, USA), recording relative luminescence units (RLU).

2.7.4 NF-κB activity assay

A luciferase-based reporter assay was performed to evaluate the impact of C1q, C4BP, FH, and FP on NF-κB activity during SARS-CoV-2 infection. The assay utilised a plasmid containing multiple copies of NF-κB consensus sequences fused to the TATA-like promoter region of the herpes simplex virus thymidine kinase (HSV-TK) promoter. This engineered vector enables direct measurement of NF-κB pathway activity by assessing the binding of the transcription factor to the κ-enhancer region. A549-hACE2+TMPRSS2 cells were transfected with the pNF-κB-LUC plasmid (T 631904; Clontech, Fitchburg, WI, USA) using the Promega FuGENETM HD Transfection Reagent. Following transfection, the cells were incubated at 37 °C in a complete

growth medium for 48 h. Subsequently, the cells (20,000 cells per well) were seeded in a 96-well plate and incubated overnight in a complete growth medium at 37 °C. The cells were then challenged with SARS-CoV-2 S protein (500ng/ml) pre-treated with 20 µg/ml of C1q, C4BP, FH, or FP for 2 h at RT. The cells were incubated for 24 h at 37 °C in an incomplete growth medium. A control group consisting of A549-hACE2+TMPRSS2 cells exposed to SARS-CoV-2 S protein without C1q, C4BP, FH or FP treatment was included. Luciferase activity was quantified as previously described to measure NF-κB activation. The luciferase activity corresponded to the level of NF-κB activation induced by the binding of endogenous NF-κB to the κ-enhancer region. The measurements were obtained using the methods mentioned above.

2.8 Cell binding assay

To investigate the impact of rfhSP-D, C1q, C4BP, FH, FP, TSR+5 or ghs (A, B, and C) C1q or C4BP treatment on the binding of SARS-CoV-2 pseudotypes to A549, D-HEK or DC THP-1 cells, a cell-binding assay was performed. A549-hACE2+TMPRSS2 , DC-HEK or DC THP-1 cells were seeded at a density of 20,000 cells per well in a 96-well plate and incubated overnight at 37 °C in a growth medium. The following day, the cells were challenged with SARS-CoV-2 lentiviral pseudoparticles that had been pretreated with 20 µg/mL of rfhSP-D, C1q, C4BP, FH, FP, TSR+5 or ghs (A, B, and C). The cells were incubated with the treated pseudoparticles in an incomplete growth medium for 2 h at 37 °C. Subsequently, the plate was washed three times with PBS to remove unbound particles. To fix the cells, they were treated with 1% v/v paraformaldehyde (PFA) at RT for 1 min. After the fixation, the cells were washed three times with PBS. Next, the cells were incubated with rabbit anti-SARS-CoV-2 spike polyclonal antibodies (1:200) for 1 h at 37 °C. Following the incubation, the wells were rewashed. The wells were probed with Alexa Fluor 488 conjugated goat anti-rabbit antibodies (1:200) (Abcam, Cambridge, UK) to detect the binding of the primary antibodies. The probing step lasted for 1 h at RT. Finally, the plate was read using a Clariostar Plus Microplate Reader (BMG Labtech, Cary, NC, USA).

2.9 Fluorescence microscopy

DC-HEK cells were cultured on 13 mm glass coverslips to form a monolayer. The cells were then incubated with SARS-CoV-2 spike pseudotypes (50 µl) at 37°C. After 30 min, the cells were rinsed with PBS and fixed using 1% w/v PFA for 1 min. Subsequently, the cells were

washed three times with PBS. The cells were treated with 5% w/v BSA in PBS for 30 min to block nonspecific binding. Followed by the cells were incubated with mouse anti-human DC-SIGN antibodies and rabbit anti-SARS-CoV-2 Spike antibodies for 30 min. Then, the cells were washed to remove any unbound antibodies. The cells were incubated with a staining buffer containing Alexa Fluor 647 conjugated goat anti-mouse antibody, Alexa Fluor 488 conjugated goat anti-rabbit antibody, and Hoechst dye for nuclear staining. This incubation step was carried out in the dark for 45 min. Following the incubation, the mounted coverslips were rinsed with PBS to remove any excess staining solution. The coverslips were then visualised using a Leica DM4000 microscope.

2.10 Modulation of SARS-CoV-2 Pseudoparticle-Induced Infection by C1q, C4BP, FH, FP or TSR4+5

2.10.1 SARS-CoV-2 S protein treatment

DC-HEK and DC-THP-1 cells were seeded overnight in a growth medium at a density of 0.5 x 10^6 cells. The following day, SARS-CoV-2 Spike protein (500 ng/mL) was pre-incubated with rfhSP-D (20 µg/mL) for 2 h at RT. The pre-incubated mixture was then added to DC-THP-1 cells in a serum-free medium. After incubation for 6h, 12h, 24h, and 48h, the cells were gently washed with PBS to remove any unbound proteins. Subsequently, the cells were pelleted for further analysis.

2.10.2 SARS-CoV-2 alphaviral pseudoparticles treatment

SARS-CoV-2 alphaviral pseudoparticles, which contain the structural proteins S, E, M, and N (Ha-CoV-2 Luc; Virongy, Manassas, VA, USA), were used for the experiment. Before challenging A549-hACE2+TMPRSS2 cells, the pseudoparticles were pre-incubated with 20 µg/mL of C1q, C4BP, FH, FP or TSR+5 for 2h at room RT. Cytokine/ chemokine gene expression was analysed through RT-qPCR (see below). SARS-CoV-2 alphaviral pseudoparticles were used in conjunction with A549-hACE2+TMPRSS2 cells alone as untreated.

2.10.3 Quantitative Real-time (qRT) Polymerase Chain Reaction (PCR) analysis

2.10.3.1 Total RNA Extraction

The RNA extraction process was performed on the SARS-CoV-2- treated and the untreated cell pellets using the GenElute Mammalian Total RNA Purification Kit (MERCK), per the manufacturer's instructions.

First, the cell pellets were lysed using a lysis solution (250 µl per 0.5 x 10^6 cells) containing 2-mercaptoethanol (2.5 µl). The lysate was vigorously vortexed until clumps disappeared. Then, 70% ethanol (250 µl) was added to the lysate, gently vortexed, and transferred to the RNA binding columns. The columns containing the lysate mixed with ethanol were centrifuged at 13,000 ×g for 15 seconds to bind the RNA to the columns. The columns were washed with washing buffer I and two washes with buffer II (provided in the RNA extraction kit). After the washes, the columns were transferred to fresh 2 ml Eppendorf tubes. 50 µl of elution buffer was added to the columns were centrifuged for 1 min at 13,000 × g to elute the RNA. That resulted in the collection of the extracted RNA.

2.10.3.2 DNase Treatment and cDNA Synthesis

To remove contaminating DNA from the purified RNA of SARS-CoV-2 challenged DC HEK, DC THP-1 or A549-hACE2 cells and their respective controls, DNase treatment with DNase I (Sigma-Aldrich) was performed. For the treatment, 5 µl of DNase I enzyme and 5 µl of 10x buffer provided in the kit were added to the previously purified total RNA extracts. The mixture was gently inverted to ensure thorough mixing. The DNase I-treated samples were then incubated at RT for 15 min. 5 µl of stop solution was added to stop the reaction. The samples were heat-inactivated at 70°C to inactivate DNase I and RNases. The concentration of total RNA was measured at A260 nm using NanoDrop 2000/2000c (Sigma-Aldrich), and the purity of RNA was assessed by calculating the A260/A280 ratio, which was between 1.8 and 2.1, respectively.

The High-Capacity RNA-to-cDNA™ Kit (Applied Biosystems™) was used per the manufacturer's instructions for cDNA synthesis. A master mix was prepared, which included 10 µl of 2x RT buffer, 1 µl of 20x enzyme mix, 2 µg of DNase I-treated total RNA extract, and nuclease-free H_2O to make a final volume of 20 µl. The samples were loaded into a thermal cycler and incubated at 37°C for 60 min, followed by a 5-min incubation at 95°C. After incubation, the samples were held at 4°C until further use and stored at -20 °C for qPCR analysis.

2.10.3.3 Primers generation

The specificity of both forward and reverse primer sequences was ensured by designing them using the Primer-BLAST software (Basic Local Alignment Search Tool). The primer sequences used in this study can be found in Table 2.2. The primers were obtained from the "Custom DNA Oligos" (MERCK).

Table 2.2: Target genes, forward primers, and reverse primers used for qPCR analysis

Gene	Forward Primer	Reverse Primer
18S	5′-ATGGCCGTTCTTAGTTGGTG-3′	5′-CGCTGAGCCAGTCAGTGTAG-3′
TNF-α	5′-AGCCCATGTTGTAGCAAACC-3′	5′-TGAGGTACAGGCCCTCTGAT-3′
IL-6	5′-GAAAGCAGCAAGAGGCACT-3	5′-TTTCACCAGGCAAGTCTCCT-3′
IL-8	5′-GTGCAGTTTTTGCCAAGGAG-3′	5′-CACCCAGTTTTCCTTGGGGT-3′
NF-κB	5′-GTATTTCAACCACAGATGGCACT-3′	5′-AACCTTTGCTGGTCCCACAT-3′
RANTES	5′-GCGGGTACCATGAAGATCTCTG-3′	5′-GGGTCAGAATCAAGAAACCCTC-3′
IFN-α	5′-TTTCTCCTGCCTGAAGGACAG-3′	5′-GCTCATGATTTCTGCTCTGACA-3′
IL-1β	5′-GTGCAGTTTTGCCAAGGAG-3′	5′-ACGTTTCGAAGATGACAGGCT-3′

2.10.3.4 Gene Expression Analysis by qPCR

The mRNA expression levels of various pro-inflammatory targeted genes, as listed in Table 2.2, were measured using a qPCR assay. Each qPCR reaction was performed in triplicates, comprising 5 µl of Power SYBR Green MasterMix (Applied Biosciences), 75 nM of forward and reverse primers obtained as described in section 2.10.3.3, 500 ng of the previously synthesised cDNA from section 2.10.3.2, and Nuclease-free H_2O to adjust the total volume to 10 µl per well. The qPCR was carried out using a StepOnePlus System (Applied Biosystems™) with the following cycling conditions: an initial denaturation at 95°C for 5 min, followed by 45 cycles of 95°C for 10 s, 60°C for 10 s, and 72°C for 10 s. The specificity of the qRT-PCR assay was determined by analysing the melting curves. The expression levels of the targeted genes were normalised using 18s RNA as an endogenous control. The relative expression (RQ) was calculated by comparing it to the calibrator and the untreated cells (DC-SIGN HEK, THP-1 or A549). The RQ value was calculated using $RQ = 2^{(-\Delta\Delta Ct)}$.

2.11 *In-silico* Docking Analysis

2.11.1 rfhSP-D interaction with Spike and DC-SIGN

A blind molecular docking approach using the ZDOCK module of Discovery Studio 2021 was employed to predict tripartite complex models of DC-SIGN tetramer, Spike trimer, and rfhSP-D trimer. The structural coordinates of DC-SIGN (CRD), Spike, and rfhSP-D were obtained from the Protein Data Bank (PDB) with the following IDs: 1K9I, 6XM3, and 1PW9. The docking process consisted of two stages. In the first stage, the DC-SIGN (CRD) tetramer was individually blind-docked with the rfhSP-D trimer (complex A) and the spike trimer (complex B). The top-ranked docking poses were analysed to assess intermolecular interactions and were compared with previous studies to validate the results (41). In the second stage, the selected docked pose from complex A was further blind docked with the spike trimer to generate a tripartite complex of DC-SIGN (CRD), Spike, and rfhSP-D (complex C). The tripartite complex was selected based on the docking score and the presence of intermolecular interactions that were consistent with previous reports (107).

2.11.2 FP interaction with Spike and ACE2

A blind docking approach was utilised to generate a fusion peptide (FP) and spike protein complex. The second-ranked docking pose was consistent with *in vitro* observations, demonstrating that the TSR4 and TSR5 domains of FP interacted with the receptor-binding domain (RBD) and N-terminal domain (NTD) of the spike protein, respectively, through hydrogen bonding, electrostatic, and hydrophobic interactions. To further investigate the interaction between FP, spike protein, and the angiotensin-converting enzyme 2 (ACE2) receptor, a tripartite complex structure was created by docking the electron microscopy structure of ACE2 onto the FP-bound spike protein. In the top-ranked pose, ACE2 was observed to interact with the spike protein, which is consistent with the electron microscopy structure (PDB ID: 7KNB). FP interacted with the spike protein and ACE2 in the tripartite complex through various non-bonded contacts in each subunit.

Additionally, the TSR4 domain of FP was found to be in proximity to the ACE2 receptor and exhibited interactions with both the spike protein and ACE2. The binding affinity of the ACE2 receptor for the unbound spike protein and the FP-bound spike protein was compared using the ZDOCK score and binding free energy. These scores indicated that the ACE2 receptor

exhibited a stronger affinity for the FP-bound spike protein than the unbound spike protein. That suggests that FP may enhance the affinity of the spike protein for ACE2 by engaging in interactions with both proteins within the tripartite complex.

2.12 Statistical analysis

The graphs were created, and statistical analysis was performed using GraphPad Prism 9.0 software. Statistical significance was determined as described in the figure legends. The mean difference between treated and untreated cells was evaluated using the unpaired t-test. The effects of distinct cytokine types and cell treatments (C1q, C4BP, and ghs or FH, FP, and TSR4+5) were simultaneously analysed using a two-way ANOVA, considering any potential interactions between these variables. The error bars represent either the standard deviation (SD) or standard error of the mean (SEM), as specified in the figure legends.

Chapter 3

Interaction between rfhSP-D and SARS-CoV-2 virus in DC-SIGN expressing cells

3.1 Abstract

C-type lectin molecules implicated in pathogen recognition include lung surfactant protein D (SP-D) and dendritic cell-specific intercellular adhesion molecules-3 grabbing non-integrin (DC-SIGN). While DC-SIGN promotes the interaction between dendritic cells and naïve T cells to develop an antiviral immune response, SP-D plays a role in detecting and clearing lung infections. It has been demonstrated that both proteins interact with SARS-CoV-2. Also, it has been shown that rfhSP-D, a recombinant fraction of human SP-D, binds to the SARS-CoV-2 Spike protein and blocks viral entrance in ACE2 expressing cells. That inhibits viral replication. Separate from ACE2, DC-SIGN has also been found to be a SARS-CoV-2 cell surface receptor. This study aimed to investigate the immune-modulation role of rfhSP-D in SARS-CoV-2 and DC-SIGN interaction. The study found that the interaction between Spike protein and DC-SIGN was enhanced when rfhSP-D and Spike protein were co-incubated. Further research using molecular dynamics showed that this interaction was stabilised by rfhSP-D. Increased binding was observed in cell binding studies utilising DC-SIGN-expressing cells challenged with SARS-CoV-2 Spike pseudotypes pre-treated rfhSP-D. Infection assay also revealed that the uptake of SARS-CoV-2 Spike pseudotypes in cells expressing DC-SIGN was enhanced by rfhSP-D. The study also measured the mRNA expression levels of pro-inflammatory cytokines and chemokines to evaluate the immunomodulatory effect of rfhSP-D on the interaction between DC-SIGN and Spike protein. In DC-SIGN-expressing cells challenged with Spike protein, it showed that rfhSP-D treatment has downregulated the mRNA expression levels of TNF-α, IFN-α, IL-1β, IL-6, IL-8, and RANTES, in addition to NF-κB. Also, MHC class II mRNA levels were downregulated when cells expressing DC-SIGN were challenged with spike protein pre-treated with rfhSP-D. In summary, rfhSP-D improved viral uptake by macrophages like cells via DC-SIGN by stabilising the interaction between SARS-CoV-2 Spike protein and DC-SIGN. That suggests rfhSP-D has an additional function in SARS-CoV-2 infection besides suppressing viral entry.

3.2 Introduction

The innate immune system recognises pathogen-associated molecular patterns (PAMPs) through pathogen recognition receptors (PRRs) (108). Numerous innate immune cells, such as monocytes, neutrophils, macrophages, and dendritic cells (DCs), express PRRS molecules (109). Key PRRs implicated in host protection against infections are C-type lectin receptors (CLRs) and toll-like receptors (TLRs) (110). CLRs are crucial for recognising pathogenic bacteria, viruses, parasites, and fungi (111). Dectin-2, Mincle, MGL, Langerin, and DC-SIGN are examples of CLRs. By interacting with their ligands, these receptors modulate the immune response by presenting antigens and releasing cytokines (112). DCs are mainly found in tissues that encounter pathogens, such as mucosal surfaces like the lungs and nasopharynx. They are primarily in charge of triggering antigen-specific immune responses (113).

The binding of cell adhesion molecule ICAM-3 on T cells to DC-SIGN, a surface molecule on DCs, improves DC-T cell interaction (114). DC-SIGN is a 44 KDa, type II integral membrane protein with a single C-terminal carbohydrate recognition domain (CRD) supported by an α-helical neck region containing tandem repeats of a 23 amino-acid residue sequence(102). On the cell surface, DC-SIGN organises into oligomers, which improves ligand binding avidity and specificity to pathogens surfaces (115). DC-SIGN was found to facilitate Zika, Dengue, Ebola, HIV, and Cytomegalovirus infections (116-120). Dendritic cells expressing DC-SIGN are found mainly on mucosal surfaces, and it has been suggested that the interaction between DCs and T cells could be critical for HIV-1 mucosal transmission (121). Additionally, recent research has shown that DC-SIGN, apart from ACE2 expression, binds to and improves SARS-CoV and SARS-CoV-2 infection (122).

Surfactant protein D (SP-D) is a lung surfactant protein vital for mucosal immunity and homeostasis (123). It recognises glycosylated ligands on pathogens and involves its opsonization, aggregation, and enhancing phagocytosis by phagocytic cells such as macrophages (123). It has been demonstrated that SP-D binds to the SARS-CoV-2 Spike protein, preventing viral replication *in vitro* (123). Recombinant human SP-D, or rfhSP-D, has immunological properties like native SP-D (124). It has been demonstrated that rfhSP-D binds to the influenza A virus's (IAV) HA protein, inhibiting its ability to infect lung epithelial cells (124). The binding and transmission of HIV-1 to CD4+ T cells can be modulated by rfhSP-D

through direct binding to DC-SIGN (41). It has also been demonstrated that rfhSP-D functions as viral entry of SARS-CoV-2 in A549 cells expressing human ACE2 and TMPRSS2 (34, 107).

Even while the relationship between the ACE2 and Spike proteins is well-established, there is still much to learn about other elements implicated in the infection process, such as how SARS-CoV-2 is delivered to the ACE2 receptor (125). The high transmission rate of SARS-CoV-2 compared to SARS-CoV could be because of effective viral adhesion factors that improve infection to ACE2+ cells (126, 127). Thus, effective SARS-CoV-2 viral attachment and immune-hyperactivation in the lungs may be facilitated by DCs that express DC-SIGN and alveolar macrophages (128-130).

Previous studies have emphasised the function of SP-D in immune surveillance in viral recognition and the modulation of inflammatory responses (34, 41, 131). Understanding how SP-D and DC-SIGN interact during HIV-1 infection can help understand how SP-D can prevent DC-SIGN-mediated viral pathogenesis (41). It has been demonstrated that SP-D and rfhSP-D bind to the Spike protein of SARS-CoV-2, preventing viral infection and replication (34). Furthermore, it has been documented that DC-SIGN functions as an entrance receptor and facilitator for SARS-CoV-2 infection without ACE2 involvement (80). Thus, this study aimed to examine the role of rfhSP-D on SARS-CoV-2 infection mediated via DC-SIGN. The study also investigated the function of rfhSP-D in SARS-CoV-2 viral uptake by macrophage-like cells, given high expression levels of DC-SIGN on DCs and macrophages.

3.3 Results

3.3.1 Both DC-SIGN and rfhSP-D bind to SARS-CoV-2 spike protein.

An indirect ELISA assessed protein-protein interaction between rfhSP-D, DC-SIGN, and SARS-CoV-2 spike protein. DC-SIGN or rfhSP-D were coated in decreasing concentrations on microtiter plates, and an anti-SARS-CoV-2 spike antibody was then used to probe the plates. All tested concentrations of DC-SIGN (Figure 3.1A) and rfhSP-D (Figure 3.1B) showed a dose-dependent increase in binding. A competitive ELISA was carried out to determine if rfhSP-D interferes with DC-SIGN and Spike protein binding. Adding rfhSP-D improved the binding between DC-SIGN and the Spike protein in a dose-dependent pattern. (Figure 3.1C).

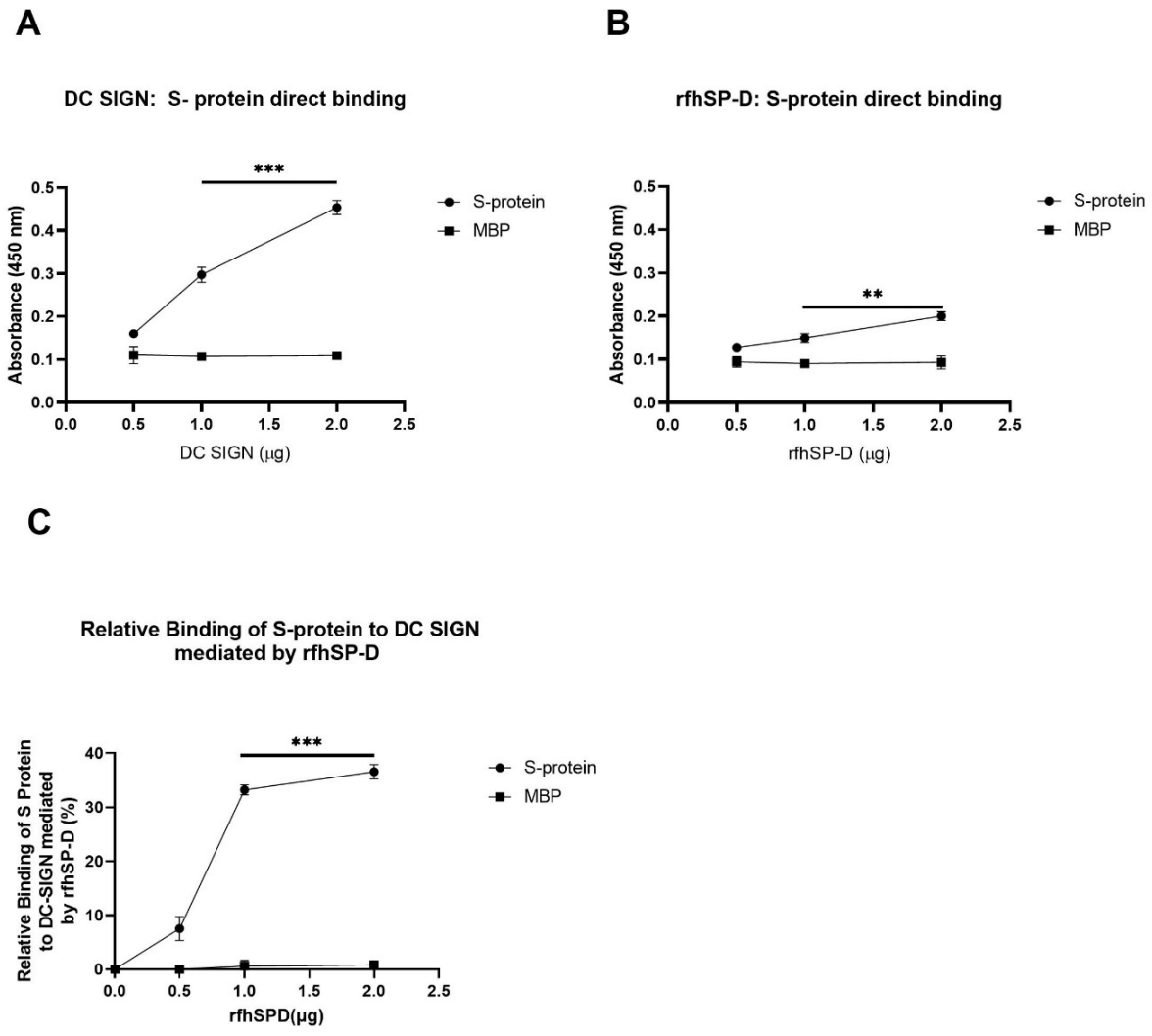

Figure 3.1: *ELISA shows SARS-CoV-2 S protein binds DC-SIGN(A) and rfhSP-D (B), where rfhSP-D increases S protein and DC-SIGN binding (C). SARS-CoV-2 Spike protein (2 µg /well) was incubated with microtiter wells coated with DC-SIGN or rfhSP-D proteins at varying doses (2, 1, 0.5, or 0 µg/ well). The binding of DC-SIGN and rfhSP-D to Spike protein was shown to be dose-dependent. A competitive ELISA (C) was performed to investigate the impact of rfhSP-D on DC-SIGN and Spike protein interaction. The addition of rfhSP-D enhanced the binding of Spike protein to DC-SIGN. The increased detectable amount of Spike protein with increasing concentrations of rfhSP-D suggests the presence of distinct binding sites for Spike protein on both C-type lectins. MBP was used as a negative control. The data were expressed as the mean of triplicates ± SD. Statistical significance was determined using the unpaired t-test (compared mean of rfhSP-D or DC-SIGN binding with S-protein to MBP) (**p < 0.01, and ***p < 0.001) (n = 3).*

3.3.2 rfhSP-D treatment enhances DC-SIGN mediated binding and uptake of SARS-CoV-2 pseudotyped viral particles

We used HEK 293T cells transfected with a full-length human DC-SIGN construct to generate a surface expression of DC-SIGN to investigate the effect of rfhSP-D on the binding of SARS-CoV-2 to DC-SIGN expressing cells. The binding of SARS-CoV-2 spike protein-expressing pseudotypes to DC-HEK cells was confirmed by microscopic examination, which agrees with a previous study (122) (Figure 3.2). The impact of rfhSP-D on pseudotype binding was then assessed by challenging DC-HEK cells with SARS-CoV-2 spike protein-expressing pseudotype pre-treated with rfhSP-D (20µg/ml). When comparing the treated samples (DC-HEK + SARS-CoV-2 spike pseudotypes + rfhSP-D) to the untreated samples (DC-HEK + SARS-CoV-2 spike pseudotypes), we found that the binding was increased by almost 50% (Figure 3.3A). Additionally, utilising THP-1 cells stimulated with PMA and IL-4 to promote the expression of native DC-SIGN, the binding of SARS-CoV-2 spike protein-expressing pseudotypes was carried out. When SARS-CoV-2 spike pseudotypes were pre-treated with rfhSP-D, their binding to DC-SIGN-expressing THP-1 cells was around 25% higher than the control (Figure 3.3B). The cells were challenged with SARS-CoV-2 Spike protein-expressing pseudotypes- pre-treated with rfhSP-D (20µg/ml) for 24 hours to assess the impact of rfhSP-D on the transduction of pseudotypes to DC-SIGN expressing cells. A notable increase in luciferase activity (~190%) was observed in the treated samples (DC-HEK + SARS-CoV-2 spike pseudotypes + rfhSP-D) compared to their untreated counterparts (DC-HEK + SARS-CoV-2 spike pseudotypes) (Figure 3.4A). Compared to the untreated controls, treatment with rfhSP-D increased the transduction efficiency of the pseudotypes in DC-THP-1 cells by around 90% (Figure 3.4B). Appendices 2 and 3 contain the data with the mean fluorescence units. The results with the mean fluorescence and luciferase units are found in appendices 2 (cell binding) and 3 (viral cell entry).

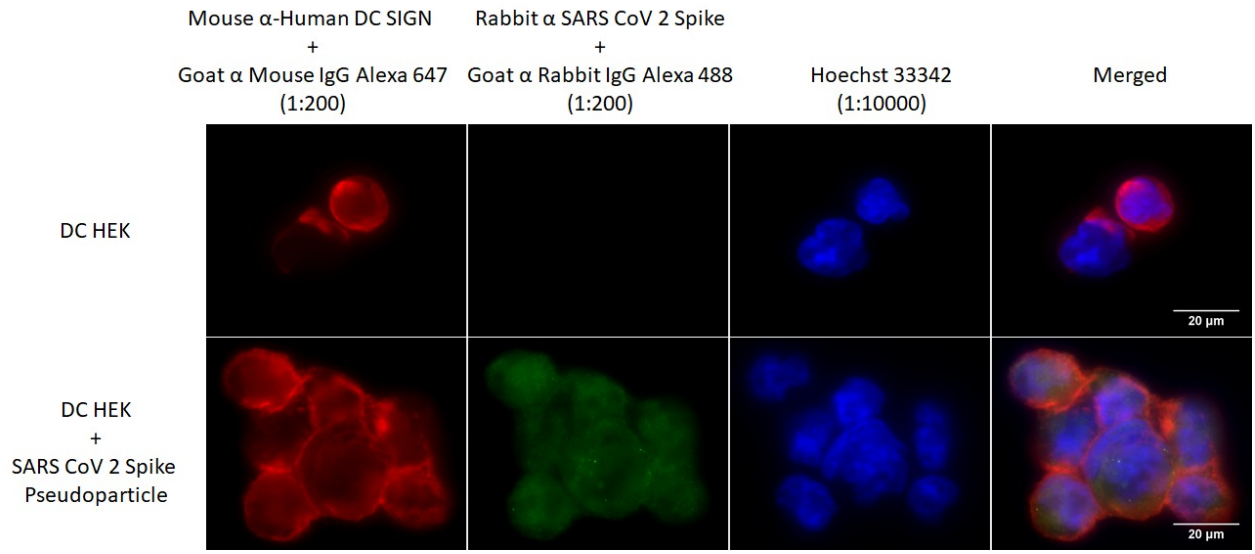

Figure 3.2: *SARS-CoV-2 Spike Pseudotypes bind to DC-SIGN expressing using fluorescence microscopy. DC-HEK cells were incubated with SARS-CoV-2 Spike Pseudotypes at 37°C for 30 minutes. After incubation, the cells were fixed using 4% paraformaldehyde, washed, and blocked with 5% FCS. The cells were probed with rabbit anti-SARS-CoV-2 Spike antibody and mouse anti-DC-SIGN antibody to detect Spike-Pseudotypes and DC-SIGN expression in the cells. Alexa Fluor 647 conjugated goat anti-mouse antibody (Abcam) and Alexa Fluor 488 conjugated goat anti-rabbit antibody (Abcam) were used to detect the primary antibodies. The nucleus was stained using Hoechst dye (Invitrogen, Life Technologies).*

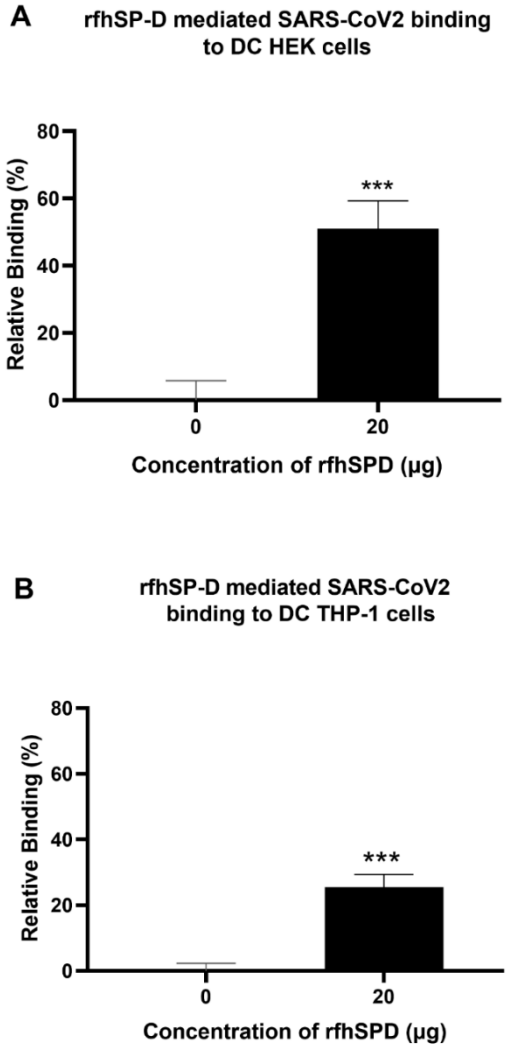

Figure 3.3: *rfhSP-D promotes the binding of SARS-CoV-2 Spike pseudotypes in DC-HEK (A) and DC-THP-1 cells (B). rfhSP-D enhances the interaction between SARS-CoV-2 Spike Pseudotypes and DC-SIGN expressing cells. DC-HEK cells (Panel A) and DC-THP-1 cells (Panel B) were treated with rfhSP-D and SARS-CoV-2 Spike Pseudotypes. The binding of cells to the pseudotypes was assessed using fluorescent probes, Alexa Fluor 488 (FTIC) and Alexa Fluor 647 (APC), and the fluorescence intensity was measured using a GloMax 96 Microplate Luminometer (Promega). Increased fluorescence intensity was observed in DC-HEK and DC-THP-1 cells treated with 20 µg/ml of rfhSP-D compared to cells challenged with Spike pseudotypes alone. The experiments were conducted in triplicates, and the error bars represent ± SEM. Statistical significance was calculated using an unpaired t-test (compared mean of treated to untreated cells) (***p < 0.001) (n = 3). The x-axis represents the treatment conditions (0 for untreated and 20 for treated samples). MBP used as a negative control; appendix 2.*

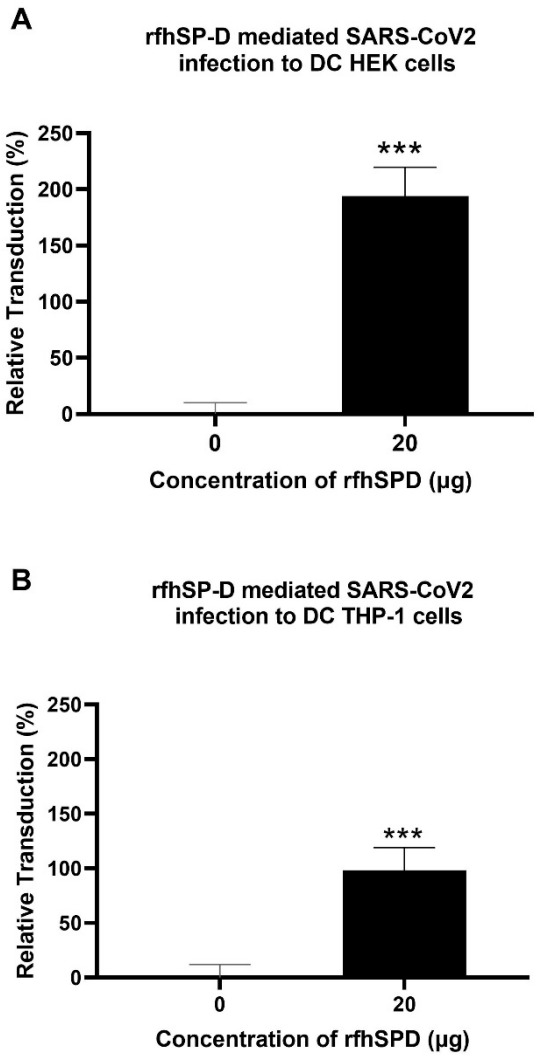

Figure 3.4: *rfhSP-D enhances the transduction of SARS-CoV-2 Spike pseudotypes in DC-HEK (A) and DC-THP-1 cells (B). Purified Spike pseudotypes were used to transduce DC-HEK cells (Panel A) and DC-THP-1 cells (Panel B), and the luciferase reporter activity was measured. Significantly higher levels of luciferase reporter activity were observed in DC-HEK and DC-THP-1 cells treated with 20 µg/ml of rfhSP-D (treated) compared to cells challenged with Spike pseudotypes alone (untreated) or cells challenged with Spike pseudotypes + MBP (negative control, appendix 3). The experiments were conducted in triplicates, and the error bars represent ± SEM. Statistical significance was calculated using an unpaired t-test (compared mean of treated to untreated cells) (***p < 0.001) (n = 3).*

3.3.3 rfhSP-D modulates pro-inflammatory cytokines and chemokines response in SARS-CoV-2 spike protein-challenged DC-HEK cells

High levels of pro-inflammatory chemokines and cytokines such as TNF-α, IFN-α, RANTES, and transcription factors NF-κB characterize the expression of DC-SIGN in SARS-CoV-2 infection in the lower respiratory epithelium. DC-HEK cells were challenged with SARS-CoV-2 Spike protein pre-treated with rfhSP-D to assess its impact on producing these pro-inflammatory mediators during SARS-CoV-2 infection. For qRT-PCR analysis, total RNA was extracted from treated and untreated cells. Treatment with rfhSP-D at 6 h reduced mRNA levels of TNF-α, IFN-α, RANTES,

and NF-κB in DC-HEK cells challenged with Spike protein. Notably, TNF-α mRNA levels were decreased by ~ -3.3 log10 (Figure 3.5C), while IFN-α mRNA levels were downregulated by ~ -2.1 log10 (Figure 3.5B). The mRNA levels of RANTES, induced upon viral component detection in infected cells, were decreased by ~ -1.3 log10 in rfhSP-D-treated DC-HEK cells challenged with Spike protein (Figure 3.5D). Additionally, the mRNA levels of the antiviral cytokines/chemokines regulated by the transcription factor NF-κB reduced by ~ -1.2 log10 (Figure 3.5A).

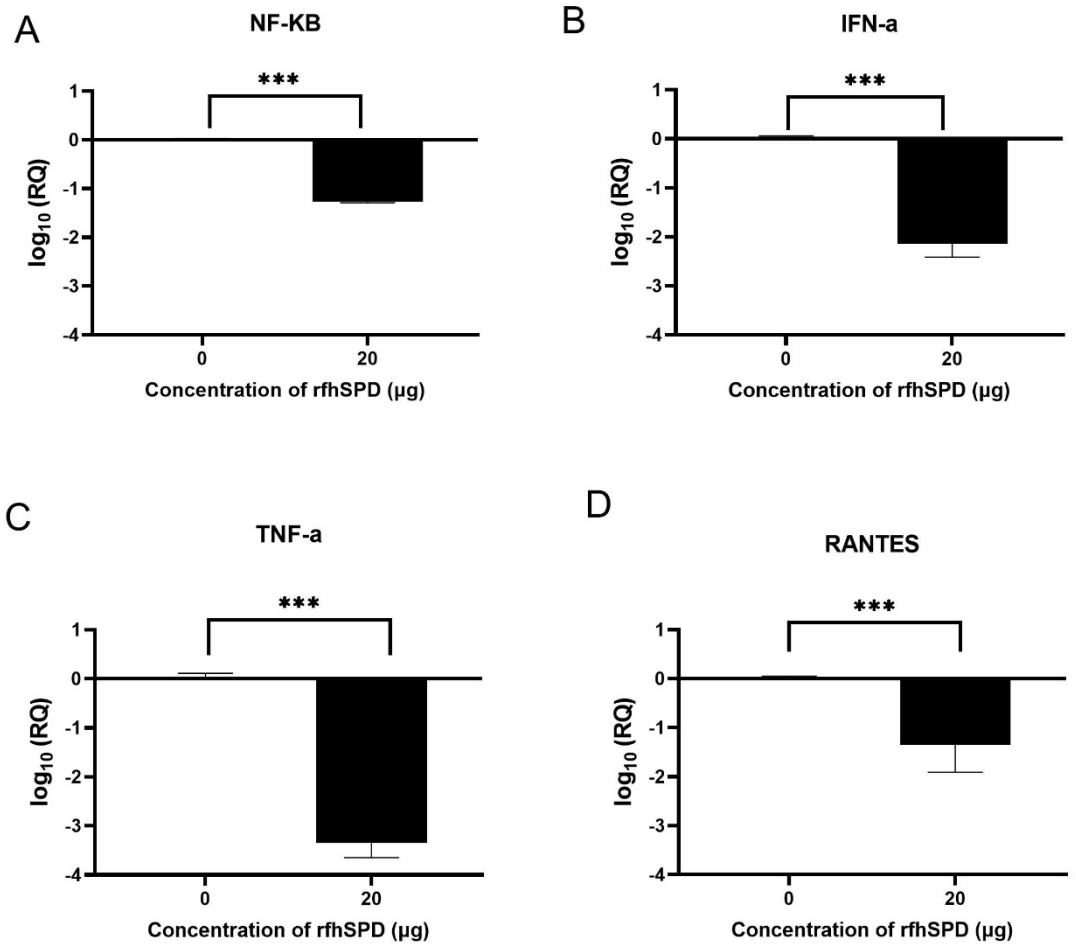

Figure 3.5: *rfhSP-D reduces the expression of pro-inflammatory cytokines and chemokines in DC-HEK cells. DC-HEK cells were challenged with SARS-CoV-2 Spike protein incubated with 20 µg/ml of rfhSP-D (treated). After 6 hours, the cells were harvested for analysis of cytokine expression. RNA was purified and converted into cDNA, and the gene expression levels of NF-κB (Panel A), IFN-α (Panel B), TNF-α (Panel C), and RANTES (Panel D) were assessed using RT-qPCR. The expression levels were normalised to the endogenous control 18S rRNA, and the relative expression (RQ) was calculated using cells challenged with Spike protein (untreated) as the calibrator. DC-HEK cells challenged with Spike pseudotypes + MBP used as negative control. The assays were performed in triplicates, and the error bars represent ± SEM. Statistical significance was determined using the two-way ANOVA test (***p < 0.0001) (n = 3).*

3.3.4 Modulation of immune response in SARS-CoV-2 spike protein-challenged DC-THP-1 cells by rfhSP-D

Lung macrophages produced higher levels of pro-inflammatory cytokines and chemokines such as TNF-α, IL-1, IL-6, and IL-8 in response to SARS-CoV-2. To investigate the effect of rfhSP-D on the inflammatory response of lung macrophages expressing DC-SIGN. DC-THP-1 cells were challenged with rfhSP-D-pre-treated or untreated SARS-CoV-2 Spike protein. The mRNA levels of pro-inflammatory cytokines and chemokines were examined utilising qRT-PCR at 6 h and 12 h time points (Figure 3.6), and in DC-THP-1 cells challenged with Spike protein, treatment with rfhSP-D resulted in a decreasing in mRNA levels of IL-1, IL-6, IL-8, TNF-α, and NF-κB (Figure 3.6). At 6 h, the mRNA levels of NF-κB were slightly decreased by ~ -1 $\log_{10}$, while at 12 h, a significant downregulation of NF-κB mRNA levels was observed, reaching ~ -4 $\log_{10}$ in rfhSP-D-treated DC-THP-1 cells challenged with Spike protein (Figure 3.6A). In cells challenged with Spike protein and treated with rfhSP-D, a decrease in gene expression levels of TNF-α was observed, with ~ -3.1 $\log_{10}$ at 6h and -6.8 $\log_{10}$ at 12 h (Figure 3.6B). Treatment with rfhSP-D reduced mRNA levels of IL-1β by ~ -2.5 $\log_{10}$ at 6 h and -4 $\log_{10}$ at 12 h in DC-THP-1 cells challenged with Spike protein (Figure 3.6C). Similarly, IL-6 levels were significantly downregulated at 12 h by ~ -5 $\log_{10}$ in rfhSP-D-treated DC-THP-1 cells challenged with Spike protein (Figure 3.6D). A reduction in IL-8 levels was observed at both 6 h (~ -2.3 $\log_{10}$) and 12 h (~ -4.8 $\log_{10}$) in DC-THP-1 cells challenged with Spike protein and treated with rfhSP-D (Figure 3.6E). Additionally, rfhSP-D treatment resulted in a reduction of the expression levels of MHC class II molecules at 6 h (~ -2 $\log_{10}$) and 12 h (~ -2.7 $\log_{10}$) in DC-THP-1 cells challenged with Spike protein (Figure 3.6F). Importantly, no effect observed on DC-THP-1 cells treated only with rfhSP-D (Appendix 4).

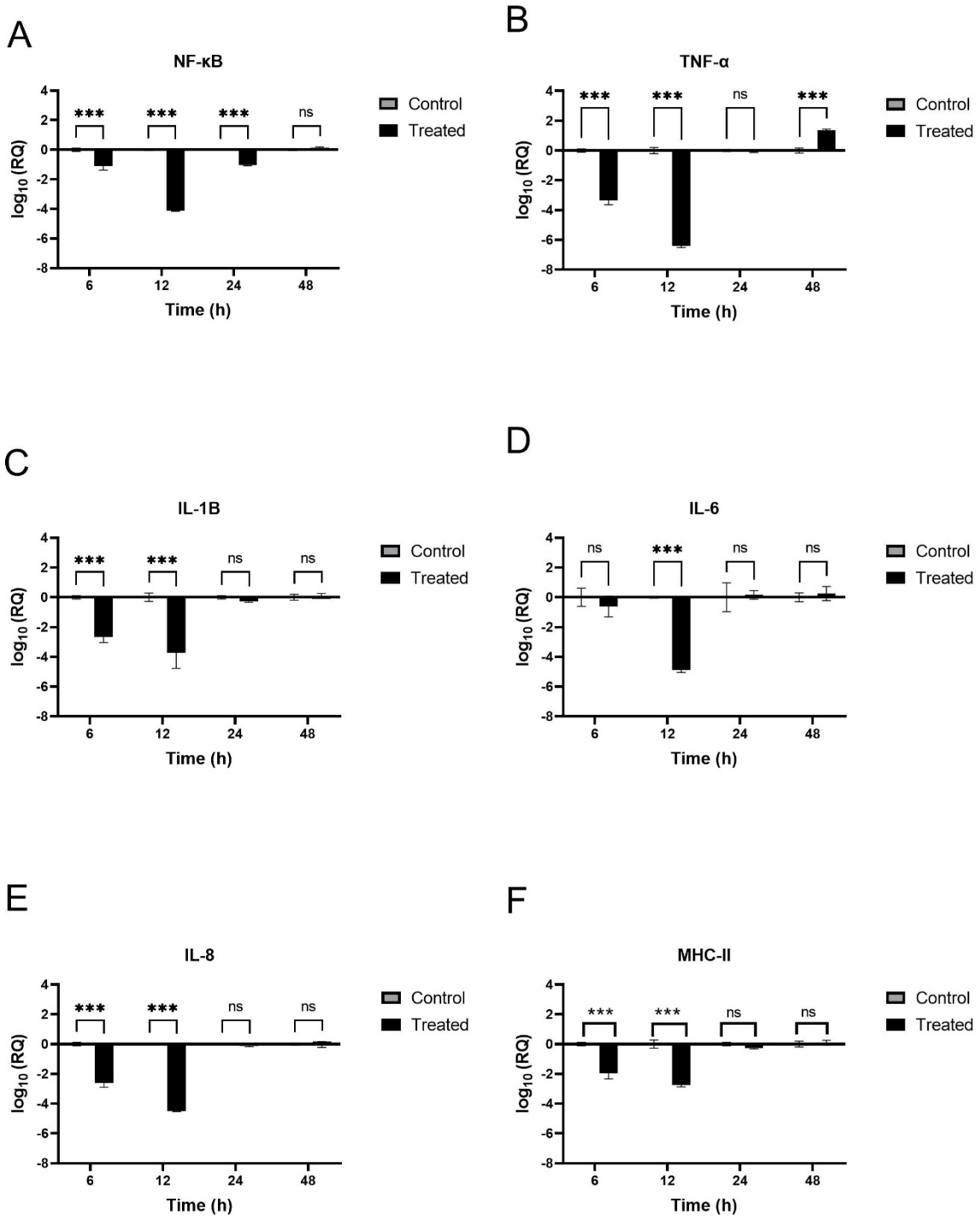

Figure 3.6: *rfhSP-D modulates the immune response in DC-THP-1 cells. DC-THP-1 cells were challenged with SARS-CoV-2 Spike protein incubated with 20 µg/ml of rfhSP-D. The cells were harvested at 6 hours, 12 hours, 24 hours, and 48 hours to analyse the expression of cytokines and MHC class II. RNA was purified from the lysed cells and converted into cDNA. The expression levels of NF-κB (Panel A), TNF-α (Panel B), IL-1β (Panel C), IL-6 (Panel D), IL-8 (Panel E), and MHC class II (Panel F) were measured using RT-qPCR, and the data were normalised against the expression of 18S rRNA as a control. The experiments were conducted in triplicates, and the error bars represent ± SEM. The relative expression (RQ) was calculated using cells challenged with Spike protein without rfhSP-D as the calibrator. The RQ value was calculated using the formula RQ = 2−ΔΔCt. Statistical significance was determined using the two-way ANOVA test (***p < 0.0001, and ns = no significance) (n = 3).*

3.3.5 SP-D interacts with RBD, and DC-SIGN interacts with NTD of the SARS-CoV-2 spike protein

DC-SIGN and SP-D interaction through their CRDs has been previously shown (132) . This study observed this interaction in complex A, which represents the second docked pose (Figure 3.7A). The specific binding site of DC-SIGN (CRD) and Spike protein remains unknown. Thus, a blind docking approach was used to generate complex B. Analysis of the top-ranked docked pose of complex B showed an interaction between Spike protein's NTD (N-terminal domain) and the CRD domain of DC-SIGN (Figure 3.7B). Based on previous knowledge that Spike protein interacts with SP-D (34) , it was hypothesised that Spike protein could interact with both SP-D and DC-SIGN (CRD) through two distinct domains, RBD and NTD, respectively. This hypothesis is further supported by the *in vitro* observation that the binding of DC-SIGN to Spike protein was improved by rfhSP-D (Figure 3.1C). A tripartite complex was generated by docking complex A (DC-SIGN and SP-D) with Spike protein to explore this further. The top two docked poses, complexes C1 and C2, were examined for their intermolecular interactions (Figure 3.8). In both C1 (Figure 3.8A) and C2 Figure 3.8B) complexes, DC-SIGN (CRD) interacted with the NTD domain of Spike protein. In C1, no molecular interactions were observed between Spike protein and rfhSP-D (Figure 3.8A). However, in C2, Spike protein interacted with rfhSP-D through its RBD (Figure 3.8B). Chandan Kumar and Susan Idicula, Biomedical Informatics Centre, National Institute for Research in Reproductive and Child Health, ICMR, Mumbai, Maharashtra, India, kindly have conducted this work.

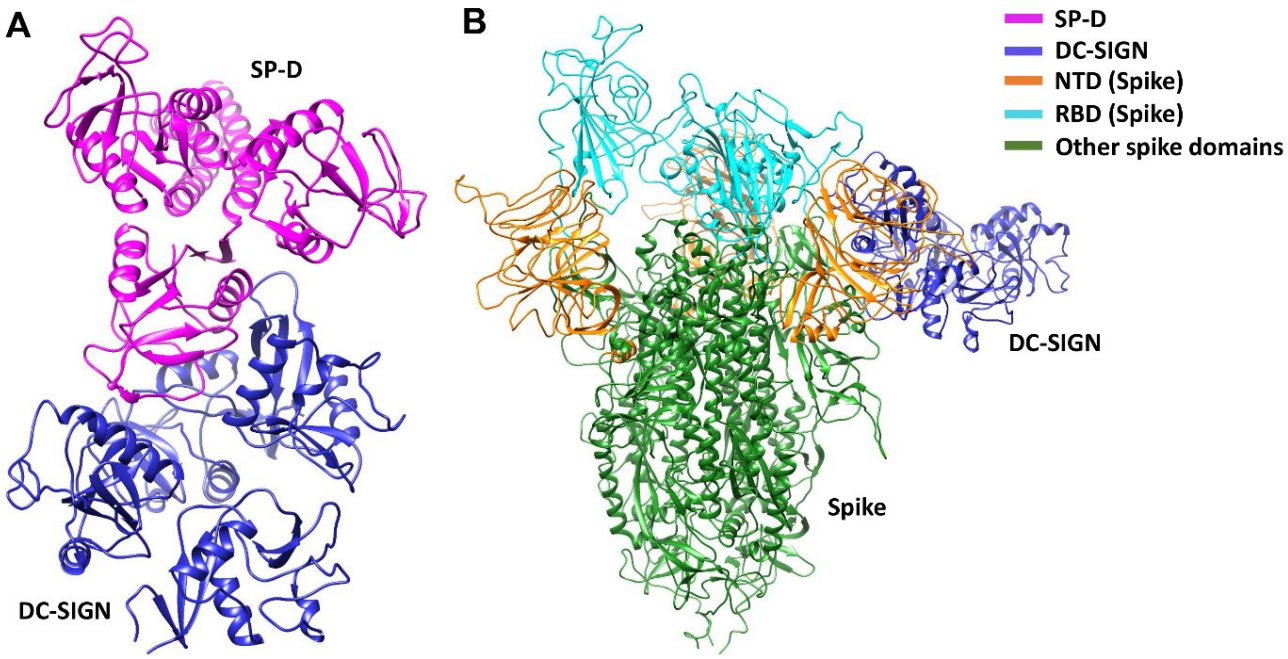

Figure 3.7: *DC-SIGN interacts with both SP-D and SARS-CoV-2 Spike. The docked poses of complex A (A) and complex B (B) were selected for docking and molecular dynamics (MD) simulations, respectively. The spike protein interacts with DC-SIGN (CRD) in complex B through the N-terminal domain (NTD, shown in orange).*

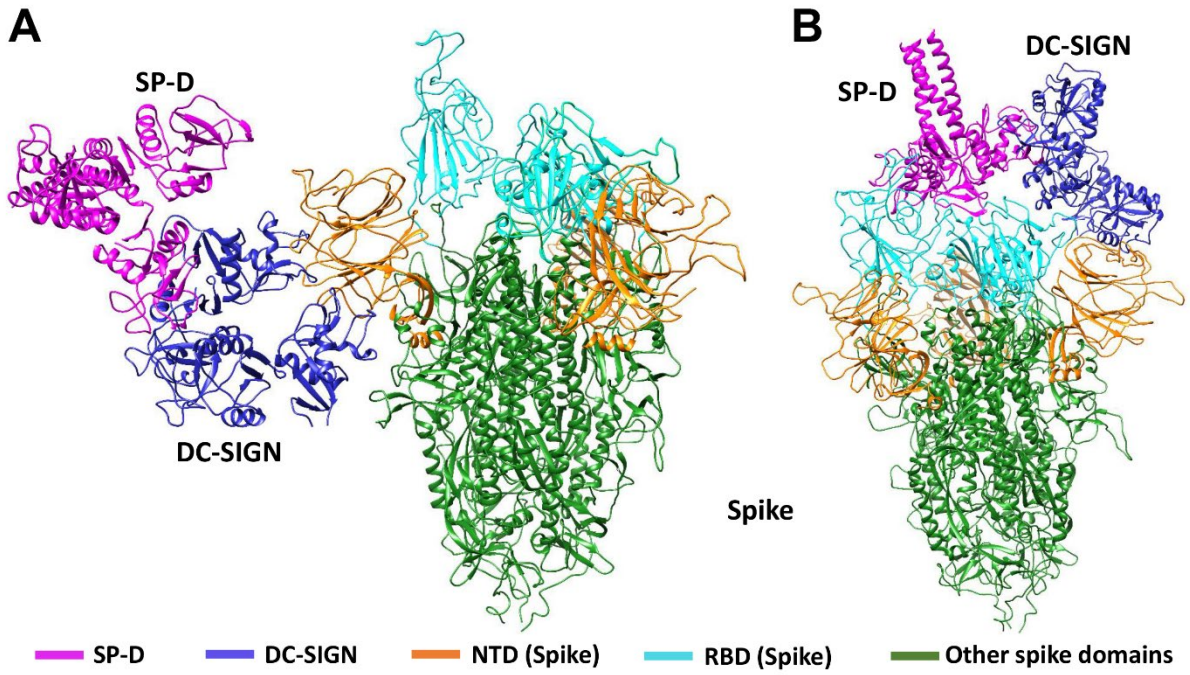

Figure 3.8: *DC-SIGN, SP-D and SARS-CoV-2 spike interaction. A tripartite complex of SP-D, DC-SIGN, and SARS-CoV-2 Spike was formed, and the docked poses of the tripartite complexes were selected for analysis using molecular dynamics (MD) simulations. In complex C1 (A), DC-SIGN (CRD) interacts with the N-terminal domain (NTD) of Spike. In complex C2 (B), DC-SIGN (CRD) interacts with the NTD of Spike, while SP-D interacts with the receptor binding domain (RBD) of Spike.*

3.3.6 SP-D stabilises DC-SIGN and SARS-CoV-2 spike protein interaction

MD simulations were carried out to assess the effect of SP-D on the interaction between DC-SIGN (CRD) and Spike protein. The root means square deviation (RMSD) analysis revealed that complexes C1 and C2 had lower RMSD values than complex B throughout the simulation, showing that SP-D improves the stability of the DC-SIGN and Spike protein interaction (Figure 9A). This result was further supported by analysing the potential energy (PE), intermolecular distance, and hydrogen bond profiles. The trajectory analysis of PE, intermolecular distance, and hydrogen bonds between DC-SIGN and Spike protein showed that complexes C1 and C2 exhibited higher stability than complex B (Figure 3.9B, Figure 3.10A–C, Figure 3.10D–F). C1 displayed slightly better stability than C2 (s 3.9 and) among the tripartite complexes. These analyses reveal that SP-D stabilises the interaction between DC-SIGN and Spike protein. Chandan Kumar and Susan Idicula, Biomedical Informatics Centre, National Institute for Research in Reproductive and Child Health, ICMR, Mumbai, Maharashtra, India, kindly have done this work.

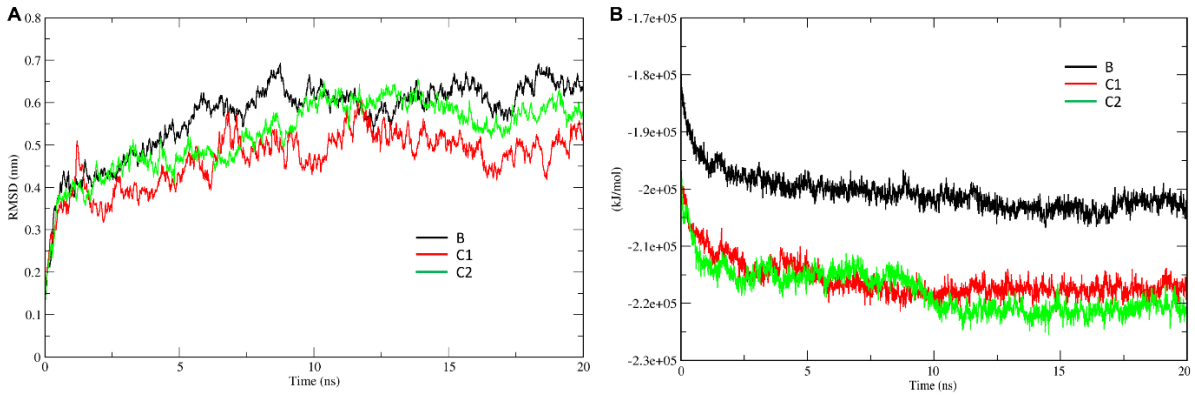

Figure 3.9: *SP-D stabilises SARS-CoV-2 Spike interaction with DC-SIGN. SP-D plays a stabilising role in the interaction between SARS-CoV-2 Spike and DC-SIGN. Comparative analysis of MD simulations was conducted for complexes B, C1, and C2, considering (A) root mean square deviation (RMSD) and (B) potential energy (PE). The RMSD and PE profiles of complexes C1 and C2 were lower than those of complex B, indicating greater tripartite complex C1 and C2 stability.*

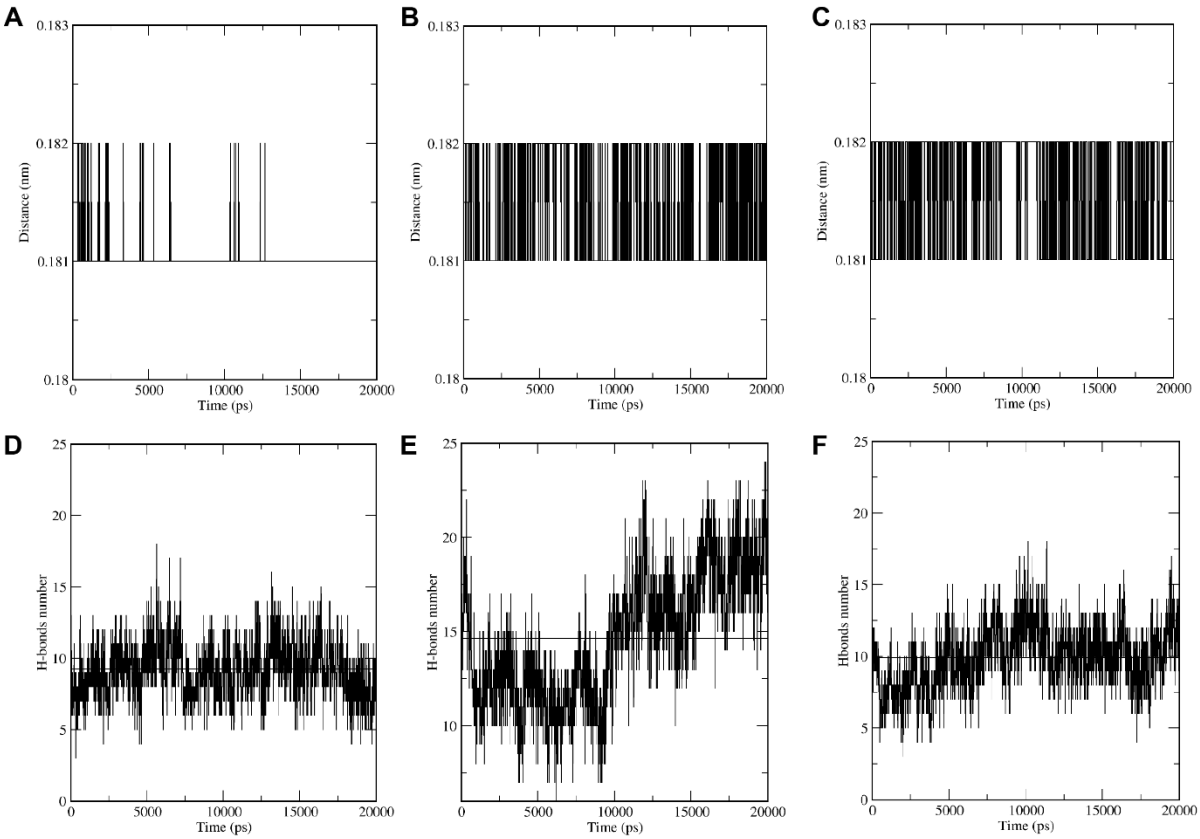

Figure 3.10: *SP-D stabilises the interaction between SARS-CoV-2 Spike and DC-SIGN. Comparative analysis of MD simulations was performed for complexes B, C1, and C2, considering the average distance (A–C) and H-bonds (D–F) between DC-SIGN and Spike. In contrast to complex B, the intermolecular distance between DC-SIGN and Spike remained relatively constant throughout the simulation period in tripartite complexes C1 and C2. Additionally, the number of intermolecular H-bonds between DC-SIGN and Spike was higher in complexes C1 and C2 compared to complex B. These findings suggest that SP-D stabilises Spike and DC-SIGN (CRD) interaction.*

3.4 Discussion

Pathogen-associated molecular patterns (PAMPs) are distinctive molecular structures on pathogens that are recognized by pattern recognition receptors (PRRs), which slso can serve as a bridge between nonspecific and specific immunity (110). By recognising and attaching to non-self-ligands, PRRs contribute to nonspecific immune responses against infection and tumours (110). Calcium is used by C-type lectin receptors (CLRs) to bind carbohydrate residues on pathogenic bacteria and viruses (133). DC-SIGN and SP-D are CLRs that crucial in antiviral immunity, including SARS-CoV-2 (2, 134). For many viruses, tissue tropism is determined by virus-host receptors and entry cofactors on host cells (135). Our findings indicated that rfhSP-D improves SARS-CoV-2's binding and entry into cells that express DC-SIGN.

Additionally, rfhSP-D treatment hinders inflammatory signalling caused by the binding of Spike protein to DC-SIGN, which in turn causes the production of pro-inflammatory mediator genes to be downregulated. To validate the observed cytokine modulation mediated by rfhSP-D, more studies are necessary to utilise DC-SIGN-expressing cells clinical isolates. Our results reveal a unique interaction between SARS-CoV-2, DC-SIGN, and rfhSP-D that may be therapeutically useful in reducing viral spread and its associated cytokine storm.

In the lungs, alveolar macrophages and dendritic cells (DCs) express high levels of DC-SIGN, which interacts with SARS-CoV-2 via the Spike protein (80). It has previously been demonstrated that DC-SIGN interacts with viral proteins of many viruses, such as SARS-CoV, HIV-1, and Ebola (129, 136, 137). DC-SIGN has been linked to the induction of DC maturation, myeloid cell cytokine response, and T-cell priming (138). Another CLR, SP-D, has shown antiviral functions against SARS-CoV-2, HIV-1, and influenza A virus (IAV) infections (40, 124). Our previous results revealed that rfhSP-D can inhibit SARS-CoV-2 S1 protein binding to cells expressing ACE2 and restricting viral entry (34). nevertheless, the role of SP-D in the interaction between DC-SIGN and SARS-CoV-2 is still unknown.

The binding of the SARS-CoV-2 Spike protein to the host cell receptor ACE2 is considered a critical step in the viral replication cycle (139). Lys31, Glu35, and Lys353 are among the ACE2 residues with which the receptor binding motif (RBM) in the receptor-binding domain (RBD) of the Spike protein binds (139). While the sequence of events about the Spike protein/ACE2 interaction is becoming increasingly evident, unknown factors still facilitate viral infection,

such as how SARS-CoV-2 is transported to the ACE2 receptor (126). The affinity of the SARS-CoV and SARS-CoV-2 Spike proteins for ACE2 is similar, but SARS-CoV-2 transmits at a substantially higher rate (127). That suggests SARS-CoV-2 could more effectively infect ACE2-expressing cells by improving viral adherence through host cell attachment proteins (127). DC-SIGN is a receptor for the SARS-CoV Spike protein, improving cell entry in ACE2+ pneumocytes (128). Recently, it has been demonstrated that DC-SIGN increases trans-infection by binding to the SARS-CoV-2 Spike protein (122). Here, we examined the potential of rfhSP-D in preventing SARS-CoV-2 interaction with DC-SIGN-expressing cells. The previous studies on the interaction between SARS-CoV-2 and rfhSP-D or DC-SIGN has been independently verified by us (34).

This study shows that rfhSP-D improves SARS-CoV-2 Spike protein binding to DC-SIGN. The findings indicated that SP-D stabilises the binding between DC-SIGN CRD, and the N-terminal domain of the SARS-CoV-2 Spike protein by in-silico molecular dynamics studies. We evaluated the effect of rfhSP-D by utilising viral lentiviral pseudotype as a safe substitute for live virus on the binding and uptake of SARS-CoV-2 in DC-SIGN-expressing cells. Our results demonstrated that rfhSP-D enhances spike protein binding and transduction in DC-SIGN expressing cells compared to the control cells (Cells + SARS-CoV-2). In vivo study has shown that SP-D improves IAV viral clearance in the lung (140).). Similarly, rfhSP-D's interaction with DC-SIGN may improve SARS-CoV-2 binding and macrophage uptake, suggesting that rfhSP-D may enhance SARS-CoV-2 clearance through DC-SIGN.

Additionally, we investigated the effect of rfhSP-D on mRNA expression levels of pro-inflammatory mediator genes in DC-HEK and DC-THP-1 cells that had been challenged with SARS-CoV-2 Spike protein. Overall, there was a reduction in mRNA levels of pro-inflammatory chemokines and cytokines such as TNF-α and IL-8, suggesting an modulatory effect of rfhSP-D in DC-SIGN-expressing cells.

DC-SIGN has been linked to the activation of the STAT3 pathway during viral infection (141). In myeloid cells infected with SARS-CoV-2, STAT3 is crucial for activating the transcription factor NF-κB, which may produce inflammatory cytokines, resulting in virus elimination and sometimes tissue destruction (142). Many cytokines, including IL-1, IL-2, IL-6, IL-12, TNF-α, LT-α, LT-β, and GM-CSF, as well as chemokines such as IL-8, MIP-1, MCP1, RANTES, and eotaxin, are expressed when NF-κB is activated during viral infection (142). These inflammatory

mediators are critical for infection resistance and play a role in antiviral immunity (142). Nonetheless, in moderate to severe SARS-CoV-2 infection cases, lung macrophages and epithelial cells produce elevated amounts of TNF-α, IL-1β, IL-6, and IL-8 mainly by activating NF-κB (143). Increased morbidity and mortality organ failure could be caused by cytokine storm (143). The severity of SARS-CoV-2 infection could be attenuated by immunomodulation of NF-κB activation (143). SARS-CoV-2 Spike protein induces pro-inflammatory mediators in THP-1 cells *in vitro* (144). Our finding indicates that rfhSP-D inhibited pro-inflammatory immune response in DC-SIGN-expressing immune cells by downregulating the NF-κB gene expression levels in DC-HEK and DC-THP-1 cells challenged with SARS-CoV-2 Spike protein.

Another key factor in the pathology of SARS-CoV-2 infection is TNF-α, which is produced in the lungs by various cell types, including macrophages, mast cells, T cells, epithelial cells, and smooth muscle cells (145, 146). Patients with severe SARS-CoV-2 infection have been shown to have elevated plasma levels of TNF-α (146). TNF-α can cause neutrophil infiltration in the lung (147). Furthermore, TNF-α promotes the synthesis of cytokines such as IL-1β and IL-6 (148). Our findings revealed that reduced mRNA levels of TNF-α in DC-HEK and DC-THP-1 cells challenged with SARS-CoV-2 Spike-treated with rfhSP-D suggesting immunomodulation function of rfhSP-D in SARS-CoV-2 inflammatory response.

IL-1β can induce inflammasome in response to various viral diseases, including SARS-CoV-2 (149). High serum levels of IL-1β were observed in patients with severe SARS-CoV-2 (149). Pyroptosis, a highly inflammatory type of programmed cell death commonly seen in cytopathic viruses, is associated with IL-1β (150).). Pyroptosis may cause an uncontrollable inflammatory response and play a role in the immune pathology of SARS-CoV-2 (151). Our results showed that lower mRNA levels of IL-1β in DC-THP-1 cells challenged with SARS-CoV-2 Spike pre-treated with rfhSP-D, indicating that rfhSP-D may lessen unnecessary inflammation via IL-1β downregulation.

IL-6 is a glycoprotein that plays a crucial role in control viral infection (152). IL-6 is expressed by T and B lymphocytes, DCs, fibroblasts, monocytes, macrophages, and endothelial cells (153, 154). Severe SARS-CoV-2 infection has been linked to elevated levels of IL-6 in the serum (152).). Our findings revealed that decreased mRNA levels of IL-6 in DC-THP-1 cells challenged with SARS-CoV-2 Spike pre-treated with rfhSP-D. This finding suggests that SP-D may attenuate IL-6-associated immunopathogenesis in SARS-CoV-2 infection.

IFN-α is an important cytokine in the control of viral infection, mainly released by virus-infected cells (155). Nonetheless, elevated interferon-stimulated gene (ISG) levels in SARS-CoV-2 may lead to immunopathology (156). Our results demonstrated that downregulation of IFN-α mRNA expression levels in DC-HEK cells challenged with SARS-CoV-2 Spike-treated with rfhSP-D. These results imply that rfhSP-D may reduce infection pathology.

MHC class II molecules are highly expressed on the surface of antigen-presenting cells and are crucial for initiating an adaptive immune response to viral infection (157). On the other hand, limited MHC class II molecule expression on type II alveolar cells and macrophages can enhance the course of respiratory viral infections (157). THP-1 cells are polarized toward an M1-like macrophage upon binding the SARS-CoV-2 Spike protein, accompanied by enhanced production of MHC class II molecules (158). Our findings revealed lower MHC class II mRNA expression levels in DC-THP-1 cells challenged with SARS-CoV-2 Spike-treated with rfhSP-D. This finding suggests that SP-D plays a role in regulating antigen presentation to prevent an overactivation of adaptive immunity.

The recruitment of inflammatory cells to the site of viral infection is induced by chemokines such as RANTES and IL-8 (159). IL-8 (CXCL8) is a key in neutrophil infiltration (159). IL-8 also causes a release of high levels of neutrophil extracellular traps (NETs), which may be involved in organ damage in severe SARS-CoV-2(160). Our results showed IL-8 mRNA levels were reduced in DC-THP-1 cells challenged with SARS-CoV-2 Spike-treated with rfhSP-D. This indicates that SP-D may attenuate inflammatory neutrophil pathology in SARS-CoV-2 infection.

Elevated serum levels of RANTES were observed in severe SARS-CoV-2 infection (161, 162). It is a chemokine important in viral immune protection; however, high levels can cause excessive pulmonary inflammation (161, 162). Our findings showed reduced mRNA expression levels of RANTES in DC-HEK cells challenged with SARS-CoV-2 Spike-treated with rfhSP-D.

In summary, our results revealed that rfhSP-D can enhance SARS-CoV-2 binding and uptake by DC-SIGN-expressing cells. Furthermore, in DC-SIGN-expressing cells, rfhSP-D suppresses the expression of chemokines like RANTES and IL-8 and pro-inflammatory cytokines, including IL-1β, TNF-α, and IL-6. These results indicate a preventive immune function of rfhSP-D against immunopathology in SARS-CoV-2 infection. Thus, rfhSP-D stabilizes SARS-CoV-2 Spike protein and DC-SIGN interaction, facilitating the viral uptake by macrophages like cells and may even

support viral clearance. Further research is necessary to evaluate the expression of DC-SIGN in patients' samples with mild, moderate, and severe SARS-CoV-2 infection. To further explore the potential of rfhSP-D as a universal treatment against SARS-CoV-2 infection, the interaction of rfhSP-D and DC-SIGN with Spike proteins of various SARS-CoV-2 variants should be examined *in vivo*, specifically in lung microenvironment using well-established COVID-19 animal models.

Chapter 4

Complement Activation-Independent Attenuation of SARS-CoV-2 Infection by C1q and C4b-Binding Protein

4.1 Abstract

The Complement system is a key component of the innate immunity. Severe COVID-19 is characterised by complement dysregulation and cytokines storm. However, recent evidence suggests that locally produced or activated complement protein may protect against SARS-CoV-2 infection. This study investigated the potential immune role of C1q and C4b-binding protein (C4BP) in SARS-CoV-2 infection, independent of complement activation. Here, we found that C1q and C4BP directly bind to the SARS-CoV-2 spike protein and receptor binding domain (RBD), which inhibits viral binding and transduction into A549 cells that express human ACE2 and TMPRSS2 (A549-hACE2+TMPRSS2 cells). Furthermore, mRNA levels of proinflammatory cytokines and chemokines, including IL-1β, IL-8, IL-6, TNF-α, IFN-α, RANTES, and NF-κB were downregulated in A549-hACE2+TMPRSS2 cells challenged with SARS-CoV-2 lentiviral pseudoparticles pre-treated with C1q or C4BP. Similar results were observed when C1q- recombinant globular heads (ghA, ghB, and ghC) were used. These findings suggest that C1q, ghs, and C4BP can bind, block viral entry and attenuate inflammatory responses in SARS-CoV-2 infection. Interestingly, although hepatocytes are the primary sources of these proteins, macrophages and alveolar type II cells in the lungs can produce C1q and C4BP locally. In summary, this study revealed protective functions of C1q and C4BP against SARS-CoV-2 infection, independent of complement activation. These results improve our knowledge of the immune response to SARS-CoV-2 infection. Further studies are required to investigate these protective roles' underlying processes and their potential clinical uses.

4.2 Introduction

The severity of COVID-19 is mainly associated with the aberration of immune response (163). The complement system is a key element of innate immunity linked to the induction of hyperinflammation in animal models by coronaviruses such as MERS-CoV (164). Likewise, it has been reported that SARS-CoV interacts with MBL, triggering the lectin pathway ((165). Dysregulation of complement activation can lead to high serum levels of C5a, C5b-9, and elevated CD11b expression in leukocytes (perhaps due to C5aR1 activation) in COVID-19, resulting in severe disease (52). Recently, it has been reported that SARS-CoV-2 activates the three pathways of complement (lectin, alternative, and classical) (166). Furthermore, it has been demonstrated that deregulation of the classical pathway contributes to pulmonary tissue injury in SARS-CoV-2 infection (167, 168). Lower serum levels of key classical pathway proteins, such as C1q and C4BP, were observed in patients with severe COVID-19 (167, 168).

C1q is a crucial classical pathway protein that plays a vital role in the induction of humoral immune response against viruses such as West Nile (WNV) (169). It modulates anti-viral antibody-mediated effector mechanisms in influenza viral infection and binds to the antibody-bound respiratory syncytial virus (RSV), activating the classical pathway (170, 171). C4b-binding protein (C4BP), another complement key, is an essential fluid phase inhibitor of the lectin and classical pathways (172). It also functions as a cofactor for factor I, preventing the synthesis of C3 and C5 convertases (172). Variants in the gene that codes for the C4BP α chain can be a risk factor for SARS-CoV-2 infection-related morbidity and mortality (173).

Although hepatocytes are the primary source of complement proteins, alveolar type II cells and macrophages can also produce C1q and C4BP locally in the pulmonary (55, 174-176) . That implies they play a vital immune function in protecting lung tissue in the early phases of viral infection (55, 174-176). Locally produced C1q and C4BP can act as PRR molecules by interacting with IAV surface proteins, inhibiting viral entry and replicating subtypes independently (55, 177).

Many recent studies have investigated the pathological role of classical pathways in SARS-CoV-2 infection; however, the protective roles of C1q and C4BP are not yet explored. Here, we examined the potential protective or pathogenic effect of purified human C1q, its recombinant globular heads (ghA, ghB, and ghC), and C4BP proteins against SARS-CoV-2

infection in a complement activation-independent manner. Additionally, we assessed the interaction between complement proteins, including C1q and C4BP, with SARS-CoV-2 S and RBD proteins. Furthermore, the potential of C1q and C4BP in habiting viral entry of the SARS-CoV-2 lentiviral pseudotype was investigated in A549-hACE2+TMPRSS2 cells. Our results revealed that C1q and C4BP could block cell entry of the SARS-CoV-2 lentiviral pseudotype in A549-hACE2+TMPRSS2 cells. Also, C1q and C4BP decreased the proinflammatory responses induced by the SARS-CoV-2 alphaviral pseudotype independently of complement activation.

4.3 Results

4.3.1 Human C1q and C4BP interact with SARS-CoV-2 Spike and RBD Proteins.

ELISA was employed to investigate the interaction between immobilised native C1q and SARS-CoV-2 S and RBD proteins (Figure 4.1 A) and vice versa (Figure 4.1B). The results revealed a dose-dependent interaction between immobilised C1q and SARS-CoV-2 S and RBD proteins when probed with the anti-SARS-CoV-2 S protein polyclonal antibody. Similarly, when probed with the rabbit anti-human C1q polyclonal antibody, immobilised SARS-CoV-2 spike protein or RBD exhibited dose-dependent binding to C1q.

Likewise, the study investigated the ability of immobilised native C4BP to interact with SARS-CoV-2 S and RBD proteins (Figure 4.1C) and vice versa (Figure 4.1D) using a direct ELISA. The results demonstrated that immobilised C4BP bound SARS-CoV-2 S and RBD proteins in a dose-dependent manner when probed with polyclonal anti-SARS-CoV-2 S protein. Moreover, when probed with rabbit anti-human C4BP, the immobilised SARS-CoV-2 S or RBD also displayed dose-dependent binding to C4BP; however, the binding was relatively weaker compared to C1q. BSA protein was utilised as a negative control.

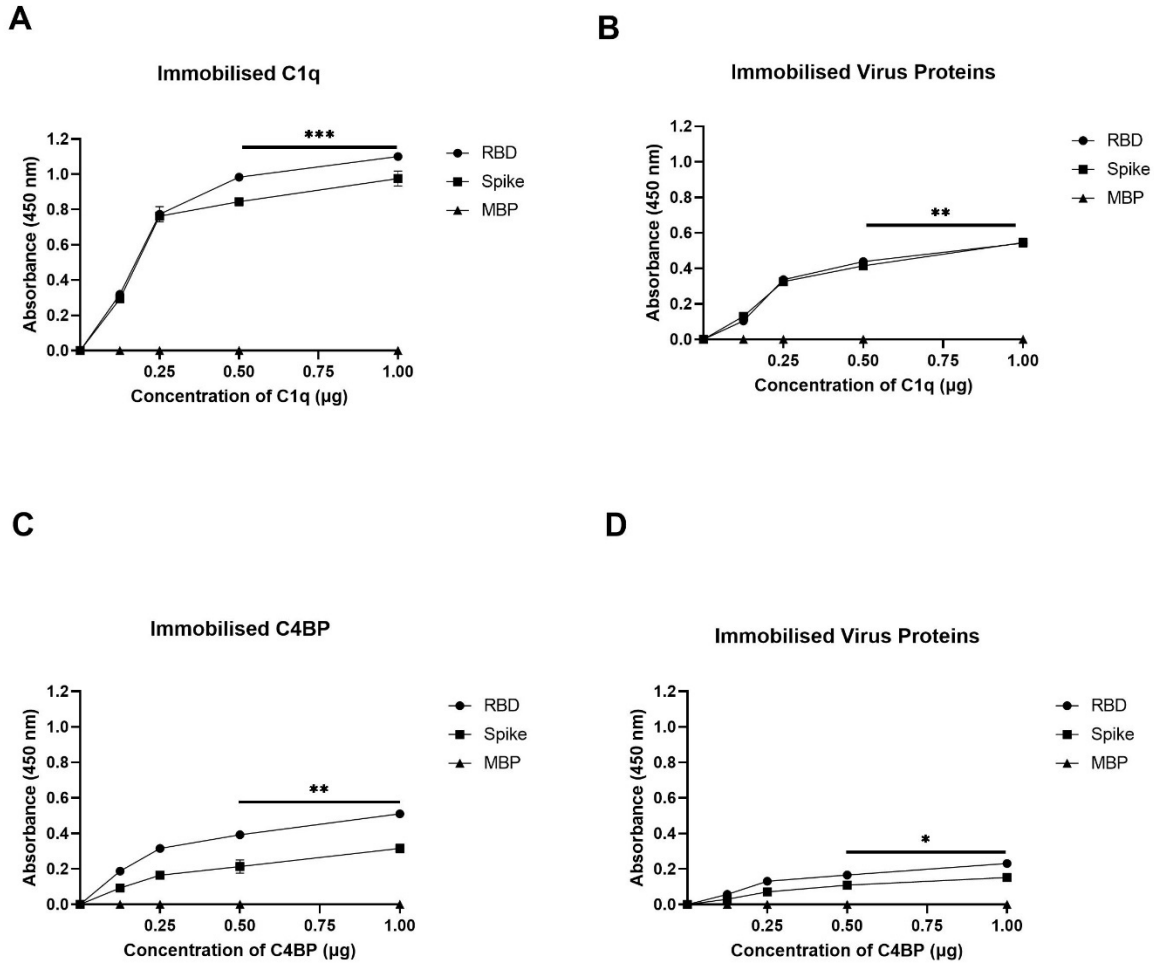

Figure 4.1: *ELISA shows that the SARS-CoV-2 S protein binds C1q (A, B) and C4BP (C, D). SARS-CoV-2 virus exhibits direct interactions with both C1q and C4BP proteins. To investigate this interaction, a 96-well plate was coated with varying concentrations of immobilised C1q (1, 0.5, 0.125, and 0 µg per well) (A, C) or constant concentrations of viral proteins (spike or RBD 1 µg per well) (B, D) using a carbonate–bicarbonate (CBC) buffer at pH 9.6, and then incubated at 4 °C overnight. Subsequently, a constant concentration of viral proteins (1 µg per well) (A) or decreasing amounts of C1q/C4BP (1, 0.5, 0.125, and 0 1 µg per well) (B) was added to the corresponding wells and incubated at 37 °C for 2 hours. After the incubation, the wells were washed, and primary antibodies (rabbit anti-SARS-CoV-2 spike or rabbit anti-human C1q/C4BP) were added (1:5000 dilution, 100 µL/well). MBP was used as a negative control. The data were expressed as the mean of triplicates ± SD. Statistical significance was determined using the two-way ANOVA (* $p < 0.05$, ** $p < 0.01$, and *** $p < 0.001$) (n = 3).*

4.3.2 Human C1q, Recombinant Globular Head Modules, and C4BP Inhibit SARS-CoV-2 Pseudoparticle Transduction

A luciferase reporter assay assessed the impact of C1q, ghA, ghB, ghC, and C4BP on SARS-CoV-2 infectivity. SARS-CoV-2 lentiviral pseudoparticles pre-treated with C1q, ghA, ghB, ghC, or C4BP exhibited reduced viral transduction in A549-hACE2+TMPRSS2 cells compared to their controls. Specifically, A549-hACE2+TMPRSS2 cells, when challenged with SARS-CoV-2 lentiviral pseudoparticles pre-treated with C1q, showed significant inhibition of viral infection by ~ 60% (Figure 4.2A), while pre-treatment with C4BP resulted in a reduction of ~ 17% (Figure 4.2B), compared to the control group (A549-hACE2+TMPRSS2 cells + SARS-CoV-2 pseudoparticles). That suggests that C1q treatment can significantly impede SARS-CoV-2 viral infection in a complement-independent manner, although the inhibition observed with C4BP was not as pronounced. Additionally, no statistically significant difference in transduction efficiency was observed between A549 cells challenged with the SARS-CoV-2 pseudotype and the control group of native A549 cells.

Next, the ability of recombinant globular heads of C1q (ghA, ghB, and ghC) to modulate SARS-CoV-2 pseudoparticle infectivity was investigated. SARS-CoV-2 lentiviral pseudoparticles pre-treated with ghA, ghB, or ghC demonstrated a significant reduction in viral transduction, ~ 20% (Figure 4.3A), ~ 30% (Figure 4.3B), and ~ 60% (Figure 4.3C), respectively, compared to the control (A549-hACE2+TMPRSS2 cells + SARS-CoV-2 lentiviral pseudoparticles + MBP). Importantly, no significant difference was observed between A549-hACE2+TMPRSS2 cells treated with the SARS-CoV-2 pseudotype + MBP and A549-hACE2+TMPRSS2 cells treated with the SARS-CoV-2 pseudotype alone. This finding suggests that the reduction in transduction efficiency was attributed to the presence of the C1q globular head modules and not influenced by the MBP fusion partner. The results with the mean luciferase units are found in Appendix 7.

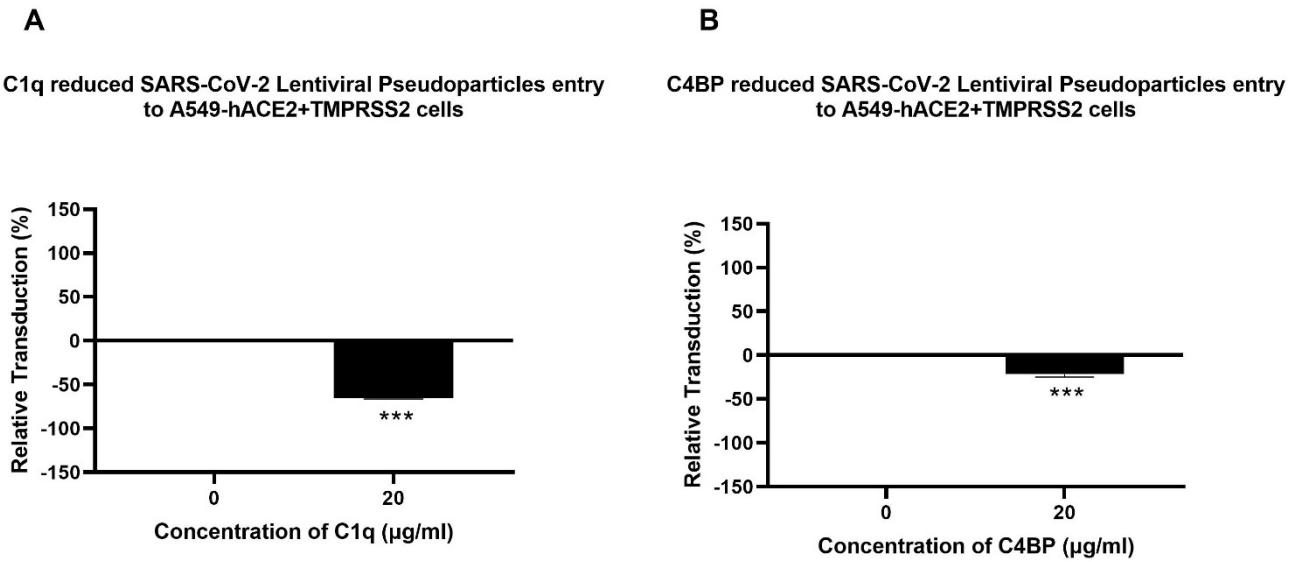

Figure 4.2: *C1q (A) and C4BP (B) inhibit the transduction of SARS-CoV-2 Spike pseudotypes in A549-hACE2+TMPRSS2 cells*. *C1q (A) and C4BP (B) were found to inhibit the entry of SARS-CoV-2 pseudoparticles into A549-hACE2+TMPRSS2 cells. To assess the impact of complement protein treatment on the ability of lentiviral pseudoparticles to enter the cells, luciferase reporter activity was measured in A549-hACE2+TMPRSS2 cells transduced with either treated or untreated SARS-CoV-2 lentiviral pseudoparticles that were pre-treated with C1q or C4BP (20µg/ml). Background values were subtracted from all data points, and the obtained data were normalised with 0% luciferase activity representing the mean relative luminescence units recorded from the control sample (A549-hACE2+TMPRSS2 cells + SARS-CoV-2 lentiviral pseudoparticles). The pseudoparticles pre-treated with C1q and C4BP demonstrated a substantial reduction in viral transduction. The data are presented as the normalised mean of three independent experiments, each carried out in triplicates, with the error bars representing the standard error of the mean (SEM). Statistical significance was determined using the two-way ANOVA test (*** $p < 0.001$) (n = 3). MBP was used as a negative control; appendix7.*

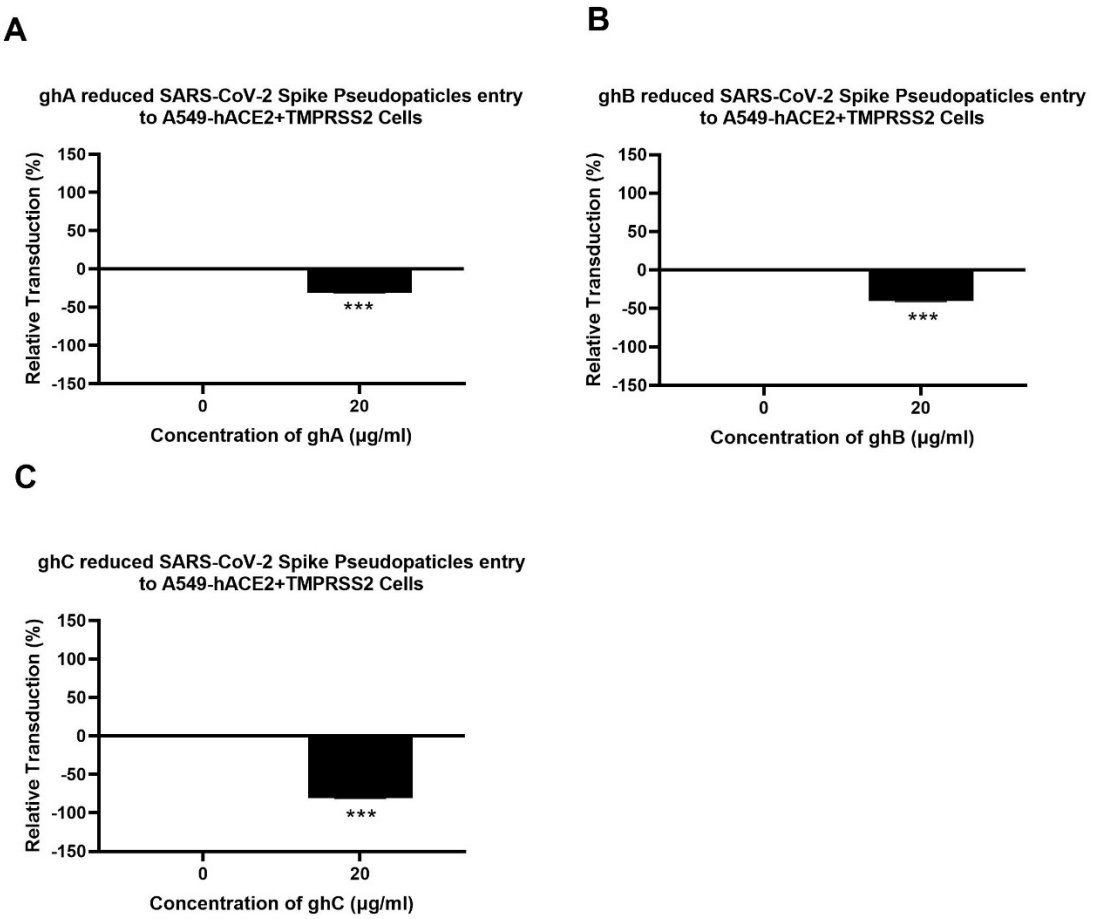

Figure 4.3: *C1q globular head modules inhibit the transduction of SARS-CoV-2 Spike pseudotypes in A549-hACE2+TMPRSS2 cells. Recombinant ghA, ghB, and ghC modules of human C1q were found to inhibit SARS-CoV-2 pseudoparticle entry into A549-hACE2+TMPRSS2 cells. To assess the interference of these recombinant C1q modules with pseudoparticle entry, SARS-CoV-2 pseudoparticles were pre-treated with ghA (A), ghB (B), or ghC (C) at a concentration of 20µg/ml. Luciferase reporter activity was measured in A549-hACE2+TMPRSS2 cells transduced with pseudoparticles pre-treated with ghA, ghB, or ghC. The background was subtracted from all data points. The obtained data were normalised, with 0% luciferase activity defined as the mean of the relative luminescence units recorded from the untreated sample (A549-hACE2+TMPRSS2 cells + MBP + SARS-CoV-2 pseudoparticles). The results are presented as the normalised mean of three independent experiments conducted in triplicates, with error bars expressed as ± SEM. Statistical significance was determined using the two-way ANOVA test (*** p < 0.001) (n = 3). MBP was used as a negative control; appendix 7.*

4.3.3 Human C1q, Recombinant Globular Head Modules, and C4BP Inhibit SARS-CoV-2 Pseudoparticle Binding to ACE2- and TMPRSS2-Expressing A549 Cells

A cell binding assay evaluated the potential interference of C1q, ghA, ghB, ghC, and C4BP with SARS-CoV-2 binding to lung epithelial-like cells. A549-hACE2+TMPRSS2 cells were challenged with SARS-CoV-2 lentiviral pseudoparticles pre-treated with C1q, ghA, ghB, ghC, or C4BP. The results demonstrated reduced viral binding to the cells compared to untreated controls. Specifically, SARS-CoV-2 pseudoparticles treated with C1q or C4BP resulted in a decrease by ~ 65% (Figure 4.4A) and ~ 37% (Figure 4.4B), respectively, in viral binding compared to the

control group (A549-hACE2+TMPRSS2 cells + SARS-CoV-2 pseudoparticles). No statistically significant difference was observed in binding efficiency between A549 cells challenged with the SARS-CoV-2 pseudotype and the control group of native A549 cells.

Furthermore, SARS-CoV-2 pseudoparticles pre-treated with ghA, ghB, or ghC exhibited a reduction in viral binding by ~38% (Figure 4.5A), ~45% (Figure 4.5B), and ~70% (Figure 4.5C), respectively, compared to the control group (A549-hACE2+TMPRSS2 cells + SARS-CoV-2 pseudoparticles + MBP). These findings strongly suggest that both C1q and C4BP can inhibit SARS-CoV-2 pseudotype binding and subsequent entry into the target cell, and this inhibition occurs independent of complement activation. Notably, no significant difference was observed between the group of A549-hACE2+TMPRSS2 cells treated with the SARS-CoV-2 pseudotype + MBP and the control group of A549-hACE2+TMPRSS2 cells treated with the SARS-CoV-2 pseudotype alone. This observation indicates that the inhibition of viral binding is driven explicitly by the presence of the globular heads (ghA, ghB, and ghC). The results with the mean fluorescence units found in Appendices 6.

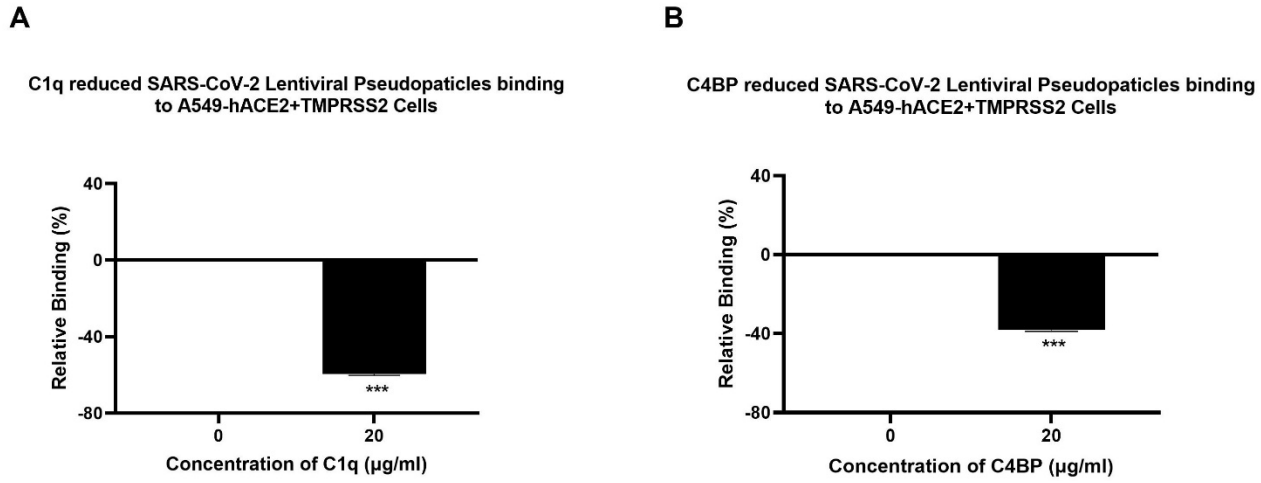

Figure 4.4: *C1q (A) and C4BP (B) reduce the binding of SARS-CoV-2 Spike pseudotypes in A549-hACE2+TMPRSS2 cells. The binding of C1q (A) or C4BP (B) treated SARS-CoV-2 pseudoparticles to A549-hACE2+TMPRSS2 cells was examined. SARS-CoV-2 lentiviral pseudoparticles were used to transduce A549-hACE2+TMPRSS2 cells pre-incubated with C1q or C4BP (20µg/ml). After washing and fixation with 1% v/v paraformaldehyde for 1 minute, the wells were probed with rabbit anti-SARS-CoV-2 spike (1:200) polyclonal antibodies. The obtained data were normalised with 0% fluorescence representing the mean of the relative fluorescence units recorded from the untreated sample (A549-hACE2+TMPRSS2 cells + SARS-CoV-2 lentiviral pseudoparticles). Three independent experiments were conducted in triplicates, and the error bars are presented as ± SEM. Statistical significance was determined using the two-way ANOVA test (*** $p < 0.001$) (n = 3). MBP was used as a negative control; appendix 6.*

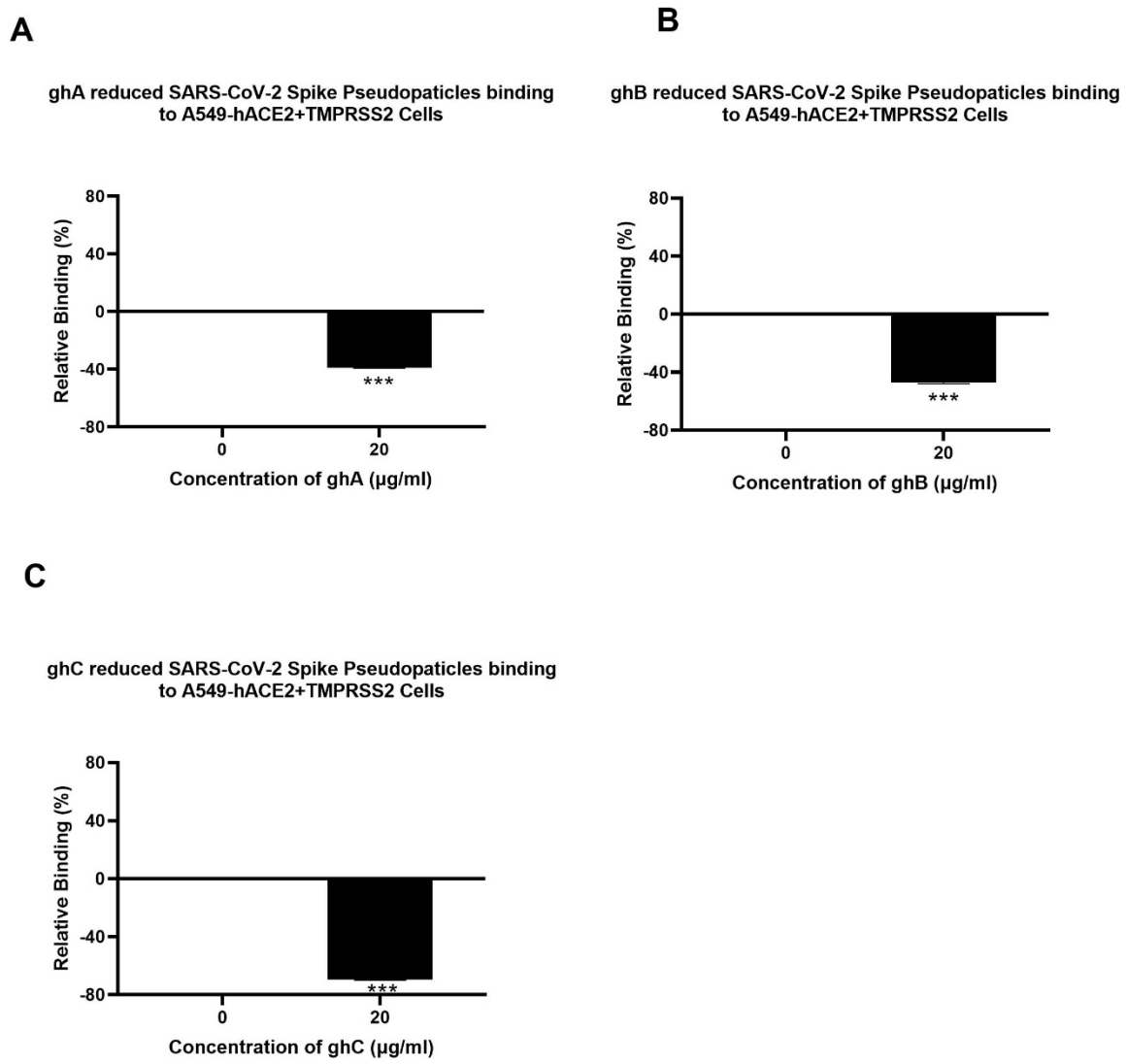

Figure 4.5: *C1q globular head modules block the binding of SARS-CoV-2 Spike pseudotypes in A549-hACE2+TMPRSS2 cells. The ability of recombinant ghA (A), ghB (B), or ghC (C) to interfere with the binding of SARS-CoV-2 lentiviral pseudoparticles to A549-hACE2+TMPRSS2 cells was investigated. A549-hACE2+TMPRSS2 cells were transduced with SARS-CoV-2 pseudoparticles following pre-incubation with or without ghA, ghB, or ghC at a 20µg/ml concentration. After removing unbound protein and viral particles, the wells were fixed with 1% v/v paraformaldehyde for 1 min and probed with rabbit anti-SARS-CoV-2 spike (1:200) polyclonal antibodies. The obtained data were normalised, with 0% fluorescence as the mean of the relative fluorescence units recorded from the untreated sample (cells + MBP + pseudoparticles). Three independent experiments were carried out in triplicates, and error bars represent ± SEM. Statistical significance was determined using the two-way ANOVA test (*** $p < 0.001$) (n = 3).*

4.3.4 C1q and C4BP Attenuate Inflammatory Response in SARS-CoV-2 Pseudoparticles Challenged A549-hACE2+TMPRSS2 Cells

The effect of C1q or C4BP on NF-κB activation in lung epithelial-like A549 cells challenged with SARS-CoV-2 pseudoparticles was assessed using a luciferase reporter assay. The NF-κB pathway is frequently associated with a proinflammatory cellular signal and responses. A549-hACE2+TMPRSS2 cells, challenged with SARS-CoV-2 S protein that was pre-treated with C1q,

showed ~65% reduction in NF-κB activation compared to the untreated control (A549-hACE2+TMPRSS2 cells + SARS-CoV-2 spike protein) (Figure 4.6A). A ~ 17% decrease in NF-κB activation was observed in A549-hACE2+ TMPRSS2 cells challenged with SARS-CoV-2 spike protein pre-treated with C4BP to the control (Figure 4.6B). These findings suggest that C1q, and to some extent C4BP, negate the SARS-CoV-2-induced inflammatory response by reducing NF-κB activation.

We also investigated the modulatory effects of C1q and C4BP on inflammatory gene expression during SARS-CoV-2 infection using RT-qPCR. That was examined by comparing the mRNA levels of proinflammatory cytokines and chemokines, such as interleukin 1 beta (IL-1β), IL-8, tumour necrosis factor-alpha (TNF-α), interferon alpha (IFN-α), nuclear factor kappa B (NF-κB), and RANTES, in treated cells (protein + SARS-CoV-2 alphaviral pseudoparticles + A549-hACE2+TMPRSS2 cells) with their respective controls (SARS-CoV2-alphaviral pseudoparticles + A549-hACE2+ TMPRSS2 cells). Our finding revealed that SARS-CoV-2 alphaviral-pseudoparticles induce Inflammatory Response in A549-hACE2 + TMPRSS2 Cells, appendix 11. The data revealed immune modulation in A549-hACE2+ TMPRSS2 cells by C1q and C4BP (Figure 4.7 and Figure 4.8). A549-hACE2+ TMPRSS2 cells, when challenged with SARS-CoV-2 alphaviral pseudoparticles that were pre-incubated with C1q (C1q-treated cells), exhibited lower mRNA levels of IFN-α, IL-6, RANTES, IL-1β, IL-8, and TNF-α, compared to their respective untreated control (Figure 4.7). C1q caused a reduction in NF-κB gene expression levels at 6 h (−0.8 $\log_{10}$-fold), with a marked effect evident at 12 h (~−2.5 $\log_{10}$) (Figure 4.7A). At 6 h, C1q-treated cells displayed a decrease in mRNA levels of IL-6 (~−1 $\log_{10}$) (Figure 4.7B), IFN-α (~−0.3 $\log_{10}$) (Figure 4.7C), IL-1β (~−1.5 $\log_{10}$) (Figure 4.7D), and TNF-α (~−1.5 $\log_{10}$) (Figure 4.7E), compared to their respective controls. Similarly, at 12 h post-infection, C1q-treated cells exhibited lower gene expression levels of IL-6 (~ −5 $\log_{10}$) (Figure 4.7B), IFN-α (~−1.9 $\log_{10}$) (Figure 4.7C), IL-1β (~−4.5 $\log_{10}$) (Figure 4.7D), and TNF-α (~−4.4 $\log_{10}$) (Figure 4.7E). RANTES mRNA levels remained unchanged at 6 h in C1q-treated cells, while at 12 h, a significant reduction was observed (~−2.3 $\log_{10}$) (Figure 4.7F). C1q-treated cells showed downregulation of IL-8 mRNA levels at 6 h (~−1.5 $\log_{10}$) and 12 h (~−4.7 $\log_{10}$) when compared to their respective controls (Figure 4.7G).

The immune modulatory effects of SARS-CoV-2 alphaviral pseudoparticles that were pre-treated with C4BP and then challenged against A549-hACE2+TMPRSS2 cells (C4BP- treated

cells) were similar to C1q (Figure 4.8). C4BP-treated cells had reduced mRNA levels of IFN-α, IL-6, RANTES, IL-1β, IL-8, TNF-α, and NF-κB compared to the control cells. At 6 h, C4BP-treated cells showed lower NF-κB gene expression levels (∼−0.4 $\log_{10}$) than untreated cells, with further reduction at 12 h (∼−1.5 $\log_{10}$) (Figure 4.8A). No significant change in the mRNA level of IL-6 was observed at 6 h; nevertheless, there was a noticeable downregulation at 12 h (∼−1.9 $\log_{10}$) in C4BP-treated cells (Figure 4.8B). Compared to their respective controls, mRNA levels at 6 h of IFN-α (∼−0.8 $\log_{10}$) (Figure 4.8C), IL-1β (∼−1.2 $\log_{10}$) (Figure 4.8D), TNF-α (−1 $\log_{10}$-fold) (Figure 4.8E), RANTES (−0.2 $\log_{10}$-fold) (Figure 4.8F), and IL-8 (∼−1 $\log_{10}$) (Figure 4.8G) were reduced in C4BP-treated cells, whereas at 12 h the mRNA levels of IFN-α, IL-1β, TNF-α, RANTES, and IL-8 were even further downregulated (∼−1 $\log_{10}$, ∼−2.4 $\log_{10}$, ∼−1 $\log_{10}$, ∼−0.4 $\log_{10}$, and ∼−1.8 $\log_{10}$, respectively). These results suggest that C1q and C4BP attenuate the inflammatory immune response in SARS-CoV-2 infection in a complement activation-independent manner.

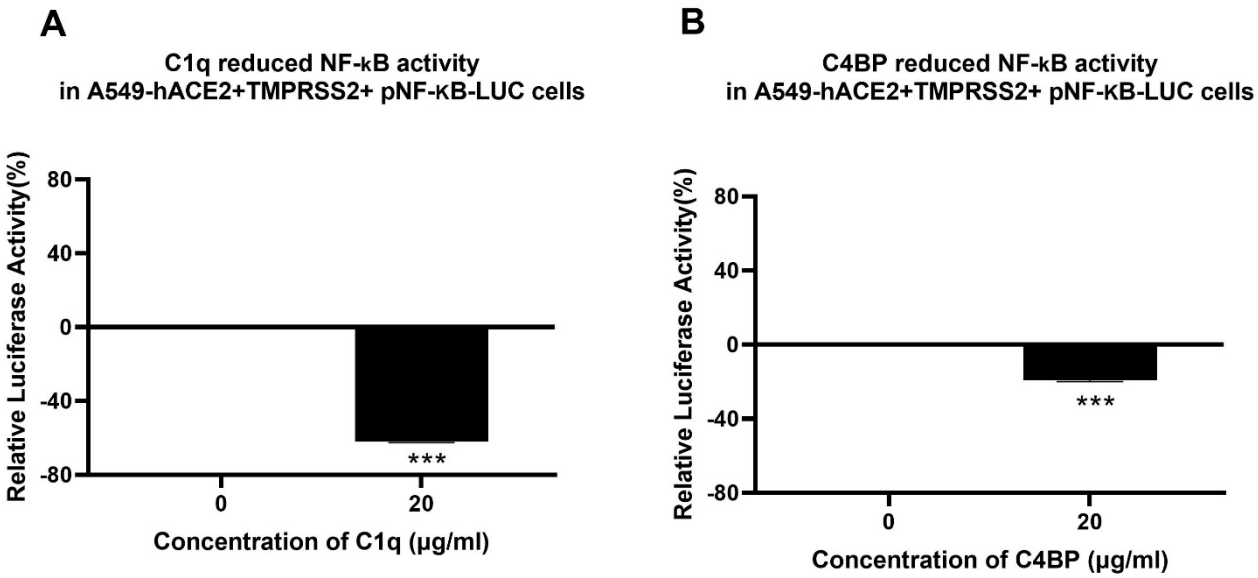

Figure 4.6: *C1q and C4BP inhibit NF-κB. C1q and C4BP exhibit inhibitory effects on NF-κB activation in A549-hACE2-TMPRSS2 cells challenged with SARS-CoV-2 spike protein. A549-hACE2+TMPRSS2 cells were transfected with pNF-κB-LUC and subsequently exposed to SARS-CoV-2 spike protein (500ng/mL) that was pre-treated with C1q (A) or C4BP (B) at a concentration of 20 µg/mL. After 24 hours of incubation, luciferase reporter activity was measured. The background was subtracted from all data points, and the obtained data were normalised, with 0% luciferase activity defined as the mean of the relative luminescence units recorded from the untreated sample (A549-hACE2+TMPRSS2 cells + SARS-CoV-2 spike protein). The data are presented as the normalised mean of three independent experiments carried out in triplicates ± SEM. Statistical significance was determined using the two-way ANOVA test (*** p < 0.001) (n = 3).*

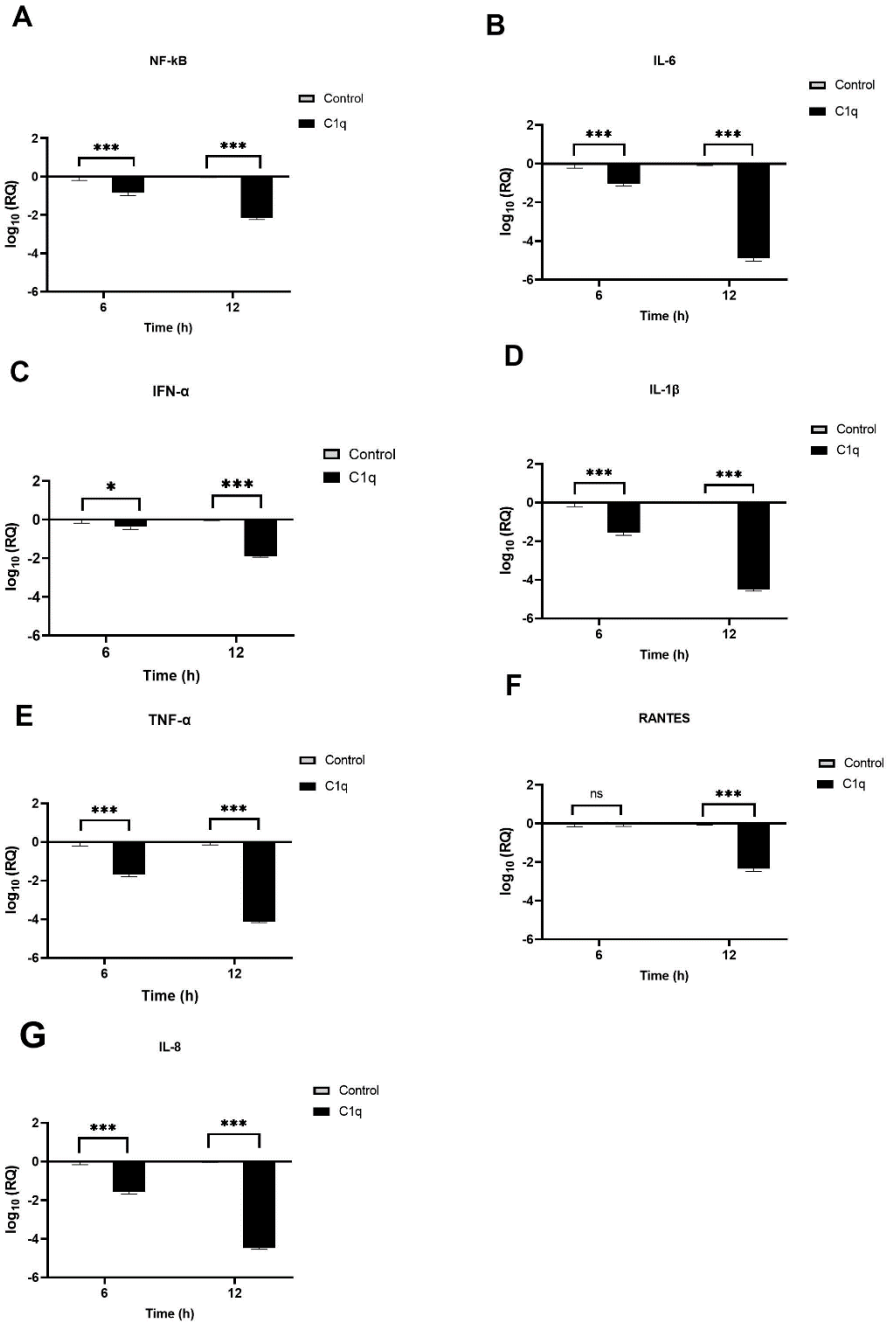

Figure 4.7: *C1q reduces the expression of proinflammatory cytokines and chemokines in A549-hACE2+TMPRSS2 cells. C1q reduces the inflammatory response in A549-hACE2+TMPRSS2 cells challenged with SARS-CoV-2 alphaviral pseudoparticles. The pseudoparticles were pre-incubated with a 20µg/ml of C1q before being used to challenge the cells. At 6 hours and 12 hours post-challenge, the cells were harvested to measure the mRNA levels of proinflammatory cytokines and chemokines. The cells were lysed, and purified RNA was converted into cDNA. RT-qPCR was then used to measure the mRNA levels of NF-κB (A), IL-6 (B), IFN-α (C), IL-1β (D), TNF-α (E), RANTES (F), and IL-8 (G). The data were normalised against 18S rRNA expression as a control, and the relative expression (RQ) was calculated using A549-hACE2+TMPRSS2 cells challenged with SARS-CoV-2 alphaviral pseudoparticles alone as the calibrator. The RQ value was determined using the RQ = $2^{\wedge(-\Delta\Delta Ct)}$. The experiments were carried out in triplicates, and error bars represent ± SEM. Statistical significance was determined using the two-way ANOVA test (* $p < 0.05$, *** $p < 0.001$, ns $p > 0.05$) (n = 3).*

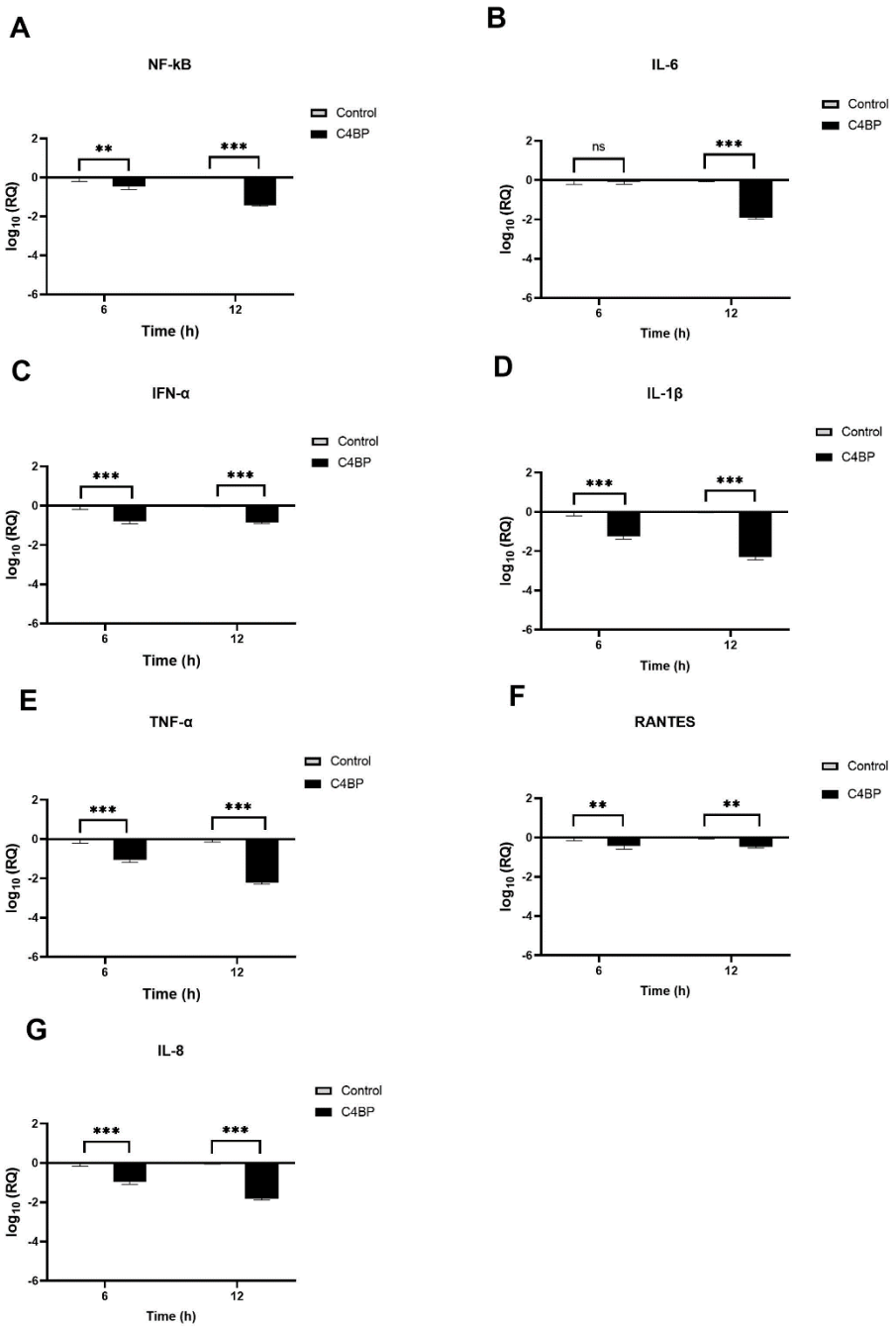

Figure 4.8: *C4BP attenuate the expression of proinflammatory cytokines and chemokines in A549-hACE2+TMPRSS2 cells. C4BP attenuates the inflammatory response in A549-hACE2+TMPRSS2 cells challenged with SARS-CoV-2 alphaviral pseudoparticles. The gene expression profile of cytokines and chemokines in these cells was examined after being challenged with SARS-CoV-2 alphaviral pseudoparticles pre-treated with and without C4BP 20µg/mlL). The expression levels of NF-κB (A), IL-6 (B), IFN-α (C), IL-1ϐ (D), TNF-α (E), RANTES (F), and IL-8 (G) were measured using RT-qPCR at 6 hours and 12 hours post-challenge. A549-hACE2+TMPRSS2 cells challenged with SARS-CoV-2 alphaviral pseudoparticles alone were used as a calibrator to calculate the relative quantitation (RQ), which was determined using the formula RQ = 2^(-ΔΔCt). The experiments were conducted in triplicates, and error bars represent ± SEM. Additionally, 18S rRNA was used as an endogenous control. Statistical significance was established using the two-way ANOVA test (** p < 0.01, *** p < 0.001, ns p > 0.05) (n = 3).*

4.4 Discussion

The COVID-19 pandemic has had a dreadful global impact, resulting in almost 20 million deaths worldwide (178). Many risk factors are claimed to be associated with the development of severe COVID-19, including pre-existing medical conditions, ageing, genetics, and immune system dysregulation. Overactivation of complement against SARS-CoV-2 has been linked with disease severity (179). Abnormality of alternative and classical complement pathways was observed in severe SARS-CoV-2 infection (167, 168). A recent study revealed complement activation is triggered by the SARS-CoV-2 S protein (180). Reduced serum C1q and C4BP levels in severe COVID-19 have been reported (167, 168). Nevertheless, the potential protective role of C1q and C4BP against SARS-CoV-2 infection remains unknown. Thus, this study aimed to examine the immune function of C1q and C4BP against SARS-CoV-2 infection, independent of complement activation.

Our findings revealed a direct interaction between SARS-CoV-2 S and RBD proteins with C1q and C4BP. In parallel, previous research showed that C1q and C4BP can directly bind to glycoproteins on the surface of many viruses, such as IAV (177, 181). SARS-CoV-2 lentiviral pseudoparticles and A549-hACE2+TMPRSS2 cells were used to investigate whether C1q and C4BP interfere with SARS-CoV-2 infection at the cellular level. SARS-CoV-2 infection can cause cellular damage in alveolar type II cells, resulting in excessive inflammation and pulmonary dysfunction (10). Alveolar type II cells are considered important players in the innate immune response to viruses because of the production of surfactant proteins A (SP-A) and D (SP-D), which act as PRRs and opsonin (33).

Additionally, human leukocyte antigen–DR isotype, CD80, and CD86, which are necessary for antigen presentation, are expressed by alveolar type II cells (182). Besides, these cells produce and secrete proinflammatory mediators (182). Nevertheles, alveolar type II cells can perform some immune functions, they are less effective than dendritic cells in antigen presentation and inducing T-cell responses (182). The A549 cell line is a physiological module for pulmonary epithelium for *in vitro* studies (183). Here we have used A549 cell expressing human ACE2 and TMPRSS2 (A549-hACE2+TMPRSS2 cells) as *in vitro* model, appendix 5.

SARS-CoV-2 is considered a BSL-3 pathogen due to its highly contagious nature; however, this study has used SARS-CoV-2 lentiviral pseudotype which expressed spike protein, and SARS-

CoV-2 alphaviral pseudotype that expresses S, E, N, and M. These pseudotyped particles have the benefit of being safe, easily to use in BSL-2 laboratories because of lack viral replication ability (106). Viral pseudotyped particles have become useful for studying sero-surveillance, antigenic properties, and viral entry mechanisms of emerging viral infections (184, 185). Many studies have shown that assays for neutralising pseudotyped particles are comparable and robust as those conducted with wild-type viruses (184, 185).

C1q is a key component of the classical pathway, which is locally produced and secreted by dendritic and macrophages (186). It has been demonstrated that C1q neutralized IAV in vitro (177). Furthermore, C1q interacts with envelope glycoproteins of other viruses, such as gp41 and gp120 of HIV-1, p15E of the murine leukaemia virus (MuLV), and gp21 of the human T lymphotropic virus (HTLV)-1, through its globular chains (ghA, ghB, and ghC) (177). Conversely, lung alveolar type II cells can produce C4BP locally, a potent fluid-phase inhibitor of the lectin and classical pathways (175). It has been revealed that C4BP can interact with cell surface heparin-sulfate proteoglycans to enhance the uptake of adenoviruses by hepatocytes (55). Moreover, C4BP inhibit IAV infection in A549 cells (55). These studies suggest that C1q and C4BP synthesis locally plays an important protective role in preventing viral infection.

The potential interference of C1q, its globular heads, ghA, ghB, ghC, and C4BP on SARS-CoV-2 binding to A549-hACE2+TMPRSS2 cells was assessed using a cell binding assay. Compared to the control, the results showed a reduction in the binding of SARS-CoV-2 lentiviral pseudoparticles to A549-hACE2+TMPRSS2 cells. Similarly, C1q and C4BP have been shown to inhibit IAV cell entry independently of complement activation (177, 181). Luciferase reporter gene assay was conducted to determine whether C1q, ghA, ghB, ghC, and C4BP on cell binding would impact viral cell entry. Our finding revealed a reduction in the transduction of SARS-CoV-2 lentiviral pseudoparticles pre-treated with C1q, ghA, ghB, ghC, or C4BP in A549-hACE2+TMPRSS2 cells. These results suggest a crucial role in C1q and C4BP in blocking SARS-CoV-2 cell entry into the lung epithelium independently of complement activation.

As it has been mentioned above, the findings showed that A549-hACE2+TMPRSS2 cells challenged with SARS-CoV-2 pretreated with C1q globular heads A, B, or C (ghA, ghB, or ghC), inhibit viral pseudotypes binding and entry of viral cells compared to MBP treated cell (as a relevant control). These results imply that distinct structural domain of each globular head can identify, interact and attach to various regions of the viral spike protein. Through this

interaction, the viral pseudotypes is effectively prevented from attaching to the cells, thereby effectively preventing viral entry and infection.

Dysregulation of inflammatory response in SARS-CoV-2 infection contributes significantly to developing severe disease (186). Elevated Serum levels of TNF-α, IL-1β, IL-6, and IL-8 have been observed in patients with severe COVID-19 (187, 188). It has been reported that the complement classical pathway is involved in the immunopathogenesis of SARS-CoV-2 infection (189). Furthermore, alveolar type II cells infected with SARS-CoV-2 have been shown to express elevated mRNA levels of IL-6, TNF-α, MIP-2, and IL-8 (190). Therefore, this study has used qPCR analysis to investigate whether C1q and C4BP may affect the expression of proinflammatory genes in A549-hACE2+TMPRSS2 cells challenged with SARS-CoV-2 viral pseudoparticles, independently from complement activation.

The structural proteins of SARS-CoV-2, Spike (S), envelope (E), and nucleocapsid (N) have been shown in many studies to induce inflammatory responses in the respiratory epithelium (191, 192). Therefore, we have used SARS-CoV-2 alphaviral pseudoparticles expressing S, E, N, and M proteins as a safe viral model to examine the expression of proinflammatory cytokines and chemokines in a lung epithelial model. RT-qPCR analysis revealed that SARS-CoV-2 alphaviral pseudoparticles could induce inflammation in A549 cells that express the human co-receptors ACE2 and TMPRSS2.

NF-κB is key to an effective and efficient immune response to viral infections (193). However, dysregulated NF-κB activity has been observed in severe SARS-CoV-2 infection, which is linked to increased levels of proinflammatory cytokines, such as RANTES, MCP1, IL-6, IL-21, IL-1, IL-2, IL-8, MIP-1, and MCP1 (193). Blocking NF-κB has been proposed as an effective therapeutic approach for severe SARS-CoV-2 infection (193). Here, we revealed that A549-hACE2+TMPRSS2 cells challenged with SARS-CoV-2 alphaviral pseudoparticles pre-treated with C1q or C4BP decreased NF-κB gene and protein expression levels. That suggests C1q and C4BP may prevent an immune system overreaction in SARS-CoV-2 infection due to dysregulation of NF-κB activity.

IL-1β plays a crucial role in inflammatory response to control viral infection (194).). It has been reported that SARS-CoV-2 causes IL-1β production which leads to TNF-α and IL-6 secretion (195, 196). Elevated IL-1β levels in patients with severe SARS-CoV-2 infection have

been observed (197). SARS-CoV-2-induced cell death is considerably inhibited by targeting IL-1ß in vitro (198). Here, we have shown that mRNA levels of IL-1β were reduced in A549-hACE2+TMPRSS2 cells challenged with SARS-CoV-2 alphaviral pseudoparticles pre-treated with C1q or C4BP. That implies an immune protective role of C1q and C4BP in lessening excessive inflammation in SARS-CoV-2 infection because of IL-1β irregularity. TNF-α plays a vital role in eliminating viral infection (199). Nevertheless, high serum levels of TNF-α have been associated with severe SARS-CoV-2 infection (199). That may lead to lung tissue damage and a poor prognosis (199). Our results indicated a reduction in mRNA levels of TNF-α in A549-hACE2+TMPRSS2 cells challenged with SARS-CoV-2 alphaviral pseudoparticles pre-treated with C1q or C4BP. That suggests that C1q and C4BP modulate TNF-α's role in SARS-CoV-2-mediated immunopathogenesis. Il-6 is considered a protective factor in viral infection (200). However, elevated serum levels of IL-6 were reported in SARS-CoV-2 pneumonia patients, which correlates with the severity of the disease (200). Here, we have shown decreased IL-6 mRNA levels in A549-hACE2+TMPRSS2 cells challenged with SARS-CoV-2 alphaviral pseudoparticles pre-treated with C1q or C4BP. The results imply the preventive roles of C1q and C4BP in the inflammatory response induced by IL-6 abnormality. IFN-α is a crucial cytokine in controlling and eliminating viral infection (201). Nevertheless, elevated serum levels of IFN-type 1 in late stage of SARS-CoV-2 infection (201). That may involve immunopathology in severe COVID-19 (201). Our findings revealed reduced mRNA levels of IFN-α in A549-hACE2+TMPRSS2 cells challenged with SARS-CoV-2 alphaviral pseudoparticles pre-treated with C1q or C4BP.

Chemokines such as IL-8 and RANTES play an essential role in attracting leukocytes to the site of viral infection, which is a key step in our immune defense mechanisms (202). High levels of neutrophil infiltration were reported due to elevated levels of IL-8 in severe SARS-CoV-2 infection (202). That can lead to respiratory failure and acute kidney injury (202). Our results showed lower IL-8 mRNA levels in A549-hACE2+TMPRSS2 cells challenged with SARS-CoV-2 alphaviral pseudoparticles pre-treated with C1q or C4BP

Another chemokine is RANTES, which play role in viral control via the recruitment of effector immune cells (203). Nevertheless, high serum levels of RANTES were found in severe COVID-19 and may contribute to disease severity (203). Here, we showed that reduced mRNA levels of RANTES in A549-hACE2+TMPRSS2 cells were challenged with SARS-CoV-2 alphaviral

pseudoparticles pre-treated with C1q or C4BP. These findings suggest the immunomodulatory role of C1q and C4BP in downregulating IL-8 and RANTES in severe SARS-CoV-2 infection.

More studies are required to understand better C1q and C4BP interaction with S protein of different SARS-CoV-2 variations. Furthermore, in vivo studies to assess the impact of locally produced C1q and C4BP in SARS-CoV-2 infection in the lung microenvironment can provide a deep understanding of infection dynamics and immune response. We showed that C1q and C4BP can directly interact with the SARS-CoV-2 spike and receptor-binding domain (RBD). Also, C1q and C4BP inhibited SARS-CoV-2 binding and viral cell entry in A549-hACE2+TMPRSS2 cells. Moreover, C1q and C4BP downregulated mRNA levels of proinflammatory cytokines and chemokines, including RANTES, TNF-α, IFN-α, IL-1β, IL-8, and IL-6, in A549-hACE2+TMPRSS2 cells independently of complement activation. These findings suggest that C1q and C4BP may act as PRR as the first lines of defence mechanism against SARS-CoV-2 infection.

Chapter 5

Human complement Properdin and Factor H differentially modulate SARS-CoV-2 Infection

5.1 Abstract

Severe SARS-CoV-2 infection characterises with immune response dysregulation resulting in acute respiratory distress syndrome (RDS), multiorgan failure and death. The complement system has been reported to contribute to the pathology of SARS-CoV-2 infection. Properdin (FP) and factor H (FH) are key regulatory proteins in the complement alternative pathway. Abnormal gene expression levels of FP and FH in severe SARS-CoV-2 infection have been observed. Here, we assessed the immune functions of FH and FH in SARS-CoV-2 infection independently of complement activation. FH and FP directly interacted with the SARS-CoV-2 spike (S) and receptor binding domain (RBD), which were examined using direct ELISA. Viral cell binding and entry assays revealed FH can reduce viral cell binding and entry in A549 o-expressing human ACE2 and TMPRSS2 (A549-hACE2+TMPRSS2 cells) challenged with SARS-CoV-2 lentiviral pseudoparticles pretreated with FH. On the contrary, FP-enhanced viral cell binding and entry in A549-hACE2+TMPRSS2 cells were challenged with SARS-CoV-2 lentiviral pseudoparticles pretreated with FP. Furthermore, lower mRNA levels of IL-1β, IL-6, TNF-α, INF-α, RANTES, and NF-κB in A549-hACE2+TMPRSS2 cells challenged with SARS-CoV-2 alphativiral pseudoparticles pretreated with FH. Controversy, upregulation in mRNA levels of IL-1β, IL-6, TNF-α, IFN-α, RANTES, and NF-κB activity in A549-hACE2+TMPRSS2 cells f TMPRSS2 have been shown when cells challenged with SARS-CoV-2 alphativiral pseudoparticles pretreated with FP. Moreover, FP enhanced NF-κB in A549-hACE2+TMPRSS2 cells challenged with SARS-CoV-2 spike protein, in which anti-FP antibodies reverse this effect. This study revealed that FH might prevent viral cell binding and entry and downregulation of proinflammatory response in SARS-CoV-2 infection in A549-hACE2+TMPRSS2 cells. On the other hand, FP can upregulate proinflammatory immune response and viral cell binding and entry in A549-hACE2+TMPRSS2 cells in SARS-CoV-2 infection. These effects of FH and FP are independent of complement activation.

5.2 Introduction

Hyperinflammation and immune response dysfunction are key hallmarks of severe SARS-Cov-2 infection (178). The complement system is part of the innate immune response, vital in eliminating viral infection. Previous research has revealed activation of the lectin pathway through the interaction of mannan-binding lectin (MBL) with SARS-CoV (204). Moreover, complement can induce hyperinflammation in Middle East respiratory syndrome coronavirus (MERS-CoV) in animal modules(164). Recently, C1q and C4BP have been shown to downregulate proinflammatory response and inhibit viral cell entry in SARS-CoV-2 infection independently of complement activation (178).

The three pathways of the complement (classical, alternative, and lectin)can be activated in SARS-CoV-2 infection (166). Severe SRAS-CoV-2 infection is associated with alternative pathway dysfunction (168). Notably, it has been shown that the SARS-CoV-2 spike protein can directly induce the activation of the alternative pathway (205). Importantly, abnormal gene expression levels of FH and FP in patients with severe COVID-19 have been reported (167, 168, 173, 206).

Complement FH is a soluble glycoprotein that acts as inhibitor of complement alternative pathways by accelerating the decay of C3 convertase C3bBb (207, 208). Serum concertation of FH is between 128 to 654 µg/ml and has a molecular weight of 155 kDa (207, 208). It is produced by hepatocytes and locally in lungs by fibroblasts and DCs (208-210). FH plays a defense role against viruses such as West Nile by interacting with the West Nile virus's NS1 protein (211). Furthermore, FH can block influenza A virus (IAV) cell entry and attenuate proinflammatory responses subtype-dependently in A549 cells (212). The full-length 3D structure of FH is found in Appendix 10.

Another alternative soluble protein is FP, which act as a positive regulator by stabilising C3-convertase and C5-convertase (55). It synthesises macrophages, Langerhans cells, monocytes, Kupffer cells, and neutrophil storage (55, 181). FP is found in cyclic polymers, including cyclic dimers, trimers, and tetramers in the serum, with concentrations ranging from 22 to 25 µg/ml (181). The FP monomer has a molecular weight of 53 kDa and comprises seven non-identical thrombospondin type 1 repeats (TSRs, 0-6) (181). TSR4 and TSR5 are essential for binding other molecules, such as C3-convertase (181). Recently, a recombinant form of TSR4+5

(expressed and produced as a double domain) can bind to C3b and inhibit alternative pathway activity (181). FP can act as a pattern recognition molecule (PRR) and block influenza A virus (H1N1 subtype) cell binding and entry, downregulating inflammation independently of complement activation (181).

The roles of FH and FP in SARS-CoV-2 infection remain unknown; therefore, this study aimed to investigate the potential immune functions of purified human FH, FP, and recombinant TSR4+5 proteins in SARS-CoV-2 infection in a complement-independent manner.

Here, we have assessed the interaction of FH and FP with SARS-CoV-2 S and RBD proteins. Additionally, the impact of FH and FP in cell viral binding and entry in SARS-CoV-2 infection was investigated by utilising A549 cells (lung epithelial-like cells) that express human ACE2 and TMPRSS2 receptors (A549-hACE2+TMPRSS2) and SARS-CoV-2 viral pseudotype as a safe model for the live virus. Our findings revealed that FH can block SARS-CoV-2 pseudotype cell binding and entry, attenuating proinflammatory response in A549-hACE2+TMPRSS2, whereas FP exhibits an enhancing effect, potentially promoting viral binding and entry. In addition, upregulation of the proinflammatory response is observed in A549-hACE2+TMPRSS2 challenged with SARS-CoV-2 viral pseudotype pre-treated with FP.

5.3 Results

5.3.1 SARS-CoV-2 Spike and RBD Proteins interact with FH and FP

The binding between purified FH and SARS-CoV-2 S and RBD proteins and the reverse binding of SARS-CoV-2 S and RBD proteins to immobilised FH were assessed using ELISA. The results revealed a dose-dependent binding of FH to both S and RBD proteins, as detected by an anti-SARS-CoV-2 S protein polyclonal antibody (Figure 5.1A). Likewise, when using a rabbit anti-human FH polyclonal antibody, the immobilised S protein or RBD exhibited dose-dependent binding to FH (Figure 5.1B).

Additionally, the direct ELISA assay was utilised to assess the binding ability of purified FP to SARS-CoV-2 S and RBD proteins. The findings demonstrated that immobilised FP showed dose-dependent binding to S and RBD proteins, which was detected with a polyclonal anti-SARS-CoV-2 S protein antibody (Figure 5.1C). Similarly, the immobilised SARS-CoV-2 S or RBD proteins displayed dose-dependent binding to FP when detected with a rabbit anti-human FP polyclonal antibody (Figure 5.1D), and similar results were obtained using recombinant TSR4+5 modules detected with anti-MBP antibodies (Appendices 7). BSA was used as a negative control protein.

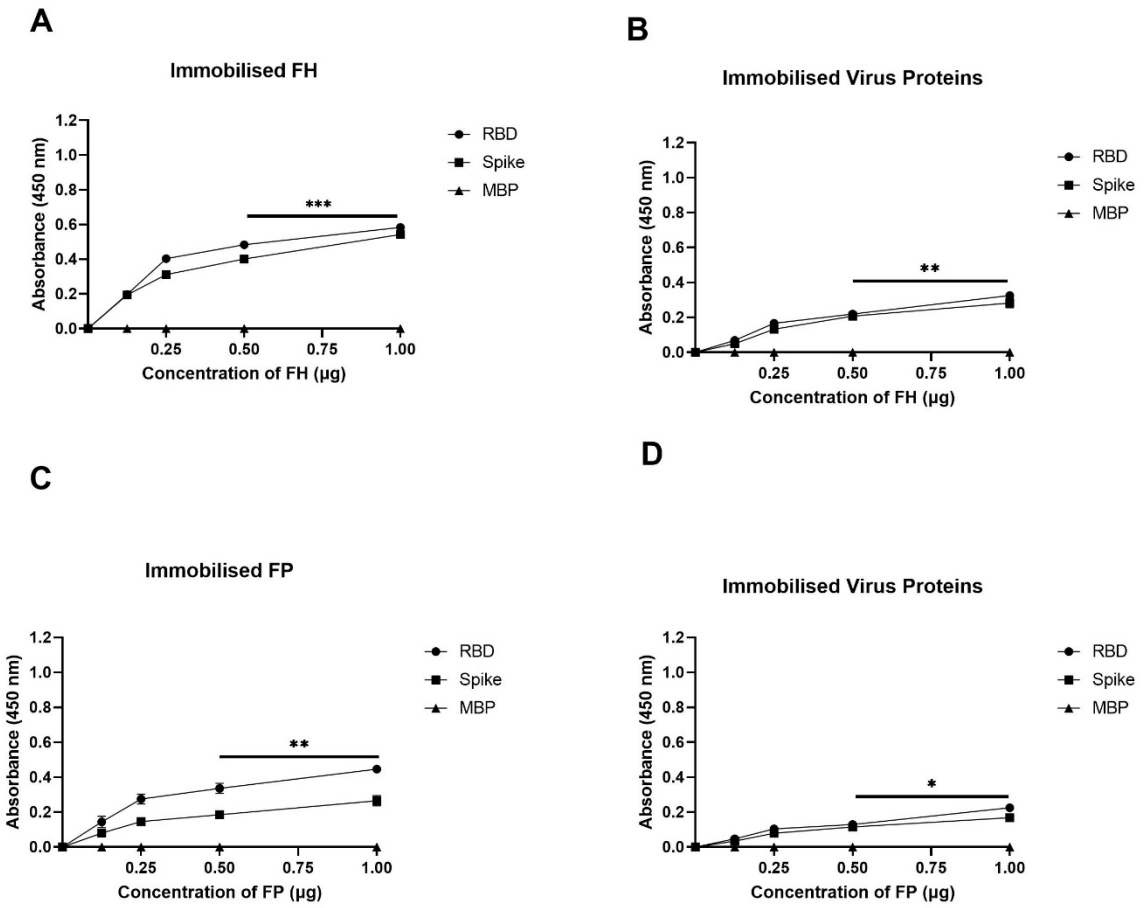

Figure 5.1: *SARS-CoV-2 Spike protein directly interacts with FH and FP via its RBD*. *In a dose-dependent manner, FH was found to bind both SARS-CoV-2 Spike and RBD proteins. Decreasing concentrations of FH or FP (1, 0.5, 1.25, and 0 µg/well) were immobilised on a 96-well plate using Carbonate-Bicarbonate (CBC) buffer, pH 9.6, and left overnight at 4°C. After washing off the excess CBC buffer with PBS, a constant concentration of viral proteins (1 µg/well) was added to the corresponding wells and incubated at 37°C for 2 hours. Unbound proteins were then washed off, and the wells were probed with corresponding primary antibodies (1:5000; 100 µl/well), namely rabbit anti-SARS-CoV-2 Spike or rabbit anti-human FH or FP polyclonal antibodies. MBP was used as a negative control. The data were expressed as the mean of triplicates ± SD. Statistical significance was determined using the two-way ANOVA (* $p < 0.05$, ** $p < 0.01$, and *** $p < 0.001$) (n = 3).*

5.3.2 FH restricted SARS-CoV-2 Pseudoparticle transduction, while FP and TSR4+5 promoted

A luciferase reporter assay was employed to assess the impact of FH, FP, and TSR4+5 (showed to bind to spike and RBD, appendix 10) on SARS-CoV-2 infectivity. When SARS-CoV-2 lentiviral pseudoparticles were pre-treated with FH, there was a reduction in viral transduction by ~ 25% in A549-hACE2+TMPRSS2 cells (Figure 5.2A). In contrast, treatment with FP or TSR4+5 increased viral transduction by ~ 80% and ~ 140% (Figure 5.2B and (Figure 5.2C), respectively, compared to their respective controls. These findings indicate that FH acts as an inhibitor, hindering the entry of SARS-CoV-2 pseudotyped particles into cells, while FP seems to facilitate viral entry, potentially enhancing the infection process. The results with the mean luciferase units found in Appendix 8.

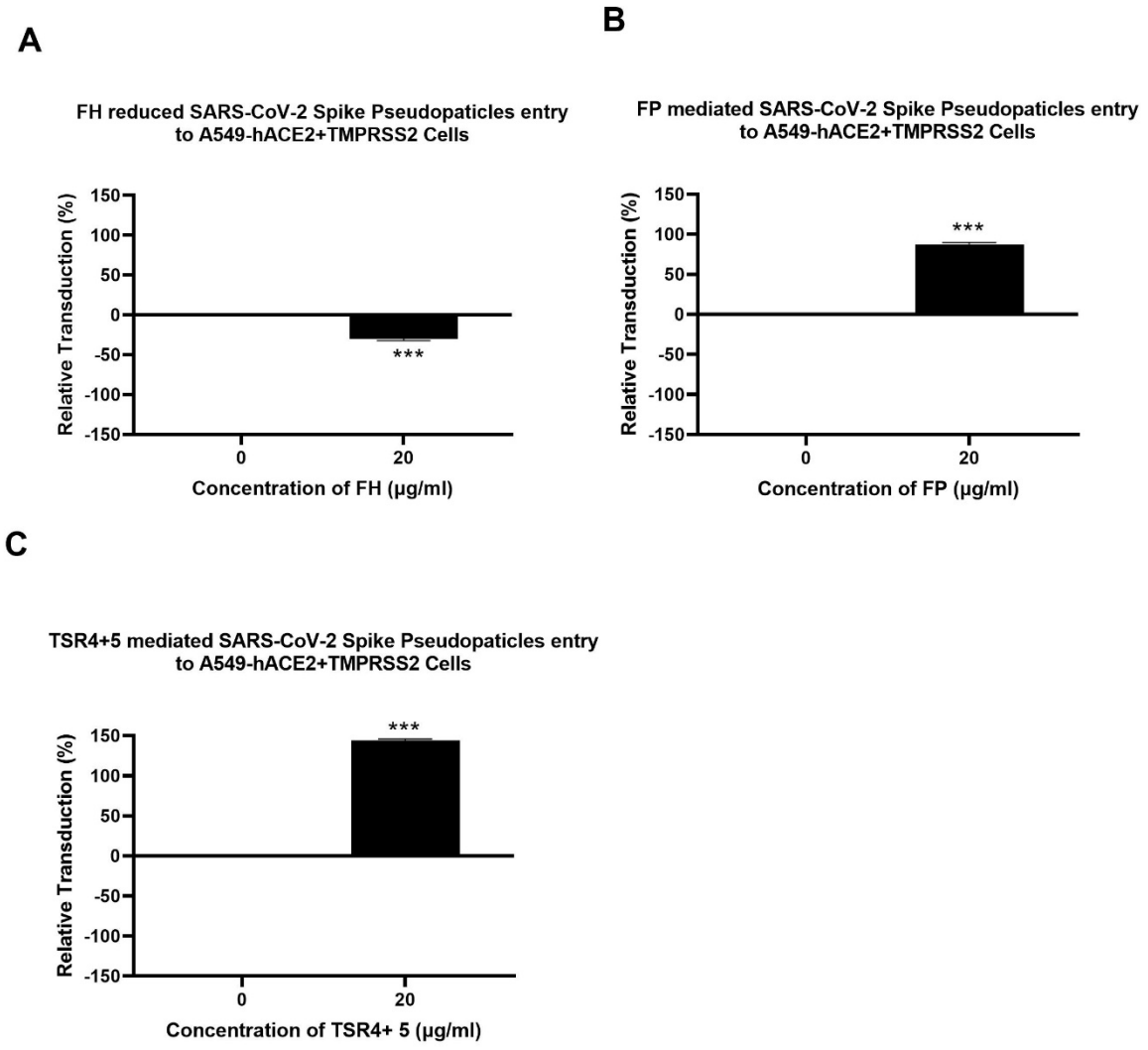

Figure 5.2: *Modulation of SARS-CoV-2 pseudotype viral entry in A549-hACE2+TMPRSS2 cells by FH, FP or TSR4+5 treatment. FH, FP, or TSR4+5 at a concentration of 20µg/ml were utilised to pre-treat SARS-CoV-2 lentiviral pseudoparticles in three separate experiments (A), (B), and (C), respectively. The objective was to assess if the treatment influenced the virus's ability to enter the cells. Both treated and untreated lentiviral pseudoparticles were then transduced into A549-hACE2+TMPRSS2 cells, and luciferase reporter activity was examined to measure viral transduction. The background signal was subtracted from all data points, and the obtained data were normalised using the mean of the relative luminescence units recorded from the untreated sample (Cells + lentiviral pseudoparticles), defined as 0% luciferase activity. The results were presented as the normalised mean of three independent experiments conducted in triplicates, with error bars expressing ±SEM. Significance was determined using the two-way ANOVA test (***p < 0.001) (n= 3).*

5.3.3 SARS-CoV-2 Pseudoparticle binding to the target cells was inhibited by FH and enhanced by FP and TSR4+5

A cell binding assay was used to assess the impact of FH, FP, and TSR4+5 on the binding of SARS-CoV-2 to lung epithelial-like cells (A549-hACE2+TMPRSS2 cells). Before challenging the cells, SARS-CoV-2 lentiviral pseudoparticles were treated with FH, FP, and TSR4+5. The results revealed that pre-treatment of SARS-CoV-2 pseudoparticles with FH reduced viral binding by ~ 35% (Figure 5.3A). On the other hand, compared to the control, both FP and TSR4+5 increased viral binding by ~30% and ~50%, respectively (Figure 5.3B and Figure 5.3 C). Anti-FP antibodies have significantly mitigated the effect of FP on viral entry and binding by ~98% and ~85%, respectively (Figure 5.4A and Figure 5.4B). These findings suggest that FH and FP influence SARS-CoV-2 viral binding, entry, and subsequent infection in lung epithelial-like cells in an antagonistic manner, independent of complement activation. Moreover, sequestering or neutralising FP could potentially limit viral binding and entry in SARS-CoV-2 infection, indicating the possibility of using anti-FP antibodies to mitigate the severity of the disease. The results with the mean fluorescence units found in Appendix 9.

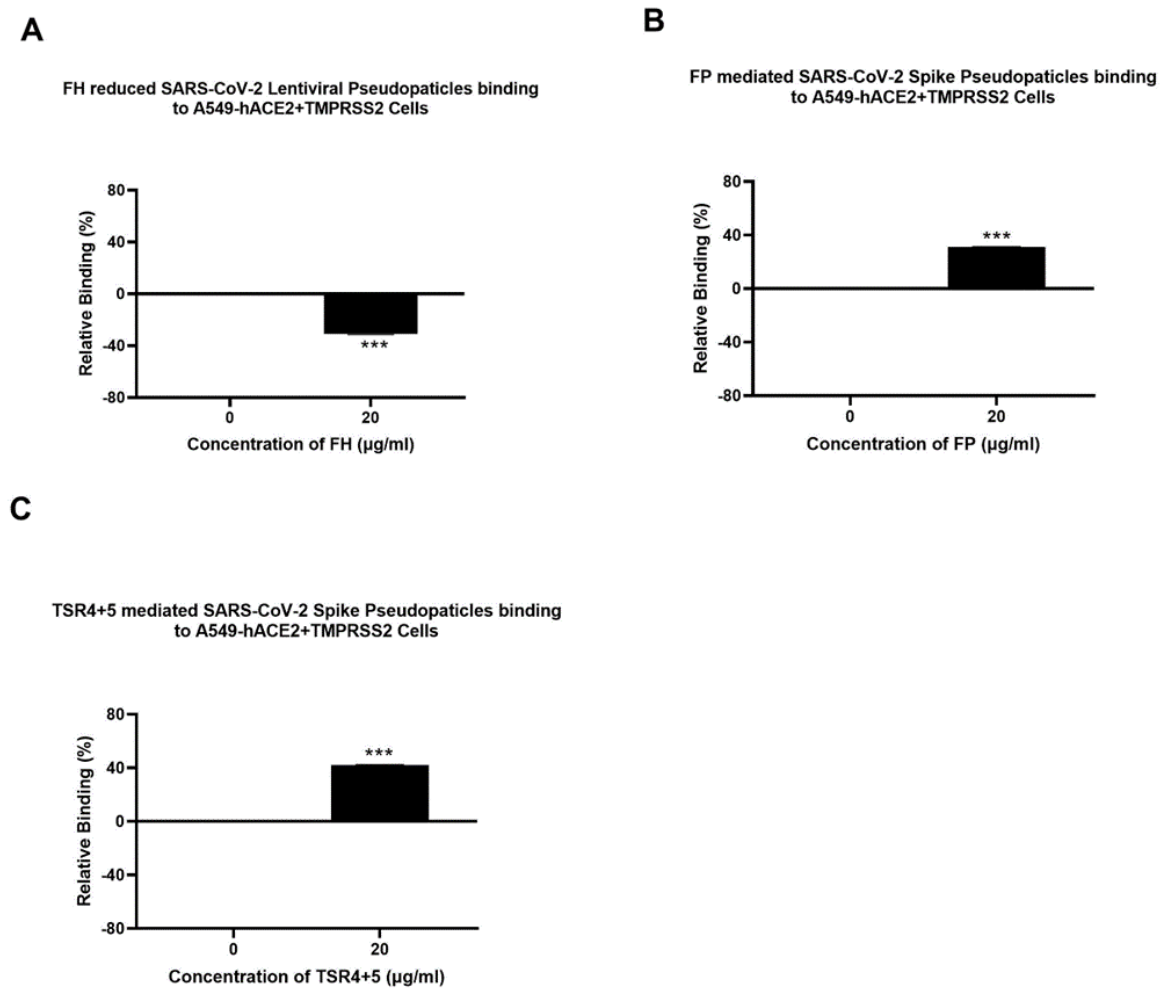

Figure 5.3: *Modulation of SARS-CoV-2 pseudoparticle binding to A549-hACE2+TMPRSS2 cells by FH, FP or TSR4+5***.** *Cell binding assay demonstrated distinct effects of FH, FP, and TSR4+5 on SARS-CoV-2 binding to cell-surface receptors, as illustrated in Figures (A), (B), and (C), respectively. For this assay, A549-hACE2+TMPRSS2 cells at a concentration of 2 × 10^4 cells/ml were exposed to SARS-CoV-2 lentiviral pseudoparticles that were pre-incubated with or without FH, FP, or TSR4+5 at a concentration of 20 µg/ml. The cells and viral particles were incubated at 37°C for 2 h. Following the incubation, unbound protein and viral particles were removed, and the wells were fixed using 1% v/v paraformaldehyde for 1 minute. Subsequently, the wells were probed with a polyclonal rabbit anti-SARS-CoV-2 spike antibody at a dilution of 1:200. The obtained data were normalised using 0% fluorescence as the mean of the relative fluorescence units recorded from the untreated sample (Cells + lentiviral pseudoparticles). The experiments were independently conducted three times in triplicates, and the error bars are expressed as ± SEM. Significance was determined using the two-way ANOVA test (***p < 0.001) (n = 3).*

A

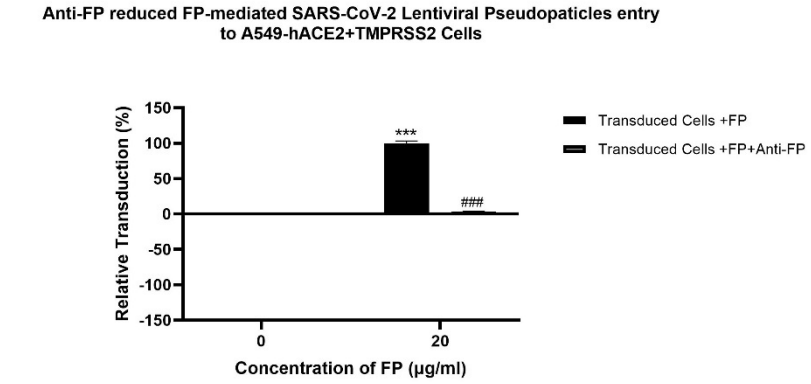

B

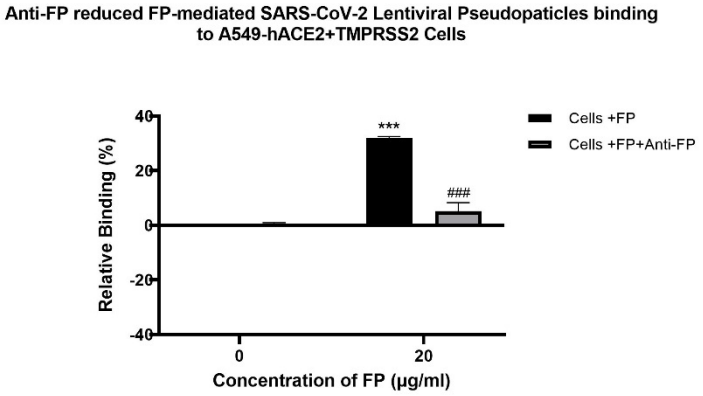

Figure 5.4: *Reversal of FP mediated-SARS-CoV-2 viral entry in and binding to A549-hACE2+TMPRSS2 cells by anti-FP antibody. Lentiviral pseudoparticles, treated with FP (with or without anti-FP antibodies) or untreated, were added to A549-hACE2+TMPRSS2 cells, and luciferase reporter activity (A) or cell binding was evaluated (B). All data points had the background subtracted. The data were normalised, with 0% luciferase activity defined as the mean of the relative luminescence units recorded from the control sample (Cells + lentiviral pseudoparticles). For binding: the obtained data were normalised using 0% fluorescence as the mean of the relative fluorescence units recorded from the untreated sample (Cells + lentiviral pseudoparticles). The data are presented as the normalised mean of three independent experiments performed in triplicates ±SEM. The significance of FP-treated cells (with and without anti-FP antibodies) compared to the untreated (cells+ viral pseudoparticles) was determined using the two-way ANOVA test (***p < 0.001). Additionally, the significance of FP-treated cells (with anti-FP antibodies) to cells treated only with FP (cells+ viral pseudoparticles + FP) was also determined (p < 0.001) (n = 3). Anti-SP-D used as a negative control; appendix 8 and 9.*

5.3.4 SARS-CoV-2 infection-associated inflammation can be attenuated by FH but promoted by FP

The NF-κB pathway, often associated with proinflammatory signals and responses, was examined in SARS-CoV-2 infection in lung epithelial-like cells treated with FP or FH. Using an NF-κB luciferase reporter assay, we found that FP pre-treatment led to a roughly 60% increase in NF-κB activation. FH treatment resulted in a roughly 25% decrease compared to the control. Using the qRT-PCR assay, we investigated the potential impact of FH, FP, and TSR4+5 on the cytokine response during SARS-CoV-2 infection. Specifically, we compared the mRNA levels of proinflammatory cytokines and chemokines in lung epithelial-like cells challenged with SARS-CoV-2 alphaviral pseudoparticles pre-treated with FH, FP, or TSR4+5 with their corresponding control samples (A549-hACE2+TMPRSS2 cells + SARS-CoV-2 alphaviral pseudoparticles). The results demonstrated distinct and differential modulation of the inflammatory immune response in A549-hACE2+TMPRSS2 cells by FH, FP, and TSR4+5, as illustrated in Figure 5.6, Figure 5.7, and Figure 5.8, respectively. Notably, in A549-hACE2+TMPRSS2 cells challenged with SARS-CoV-2 alphaviral pseudoparticles pre-treated with FH (FH-treated cells), the mRNA levels of various proinflammatory cytokines, such as IFN-α, IL-6, RANTES, IL-1β, IL-8, TNF-α (and NF-κB), were found to be downregulated when compared to the control cells (Figure 5.6).

The expression levels of the NF-κB gene decreased in FH-treated cells, reaching ~ -0.9 log10 at 6 h and reaching a peak decrease of about ~-1.7 log10 at 12 h (Figure 5.6A). At 6 h post-treatment, FH-treated cells exhibited reduced gene expression levels of IL-1β (~-1.3 log10) (Figure 5.6D), TNF-α (~ -2.0 log10) (Figure 5.6E), and IL-8 (~ -0.1 log10) (Figure 5.6G) compared to their respective controls. Similarly, at 12 hours after infection, FH-treated cells showed decreased mRNA levels of IL-6 (~-1.2 log10) (Figure 5.6B), IFN-α (~ -1.9 log10) (Figure 5.6C), IL-1β (~ -2.7 log10) (Figure 5.6D), RANTES (~ -2.9 log10) (Figure 5.6F), and IL-8 (~ -2.1 log10) (Figure 5.6G) compared to untreated cells (Figure 5.6E). However, there were no significant changes in the mRNA levels of IL-6 at 6 h (Figure 5.6B), IFN-α (Figure 5.6C), and RANTES (Figure 5.6F) in FH-treated cells as compared to their controls.

In A549-hACE2+TMPRSS2 cells challenged with SARS-CoV-2 alphaviral pseudoparticles pre-treated with either FP or TSR4+5, the proinflammatory immune response was observed to be upregulated, as depicted in Figures 7 and 8. Notably, the NF-κB gene expression levels in FP-treated cells were elevated, showing an increase of ~ 0.7 log10 at 6 h compared to control

cells and a further significant elevation of about 2.8 log10 at 12 h (Figure 5.7A). Additionally, at 6 h, the mRNA levels of IL-6, IFN-α, IL-1β, RANTES, and IL-8 were found to be upregulated in FP-treated cells, exhibiting increase of ~ 0.7 log10, ~1.5 log10, ~0.5 log10, ~0.7 log10, and ~0.3 log10, respectively (Figure 5.7B, Figure 5.7C, Figure 5.7D, Figure 5.7F, and Figure 5.7G). However, at 12 hours, the mRNA levels of IL-6, IFN-α, IL-1β, TNF-α, RANTES, and IL-8 in FP-treated cells were significantly upregulated, showing increases of ~ 2.7 log10, ~3.4 log10, ~1.5 log10, ~0.2 log10, ~3.0 log10, and ~1.4 log10, respectively (Figure 5.7B, Figure 5.7C, 7Figure 5.7D, Figure 5.7F, and Figure 5.7G). Notably, no significant alterations in the mRNA levels of IFN-α at 6 hours were observed in FP-treated cells compared to the control (Figure 5.7E).

Likewise, cells treated with TSR4+5 exhibited elevated NF-κB gene expression levels, with an increase of approximately 0.2 log10 compared to control cells at 6 h and a more significant elevation of about 2.0 log10 at 12 h (Figure 5.8A). On the other hand, there were no notable differences between the control and MBP-treated cells (TSR4+5 fusion protein) (Figure 5.8). Moreover, at 6 h, TSR4+5-treated cells displayed increased mRNA levels of IL-6, IFN-α, IL-1β, TNF-α, RANTES, and IL-8, with upregulations of ~ 0.5 log10, ~ 1.9 log10, ~0.7 log10, ~0.1 log10, ~0.2 log10, and ~0.8 log10, respectively, compared to the control (Figure 5.8, Figure 5.8B, Figure 5.8C, Figure 5.8D, Figure 5.8E, Figure 5.8F, and Figure 5.8G). At 12 h, the upregulation in mRNA levels of IL-6, IFN-α, IL-1β, TNF-α, RANTES, and IL-8 in TSR4+5-treated cells was even more pronounced, showing increases of ~ 2.2 log10, ~3.7 log10, ~2.7 log10, ~0.6 log10, ~2.3 log10, and ~2.2 log10, respectively, compared to the untreated control (Figure 5.8B, Figure 5.8C, Figure 5.8D, Figure 5.8E, Figure 5.8F, and Figure 5.8G). These findings indicate that FP and FH treatments differentially modulate NF-κB activation and the associated enhancing inflammatory response in SARS-CoV-2 infection.

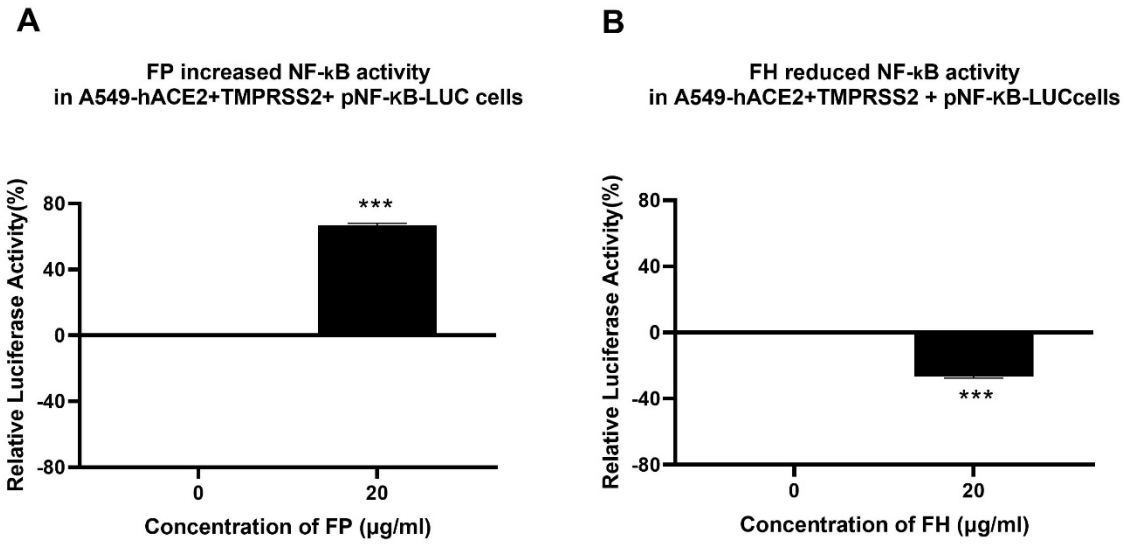

Figure 5.5: *FP increases while FH reduces NF-κB activation in SARS-CoV-2-Spike protein-challenged A549-hACE2-TMPRSS2 cells. SARS-CoV-2 Spike protein pre-treatment with FP (Panel A) or FH (Panel B) led to significant alterations in NF-κB activation. To investigate the immunological impact of FP and FH on NF-κB activation, A549-hACE2+TMPRSS2 cells were transfected with pNF-κB-LUC and then exposed to SARS-CoV-2 Spike protein (500 ng/ml) following pre-treatment with FP or FH (20 µg/ml). After 24 h of incubation, luciferase reporter activity was examined, and the background was subtracted from all data points. The obtained data were normalised, with 0% luciferase activity defined as the mean of the relative luminescence units recorded from the untreated sample (A549-hACE2+TMPRSS2 cells + SARS-CoV-2 Spike protein). The results are the normalised mean of three independent experiments conducted in triplicates ± SEM. Statistical significance was determined using the two-way ANOVA test (***p < 0.001) (n = 3).*

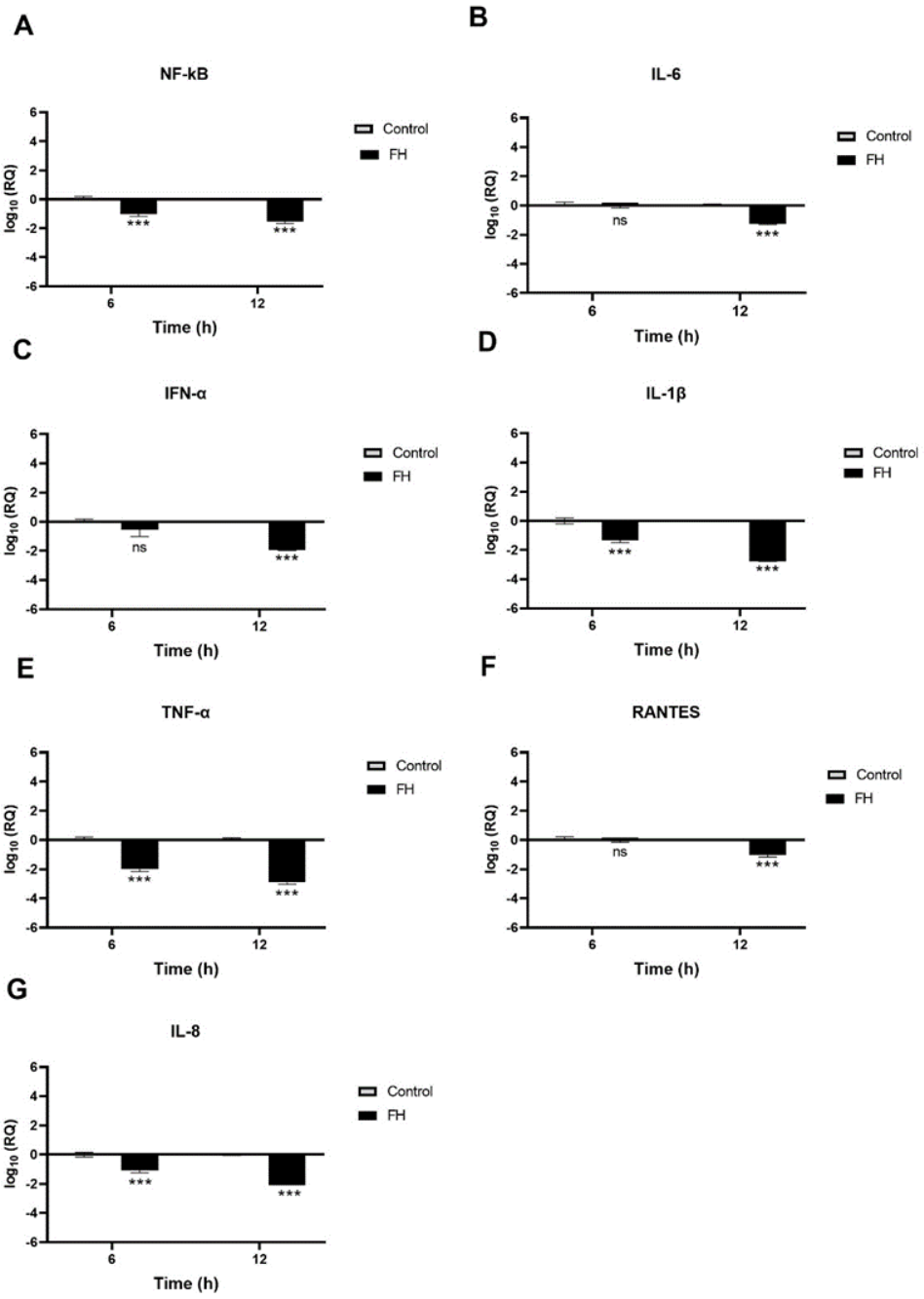

Figure 5.6: *SARS-CoV-2 FH attenuates associated inflammation in A549-hACE2+TMPRSS2 cells. A549-hACE2+TMPRSS2 cells were challenged with SARS-CoV-2 alphaviral pseudoparticles, with and without pre-treatment of FH (20 µg/ml). The mRNA levels of various cytokines and chemokines, including NF-κB (Panel A), IL-6 (Panel B), IFN-α (Panel C), IL-1ß (Panel D), TNF-α (Panel E), RANTES (Panel F), and IL-8 (Panel G), were assessed using RT-qPCR. Each target gene's relative expression (RQ) was calculated using untreated cells (A549-hACE2+TMPRSS2 cells + SARS-CoV-2 alphaviral pseudoparticles) as the calibrator. The RQ value was determined using RQ = $2^{-\Delta\Delta Ct}$. The experiments were performed in triplicates, and the error bars represent ± SEM (n = 3). Statistical significance was assessed using the two-way ANOVA test (****p < 0.0001, and ns= no significance).*

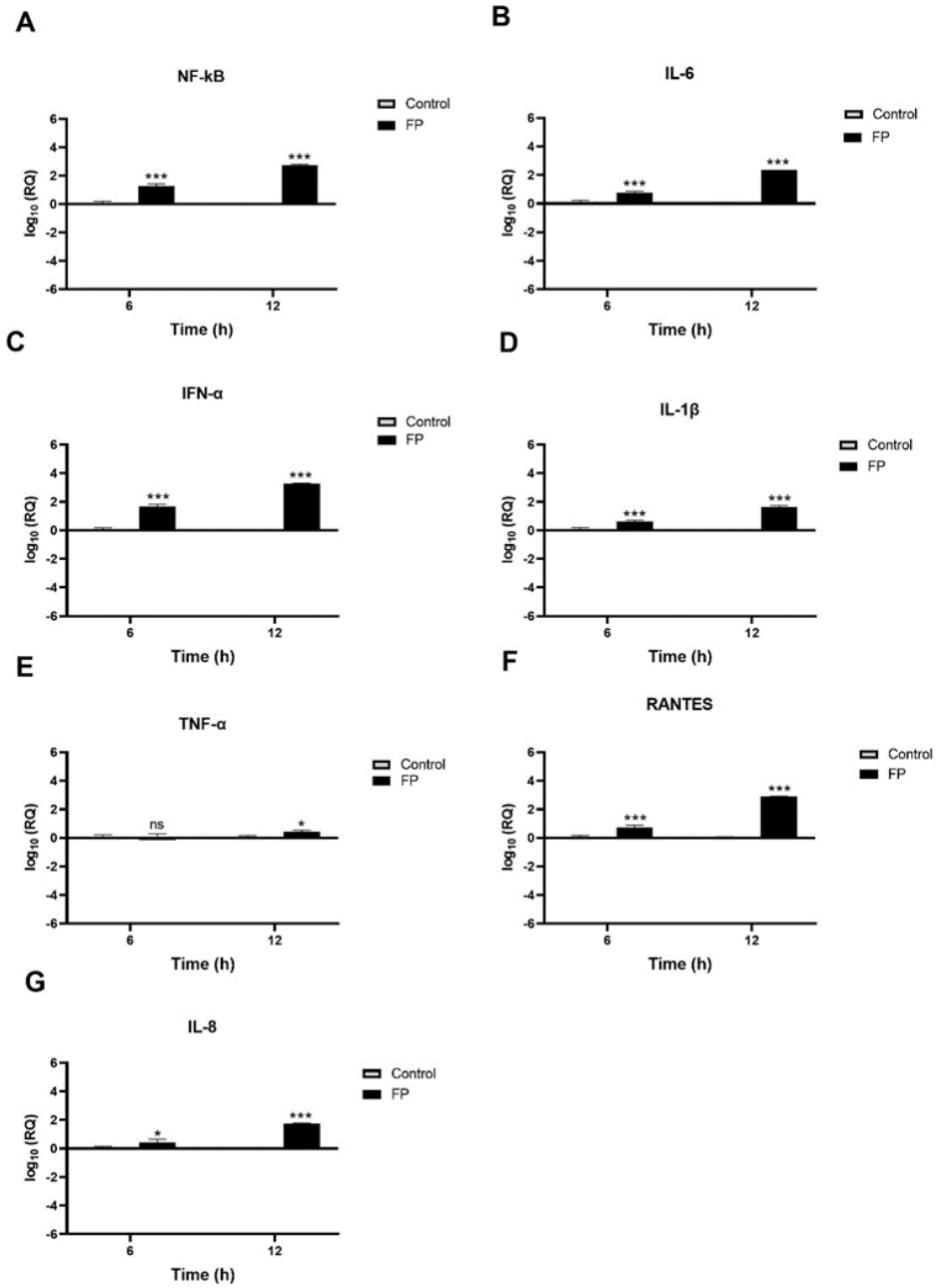

Figure 5.7: FP promotes SARS-CoV-2-associated inflammation in A549-hACE2+TMPRSS2 cells**.** *FP (20 µg/ml). pre-treated SARS-CoV-2 alphaviral pseudoparticles were assessed on the proinflammatory response in A549-hACE2+TMPRSS2 cells at 6h and 12h post-infection. We measured the mRNA expression levels of targeted cytokines and chemokines, including NF-κB (Panel A), IL-6 (Panel B), IFN-α (Panel C), IL-1ß (Panel D), TNF-α, RANTES (Panel F), and IL-8 (Panel G), using RT-qPCR. We used 18S rRNA expression as an endogenous control to ensure accurate normalisation. The relative expression (RQ) was calculated by comparing the data with untreated cells (A549-hACE2+TMPRSS2 cells + SARS-CoV-2 alphaviral pseudoparticles) as the calibrator, and the RQ value was determined using RQ = 2 $^{-\Delta\Delta Ct}$. All assays were performed in triplicates, and the error bars represent ± SEM. Statistical significance was assessed using the two-way ANOVA test (*p < 0.05, ****p < 0.0001, and ns= no significance) (n = 3).*

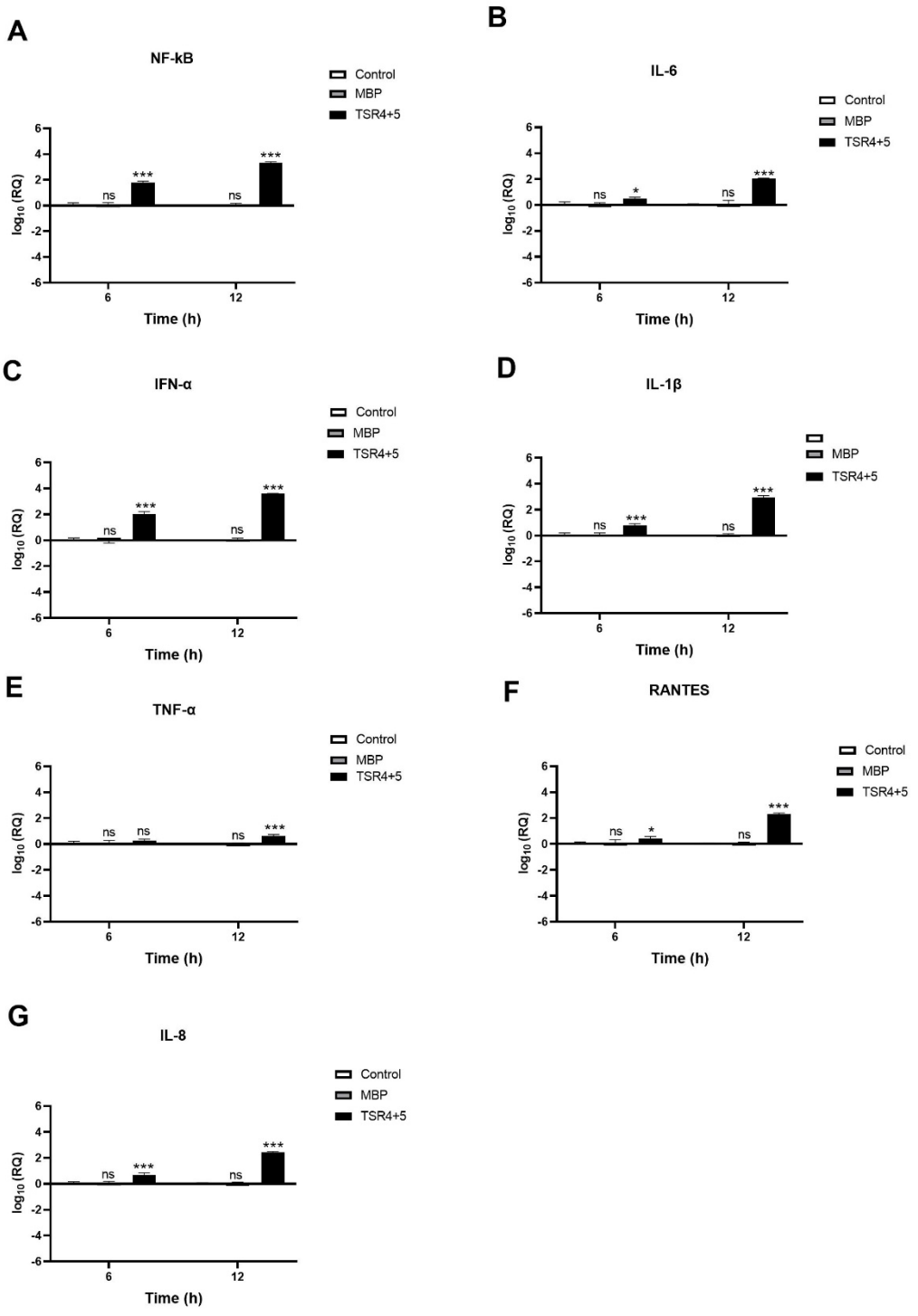

Figure 5.8: *SARS-CoV-2 infection of A549-hACE2+TMPRSS2 cells induced a greater proinflammatory response in the presence of TSR4+5. In A549-hACE2+TMPRSS2 cells challenged with SARS-CoV-2 alphaviral pseudoparticles pre-treated with TSR4+5 (20 µg/ml) or MBP (20 µg/ml). proinflammatory responses were observed at 6 h and 12 h post-infection. The levels of gene expression for cytokines and chemokines were measured using qRT-PCR, specifically for NF-kB (A), IL-6 (B), IFN-α (C), IL-1ß (D), TNF-α (E), RANTES (F), and IL-8 (G). The data were normalised against 18S rRNA expression as a control. Experiments were conducted in triplicates, and error bars represent ±SEM. The relative expression (RQ) was calculated using A549-hACE2+TMPRSS2 cells exposed to SARS-CoV-2 alphaviral pseudoparticles without TSR4+5 as the calibrator. RQ = $2^{-\Delta\Delta Ct}$ was used to calculate the RQ value. The significance of the results was determined using the two-way ANOVA test (*p < 0.05, ****p < 0.0001, and ns= no significance) (n = 3).*

5.3.5 FP interacts with spike and ACE2 in a tripartite complex

A blind docking approach was employed to generate a complex of FP with the spike protein. Interestingly, the second-ranked docked pose aligned with the *in vitro* findings, revealing that the TSR4 and TSR5 domains of FP interacted with the RBD (Receptor-Binding Domain) and NTD (N-terminal domain) of the spike protein, respectively, through hydrogen bonding, electrostatic interactions, and hydrophobic interactions (Figure 5.9A). A tripartite complex structure consisting of FP, the spike protein, and ACE2 was created by docking the electron microscopy structure of ACE2 to the FP-bound spike protein to understand the interactions further. ACE2 interacted with the spike protein in the top-ranked pose, as previously observed in the electron microscopy structure (PDB ID: 7KNB). Notably, FP was observed to interact with both the spike protein and ACE2 in the tripartite complex, forming various non-bonded contacts with each subunit (Figure 5.9B and Figure 5.9C).

Additionally, the TSR4 domain of FP was found to be near the ACE2 receptor, showing interactions with both the spike protein and ACE2. To compare the binding affinity of the ACE2 receptor with unbound spike protein and FP-bound spike protein, the Zdock score and binding free energy were assessed. The scores indicated that the ACE2 receptor exhibited a stronger affinity for the FP-bound spike protein than the unbound spike protein. That suggests that FP may enhance the affinity of the spike protein for ACE2 by interacting with both proteins through the formation of a tripartite complex. Chandan Kumar and Susan Idicula, Biomedical Informatics Centre, National Institute for Research in Reproductive and Child Health, ICMR, Mumbai, Maharashtra, India, kindly have done this work.

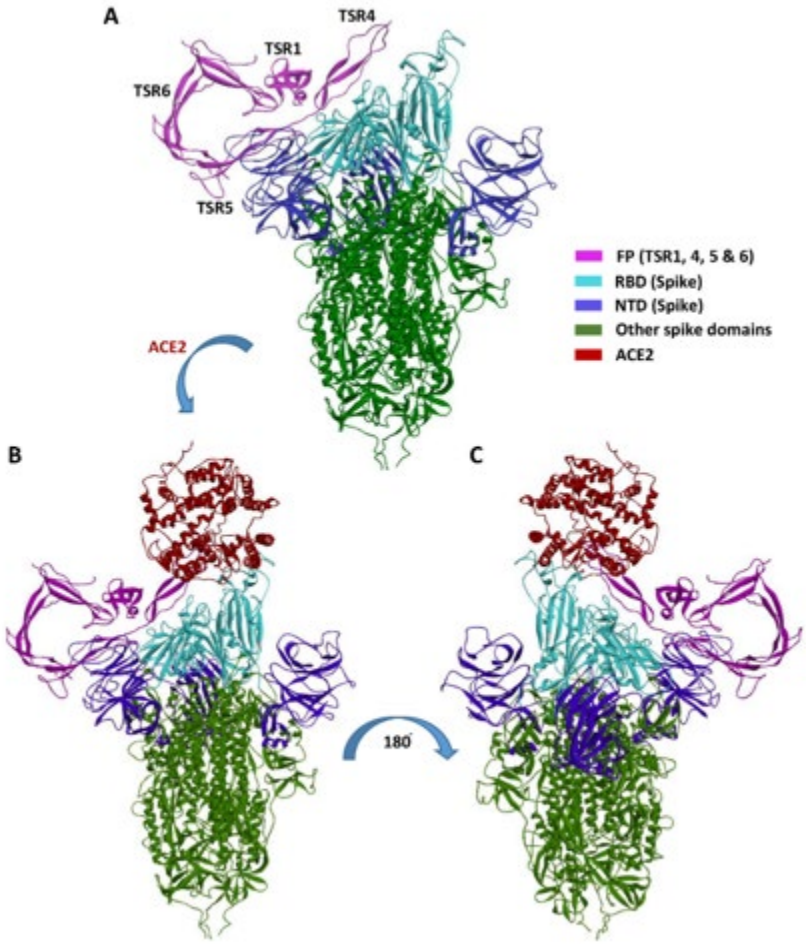

Figure 5.9: *Cartoon representation of FP interaction with spike and ACE2. (A) Interaction of FP with spike RBD and NTD through TSR4 and TSR5 domains. (B) & (C) A tripartite complex representation of FP, spike and ACE2.*

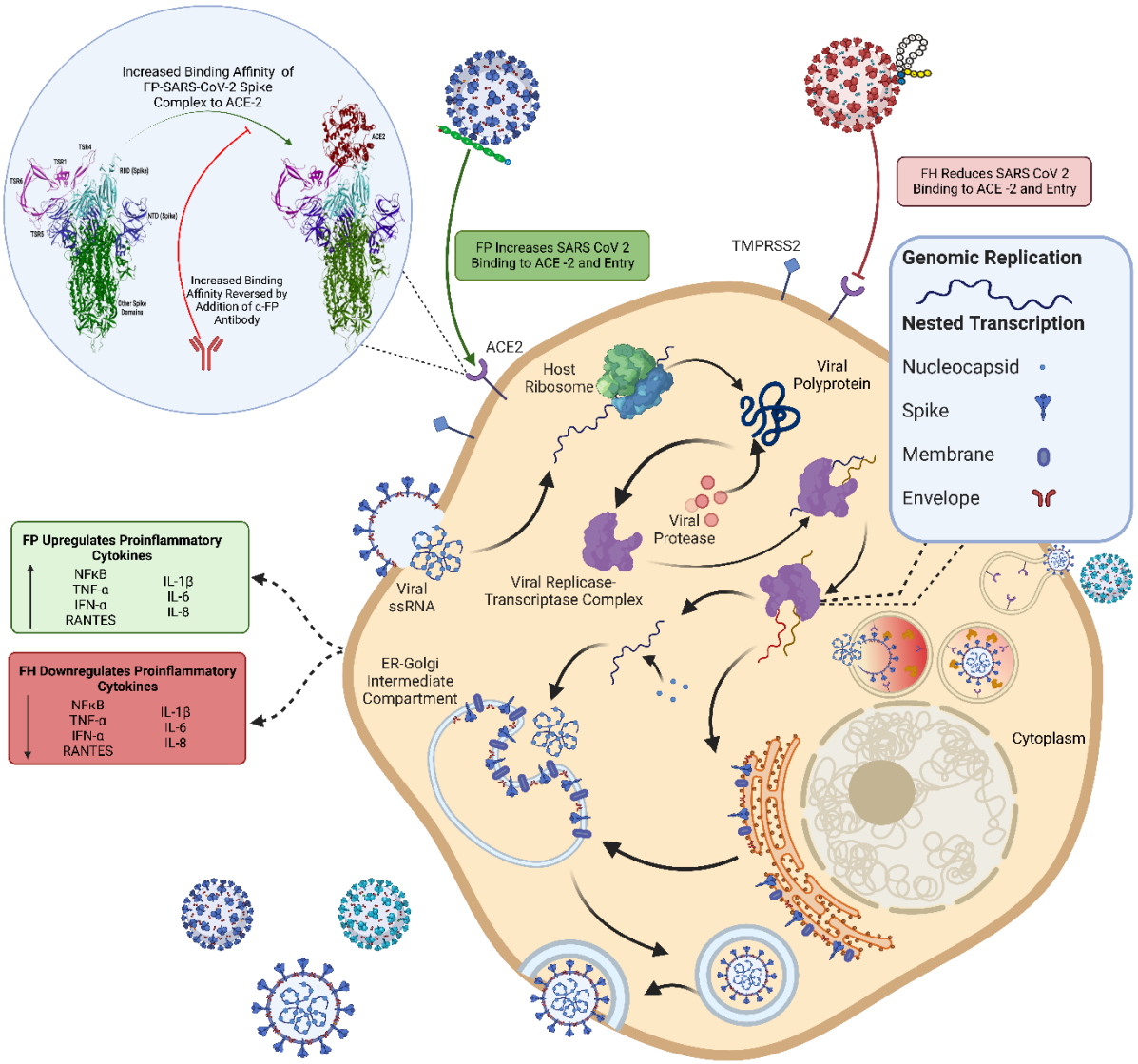

Figure 5.10: *Immune modulator function of FP and FH in SARS-CoV-2 Infection Independent of Complement Activation. The SARS-CoV-2 virus enters host cells by binding to the ACE2 receptor via its spike protein. Upon fusion with the cell membrane, viral RNA is released into the host cytoplasm, initiating viral replication, protein synthesis, and subsequent release of new virions into the extracellular environment, contributing to the spread of SARS-CoV-2 infection. This study investigated the effects of FP and FH separately to understand their roles in SARS-CoV-2 infection without activating the complement cascade. FP enhanced the binding affinity between the SARS-CoV-2 spike protein and ACE2, increasing viral entry into host cells and subsequent infection. This higher viral load triggered the upregulation of proinflammatory cytokines, contributing to the inflammatory response. On the other hand, FH was observed to reduce the binding and entry of SARS-CoV-2 into host cells. Consequently, the decreased viral entry mediated by FH reduced the production of proinflammatory cytokines, potentially mitigating the immune response. These findings provide valuable insights into FH's immunomodulatory role and FP's immunopathological role in COVID-19. Furthermore, they offer important clues regarding the potential association between elevated levels of properdin and insufficient levels of FH, as observed in severe COVID-19 patients.*

5.4 Discussion

The COVID-19 pandemic has caused millions of deaths and substantial financial losses (168). Thus, a better understanding of the immune response in SARS-CoV-2 infection as a protective or pathological role may enable an effective strategy for managing the infection and preventing future outbreaks. Various studies have reported the involvement of the complement system, particularly alternative pathways in immunopathology in severe COVID-19 patients (53, 54, 166). SARS-CoV-2 spike protein has been shown to induce alternative pathway activation (205). Notably, reduced gene expression levels of FH and increased FP levels have been associated with the severity of SARS-CoV-2 infection (167).

Nonetheless, immune functions of FH and FP in the SARS-CoV-2 infection remain unknown. Therefore, this study aimed to investigate the immune roles of FH and FP in SARS-CoV-2 infection independently of complement activation. FH and FP can directly interact with both the SARS-CoV-2 spike and receptor-binding domain (RBD), potentially influencing SARS-CoV-2 infectivity. Our work used A549 cells expressing human ACE2 and TMPRSS2 (A549-hACE2+TMPRSS2 cells) (178) as an in vitro biological model of pulmonary epithelium, appendix 5. In addition, we employed SARS-CoV-2 viral pseudoparticles (178) as a safe model of the live virus.

Factor H (FH) is a key inhibitory regulator of the alternative pathway (212). Lung fibroblasts can produce local FH, highlighting its crucial role in modulating immune responses and preserving viral infection in the pulmonary (210). Properdin (FP) is another complement regulatory protein that enhances alternative pathway activation (181). It is mainly stored and secreted locally in the lung by neutrophils (181). Interestingly, FH and FP act as PRR molecules in viral infection, such as binding to the influenza A virus (IAV) and inhibiting its entry into lung epithelial-like cells (181, 212). However, their inhibitory effect on IAV infection was in a subtype-dependent manner. Furthermore, FH and FP have been shown to attenuate proinflammatory response in A549 cells infected with IAV, further emphasising their roles in modulating immune responses (181, 212).

Here, in this study, we showed that Factor H (FH) reduced viral binding and entry into A549-hACE2+TMPRSS2 cells infection of lentiviral pseudoparticles to A549-hACE2+TMPRSS2 cells challenged with SARS-CoV-2 lentiviral pseudoparticles pretreated with FH. In contrast,

Properdin (FP) and TSR4+5 have enhanced viral cell binding and entry. In-silico analysis demonstrated that FP interacts with the spike protein through TSR4+5 domains, generating a complex with a high binding affinity to the host ACE2 receptor via TSR4. Compared to the virus alone, That leads to improved affinity between the virus and host ACE2, indicating a possible mechanism by which FP amplifies virus infection and replication, resulting in poor outcomes in infected individuals. On the contrary, we found that anti-FP polyclonal antibodies can counteract the FP-mediated enhancement of viral cell entry and binding.

Neutrophils function as a reservoir for properdin and can promptly secrete it locally through secretory granules upon activation in the lung (213). That local release of properdin is understood to be a key factor inducing alternative pathway activation (213). Importantly, infiltrated neutrophils and neutrophilia have been associated with immune response dysregulation in severe SARS-CoV-2 infection (214). This study suggests controlling excessive properdin could mitigate immunopathology in severe SARS-CoV-2 infection.

Excessive inflammation has been reported as a critical factor for developing severe SARS-CoV-2 infection (187, 188). Specifically, elevated serum levels of IL-1β, IL-6, IL-8, and TNF-α have been linked to the severity of the disease (187, 188). *In-vitro* work has shown high levels of IL-6, TNF-α, MIP-2, and IL-8 gene expression found in alveolar type II cells when infected with SARS-CoV-2 (215). The production and secretion of these proinflammatory cytokines and chemokines are induced by the activation of the NF-κB signalling pathway, which is vital for an effective immune response to viral infection (216). Dysregulation of NF-κB activation has been reported in severe SARS-CoV-2 infections (143, 217, 218). That leads to elevated serum levels of proinflammatory mediators, including IL-1, IL-2, IL-6, IL-12, TNF-α, IL-8, MIP-1, MCP1 and RANTES (143, 219-221). Here, we showed reduced NF-κB gene expression levels in A549-hACE2+TMPRSS2 cells challenged with SARS-CoV-2 alphaviral pseudoparticle pre-treated FH, whereas increased in the case of FP or TSR4+5 treatment. We also observed a reduction in NF-κB activation in A549-hACE2+TMPRSS2 cells challenged with SARS-CoV-2 spike protein pretreated FH, while FP treatment resulted in elevating NF-κB activation. Therefore, by downregulating NF-κB, FH may reduce hyperinflammation, whereas FP may increase the proinflammatory response in lung tissues infected with SARS-CoV-2.

IL-1β is a critical cytokine in inflammatory response to viral infections, including SARS-CoV-2, and it can also induce IL-6 and TNF-α secretions(222, 223). High levels of IL-1β found in the

serum and bronchoalveolar lavage fluid in patients with severe SARS-CoV-2 infection (224, 225). Blocking the IL-1 receptor has been reported as an effective treatment against cytokine storm and respiratory failure in COVID-19 patients (226, 227). Here, we revealed decreased IL-1β mRNA levels in A549-hACE2+TMPRSS2 cells challenged with SARS-CoV-2 alphaviral pseudoparticle pre-treated FH, whereas increased in the case of FP or TSR4+5 treatment. These results imply that FH may mitigate excessive inflammatory response induced by IL-1β in SARS-CoV-2 infection, while FP and TSR4+5 may exacerbate it.

TNF-α is a vital cytokine essential in limiting viral infections; however, high serum of TNF-α has been linked to lung tissue damage in severe COVID-19 cases (228). Combined therapy targeting TNF-α and IFN-γ has decreased tissue damage and mortality in severe SARS-CoV-2 infection (229). Our findings showed lower TNF-α mRNA levels in A549-hACE2+TMPRSS2 cells challenged with SARS-CoV-2 alphaviral pseudoparticle pre-treated FH while upregulated in FP or TSR4+5 treatment. These results suggest that FH might alleviate immune-complications related to TNF-α in SARS-CoV-2 infection, whereas FP and TSR4+5 could potentially worsen them.

IL-6 is one of the essential cytokines in the body's defense against viral infection(230). High serum levels of IL-6 have been associated with pneumonia-related SARS-CoV-2 and unfavourable prognoses (230). COVID-19 patients at risk of a cytokine storm have shown positive responses to tocilizumab (a monoclonal antibody that targets IL-6 receptors) (230). Here, we showed downregulation of mRNA levels of IL-6 in A549-hACE2+TMPRSS2 cells challenged with SARS-CoV-2 alphaviral pseudoparticle pre-treated FH while elevated in FP or TSR4+5 treatment. These findings indicate that FH may act as a protective PRR molecule controlling IL-6 dysfunction in SARS-CoV-2 infection, thereby preventing severe disease progression. Conversely, FP could play a role in exacerbating the infection severity.

Type I Interferon (IFN-α & IFN-β) is a pivotal cytokine that is important in controlling and preventing viral infections by triggering interferon-stimulated genes (ISGs) (231). Nevertheless, high Type I IFN (IFN-1) levels can induce hyperinflammation, causing severe SARS-CoV-2 infection via various pathways (231). A recent study has shown a limited IFN-1 response in SARS-CoV-2 infection (231). Yet, it has highlighted the crucial function of IFN-1 in the progression of severe disease (231). A retrospective study also demonstrated that early administration of IFN-α reduced mortality while utilising it in severe cases increased mortality

and delayed recovery (232). Our findings revealed a reduction in IFN-α mRNA levels in A549-hACE2+TMPRSS2 cells challenged with SARS-CoV-2 alphaviral pseudoparticle pre-treated FH, whereas elevated in FP or TSR4+5 treatment.

The chemokines IL-8 and RANTES are essential in attracting leukocytes to the site of viral infection (233, 234). IL-8 is linked with high neutrophil infiltration and respiratory failure in severe COVID-19 patients (235). Targeting CXCL-8 has prevented severe lung injury in viral pneumonia (236). Here, we showed downregulation in mRNA levels of IL-8 in A549-hACE2+TMPRSS2 cells challenged with SARS-CoV-2 alphaviral pseudoparticle pre-treated FH while upregulation FP or TSR4+5 treatment. On the other hand, elevated levels of RANTES have been correlated with liver damage and acute kidney failure in severe COVID-19 patients (237). Early targeting of RANTES in viral infections could improve viral clearance (238). Our results indicated decreased RANTES mRNA levels in A549-hACE2+TMPRSS2 cells challenged with SARS-CoV-2 alphaviral pseudoparticle pre-treated FH, whereas increased in FP or TSR4+5 treatment.

Various studies have demonstrated high neutrophil infiltration in severe SARS-CoV-2 infection linked to adverse clinical outcomes (239). Since neutrophils are known to release properdin (FP) from specific granules (181), FP might induce a feedback loop in which more IL-8 is produced during SARS-CoV-2 infection, leading to increased neutrophil infiltration. That, in turn, could result in higher levels of FP being secreted, exacerbating the infection and inflammation. Conversely, inadequate levels of FH in severe SARS-CoV-2 cases might contribute to disease progression. Here, we offer valued insights into FH's potential immune protective role and FP's immunopathological role in COVID-19. Nevertheless, further studies utilising clinical isolates from various virus variants and lineages are essential to understand the dynamics of the infection. Additionally, evaluation of the effect of local FH and FP in the lung microenvironment and exploring effective combination therapies is required to alleviate complications linked to SARS-CoV-2 infection.

Our finding has made a meaningful discovery, showing that FH and FP can directly interact with the receptor-binding domain (RBD) of the SARS-CoV-2 spike protein independently of complement activation. In addition, FH can inhibit SARS-CoV-2 pseudotype cell binding and entry and attenuate mRNA levels of IL-1β, IL-8, IL-6, TNF-α, IFN-α, NF-κB, and RANTES in A549-hACE2+TMPRSS2. In contrast, FP enhanced viral binding and entry, proinflammatory response

independent of complement activation. This study provides additional understanding into our innate immune system's sophisticated interplay in safeguarding against SARS-CoV-2 and contributing to its immunopathology.

Chapter 6

Conclusion

Severe SARS-CoV-2 infection is characterised by an imbalanced immune response, leading to excessive inflammation and acute respiratory distress syndrome, ultimately resulting in multiorgan failure and death. While the innate immune response generally plays a protective role, there are instances where it may contribute to the pathogenesis of SARS-CoV-2 infection. Therefore, this study aimed to investigate the immune functions of key innate immune molecules, both cell membrane-bound and soluble proteins, including SP-D, DC-SIGN, C1q, C4BP, FH, and FP in SARS-CoV-2 infection.

Firstly, the study focused on understanding the possible role of SP-D in DC-SIGN and SARS-CoV-2 interaction. Both SP-D and DC-SIGN are C-type lectin molecules involved in pathogen recognition. SP-D plays a critical role in detecting and clearing pulmonary pathogens. At the same time, DC-SIGN facilitates the interaction between dendritic cells and naïve T cells, thereby triggering an antiviral immune response. A recombinant fragment of human SP-D (rfhSP-D), consisting of a homotrimeric neck and CRD regions, has been demonstrated to exert immune functions against pathogens comparable to native SP-D. Our results showed that rfhSP-D binds to both DC-SIGN and SARS-CoV-2, enhancing viral uptake in cells expressing DC-SIGN. Furthermore, the study highlighted the immunomodulatory effects of rfhSP-D, as treatment led to the downregulation of pro-inflammatory cytokines and chemokines in macrophage-like cells expressing DC-SIGN when challenged with SARS-CoV-2 Spike protein.

Secondly, the study investigated the roles of C1q and C4BP in SARS-CoV-2 infection. The complement system, a crucial component of the innate immune response, plays a dual role in SARS-CoV-2 infection. While excessive complement activation has been associated with the cytokine storm observed in severe cases, recent evidence suggests that locally produced or activated complement regulatory proteins may have a protective effect independent of complement activation. C1q and C4BP are crucial regulators of the complement classical pathway, which have been shown to act as PRR molecules in viral infection. Our findings revealed that C1q and C4BP directly bind to RBD and spike proteins of the SARS-CoV-2. That reduces viral attachment and entry into lung-like cells expressing human ACE2 and TMPRSS2 (A549-hACE2+TMPRSS2 cells). Moreover, treatment with C1q and C4BP resulted in the downregulation of pro-inflammatory cytokines and chemokines in these cells independently of complement activation. That suggests a potential role of C1q and C4BP in mitigating the inflammatory response associated with SARS-CoV-2 infection. Notably, these complement

proteins can be locally produced in the lungs, offering additional protection against SARS-CoV-2 infection.

Lastly, the study evaluated the role of FH and FP in SARS-CoV-2 infection. FH and FP are critical regulatory proteins of the complement alternative pathway. These proteins have been demonstrated to play a role in controlling viral infection. Here, we found that FH exhibited an inhibitory effect on SARS-CoV-2 binding and cell entry, attenuating the infection-associated inflammatory response in A549-hACE2+TMPRSS2 cells. Conversely, FP demonstrated the opposite effect, promoting viral cell entry, binding, and enhancing inflammatory response, potentially influencing the severity of the infection. Importantly, these effects were independent of complement activation.

The study's main limitations in this thesis include its reliance on SARS-CoV-2 pseudotyped particles and *in vitro* models, which might not adequately represent in vivo settings. To provide a more thorough knowledge of these complement proteins' immunological involvement in COVID-19, future studies should investigate how they interact with other receptors and co-factors. Therefore, animal models are the next logical step to validate these findings further. Transgenic mouse models present an ideal platform for investigating these innate immune proteins' protective and pathogenic functions (240-242). Their advantages include low cost, easy accessibility, rapid breeding capabilities, ease of manipulation, and ample availability of reagents (240, 241). Among the available models, the K18-hACE2 model, initially designed for evaluating SARS-CoV in vivo, has emerged as a prominent choice for SARS-CoV-2 research(240, 241). This model expresses human ACE2 on epithelial tissues and relies on intranasal infection despite inefficient transmission (240, 241). Histopathological examination of lung tissue from the K18-hACE2 model reveals features resembling pneumonia associated with severe SARS-CoV-2 infection, including diffuse alveolar damage and inflammation (240-242). Infection of the K18-hACE2 model with SARS-CoV-2 triggers a significant innate immune response characterized by migration of immune cells to the lungs, including dendritic cells, monocytes, macrophages, CD4+, and CD8+ T cells, resulting in notable morbidity and mortality (240-242). Thus, our study findings are required to be validated in vivo using K18-hACE2 mice. The binding and viral cell entry will be assessed by administering C1q, its globular heads (ghs), FH, FP, TSR4+5, or rfhSP-D to K18-hACE2 mice, after these mice are infected with SARS-CoV-2 virus, with untreated K18-hACE2 mice serving as controls. Plaque assays and qPCR will be used to

measure the virus load in the lung tissues. Following this, clinical signs, weight loss, and histological changes in lung tissues will be monitored to assess the course and severity of the disease. At various time points post-infection, blood and tissue samples from treated and control mice will be taken to investigate the immune response and cytokine profile. ELISA and multiplex assays will be used to quantify the amounts of cytokines and chemokines, and flow cytometry will be employed to evaluate immune cell populations and activation status. By carrying out these studies in K18-hACE2 mice, a thorough understanding of the processes by which the tested proteins prevent viral binding and entry as well as their overall effects on SARS-CoV-2 infection and immune response will be obtained. That could pave the way for better disease management in severe cases of COVID-19.

In conclusion, our study has shed light on key innate immune molecules in SARS-CoV-2 infection. These results showed the potential immunomodulatory effects of rfhSP-D and its role in enhancing viral uptake via DC-SIGN. Additionally, C1q and C4BP were found to have protective roles by inhibiting viral cell entry and binding and mitigating the inflammatory response. FH exhibited potential as an inhibitor of viral cell entry and binding, while FP showed a propensity to enhance viral entry and promote inflammation. These findings hold significant implications for understanding the immune response to COVID-19 and offer promising avenues for developing therapeutic interventions targeting these innate immune proteins. However, further research is necessary to unravel these immune-protective and immune-pathogenic effects' precise underlying mechanisms and explore their potential clinical applications in managing SARS-CoV-2 infection.

References

1. Helmy YA, Fawzy M, Elaswad A, Sobieh A, Kenney SP, Shehata AA. The COVID-19 pandemic: a comprehensive review of taxonomy, genetics, epidemiology, diagnosis, treatment, and control. Journal of clinical medicine. 2020;9(4):1225.

2. Hu B, Guo H, Zhou P, Shi Z-L. Characteristics of SARS-CoV-2 and COVID-19. Nature Reviews Microbiology. 2021;19(3):141-54.

3. Wang H, Paulson KR, Pease SA, Watson S, Comfort H, Zheng P, et al. Estimating excess mortality due to the COVID-19 pandemic: a systematic analysis of COVID-19-related mortality, 2020–21. The Lancet. 2022;399(10334):1513-36.

4. Stein C, Nassereldine H, Sorensen RJ, Amlag JO, Bisignano C, Byrne S, et al. Past SARS-CoV-2 infection protection against re-infection: a systematic review and meta-analysis. The Lancet. 2023;401(10379):833-42.

5. Singh D, Yi SV. On the origin and evolution of SARS-CoV-2. Experimental & Molecular Medicine. 2021;53(4):537-47.

6. Yang H, Rao Z. Structural biology of SARS-CoV-2 and implications for therapeutic development. Nature Reviews Microbiology. 2021;19(11):685-700.

7. Naqvi AAT, Fatima K, Mohammad T, Fatima U, Singh IK, Singh A, et al. Insights into SARS-CoV-2 genome, structure, evolution, pathogenesis and therapies: Structural genomics approach. Biochimica et Biophysica Acta (BBA)-Molecular Basis of Disease. 2020;1866(10):165878.

8. Wang M-Y, Zhao R, Gao L-J, Gao X-F, Wang D-P, Cao J-M. SARS-CoV-2: structure, biology, and structure-based therapeutics development. Frontiers in cellular and infection microbiology. 2020;10:587269.

9. Hardenbrook NJ, Zhang P. A structural view of the SARS-CoV-2 virus and its assembly. Current opinion in virology. 2022;52:123-34.

10. Varghese PM, Tsolaki AG, Yasmin H, Shastri A, Ferluga J, Vatish M, et al. Host-pathogen interaction in COVID-19: Pathogenesis, potential therapeutics and vaccination strategies. Immunobiology. 2020;225(6):152008.

11. V'kovski P, Kratzel A, Steiner S, Stalder H, Thiel V. Coronavirus biology and replication: implications for SARS-CoV-2. Nature Reviews Microbiology. 2021;19(3):155-70.

12. Shang J, Ye G, Shi K, Wan Y, Luo C, Aihara H, et al. Structural basis of receptor recognition by SARS-CoV-2. Nature. 2020;581(7807):221-4.

13. Jackson CB, Farzan M, Chen B, Choe H. Mechanisms of SARS-CoV-2 entry into cells. Nature reviews Molecular cell biology. 2022;23(1):3-20.

14. Baggen J, Vanstreels E, Jansen S, Daelemans D. Cellular host factors for SARS-CoV-2 infection. Nature Microbiology. 2021;6(10):1219-32.

15. Wang Q, Zhang Y, Wu L, Niu S, Song C, Zhang Z, et al. Structural and functional basis of SARS-CoV-2 entry by using human ACE2. Cell. 2020;181(4):894-904. e9.

16. Datta PK, Liu F, Fischer T, Rappaport J, Qin X. SARS-CoV-2 pandemic and research gaps: Understanding SARS-CoV-2 interaction with the ACE2 receptor and implications for therapy. Theranostics. 2020;10(16):7448.

17. Lambotin M, Raghuraman S, Stoll-Keller F, Baumert TF, Barth H. A look behind closed doors: interaction of persistent viruses with dendritic cells. Nature Reviews Microbiology. 2010;8(5):350-60.

18. Cunningham AL, Harman AN, Donaghy H. DC-SIGN'AIDS'HIV immune evasion and infection. Nature immunology. 2007;8(6):556-8.

19. Lozach P-Y, Burleigh L, Staropoli I, Amara A. The C type lectins DC-SIGN and L-SIGN: receptors for viral glycoproteins. Glycovirology Protocols. 2007:51-68.

20. Khoo U-S, Chan KY, Chan VS, Lin CS. DC-SIGN and L-SIGN: the SIGNs for infection. Journal of molecular medicine. 2008;86:861-74.

21. Lempp FA, Soriaga LB, Montiel-Ruiz M, Benigni F, Noack J, Park Y-J, et al. Lectins enhance SARS-CoV-2 infection and influence neutralizing antibodies. Nature. 2021;598(7880):342-7.

22. Tay MZ, Poh CM, Rénia L, MacAry PA, Ng LF. The trinity of COVID-19: immunity, inflammation and intervention. Nature Reviews Immunology. 2020;20(6):363-74.

23. Lamers MM, Haagmans BL. SARS-CoV-2 pathogenesis. Nature reviews microbiology. 2022;20(5):270-84.

24. Flerlage T, Boyd DF, Meliopoulos V, Thomas PG, Schultz-Cherry S. Influenza virus and SARS-CoV-2: pathogenesis and host responses in the respiratory tract. Nature Reviews Microbiology. 2021;19(7):425-41.

25. Shivshankar P, Karmouty-Quintana H, Mills T, Doursout M-F, Wang Y, Czopik AK, et al. SARS-CoV-2 infection: host response, immunity, and therapeutic targets. Inflammation. 2022;45(4):1430-49.

26. Phetsouphanh C, Darley DR, Wilson DB, Howe A, Munier CML, Patel SK, et al. Immunological dysfunction persists for 8 months following initial mild-to-moderate SARS-CoV-2 infection. Nature immunology. 2022;23(2):210-6.

27. Diamond MS, Kanneganti T-D. Innate immunity: the first line of defense against SARS-CoV-2. Nature immunology. 2022;23(2):165-76.

28. Madden EA, Diamond MS. Host cell-intrinsic innate immune recognition of SARS-CoV-2. Current Opinion in Virology. 2022;52:30-8.

29. Yamada T, Takaoka A. Innate immune recognition against SARS-CoV-2. Inflammation and Regeneration. 2023;43(1):7.

30. Kasuga Y, Zhu B, Jang K-J, Yoo J-S. Innate immune sensing of coronavirus and viral evasion strategies. Experimental & molecular medicine. 2021;53(5):723-36.

31. Vasta GR. Roles of galectins in infection. Nature Reviews Microbiology. 2009;7(6):424-38.

32. Labarrere CA, Kassab GS. Pattern recognition proteins: first line of defense against coronaviruses. Frontiers in Immunology. 2021;12:652252.

33. Murugaiah V, Tsolaki AG, Kishore U. Collectins: innate immune pattern recognition molecules. Lectin in Host Defense Against Microbial Infections. 2020:75-127.

34. Hsieh M-H, Beirag N, Murugaiah V, Chou Y-C, Kuo W-S, Kao H-F, et al. Human surfactant protein D binds spike protein and acts as an entry inhibitor of SARS-CoV-2 pseudotyped viral particles. Frontiers in Immunology. 2021;12:641360.

35. Gupta A, Gupta G. Status of mannose-binding lectin (MBL) and complement system in COVID-19 patients and therapeutic applications of antiviral plant MBLs. Molecular and Cellular Biochemistry. 2021;476(8):2917-42.

36. Madan T, Kishore U. Surfactant protein D recognizes multiple fungal ligands: a key step to initiate and intensify the anti-fungal host defense. Frontiers in Cellular and Infection Microbiology. 2020;10:229.

37. Kishore U, Greenhough TJ, Waters P, Shrive AK, Ghai R, Kamran MF, et al. Surfactant proteins SP-A and SP-D: structure, function and receptors. Molecular immunology. 2006;43(9):1293-315.

38. Nayak A, Dodagatta-Marri E, Tsolaki AG, Kishore U. An insight into the diverse roles of surfactant proteins, SP-A and SP-D in innate and adaptive immunity. Frontiers in immunology. 2012;3:131.

39. Meschi J, Crouch EC, Skolnik P, Yahya K, Holmskov U, Leth-Larsen R, et al. Surfactant protein D binds to human immunodeficiency virus (HIV) envelope protein gp120 and inhibits HIV replication. Journal of general virology. 2005;86(11):3097-107.

40. Pandit H, Gopal S, Sonawani A, Yadav AK, Qaseem AS, Warke H, et al. Surfactant protein D inhibits HIV-1 infection of target cells via interference with gp120-CD4 interaction and modulates pro-inflammatory cytokine production. PloS one. 2014;9(7):e102395.

41. Dodagatta-Marri E, Mitchell DA, Pandit H, Sonawani A, Murugaiah V, Idicula-Thomas S, et al. Protein–protein interaction between surfactant protein d and DC-SIGN via c-type lectin domain can suppress HIV-1 transfer. Frontiers in immunology. 2017;8:834.

42. Wu Y, Liu Z, Wei R, Pan S, Mao N, Chen B, et al. Elevated plasma surfactant protein d (SP-D) levels and a direct correlation with anti-severe acute respiratory syndrome

coronavirus-specific IgG antibody in SARS patients. Scandinavian journal of immunology. 2009;69(6):508-15.

43. Leth-Larsen R, Zhong F, Chow VT, Holmskov U, Lu J. The SARS coronavirus spike glycoprotein is selectively recognized by lung surfactant protein D and activates macrophages. Immunobiology. 2007;212(3):201-11.

44. Reading PC, Holmskov U, Anders EM. Antiviral activity of bovine collectins against rotaviruses. Journal of General Virology. 1998;79(9):2255-63.

45. Favier A-L, Reynard O, Gout E, Van Eijk M, Haagsman HP, Crouch E, et al. Involvement of surfactant protein D in ebola virus infection enhancement via glycoprotein interaction. Viruses. 2018;11(1):15.

46. Perino J, Thielens NM, Crouch E, Spehner D, Crance J-M, Favier A-L. Protective effect of surfactant protein d in pulmonary vaccinia virus infection: implication of A27 viral protein. Viruses. 2013;5(3):928-53.

47. York IA, Stevens J, Alymova IV. Influenza virus N-linked glycosylation and innate immunity. Bioscience reports. 2019;39(1).

48. van Eijk M, van de Lest CH, Batenburg JJ, Vaandrager AB, Meschi J, Hartshorn KL, et al. Porcine surfactant protein D is N-glycosylated in its carbohydrate recognition domain and is assembled into differently charged oligomers. American journal of respiratory cell and molecular biology. 2002;26(6):739-47.

49. Reading PC, Morey LS, Crouch EC, Anders EM. Collectin-mediated antiviral host defense of the lung: evidence from influenza virus infection of mice. Journal of virology. 1997;71(11):8204-12.

50. Job ER, Deng Y-M, Tate MD, Bottazzi B, Crouch EC, Dean MM, et al. Pandemic H1N1 influenza A viruses are resistant to the antiviral activities of innate immune proteins of the collectin and pentraxin superfamilies. The Journal of Immunology. 2010;185(7):4284-91.

51. Boechat JL, Chora I, Morais A, Delgado L. The immune response to SARS-CoV-2 and COVID-19 immunopathology–current perspectives. Pulmonology. 2021;27(5):423-37.

52. Wong L-YR, Perlman S. Immune dysregulation and immunopathology induced by SARS-CoV-2 and related coronaviruses—are we our own worst enemy? Nature Reviews Immunology. 2022;22(1):47-56.

53. Afzali B, Noris M, Lambrecht BN, Kemper C. The state of complement in COVID-19. Nature Reviews Immunology. 2022;22(2):77-84.

54. Chauhan AJ, Wiffen LJ, Brown TP. COVID-19: a collision of complement, coagulation and inflammatory pathways. Journal of Thrombosis and Haemostasis. 2020;18(9):2110-7.

55. Murugaiah V, Varghese PM, Beirag N, DeCordova S, Sim RB, Kishore U. Complement proteins as soluble pattern recognition receptors for pathogenic viruses. Viruses. 2021;13(5):824.

56. Shah A, Kishore U, Shastri A. Complement System in Alzheimer's Disease. International Journal of Molecular Sciences. 2021;22(24):13647.

57. Merle NS, Noe R, Halbwachs-Mecarelli L, Fremeaux-Bacchi V, Roumenina LT. Complement system part II: role in immunity. Frontiers in immunology. 2015;6:257.

58. Son M. Understanding the contextual functions of C1q and LAIR-1 and their applications. Experimental & Molecular Medicine. 2022;54(5):567-72.

59. Gaboriaud C, Frachet P, Thielens NM, Arlaud GJ. The human c1q globular domain: structure and recognition of non-immune self ligands. Frontiers in immunology. 2012;2:92.

60. Thielens NM, Tedesco F, Bohlson SS, Gaboriaud C, Tenner AJ. C1q: A fresh look upon an old molecule. Molecular immunology. 2017;89:73-83.

61. Kishore U, Gaboriaud C, Waters P, Shrive AK, Greenhough TJ, Reid KB, et al. C1q and tumor necrosis factor superfamily: modularity and versatility. Trends in immunology. 2004;25(10):551-61.

62. Ermert D, Weckel A, Agarwal V, Frick I-M, Björck L, Blom AM. Binding of complement inhibitor C4b-binding protein to a highly virulent Streptococcus pyogenes M1 strain is mediated by protein H and enhances adhesion to and invasion of endothelial cells. Journal of Biological Chemistry. 2013;288(45):32172-83.

63. Blom AM, Kask L, Dahlbäck Br. Structural requirements for the complement regulatory activities of C4BP. Journal of Biological Chemistry. 2001;276(29):27136-44.

64. Linse S, Härdig Y, Schultz DA, Dahlbäck Br. A region of vitamin K-dependent protein S that binds to C4b binding protein (C4BP) identified using bacteriophage peptide display libraries. Journal of Biological Chemistry. 1997;272(23):14658-65.

65. Cipriani V, Lorés-Motta L, He F, Fathalla D, Tilakaratna V, McHarg S, et al. Increased circulating levels of Factor H-Related Protein 4 are strongly associated with age-related macular degeneration. Nature communications. 2020;11(1):778.

66. Ferreira VP, Pangburn MK, Cortés C. Complement control protein factor H: the good, the bad, and the inadequate. Molecular immunology. 2010;47(13):2187-97.

67. Kopp A, Hebecker M, Svobodová E, Józsi M. Factor h: a complement regulator in health and disease, and a mediator of cellular interactions. Biomolecules. 2012;2(1):46-75.

68. Braunger K, Ahn J, Jore MM, Johnson S, Tang TT, Pedersen DV, et al. Structure and function of a family of tick-derived complement inhibitors targeting properdin. Nature communications. 2022;13(1):317.

69. Pedersen DV, Gadeberg TA, Thomas C, Wang Y, Joram N, Jensen RK, et al. Structural basis for properdin oligomerization and convertase stimulation in the human complement system. Frontiers in Immunology. 2019;10:2007.

70. Blatt AZ, Pathan S, Ferreira VP. Properdin: a tightly regulated critical inflammatory modulator. Immunological reviews. 2016;274(1):172-90.

71. Michels MA, Volokhina EB, van de Kar NC, van den Heuvel LP. The role of properdin in complement-mediated renal diseases: a new player in complement-inhibiting therapy? Pediatric Nephrology. 2019;34:1349-67.

72. Qin G, Liu S, Yang L, Yu W, Zhang Y. Myeloid cells in COVID-19 microenvironment. Signal Transduction and Targeted Therapy. 2021;6(1):372.

73. Knoll R, Schultze JL, Schulte-Schrepping J. Monocytes and Macrophages in COVID-19. Frontiers in immunology. 2021;12:720109.

74. Meidaninikjeh S, Sabouni N, Marzouni HZ, Bengar S, Khalili A, Jafari R. Monocytes and macrophages in COVID-19: Friends and foes. Life sciences. 2021;269:119010.

75. Matic S, Popovic S, Djurdjevic P, Todorovic D, Djordjevic N, Mijailovic Z, et al. SARS-CoV-2 infection induces mixed M1/M2 phenotype in circulating monocytes and alterations in both dendritic cell and monocyte subsets. PLoS One. 2020;15(12):e0241097.

76. Lv J, Wang Z, Qu Y, Zhu H, Zhu Q, Tong W, et al. Distinct uptake, amplification, and release of SARS-CoV-2 by M1 and M2 alveolar macrophages. Cell discovery. 2021;7(1):24.

77. Borges RC, Hohmann MS, Borghi SM. Dendritic cells in COVID-19 immunopathogenesis: insights for a possible role in determining disease outcome. International Reviews of Immunology. 2021;40(1-2):108-25.

78. Galati D, Zanotta S, Capitelli L, Bocchino M. A bird's eye view on the role of dendritic cells in SARS-CoV-2 infection: Perspectives for immune-based vaccines. Allergy. 2022;77(1):100-10.

79. Van der Sluis RM, Holm CK, Jakobsen MR. Plasmacytoid dendritic cells during COVID-19: Ally or adversary? Cell Reports. 2022:111148.

80. Amraei R, Yin W, Napoleon MA, Suder EL, Berrigan J, Zhao Q, et al. CD209L/L-SIGN and CD209/DC-SIGN act as receptors for SARS-CoV-2. ACS Central Science. 2021;7(7):1156-65.

81. Björkström NK, Strunz B, Ljunggren H-G. Natural killer cells in antiviral immunity. Nature Reviews Immunology. 2022;22(2):112-23.

82. Di Vito C, Calcaterra F, Coianiz N, Terzoli S, Voza A, Mikulak J, et al. Natural killer cells in SARS-CoV-2 infection: pathophysiology and therapeutic implications. Frontiers in immunology. 2022:3295.

83. Zafarani A, Razizadeh MH, Pashangzadeh S, Amirzargar MR, Taghavi-Farahabadi M, Mahmoudi M. Natural killer cells in COVID-19: from infection, to vaccination and therapy. Future Virology. 2023;18(3):177-91.

84. van Eeden C, Khan L, Osman MS, Cohen Tervaert JW. Natural killer cell dysfunction and its role in COVID-19. International journal of molecular sciences. 2020;21(17):6351.

85. Ackermann M, Anders H-J, Bilyy R, Bowlin GL, Daniel C, De Lorenzo R, et al. Patients with COVID-19: in the dark-NETs of neutrophils. Cell Death & Differentiation. 2021;28(11):3125-39.

86. Castanheira FV, Kubes P. Neutrophils during SARS-CoV-2 infection: Friend or foe? Immunological Reviews. 2023;314(1):399-412.

87. Cavalcante-Silva LHA, Carvalho DCM, de Almeida Lima É, Galvao JG, da Silva JSdF, de Sales-Neto JM, et al. Neutrophils and COVID-19: The road so far. International immunopharmacology. 2021;90:107233.

88. Panda R, Castanheira FV, Schlechte JM, Surewaard BG, Shim HB, Zucoloto AZ, et al. A functionally distinct neutrophil landscape in severe COVID-19 reveals opportunities for adjunctive therapies. JCI insight. 2022;7(2).

89. Neufeldt CJ, Cerikan B, Cortese M, Frankish J, Lee J-Y, Plociennikowska A, et al. SARS-CoV-2 infection induces a pro-inflammatory cytokine response through cGAS-STING and NF-κB. Communications biology. 2022;5(1):45.

90. Costela-Ruiz VJ, Illescas-Montes R, Puerta-Puerta JM, Ruiz C, Melguizo-Rodríguez L. SARS-CoV-2 infection: The role of cytokines in COVID-19 disease. Cytokine & growth factor reviews. 2020;54:62-75.

91. Montazersaheb S, Hosseiniyan Khatibi SM, Hejazi MS, Tarhriz V, Farjami A, Ghasemian Sorbeni F, et al. COVID-19 infection: An overview on cytokine storm and related interventions. Virology Journal. 2022;19(1):1-15.

92. Hasanvand A. COVID-19 and the role of cytokines in this disease. Inflammopharmacology. 2022;30(3):789-98.

93. Stokel-Walker C. What do we know about the adaptive immune response to covid-19? bmj. 2023;380.

94. Sette A, Crotty S. Adaptive immunity to SARS-CoV-2 and COVID-19. Cell. 2021;184(4):861-80.

95. Primorac D, Vrdoljak K, Brlek P, Pavelić E, Molnar V, Matišić V, et al. Adaptive immune responses and immunity to SARS-CoV-2. Frontiers in Immunology. 2022;13:848582.

96. Silva MJA, Ribeiro LR, Lima KVB, Lima LNGC. Adaptive immunity to SARS-CoV-2 infection: A systematic review. Frontiers in immunology. 2022;13:1001198.

97. Tan LA, Yu B, Sim FC, Kishore U, Sim RB. Complement activation by phospholipids: the interplay of factor H and C1q. Protein & cell. 2010;1(11):1033-49.

98. Sim R, Day A, Moffatt B, Fontaine M. [1] Complement factor I and cofactors in control of complement system convertase enzymes. Methods in enzymology. 1993;223:13-35.

99. Sim E, Sim R. Enzymic assay of C3b receptor on intact cells and solubilized cells. Biochemical Journal. 1983;210(2):567-76.

100. Kouser L, Abdul-Aziz M, Tsolaki AG, Singhal D, Schwaeble WJ, Urban BC, et al. A recombinant two-module form of human properdin is an inhibitor of the complement alternative pathway. Molecular Immunology. 2016;73:76-87.

101. Murugaiah V, Agostinis C, Varghese PM, Belmonte B, Vieni S, Alaql FA, et al. Hyaluronic acid present in the tumor microenvironment can negate the pro-apototic effect of a recombinant fragment of human surfactant protein D on breast cancer cells. Frontiers in Immunology. 2020;11:1171.

102. Pednekar L, Pandit H, Paudyal B, Kaur A, Al-Mozaini MA, Kouser L, et al. Complement protein C1q interacts with DC-SIGN via its globular domain and thus may interfere with HIV-1 transmission. Frontiers in immunology. 2016;7:600.

103. Kishore U, Gupta SK, Perdikoulis MV, Kojouharova MS, Urban BC, Reid K. Modular organization of the carboxyl-terminal, globular head region of human C1q A, B, and C chains. The Journal of Immunology. 2003;171(2):812-20.

104. Perdikoulis MV, Kishore U, Reid KB. Expression and characterisation of the thrombospondin type I repeats of human properdin. Biochimica et Biophysica Acta (BBA)-Protein Structure and Molecular Enzymology. 2001;1548(2):265-77.

105. Jin C, Wu L, Li J, Fang M, Cheng L, Wu N. Multiple signaling pathways are involved in the interleukine-4 regulated expression of DC-SIGN in THP-1 cell line. BioMed Research International. 2012;2012.

106. Di Genova C, Sampson A, Scott S, Cantoni D, Mayora-Neto M, Bentley E, et al. Production, titration, neutralisation, storage and lyophilisation of severe acute respiratory syndrome coronavirus 2 (SARS-CoV-2) lentiviral pseudotypes. Bio-protocol. 2021;11(21):e4236-e.

107. Madan T, Biswas B, Varghese PM, Subedi R, Pandit H, Idicula-Thomas S, et al. A recombinant fragment of human surfactant protein D binds spike protein and inhibits infectivity and replication of SARS-CoV-2 in clinical samples. American journal of respiratory cell and molecular biology. 2021;65(1):41-53.

108. Takeuchi O, Akira S. Pattern recognition receptors and inflammation. Cell. 2010;140(6):805-20.

109. Kumar H, Kawai T, Akira S. Pathogen recognition in the innate immune response. Biochemical Journal. 2009;420(1):1-16.

110. Akira S. Pathogen recognition by innate immunity and its signaling. Proceedings of the Japan Academy, Series B. 2009;85(4):143-56.

111. Drickamer K, Taylor ME. Recent insights into structures and functions of C-type lectins in the immune system. Current opinion in structural biology. 2015;34:26-34.

112. Qian C, Cao X, editors. Dendritic cells in the regulation of immunity and inflammation. Seminars in immunology; 2018: Elsevier.

113. Worbs T, Hammerschmidt SI, Förster R. Dendritic cell migration in health and disease. Nature Reviews Immunology. 2017;17(1):30-48.

114. Geijtenbeek TB, Torensma R, van Vliet SJ, van Duijnhoven GC, Adema GJ, van Kooyk Y, et al. Identification of DC-SIGN, a novel dendritic cell–specific ICAM-3 receptor that supports primary immune responses. Cell. 2000;100(5):575-85.

115. Frison N, Taylor ME, Soilleux E, Bousser M-T, Mayer R, Monsigny M, et al. Oligolysine-based oligosaccharide clusters: selective recognition and endocytosis by the mannose receptor and dendritic cell-specific intercellular adhesion molecule 3 (ICAM-3)-grabbing nonintegrin. Journal of Biological Chemistry. 2003;278(26):23922-9.

116. Halary F, Amara A, Lortat-Jacob H, Messerle M, Delaunay T, Houlès C, et al. Human cytomegalovirus binding to DC-SIGN is required for dendritic cell infection and target cell trans-infection. Immunity. 2002;17(5):653-64.

117. Alvarez CP, Lasala F, Carrillo J, Muñiz O, Corbí AL, Delgado R. C-type lectins DC-SIGN and L-SIGN mediate cellular entry by Ebola virus in cis and in trans. Journal of virology. 2002;76(13):6841-4.

118. Geijtenbeek TB, Kwon DS, Torensma R, Van Vliet SJ, Van Duijnhoven GC, Middel J, et al. DC-SIGN, a dendritic cell–specific HIV-1-binding protein that enhances trans-infection of T cells. Cell. 2000;100(5):587-97.

119. Carbaugh DL, Baric RS, Lazear HM. Envelope protein glycosylation mediates Zika virus pathogenesis. Journal of virology. 2019;93(12):10.1128/jvi. 00113-19.

120. Navarro-Sanchez E, Altmeyer R, Amara A, Schwartz O, Fieschi F, Virelizier J. renzana-Seisdedos F, Despres P (2003) Dendritic-cell-specific ICAM3-grabbing non-integrin is essential for the productive infection of human dendritic cells by mosquitocell-derived dengue viruses. EMBO Rep.4(7):723-8.

121. Manches O, Frleta D, Bhardwaj N. Dendritic cells in progression and pathology of HIV infection. Trends in immunology. 2014;35(3):114-22.

122. Thépaut M, Luczkowiak J, Vivès C, Labiod N, Bally I, Lasala F, et al. DC/L-SIGN recognition of spike glycoprotein promotes SARS-CoV-2 trans-infection and can be inhibited by a glycomimetic antagonist. PLoS pathogens. 2021;17(5):e1009576.

123. Arroyo R, Grant SN, Colombo M, Salvioni L, Corsi F, Truffi M, et al. Full-length recombinant hSP-D binds and inhibits SARS-CoV-2. Biomolecules. 2021;11(8):1114.

124. Al-Ahdal MN, Murugaiah V, Varghese PM, Abozaid SM, Saba I, Al-Qahtani AA, et al. Entry inhibition and modulation of pro-inflammatory immune response against influenza A virus by a recombinant truncated surfactant protein D. Frontiers in immunology. 2018;9:1586.

125. Ni W, Yang X, Yang D, Bao J, Li R, Xiao Y, et al. Role of angiotensin-converting enzyme 2 (ACE2) in COVID-19. Critical Care. 2020;24(1):1-10.

126. Walls AC, Park Y-J, Tortorici MA, Wall A, McGuire AT, Veesler D. Structure, function, and antigenicity of the SARS-CoV-2 spike glycoprotein. Cell. 2020;181(2):281-92. e6.

127. Petersen E, Koopmans M, Go U, Hamer DH, Petrosillo N, Castelli F, et al. Comparing SARS-CoV-2 with SARS-CoV and influenza pandemics. The Lancet infectious diseases. 2020;20(9):e238-e44.

128. Yang Z-Y, Huang Y, Ganesh L, Leung K, Kong W-P, Schwartz O, et al. pH-dependent entry of severe acute respiratory syndrome coronavirus is mediated by the spike glycoprotein and enhanced by dendritic cell transfer through DC-SIGN. Journal of virology. 2004;78(11):5642-50.

129. Marzi A, Gramberg T, Simmons G, Möller P, Rennekamp AJ, Krumbiegel M, et al. DC-SIGN and DC-SIGNR interact with the glycoprotein of Marburg virus and the S protein of severe acute respiratory syndrome coronavirus. Journal of virology. 2004;78(21):12090-5.

130. Mangalmurti N, Hunter CA. Cytokine storms: understanding COVID-19. Immunity. 2020;53(1):19-25.

131. Al-Ahdal MN, Murugaiah V, Varghese PM, Abozaid SM, Saba I, Al-Qahtani AA, et al. Entry inhibition and modulation of pro-inflammatory immune response against influenza A virus by a recombinant truncated surfactant protein D. Frontiers in immunology. 2018;9:363811.

132. Dodagatta-Marri E, Mitchell DA, Pandit H, Sonawani A, Murugaiah V, Idicula-Thomas S, et al. Protein–protein interaction between surfactant protein d and DC-SIGN via c-type lectin domain can suppress HIV-1 transfer. Frontiers in immunology. 2017;8:250465.

133. Li D, Wu M. Pattern recognition receptors in health and diseases. Signal transduction and targeted therapy. 2021;6(1):291.

134. Lai C-C, Shih T-P, Ko W-C, Tang H-J, Hsueh P-R. Severe acute respiratory syndrome coronavirus 2 (SARS-CoV-2) and coronavirus disease-2019 (COVID-19): The epidemic and the challenges. International journal of antimicrobial agents. 2020;55(3):105924.

135. Perrotta F, Matera MG, Cazzola M, Bianco A. Severe respiratory SARS-CoV2 infection: Does ACE2 receptor matter? Respiratory medicine. 2020;168:105996.

136. Marzi A, Möller P, Hanna SL, Harrer T, Eisemann J, Steinkasserer A, et al. Analysis of the Interaction of Ebola Virus Glycoprotein with DC-SIGN (Dendritic Cell—Specific Intercellular Adhesion Molecule 3—Grabbing Nonintegrin) and Its Homologue DC-SIGNR. The Journal of infectious diseases. 2007;196(Supplement_2):S237-S46.

137. Pöhlmann S, Leslie GJ, Edwards TG, Macfarlan T, Reeves JD, Hiebenthal-Millow K, et al. DC-SIGN interactions with human immunodeficiency virus: virus binding and transfer are dissociable functions. Journal of virology. 2001;75(21):10523-6.

138. Freer G, Matteucci D. Influence of dendritic cells on viral pathogenicity. PLoS pathogens. 2009;5(7):e1000384.

139. Benton DJ, Wrobel AG, Xu P, Roustan C, Martin SR, Rosenthal PB, et al. Receptor binding and priming of the spike protein of SARS-CoV-2 for membrane fusion. Nature. 2020;588(7837):327-30.

140. LeVine AM, Whitsett JA, Hartshorn KL, Crouch EC, Korfhagen TR. Surfactant protein D enhances clearance of influenza A virus from the lung in vivo. The Journal of Immunology. 2001;167(10):5868-73.

141. Marongiu L, Valache M, Facchini FA, Granucci F. How dendritic cells sense and respond to viral infections. Clinical Science. 2021;135(19):2217-42.

142. Farahani M, Niknam Z, Amirabad LM, Amiri-Dashatan N, Koushki M, Nemati M, et al. Molecular pathways involved in COVID-19 and potential pathway-based therapeutic targets. Biomedicine & Pharmacotherapy. 2022;145:112420.

143. Kircheis R, Haasbach E, Lueftenegger D, Heyken WT, Ocker M, Planz O. NF-κB pathway as a potential target for treatment of critical stage COVID-19 patients. Frontiers in immunology. 2020;11:598444.

144. Chiok K, Hutchison K, Miller LG, Bose S, Miura TA. Proinflammatory Responses in SARS-CoV-2 and Soluble Spike Glycoprotein S1 Subunit Activated Human Macrophages. Viruses. 2023;15(3):754.

145. Mukhopadhyay S, Hoidal JR, Mukherjee TK. Role of TNFα in pulmonary pathophysiology. Respiratory research. 2006;7(1):1-9.

146. Qin C, Ziwei MPLZM, Tao SYMY, Ke PCXMP, Shang MMPK. Dysregulation of immune response in patients with COVID-19 in Wuhan, China; clinical infectious diseases; Oxford academic. Clinical Infectious Diseases. 2020.

147. Makwana R, Gozzard N, Spina D, Page C. TNF-α-induces airway hyperresponsiveness to cholinergic stimulation in guinea pig airways. British journal of pharmacology. 2012;165(6):1978-91.

148. Peiris J, Lai S, Poon L, Guan Y, Yam L, Lim W, et al. Coronavirus as a possible cause of severe acute respiratory syndrome. The Lancet. 2003;361(9366):1319-25.

149. Chen I-Y, Moriyama M, Chang M-F, Ichinohe T. Severe acute respiratory syndrome coronavirus viroporin 3a activates the NLRP3 inflammasome. Frontiers in microbiology. 2019;10:50.

150. Warke T, Fitch P, Brown V, Taylor R, Lyons J, Ennis M, et al. Exhaled nitric oxide correlates with airway eosinophils in childhood asthma. Thorax. 2002;57(5):383-7.

151. Wang X, Jiang W, Yan Y, Gong T, Han J, Tian Z, et al. RNA viruses promote activation of the NLRP3 inflammasome through a RIP1-RIP3-DRP1 signaling pathway. Nature immunology. 2014;15(12):1126-33.

152. Copaescu A, Smibert O, Gibson A, Phillips EJ, Trubiano JA. The role of IL-6 and other mediators in the cytokine storm associated with SARS-CoV-2 infection. Journal of Allergy and Clinical Immunology. 2020;146(3):518-34. e1.

153. Jones SA, Jenkins BJ. Recent insights into targeting the IL-6 cytokine family in inflammatory diseases and cancer. Nature reviews immunology. 2018;18(12):773-89.

154. Tanaka T, Narazaki M, Kishimoto T. IL-6 in inflammation, immunity, and disease. Cold Spring Harbor perspectives in biology. 2014;6(10):a016295.

155. Lee AJ, Ashkar AA. The dual nature of type I and type II interferons. Frontiers in immunology. 2018:2061.

156. Channappanavar R. Interferons in coronavirus pathogenesis: The good, the bad, and the ugly. Cell Host & Microbe. 2022;30(4):427-30.

157. Hargadon KM, Zhou H, Albrecht RA, Dodd HA, García-Sastre A, Braciale TJ. Major histocompatibility complex class II expression and hemagglutinin subtype influence the infectivity of type A influenza virus for respiratory dendritic cells. Journal of virology. 2011;85(22):11955-63.

158. Barhoumi T, Alghanem B, Shaibah H, Mansour FA, Alamri HS, Akiel MA, et al. SARS-CoV-2 coronavirus spike protein-induced apoptosis, inflammatory, and oxidative stress responses in THP-1-like-macrophages: potential role of angiotensin-converting enzyme inhibitor (perindopril). Frontiers in Immunology. 2021;12:3771.

159. Sokol CL, Luster AD. The chemokine system in innate immunity. Cold Spring Harbor perspectives in biology. 2015;7(5):a016303.

160. Kobayashi Y. The role of chemokines in neutrophil biology. Frontiers in Bioscience-Landmark. 2008;13(7):2400-7.

161. Posch W, Vosper J, Noureen A, Zaderer V, Witting C, Bertacchi G, et al. C5aR inhibition of nonimmune cells suppresses inflammation and maintains epithelial integrity in SARS-CoV-2–infected primary human airway epithelia. Journal of Allergy and Clinical Immunology. 2021;147(6):2083-97. e6.

162. Patterson BK, Seethamraju H, Dhody K, Corley MJ, Kazempour K, Lalezari J, et al. Disruption of the CCL5/RANTES-CCR5 pathway restores immune homeostasis and reduces plasma viral load in critical COVID-19. MedRxiv. 2020:2020.05. 02.20084673.

163. Gusev E, Sarapultsev A, Solomatina L, Chereshnev V. SARS-CoV-2-specific immune response and the pathogenesis of COVID-19. International journal of molecular sciences. 2022;23(3):1716.

164. Houser KV, Broadbent AJ, Gretebeck L, Vogel L, Lamirande EW, Sutton T, et al. Enhanced inflammation in New Zealand white rabbits when MERS-CoV reinfection occurs in the absence of neutralizing antibody. PLoS pathogens. 2017;13(8):e1006565.

165. Duchateau J, Haas M, Schreyen H, Radoux L, Sprangers I, Noel F, et al. Complement activation in patients at risk of developing the adult respiratory distress syndrome. American Review of Respiratory Disease. 1984;130(6):1058-64.

166. Java A, Apicelli AJ, Liszewski MK, Coler-Reilly A, Atkinson JP, Kim AH, et al. The complement system in COVID-19: friend and foe? JCI insight. 2020;5(15).

167. Alosaimi B, Mubarak A, Hamed ME, Almutairi AZ, Alrashed AA, AlJuryyan A, et al. Complement anaphylatoxins and inflammatory cytokines as prognostic markers for COVID-19 severity and in-hospital mortality. Frontiers in immunology. 2021;12:668725.

168. Siggins MK, Davies K, Fellows R, Thwaites RS, Baillie JK, Semple MG, et al. Alternative pathway dysregulation in tissues drives sustained complement activation and predicts outcome across the disease course in COVID-19. Immunology. 2023;168(3):473-92.

169. Mehlhop E, Diamond MS. Protective immune responses against West Nile virus are primed by distinct complement activation pathways. The Journal of experimental medicine. 2006;203(5):1371-81.

170. Van Erp EA, Luytjes W, Ferwerda G, Van Kasteren PB. Fc-mediated antibody effector functions during respiratory syncytial virus infection and disease. Frontiers in immunology. 2019;10:548.

171. Feng JQ, Mozdzanowska K, Gerhard W. Complement component C1q enhances the biological activity of influenza virus hemagglutinin-specific antibodies depending on their fine antigen specificity and heavy-chain isotype. Journal of virology. 2002;76(3):1369-78.

172. Merle NS, Church SE, Fremeaux-Bacchi V, Roumenina LT. Complement system part I–molecular mechanisms of activation and regulation. Frontiers in immunology. 2015;6:262.

173. Ramlall V, Thangaraj PM, Meydan C, Foox J, Butler D, Kim J, et al. Immune complement and coagulation dysfunction in adverse outcomes of SARS-CoV-2 infection. Nature medicine. 2020;26(10):1609-15.

174. Rodríguez de Córdoba S, Sanchez-Corral P, Rey-Campos J. Structure of the gene coding for the alpha polypeptide chain of the human complement component C4b-binding protein. The Journal of experimental medicine. 1991;173(5):1073-82.

175. Chaudhary N, Jayaraman A, Reinhardt C, Campbell JD, Bosmann M. A single-cell lung atlas of complement genes identifies the mesothelium and epithelium as prominent sources of extrahepatic complement proteins. Mucosal immunology. 2022;15(5):927-39.

176. Varghese PM, Murugaiah V, Beirag N, Temperton N, Khan HA, Alrokayan SH, et al. C4b binding protein acts as an innate immune effector against influenza a virus. Frontiers in Immunology. 2021;11:585361.

177. Varghese PM, Kishore U, Rajkumari R. Human C1q Regulates Influenza A Virus Infection and Inflammatory Response via Its Globular Domain. International Journal of Molecular Sciences. 2022;23(6):3045.

178. Beirag N, Varghese PM, Neto MM, Al Aiyan A, Khan HA, Qablan M, et al. Complement activation-independent attenuation of SARS-CoV-2 infection by C1q and C4b-binding protein. Viruses. 2023;15(6):1269.

179. Antos A, Kwong ML, Balmorez T, Villanueva A, Murakami S. Unusually high risks of COVID-19 mortality with age-related comorbidities: An adjusted meta-analysis method to improve the risk assessment of mortality using the comorbid mortality data. Infectious disease reports. 2021;13(3):700-11.

180. Yu J, Yuan X, Chen H, Chaturvedi S, Braunstein EM, Brodsky RA. Direct activation of the alternative complement pathway by SARS-CoV-2 spike proteins is blocked by factor D inhibition. Blood, The Journal of the American Society of Hematology. 2020;136(18):2080-9.

181. Varghese PM, Mukherjee S, Al-Mohanna FA, Saleh SM, Almajhdi FN, Beirag N, et al. Human properdin released by infiltrating neutrophils can modulate Influenza A virus infection. Frontiers in Immunology. 2021;12:747654.

182. Zissel G, Ernst M, Rabe K, Papadopoulos T, Magnussen H, Schlaak M, et al. Human alveolar epithelial cells type II are capable of regulating T-cell activity. Journal of investigative medicine: the official publication of the American Federation for Clinical Research. 2000;48(1):66-75.

183. Chang C-W, Parsi KM, Somasundaran M, Vanderleeden E, Liu P, Cruz J, et al. A newly engineered A549 cell line expressing ACE2 and TMPRSS2 is highly permissive to SARS-CoV-2, including the delta and omicron variants. Viruses. 2022;14(7):1369.

184. Cantoni D, Mayora-Neto M, Temperton N. The role of pseudotype neutralization assays in understanding SARS CoV-2. Oxford open immunology. 2021;2(1):iqab005.

185. Focosi D, Maggi F, Mazzetti P, Pistello M. Viral infection neutralization tests: A focus on severe acute respiratory syndrome-coronavirus-2 with implications for convalescent plasma therapy. Reviews in medical virology. 2021;31(2):e2170.

186. Yasmin H, Saha S, Butt MT, Modi RK, George AJ, Kishore U. SARS-CoV-2: Pathogenic mechanisms and host immune response. Microbial Pathogenesis: Infection and Immunity. 2021:99-134.

187. Del Valle DM, Kim-Schulze S, Huang H-H, Beckmann ND, Nirenberg S, Wang B, et al. An inflammatory cytokine signature predicts COVID-19 severity and survival. Nature medicine. 2020;26(10):1636-43.

188. Liu QQ, Cheng A, Wang Y, Li H, Hu L, Zhao X, et al. Cytokines and their relationship with the severity and prognosis of coronavirus disease 2019 (COVID-19): a retrospective cohort study. BMJ Open. 2020;10(11):e041471.

189. Satyam A, Tsokos MG, Brook OR, Hecht JL, Moulton VR, Tsokos GC. Activation of classical and alternative complement pathways in the pathogenesis of lung injury in COVID-19. Clin Immunol. 2021;226:108716.

190. Huang J, Hume AJ, Abo KM, Werder RB, Villacorta-Martin C, Alysandratos KD, et al. SARS-CoV-2 Infection of Pluripotent Stem Cell-Derived Human Lung Alveolar Type 2 Cells Elicits a Rapid Epithelial-Intrinsic Inflammatory Response. Cell Stem Cell. 2020;27(6):962-73.e7.

191. Chen L, Guan WJ, Qiu ZE, Xu JB, Bai X, Hou XC, et al. SARS-CoV-2 nucleocapsid protein triggers hyperinflammation via protein-protein interaction-mediated intracellular Cl(-) accumulation in respiratory epithelium. Signal Transduct Target Ther. 2022;7(1):255.

192. Anand G, Perry AM, Cummings CL, St Raymond E, Clemens RA, Steed AL. Surface Proteins of SARS-CoV-2 Drive Airway Epithelial Cells to Induce IFN-Dependent Inflammation. J Immunol. 2021;206(12):3000-9.

193. Kircheis R, Haasbach E, Lueftenegger D, Heyken WT, Ocker M, Planz O. NF-κB Pathway as a Potential Target for Treatment of Critical Stage COVID-19 Patients. Front Immunol. 2020;11:598444.

194. Dinarello CA. Overview of the IL-1 family in innate inflammation and acquired immunity. Immunol Rev. 2018;281(1):8-27.

195. DeDiego ML, Nieto-Torres JL, Regla-Nava JA, Jimenez-Guardeño JM, Fernandez-Delgado R, Fett C, et al. Inhibition of NF-κB-mediated inflammation in severe acute respiratory syndrome coronavirus-infected mice increases survival. J Virol. 2014;88(2):913-24.

196. Siu KL, Yuen KS, Castaño-Rodriguez C, Ye ZW, Yeung ML, Fung SY, et al. Severe acute respiratory syndrome coronavirus ORF3a protein activates the NLRP3 inflammasome by promoting TRAF3-dependent ubiquitination of ASC. Faseb j. 2019;33(8):8865-77.

197. Jamilloux Y, Henry T, Belot A, Viel S, Fauter M, El Jammal T, et al. Should we stimulate or suppress immune responses in COVID-19? Cytokine and anti-cytokine interventions. Autoimmun Rev. 2020;19(7):102567.

198. Ferreira AC, Soares VC, de Azevedo-Quintanilha IG, Dias S, Fintelman-Rodrigues N, Sacramento CQ, et al. SARS-CoV-2 engages inflammasome and pyroptosis in human primary monocytes. Cell Death Discov. 2021;7(1):43.

199. Qin C, Zhou L, Hu Z, Zhang S, Yang S, Tao Y, et al. Dysregulation of Immune Response in Patients With Coronavirus 2019 (COVID-19) in Wuhan, China. Clin Infect Dis. 2020;71(15):762-8.

200. Luo P, Liu Y, Qiu L, Liu X, Liu D, Li J. Tocilizumab treatment in COVID-19: A single center experience. J Med Virol. 2020;92(7):814-8.

201. Lee JS, Shin EC. The type I interferon response in COVID-19: implications for treatment. Nat Rev Immunol. 2020;20(10):585-6.

202. Cesta MC, Zippoli M, Marsiglia C, Gavioli EM, Mantelli F, Allegretti M, et al. The Role of Interleukin-8 in Lung Inflammation and Injury: Implications for the Management of COVID-19 and Hyperinflammatory Acute Respiratory Distress Syndrome. Front Pharmacol. 2021;12:808797.

203. Thevarajan I, Nguyen THO, Koutsakos M, Druce J, Caly L, van de Sandt CE, et al. Breadth of concomitant immune responses prior to patient recovery: a case report of non-severe COVID-19. Nat Med. 2020;26(4):453-5.

204. Ip WE, Chan KH, Law HK, Tso GH, Kong EK, Wong WH, et al. Mannose-binding lectin in severe acute respiratory syndrome coronavirus infection. The Journal of infectious diseases. 2005;191(10):1697-704.

205. Yu J, Yuan X, Chen H, Chaturvedi S, Braunstein EM, Brodsky RA. Direct activation of the alternative complement pathway by SARS-CoV-2 spike proteins is blocked by factor D inhibition. Blood. 2020;136(18):2080-9.

206. Meroni PL, Croci S, Lonati PA, Pregnolato F, Spaggiari L, Besutti G, et al. Complement activation predicts negative outcomes in COVID-19: The experience from Northen Italian patients. Autoimmunity Reviews. 2022:103232.

207. Moore A, Ansari M, McKeigue P, Skerka C, Hayward C, Rudan I, et al. Genetic influences on plasma CFH and CFHR1 concentrations and their role in susceptibility to age-related macular degeneration. 2013.

208. Ferluga J, Kouser L, Murugaiah V, Sim RB, Kishore U. Potential influences of complement factor H in autoimmune inflammatory and thrombotic disorders. Molecular immunology. 2017;84:84-106.

209. Leatherdale A, Stukas S, Lei V, West HE, Campbell CJ, Hoiland RL, et al. Persistently elevated complement alternative pathway biomarkers in COVID-19 correlate with hypoxemia and predict in-hospital mortality. Medical microbiology and immunology. 2022;211(1):37-48.

210. Blaum BS, Hannan JP, Herbert AP, Kavanagh D, Uhrín D, Stehle T. Structural basis for sialic acid–mediated self-recognition by complement factor H. Nature chemical biology. 2015;11(1):77-82.

211. Kouser L, Abdul-Aziz M, Nayak A, Stover CM, Sim RB, Kishore U. Properdin and factor h: opposing players on the alternative complement pathway “see-saw”. Frontiers in immunology. 2013;4:93.

212. Murugaiah V, Varghese PM, Saleh SM, Tsolaki AG, Alrokayan SH, Khan HA, et al. Complement-independent Modulation of influenza A virus infection by Factor H. Frontiers in Immunology. 2020;11:355.

213. Segers FM, Verdam FJ, de Jonge C, Boonen B, Driessen A, Shiri-Sverdlov R, et al. Complement alternative pathway activation in human nonalcoholic steatohepatitis. PLoS One. 2014;9(10):e110053.

214. McKenna E, Wubben R, Isaza-Correa JM, Melo AM, Mhaonaigh AU, Conlon N, et al. Neutrophils in COVID-19: Not innocent bystanders. Frontiers in Immunology. 2022:2548.

215. Huang J, Hume AJ, Abo KM, Werder RB, Villacorta-Martin C, Alysandratos K-D, et al. SARS-CoV-2 infection of pluripotent stem cell-derived human lung alveolar type 2 cells elicits a rapid epithelial-intrinsic inflammatory response. Cell Stem Cell. 2020;27(6):962-73. e7.

216. Rahman MM, McFadden G. Modulation of NF-κB signalling by microbial pathogens. Nature Reviews Microbiology. 2011;9(4):291-306.

217. Davies DA, Adlimoghaddam A, Albensi BC. The effect of COVID-19 on NF-κB and neurological manifestations of disease. Molecular Neurobiology. 2021;58(8):4178-87.

218. Milani D, Caruso L, Zauli E, Al Owaifeer AM, Secchiero P, Zauli G, et al. p53/NF-kB Balance in SARS-CoV-2 Infection: From OMICs, Genomics and Pharmacogenomics Insights to Tailored Therapeutic Perspectives (COVIDomics). Frontiers in Pharmacology. 2022;13.

219. Yang L, Xie X, Tu Z, Fu J, Xu D, Zhou Y. The signal pathways and treatment of cytokine storm in COVID-19. Signal transduction and targeted therapy. 2021;6(1):1-20.

220. Nazerian Y, Vakili K, Ebrahimi A, Niknejad H. Developing Cytokine Storm-Sensitive Therapeutic Strategy in COVID-19 Using 8P9R Chimeric Peptide and Soluble ACE2. Frontiers in Cell and Developmental Biology. 2021;9.

221. Carcaterra M, Caruso C. Alveolar epithelial cell type II as main target of SARS-CoV-2 virus and COVID-19 development via NF-Kb pathway deregulation: A physio-pathological theory. Medical Hypotheses. 2021;146:110412.

222. DeDiego ML, Nieto-Torres JL, Regla-Nava JA, Jimenez-Guardeño JM, Fernandez-Delgado R, Fett C, et al. Inhibition of NF-κB-mediated inflammation in severe acute respiratory syndrome coronavirus-infected mice increases survival. Journal of virology. 2014;88(2):913-24.

223. Siu K-L, Yuen K-S, Castaño-Rodriguez C, Ye Z-W, Yeung M-L, Fung S-Y, et al. Severe acute respiratory syndrome coronavirus ORF3a protein activates the NLRP3 inflammasome by promoting TRAF3-dependent ubiquitination of ASC. The FASEB Journal. 2019;33(8):8865.

224. Jamilloux Y, Henry T, Belot A, Viel S, Fauter M, El Jammal T, et al. Should we stimulate or suppress immune responses in COVID-19? Cytokine and anti-cytokine interventions. Autoimmunity reviews. 2020;19(7):102567.

225. Martinon F, Burns K, Tschopp J. The inflammasome: a molecular platform triggering activation of inflammatory caspases and processing of proIL-β. Molecular cell. 2002;10(2):417-26.

226. Ferreira AC, Soares VC, de Azevedo-Quintanilha IG, Dias SdSG, Fintelman-Rodrigues N, Sacramento CQ, et al. SARS-CoV-2 engages inflammasome and pyroptosis in human primary monocytes. Cell death discovery. 2021;7(1):1-12.

227. Cauchois R, Koubi M, Delarbre D, Manet C, Carvelli J, Blasco VB, et al. Early IL-1 receptor blockade in severe inflammatory respiratory failure complicating COVID-19. Proceedings of the National Academy of Sciences. 2020;117(32):18951-3.

228. Qin C, Zhou L, Hu Z, Zhang S, Yang S, Tao Y, et al. Dysregulation of immune response in patients with coronavirus 2019 (COVID-19) in Wuhan, China. Clinical infectious diseases. 2020;71(15):762-8.

229. Karki R, Sharma BR, Tuladhar S, Williams EP, Zalduondo L, Samir P, et al. Synergism of TNF-α and IFN-γ triggers inflammatory cell death, tissue damage, and mortality in SARS-CoV-2 infection and cytokine shock syndromes. Cell. 2021;184(1):149-68. e17.

230. Luo P, Liu Y, Qiu L, Liu X, Liu D, Li J. Tocilizumab treatment in COVID-19: a single center experience. Journal of medical virology. 2020;92(7):814-8.

231. Lee JS, Shin E-C. The type I interferon response in COVID-19: implications for treatment. Nature Reviews Immunology. 2020;20(10):585-6.

232. Wang N, Zhan Y, Zhu L, Hou Z, Liu F, Song P, et al. Retrospective multicenter cohort study shows early interferon therapy is associated with favorable clinical responses in COVID-19 patients. Cell host & microbe. 2020;28(3):455-64. e2.

233. Alturaiki WH. Evaluation of CC chemokine ligand 5 (CCL5) chemokine, interleukin 5 (IL-5) cytokine, and eosinophil counts as potential biomarkers in Saudi patients with chronic asthma during sandstorms. Cureus. 2020;12(4).

234. Marques RE, Guabiraba R, Russo RC, Teixeira MM. Targeting CCL5 in inflammation. Expert opinion on therapeutic targets. 2013;17(12):1439-60.

235. Cesta MC, Zippoli M, Marsiglia C, Gavioli EM, Mantelli F, Allegretti M, et al. The role of interleukin-8 in lung inflammation and injury: Implications for the management of COVID-19 and hyperinflammatory acute respiratory distress syndrome. Frontiers in pharmacology. 2022;12:3931.

236. Folkesson H, Matthay M, Hebert C, Broaddus V. Acid aspiration-induced lung injury in rabbits is mediated by interleukin-8-dependent mechanisms. The Journal of clinical investigation. 1995;96(1):107-16.

237. Patterson BK, Seethamraju H, Dhody K, Corley MJ, Kazempour K, Lalezari J, et al. CCR5 inhibition in critical COVID-19 patients decreases inflammatory cytokines, increases CD8 T-cells, and decreases SARS-CoV2 RNA in plasma by day 14. International Journal of Infectious Diseases. 2021;103:25-32.

238. Alosaimi B, Mubarak A, Hamed ME, Almutairi AZ, Alrashed AA, AlJuryyan A, et al. Complement anaphylatoxins and inflammatory cytokines as prognostic markers for COVID-19 severity and in-hospital mortality. Frontiers in Immunology. 2021:2298.

239. Zeng Z-Y, Feng S-D, Chen G-P, Wu J-N. Predictive value of the neutrophil to lymphocyte ratio for disease deterioration and serious adverse outcomes in patients with COVID-19: a prospective cohort study. BMC Infectious Diseases. 2021;21(1):1-6.

240. Chen Z, Yuan Y, Hu Q, Zhu A, Chen F, Li S, et al. SARS-CoV-2 immunity in animal models. Cellular & Molecular Immunology. 2024:1-15.

241. Chu H, Chan JF-W, Yuen K-Y. Animal models in SARS-CoV-2 research. Nature Methods. 2022;19(4):392-4.

242. Fan C, Wu Y, Rui X, Yang Y, Ling C, Liu S, et al. Animal models for COVID-19: advances, gaps and perspectives. Signal Transduction and Targeted Therapy. 2022;7(1):220.

Appendices

A

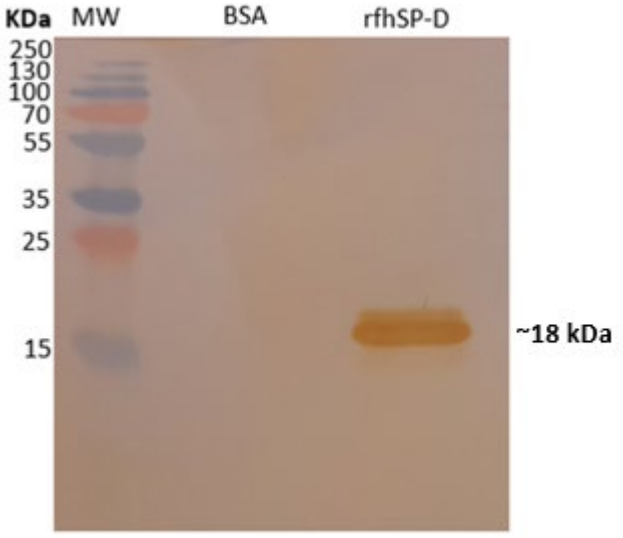
KDa
MW
BSA
rfhSP-D
250
130
100
70
55
35
25
15
~18 kDa

B

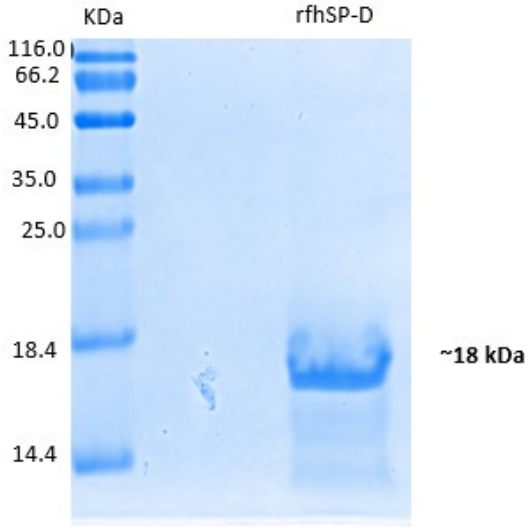
KDa
rfhSP-D
116.0
66.2
45.0
35.0
25.0
18.4
14.4
~18 kDa

C

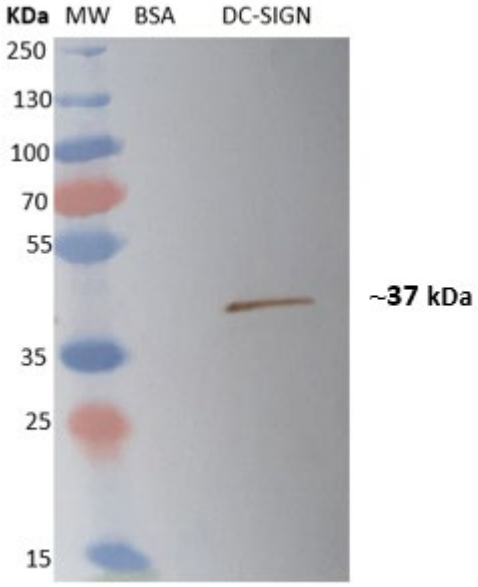
KDa
MW
BSA
DC-SIGN
250
130
100
70
55
35
25
15
~37 kDa

D

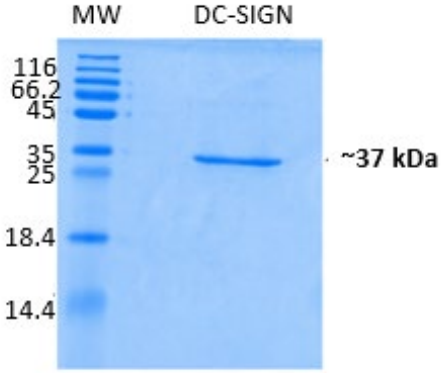
MW
DC-SIGN
116
66.2
45
35
25
18.4
14.4
~37 kDa

E

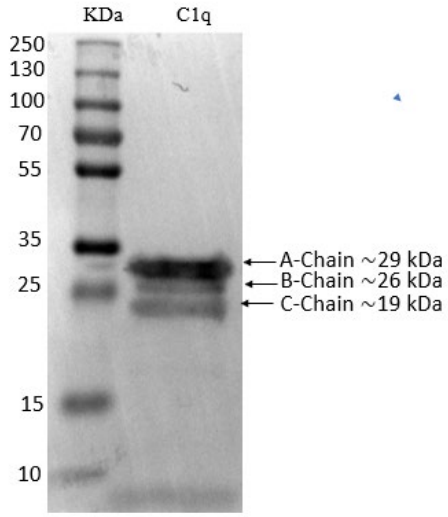
KDa
C1q
250
130
100
70
55
35
25
15
10
A-Chain ~29 kDa
B-Chain ~26 kDa
C-Chain ~19 kDa

F

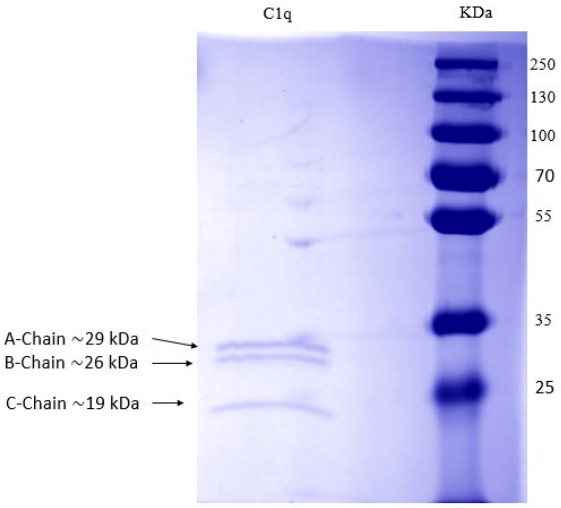
C1q
KDa
250
130
100
70
55
35
25
A-Chain ~29 kDa
B-Chain ~26 kDa
C-Chain ~19 kDa

G

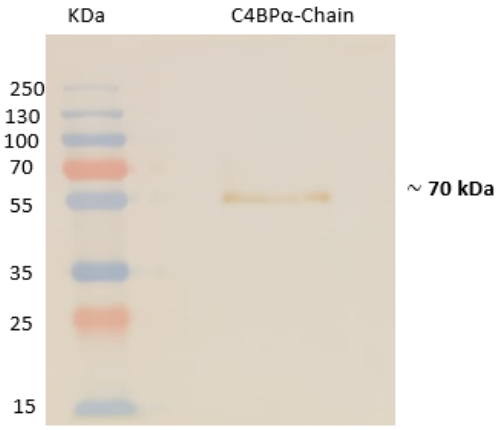
KDa
C4BPα-Chain
250
130
100
70
55
35
25
15
~ 70 kDa

H

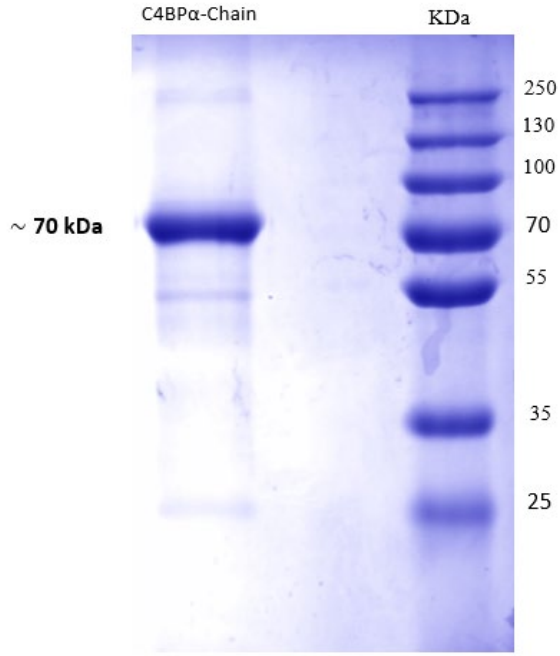
C4BPα-Chain
KDa
~ 70 kDa
250
130
100
70
55
35
25

I

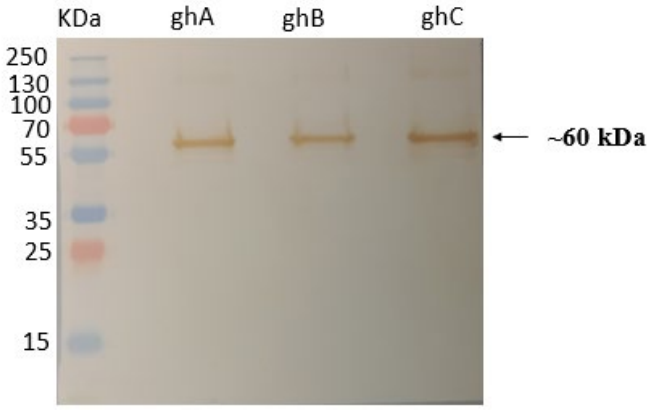
KDa
ghA
ghB
ghC
250
130
100
70
55
35
25
15
~60 kDa

J

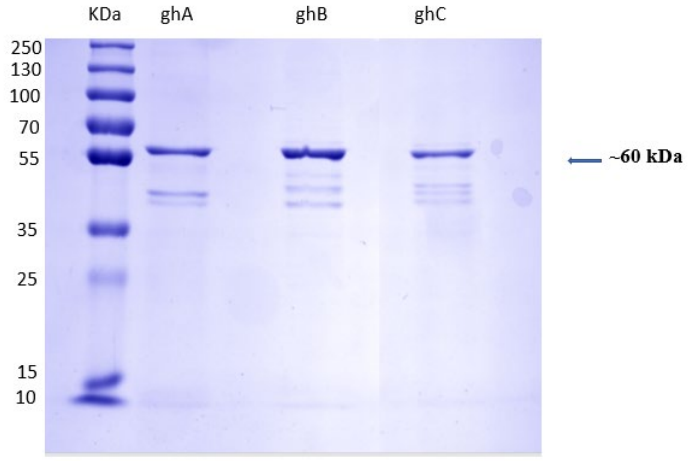
KDa
ghA
ghB
ghC
250
130
100
70
55
35
25
15
10
~60 kDa

K

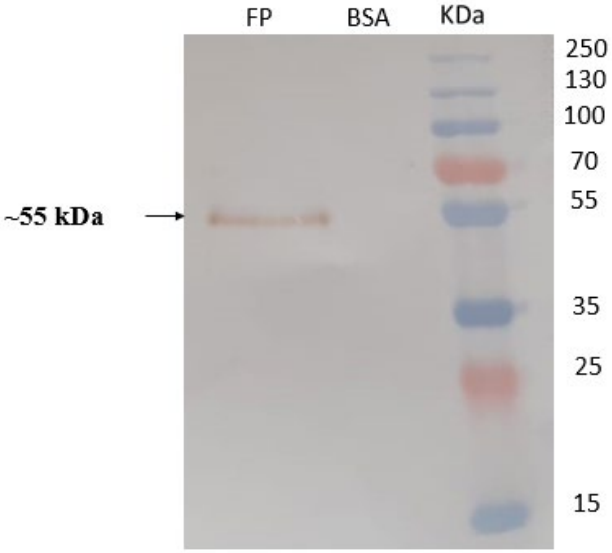
FP
BSA
KDa
~55 kDa
250
130
100
70
55
35
25
15

L

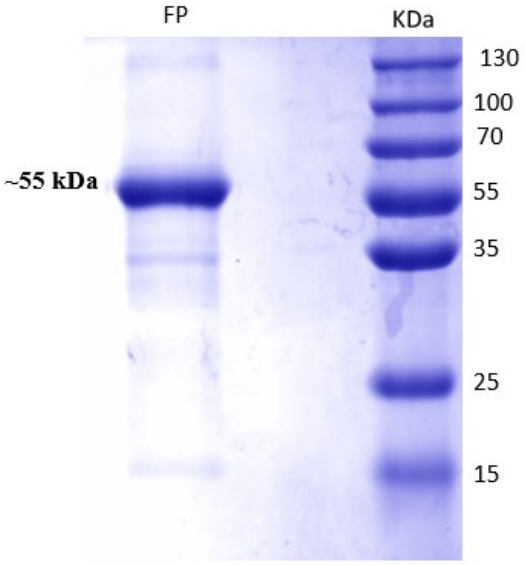
FP
KDa
~55 kDa
130
100
70
55
35
25
15

M

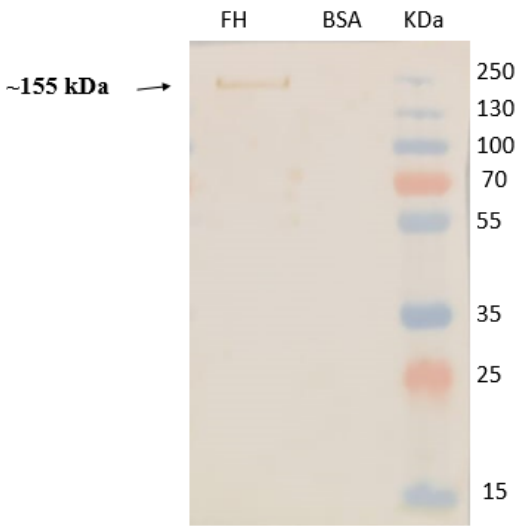
FH
BSA
KDa
~155 kDa
250
130
100
70
55
35
25
15

N

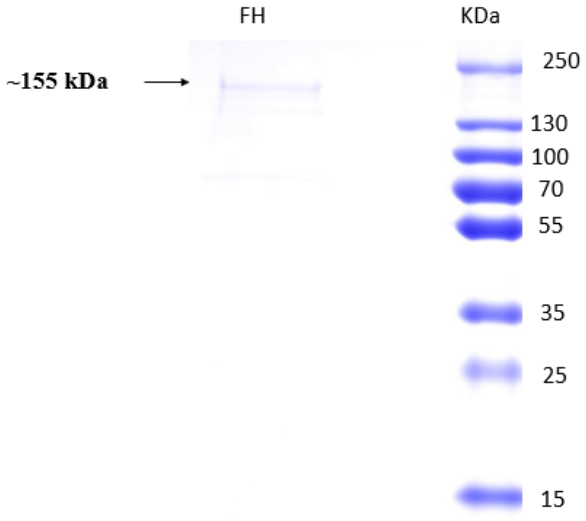
FH
KDa
~155 kDa
250
130
100
70
55
35
25
15

O

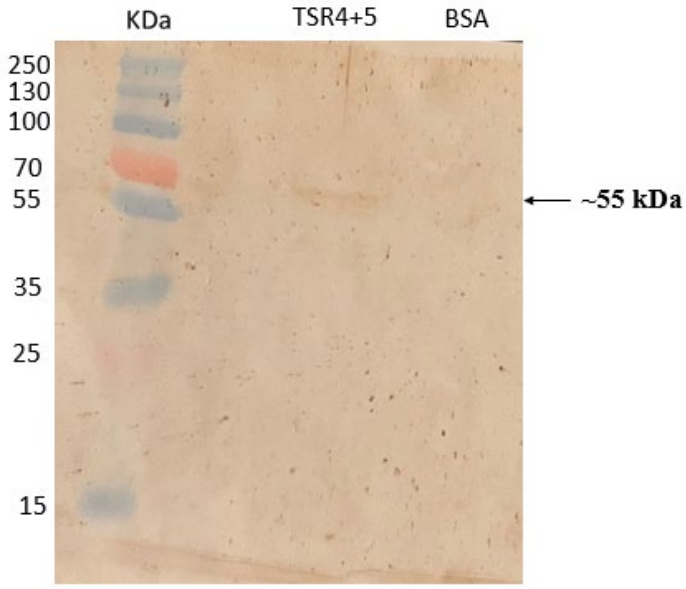
KDa
TSR4+5
BSA
250
130
100
70
55
35
25
15
~55 kDa

P

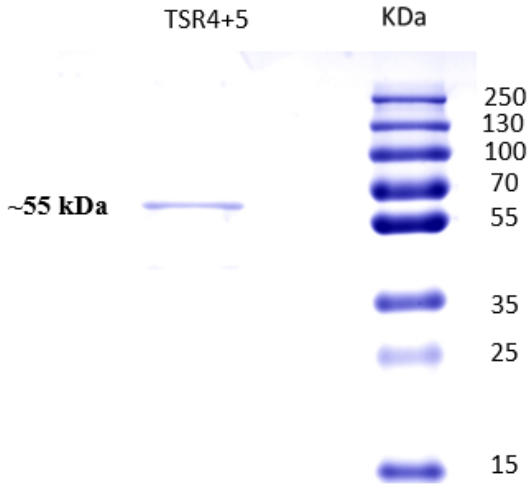
TSR4+5
KDa
~55 kDa
250
130
100
70
55
35
25
15

Appendix 1: Characterization of purified protein. SDS-PAGE (12% w/v acrylamide/bisacrylamide) were loaded with either rfhSP-D (B), CD-SIGN (D), C1q (F), C4BP (H), ghs (A, B, and C) (J), FH (L), FP (N), or TSR4+5 (P) along with a protein ladder with a range of 250 to 10 kDa (Thermofisher). The denatured and reduced samples were run for 120 min at 90 V and stained with Coomassie brilliant blue to show protein bands corresponding to the respective proteins, rfhSP-D (~18 kDa), CD-SIGN (~37 kDa)C1q [A chain (~ 29 kDa), B chain (~26 kDa), C chain (~19 kDa)], C4BP α-chain (~70kDa), ghs (A, B, and C) each gh ~60 kDa, FH (~ 155 kDa), Properdin (~55 kDa), and TSR4+5(~55 kDa). Similarly, the immunoreactivity of the purified proteins was analysed by western blotting. A PVDF membrane with either purified either rfhSP-D (A), CD-SIGN (C), C1q (E), C4BP (G), ghs (A, B, and C) (I), FH (K), FP (M), or TSR4+5 (O), along with a protein ladder with a range of 250 to 10 kDa was probed at room temperature for 1 h using respective antibodies (1:1,000)[rabbit-anti-human SP-D polyclonal antibody, rabbit-anti-human DC-SIGN polyclonal antibody, rabbit-anti-human C1q polyclonal antibody, rabbit-anti-human C4BP polyclonal antibody, mouse-anti- MBP monoclonal antibody, anti-human FH monoclonal antibody (MRCOX23)], and rabbit-anti-human Properdin polyclonal antibodies], followed by incubation with secondary goat anti-rabbit IgG HRP-conjugate or secondary goat anti-mouse IgG HRP-conjugate (1:1,000) for 1 h at room temperature. Bands corresponding to corresponding to the respective proteins, rfhSP-D (~18 kDa), CD-SIGN (~37 kDa)C1q [A chain (~ 29 kDa), B chain (~26 kDa), C chain (~19 kDa)], C4BP α-chain (~70kDa), ghs (A, B, and C) each gh ~60 kDa, FH (~ 155 kDa), Properdin (~55 kDa), and TSR4+5(~55 kDa) were observed after developing the colour using 3,3'-diaminobenzidine (DAB) substrate. Notably, the bands of C1q western blot were visualised utilising Enhanced Chemiluminescence (ECL; Thermo Fisher; Cat: 32106) in the BioRad ChemiDoc MP imaging system.

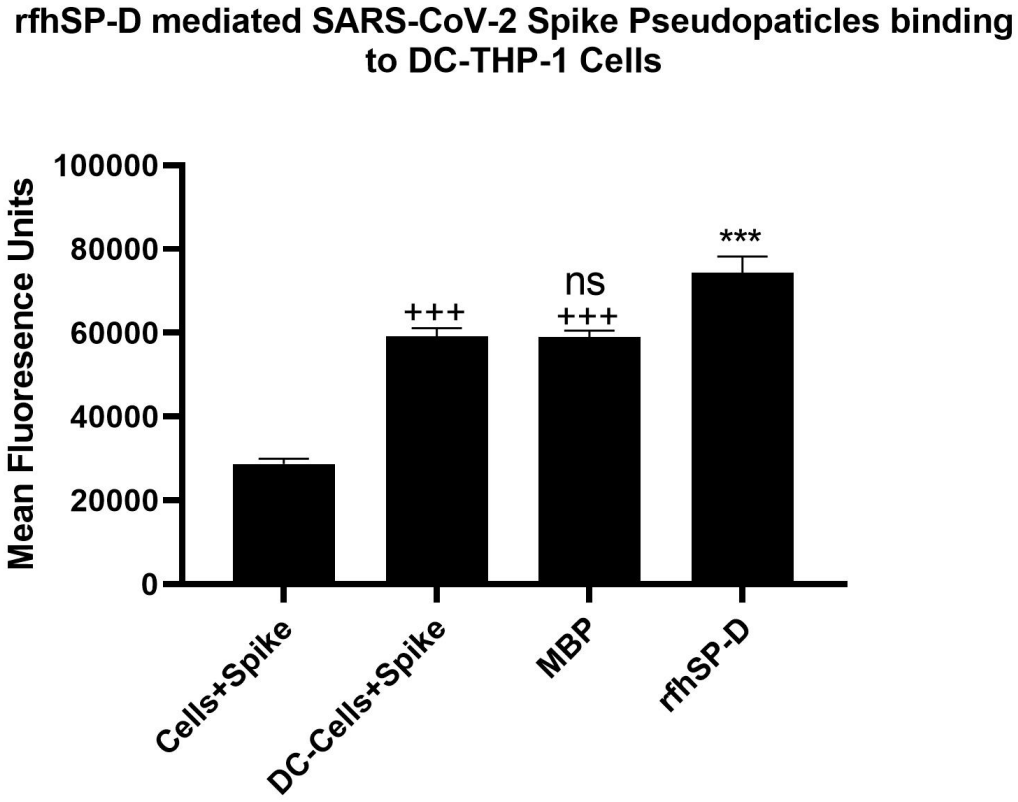

Appendix 2: Binding of rfhSP-D pre-treated SARS-CoV-2 pseudoparticles to DC-THP-1 cells. SARS-CoV-2 lentiviral pseudoparticles were used to bind DC-THP-1 cells pre-incubated with rfhSP-D (20 µg/mL). The wells were probed with rabbit anti-SARS-CoV-2 spike (1:200) polyclonal antibodies after being washed and fixed with 1% v/v paraformaldehyde for 1 min. Viral binding assay was conducted in triplicates, and error bars represent ± SEM. Statistical significance was determined using the two-way ANOVA ($^{+++}p < 0.05$) for DC- THP-1 cells treated with Spike or BSA compared to THP-1 native cells with Spike. For cells pre-treated with and then challenged with SARS-CoV-2 lentiviral pseudoparticles, significance was compared to cells only challenged with pseudotypes or BSA (***$p < 0.05$). No significance was found compared to DC -cells treated with Spike to BSA (ns > 0.05). These results indicated that rfhSP-D pretreatment enhanced viral binding.

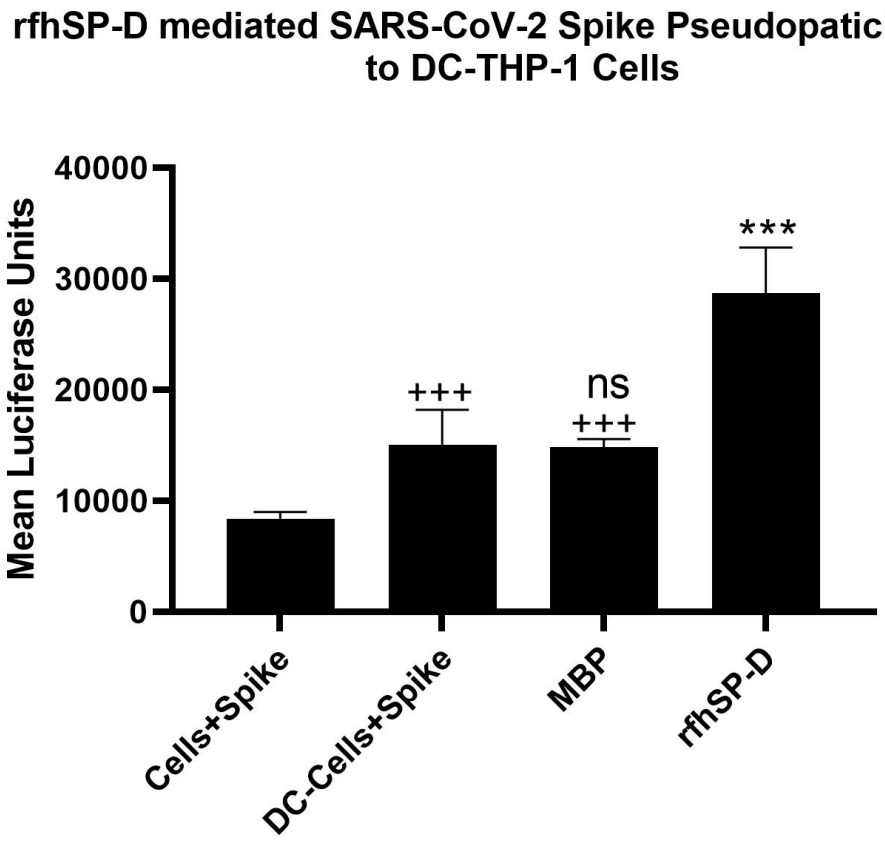

Appendix 3: Modulation of cell viral entry of rfhSP-D pre-treated SARS-CoV-2 pseudoparticles to DC-THP-1 cells. Luciferase reporter activity of rfhSP-D (20 µg/mL) pre-treated cells transduced with SARS-CoV-2 lentiviral pseudoparticles for 24h was measured. Viral entry assay was conducted in triplicates, and error bars represent ± SEM. Statistical significance was determined using the two-way ANOVA ($^{+++}p < 0.05$) for DC- THP-1 cells treated with Spike or BSA compared to THP-1 native cells with Spike. For cells pre-treated with and then challenged with SARS-CoV-2 lentiviral pseudoparticles, significance was compared to cells only challenged with pseudotypes or BSA (***$p < 0.05$). No significance was found compared to DC -cells treated with Spike to BSA (ns > 0.05). These findings revealed that rfhSP-D pretreatment increased viral entry.

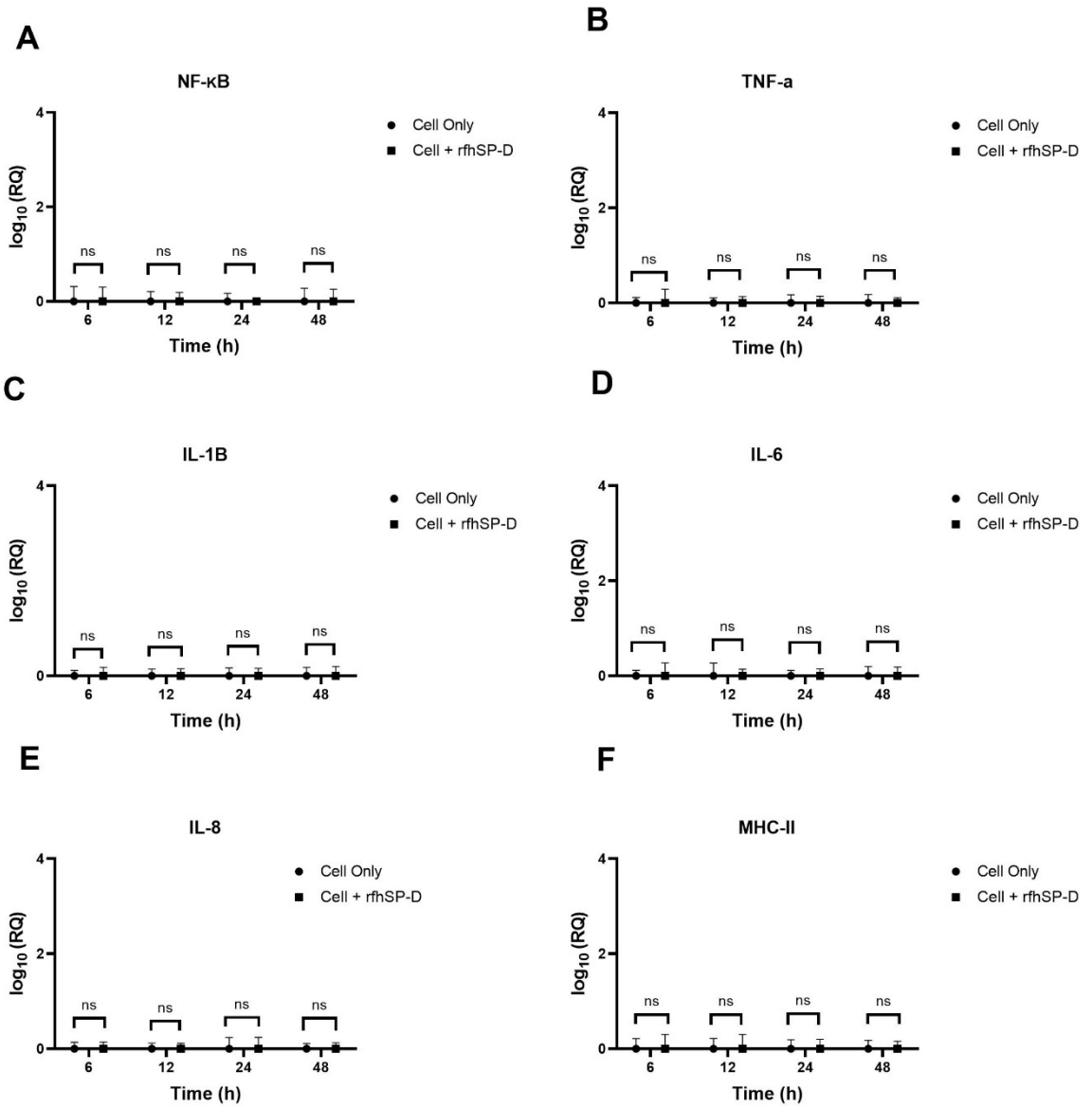

Appendix 4: rfhSP-D effect on inflammatory response in DC-THP-1 cells. DC-THP-1 cells were treated with 20 µg/ml of rfhSP-D. The cells were harvested at 6 hours, 12 hours, 24 hours, and 48 hours to analyse the expression of cytokines and MHC class II. RNA was purified from the lysed cells and converted into cDNA. The expression levels of NF-κB (A), TNF-α (B), IL-1β (C), IL-6 (D), IL-8 (E), and MHC class II (F) were measured using RT-qPCR, and the data were normalised against the expression of 18S rRNA as a control. The experiments were conducted in triplicates, and the error bars represent ± SEM. The relative expression (RQ) was calculated using DC-THP-1 cells only as the calibrator. The RQ value was calculated using the formula RQ = $2^{-\Delta\Delta Ct}$. Statistical significance was determined using the unpaired test (ns = no significance) (n = 3).

A

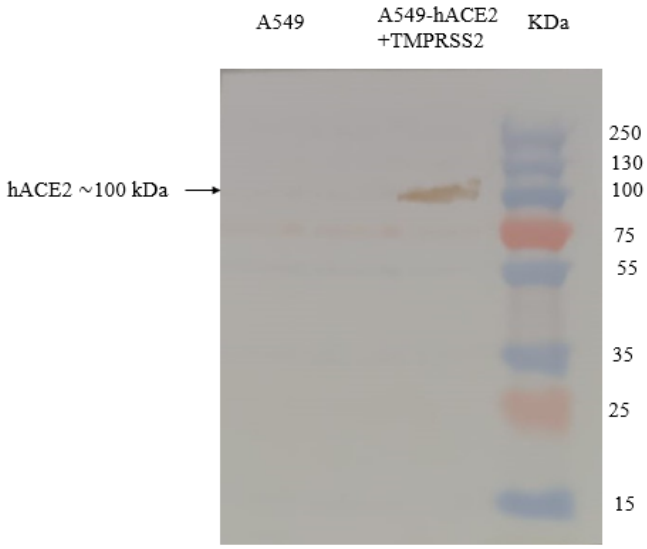

B

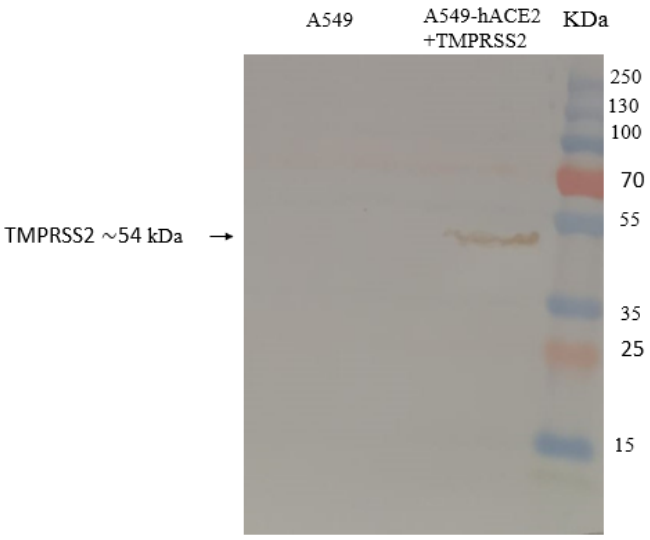

Appendix 5: Western blot analysis for A549- hACE2 +TMPRSS2 cells expressed hACE2 and TMPRSS2. A549 and A549-hACE2+TMPRSS2 cells were harvested and lysed using RIPA buffer.

Cell lysates were heated for 10 mins at 95 °C, subjected to SDS-PAGE and transferred onto a PVDF membrane. Membranes were blocked in 5% skim milk in PBS and incubated for 2h at 4 °C. Next day, the membranes were probed at room temperature for 1 h using the corresponding antibodies (1:1,000) [rabbit-anti-human ACE2 polyclonal antibody and rabbit-anti-human TMPRSS2 polyclonal antibody. After developing the colour using a 3,3'-diaminobenzidine (DAB) substrate, bands corresponding to the respective proteins, hACE2(~100 kDa) (A), and TMPRSS2 (~54 kDa) (B) were observed.

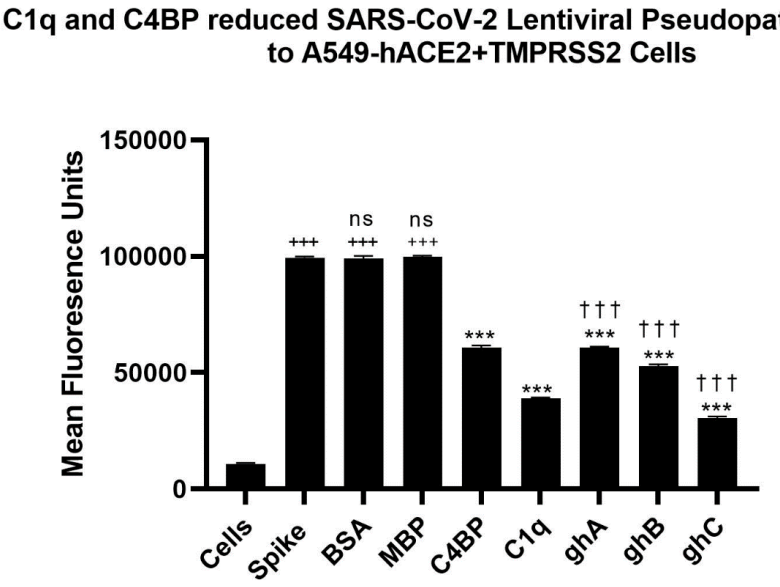

Appendix 6: Binding of C1q or C4BP pre-treated SARS-CoV-2 pseudoparticles to A549-hACE2+TMPRSS2 cells. SARS-CoV-2 lentiviral pseudoparticles were used to bind A549-hACE2+TMPRSS2 cells pre-incubated with C1q or C4BP (20 µg/mL). The wells were probed with rabbit anti-SARS-CoV-2 spike (1:200) polyclonal antibodies after being washed and fixed with 1% v/v paraformaldehyde for 1 min. Binding entry assay was conducted in triplicates, and error bars represent ± SEM. Statistical significance was determined using the two-way ANOVA ($^{+++}p < 0.05$) for cells treated with Spike, BSA, or MBP compared to untreated cells. For cells pre-treated with C1q, ghA, ghB, and ghC or C4BP and then challenged with SARS-CoV-2 lentiviral pseudoparticles, significance was compared to cells only challenged with pseudotypes or to BSA (***$p < 0.05$). Recombinant ghA, ghB, and ghC (tagged with MBP), the significance of ghs pre-treated cells challenged with pseudotypes was assessed against cells

pre-treated with MBP followed by a pseudotype challenge ($^{+++}p < 0.05$). These results demonstrated revealed that C1q and C4BP pretreatment reduced viral binding. No significant difference was observed between BSA or MBP pre-treated cells and those directly challenged with pseudotypes (ns > 0.05).

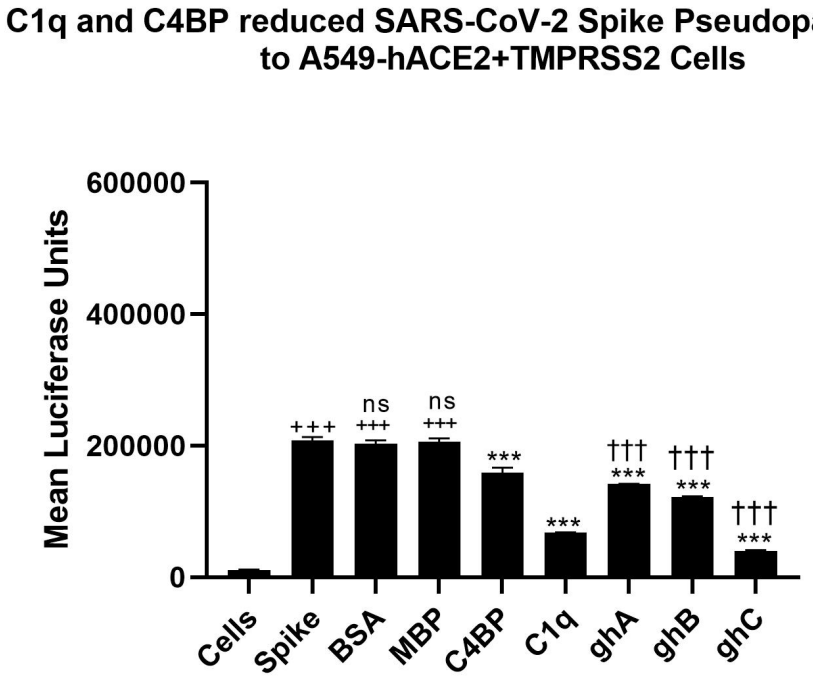

Appendix 7: C1q and C4BP reduced SARS-CoV-2 pseudoparticles entry into A549-hACE2+TMPRSS2 cells. Luciferase reporter activity of C1q or C4BP (20 µg/mL) pre-treated cells transduced with SARS-CoV-2 lentiviral pseudoparticles for 24h was measured. The assay was conducted in triplicates, and error bars represent ± SEM. The statistical significance of Spike, BSA or MBP-treated cells was compared to untreated cells and was determined using two-way ANOVA ($^{+++}p < 0.05$). Similarly, the statistical significance of C1q, ghA, ghB, and ghC or C4BP pre-treated cells challenged with SARS-CoV-2 lentiviral pseudoparticles was also determined by using the two-way ANOVA by comparing to cells that were only challenged with the pseudotypes (***$p < 0.05$), or to BSA pretreated cells challenged with the

pseudotypes ($^{###}p < 0.05$). Since the recombinant ghA, ghB, and ghC are tagged with MBP, the statistical significance of ghs pre-treated cells challenged with the pseudotypes was assessed using the two-way ANOVA by comparing to cells that were pretreated with MBP and then challenged with the pseudotypes ($^{†††}p < 0.05$). The findings showed that C1q and C4BP pretreatment significantly reduces viral entry. No statistically significant difference using the two-way ANOVA was identified between BSA or MBP pre-treated cells compared to cells directly challenged with the pseudotypes (ns > 0.05).

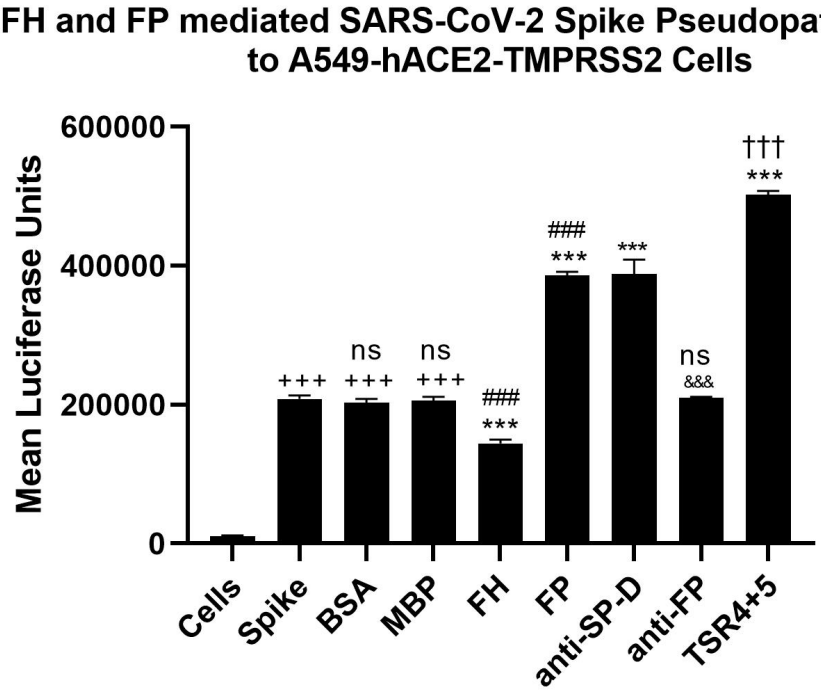

Appendix 8: FH, FP and TRS4+5 modulate SARS-CoV-2 pseudoparticles entry into A549-hACE2+TMPRSS2 cells. Luciferase reporter activity of FH, FP or TRS4+5 (20 µg/mL) pre-treated cells transduced with SARS-CoV-2 lentiviral pseudoparticles for 24h was measured. The assay was conducted in triplicates, and error bars represent ± SEM. The statistical significance of Spike, BSA or MBP-treated cells was compared to untreated cells and was determined using two-way ANOVA ($+++p < 0.05$). For cells pre-treated with FH or FP and then challenged with SARS-CoV-2 lentiviral pseudoparticles, significance was compared to cells only challenged with pseudotypes ($***p < 0.05$) or to MBP /BSA pre-treated cells subsequently challenged with pseudotypes ($^{###}p < 0.05$). Recombinant TSR4+5 (tagged with MBP), the significance of

TSR4+5 pre-treated cells challenged with pseudotypes was evaluated against cells pre-treated with MBP followed by viral pseudotypes challenge ($^{\dagger\dagger\dagger}p < 0.05$). Importantly, anti-FP has statistically significant ($^{\&\&\&}p < 0.05$) reversed the transduction effect of FP-treated cells (anti-SP-D, control), whereas no significance was found when compared to cells treated with Spike or MBP/BSA (ns > 0.05. The findings showed that FH pretreatment significantly reduces viral entry, whereas FP and TSR4+5 increased. No statistically significant difference using the two-way ANOVA was identified between BSA or MBP pre-treated cells compared to cells directly challenged with the pseudotypes (ns > 0.05).

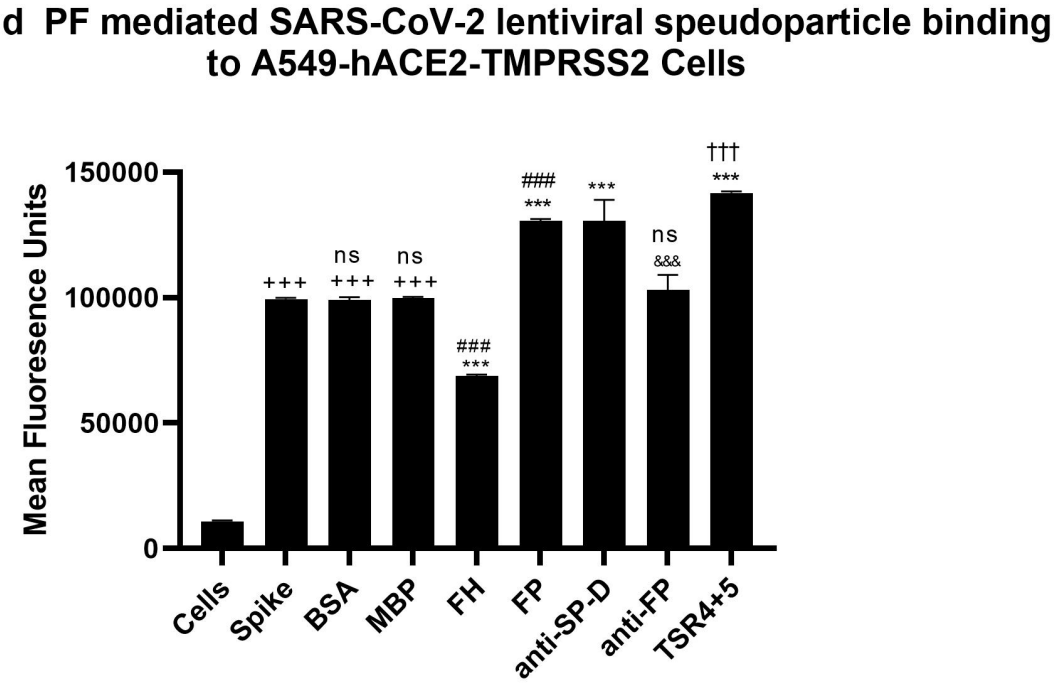

Appendix 9: Binding of FH or PF pre-treated SARS-CoV-2 pseudoparticles to A549-hACE2+TMPRSS2 cells. SARS-CoV-2 lentiviral pseudoparticles were used to bind A549-hACE2+TMPRSS2 cells pre-incubated with FH or FP (20 µg/mL). The wells were probed with rabbit anti-SARS-CoV-2 spike (1:200) polyclonal antibodies after being washed and fixed with

1% v/v paraformaldehyde for 1 min. Binding entry assay was conducted in triplicates, and error bars represent ± SEM. Statistical significance was determined using the two-way ANOVA ($^{+++}p < 0.05$) for cells treated with Spike, BSA, or MBP compared to untreated cells. For cells pre-treated with FH or FP and then challenged with SARS-CoV-2 lentiviral pseudoparticles, significance was compared to cells only challenged with pseudotypes (***$p < 0.05$) or to MBP /BSA pre-treated cells subsequently challenged with pseudotypes ($^{###}p < 0.05$). Recombinant TSR4+5 (tagged with MBP), the significance of TSR4+5 pre-treated cells challenged with pseudotypes was evaluated against cells pre-treated with MBP followed by a pseudotype challenge ($^{†††}p < 0.05$). Importantly, anti-FP has statistically significant ($^{\&\&\&}p < 0.05$) reversed the binding effect of FP-treated cells (anti-SP-D, control), whereas no significance was found when compared to cells treated with Spike or BSA (ns > 0.05). These findings revealed that FH pretreatment reduced viral binding, whereas FP or TSR 4+5 pretreatment enhanced it. No significant difference was observed between MBP/BSA pre-treated cells and those directly challenged with pseudotypes (ns > 0.05).

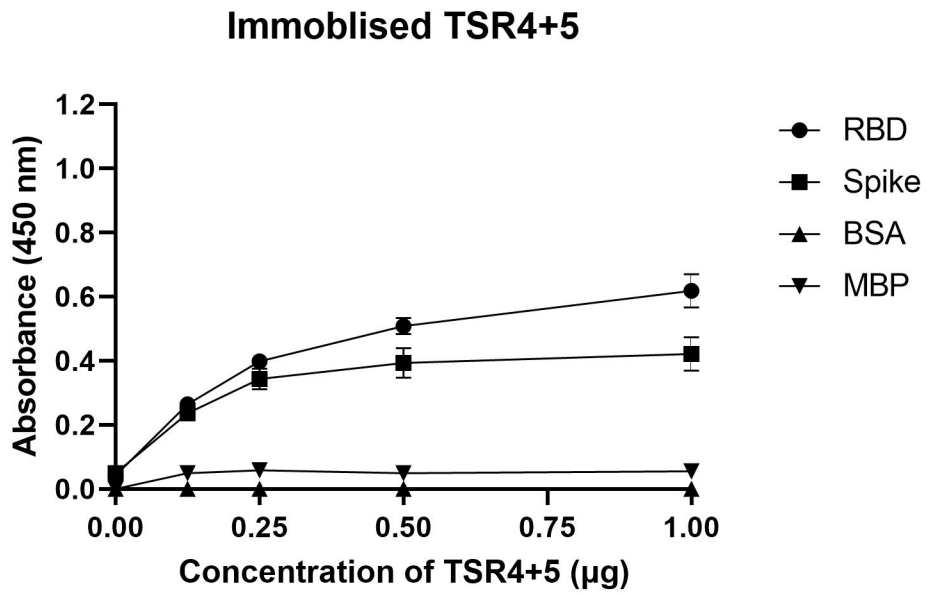

Appendix 10: SARS-CoV-2 interacted with TSR4+5 via its S Protein RBD. TSR4+5 bound both SARS-CoV-2 Spike and RBD proteins in a dose-dependent manner. Decreasing concentrations of immobilised TSR4+5 (1, 0.5, 1.25, and 0 µg/well) were coated in a 96-well plate using Carbonate-Bicarbonate (CBC) buffer, pH 9.6 at 4°C overnight. After washing out the excess

CBC buffer with PBS three times, a constant concentration of virus proteins (1 µg/well) was added to corresponding wells, followed by incubation at 37°C for 2h. After washing out the unbound proteins, the wells were probed with rabbit anti-SARS-CoV-2 Spike (1:5000; 100 µ/well). MBP and BSA were used as negative controls.

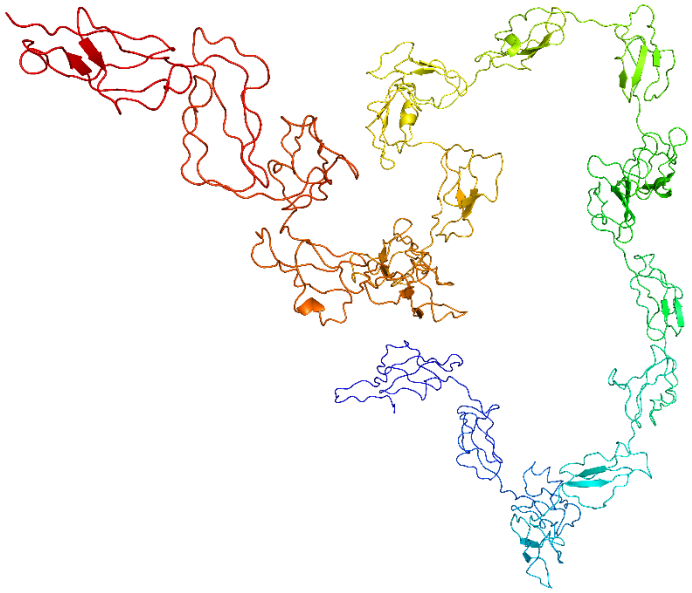

Appendix 11: Cartoon representation of modelled FH structure. The full-length 3D structure of FH was modelled using Modeller10.1. Chandan Kumar and Susan Idicula, Biomedical Informatics Centre, National Institute for Research in Reproductive and Child Health, ICMR, Mumbai, Maharashtra, India, kindly have done this work.

A

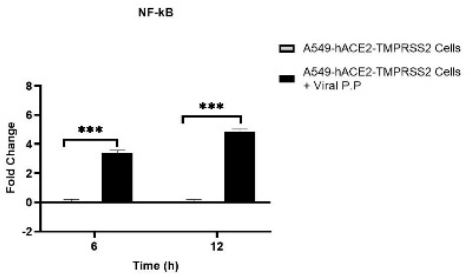
NF-kB
A549-hACE2-TMPRSS2 Cells
A549-hACE2-TMPRSS2 Cells + Viral P.P
Fold Change
Time (h)
***
***

B

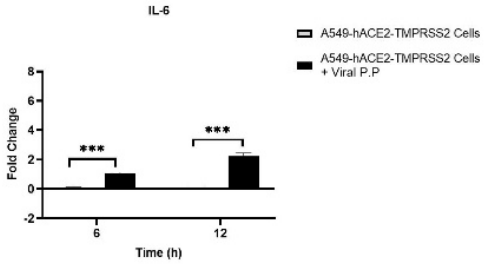
IL-6
A549-hACE2-TMPRSS2 Cells
A549-hACE2-TMPRSS2 Cells + Viral P.P
Fold Change
Time (h)
***
***

C

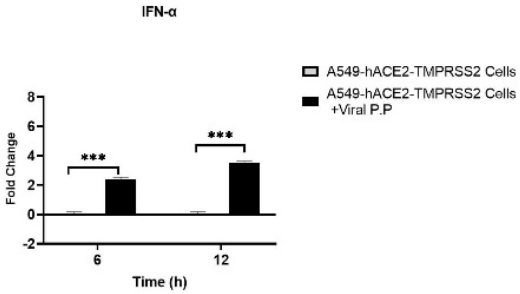
IFN-α
A549-hACE2-TMPRSS2 Cells
A549-hACE2-TMPRSS2 Cells +Viral P.P
Fold Change
Time (h)
***
***

D

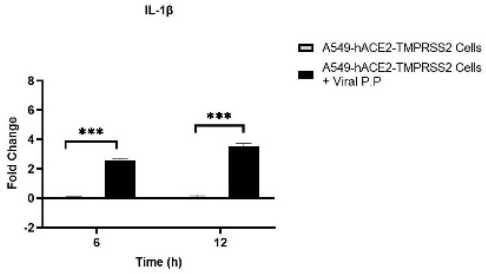
IL-1β
A549-hACE2-TMPRSS2 Cells
A549-hACE2-TMPRSS2 Cells + Viral P.P
Fold Change
Time (h)
***
***

E

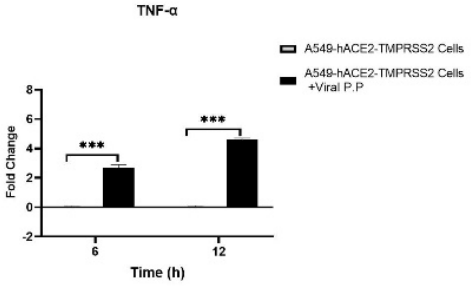
TNF-α
A549-hACE2-TMPRSS2 Cells
A549-hACE2-TMPRSS2 Cells +Viral P.P
Fold Change
Time (h)
***
***

F

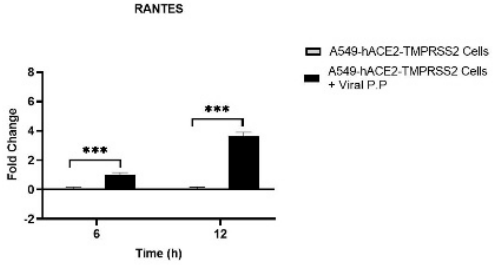
RANTES
A549-hACE2-TMPRSS2 Cells
A549-hACE2-TMPRSS2 Cells + Viral P.P
Fold Change
Time (h)
***
***

G

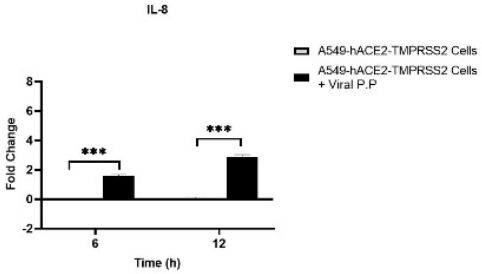
IL-8
A549-hACE2-TMPRSS2 Cells
A549-hACE2-TMPRSS2 Cells + Viral P.P
Fold Change
Time (h)
***
***

Appendix 12: SARS-CoV-2 alphaviral-pseudoparticles induce Inflammatory Response in A549-hACE2 + TMPRSS2 Cells. SARS-CoV-2 alphaviral-pseudoparticles incubated with A549-hACE2+TMPRSS2 cells. The cells were harvested at 6h and 12h to assess the mRNA levels of proinflammatory cytokines and chemokines. Cells were lysed, and purified RNA was converted into cDNA. The mRNA levels of NF-κB(A), IL-6 (B), IFN-α (C), IL-1β (D), TNF-α (E), RANTES (F) and IL-8 (G) were measured using RT-qPCR, and the data were normalised against 18S rRNA expression as a control. The relative expression (RQ) was calculated using A549-hACE2+TMPRSS2 cells only as the calibrator. $RQ = 2^{-\Delta\Delta Ct}$ was used to calculate the RQ value. SARS-CoV-2 alphaviral-pseudoparticles induce inflammatory response in A549-hACE2+TMPRSS2 cells. Experiments were carried out in triplicates, and error bars represent ± SEM. Significance was determined using the two-way ANOVA test (***$p < 0.001$) ($n = 3$).